THÈSE

En vue de l'obtention du

DOCTORAT DE L'UNIVERSITÉ DE TOULOUSE

Délivré par l'Université Paul Sabatier III
Discipline ou spécialité : Chimie-Océanographie

Présentée et soutenue par

Justyna Elżbieta Jońca

Le 1 Octobre 2012

Titre : Méthodes électrochimiques pour la surveillance autonome des espèces chimiques (oxygène et phosphate) dans l'eau de mer : Application aux Zones de Minimum d'Oxygène

JURY

V. Garçon – Directrice de Recherches, CNRS, LEGOS, Toulouse, France
M. Comtat – Professeur, Université Paul Sabatier Toulouse III, France
D. Connelly – Senior Research Scientist, National Oceanography Center, Royaume-Uni
G. W. Luther III – Professeur, Université de Delaware, États-Unis
J.-L. Marty – Professeur, Université de Perpignan, France
N. P. Revsbech – Professeur, Université d'Aarhus, Danemark
M. Trojanowicz – Professeur, Université de Varsovie, Pologne

Ecole doctorale : SDU2E
Unité de recherche : Laboratoire d'Etudes en Géophysique et Océanographie Spatiales
Directeur(s) de Thèse : Véronique Garçon
Co-directeur de Thèse : Maurice Comtat

I dedicate this work to my beloved mother.

Niniejszą pracę dedykuję mojej ukochanej mamie.

Acknowledgments

Working on the Ph.D. has been a wonderful experience. It is hard to say whether it has been grappling with the topic itself which has been the real learning experience, or grappling with how to write papers, give talks, work in a group, and stay focussed to the late night hours...In any case, I am indebted to many people for making the time working on my Ph.D. an unforgettable experience.

First of all, I am deeply grateful to my advisor **Véronique Garçon** for introducing me into the fascinating world of oceanography. Working with her has been a real pleasure to me. She has oriented and supported me with care, and has always been patient and encouraging in times of new ideas and difficulties. Her ability to select and approach compelling research problems, her high scientific standards, and her hard work set an example. Despite many responsibilities, she always had a moment to correct my manuscripts and prepare me for conferences. Above all, she made me feel friend, which I appreciate from my heart.

I will forever be thankful to my co-advisor **Maurice Comtat** for his scientific advice and knowledge and many insightful discussions and suggestions. He was my primary resource for getting my electrochemical questions answered. I am also grateful for our long discussions about french cooking and wines.

I also thank my scientific advisor **Niels Peter Revsbech** from Aarhus University in Denmark for choosing a very interesting topic for my secondment in his laboratory and for helping me achieve excellent results in a very short period of time.

I also have to thank the members of my PhD committee: **George Luther III, Douglas Connelly, Niels Peter Revsbech, Marek Trojanowicz and Jean-Louis Marty** for their helpful suggestions and hard questions. Thank you all for having accepted this additional work.

SUMMARY

GENERAL INTRODUCTION

Water has "extraordinary" properties, which play an important role in shaping the climate and make life on Earth possible. Circulation in the ocean helps distribute heat from tropical areas to polar regions of the Earth. In addition, the oceans absorb large quantities of CO_2 from the atmosphere. Approximately one quarter of CO_2 emitted by human activities goes into the oceans (Balino et al., 2001; Denman et al., 2007), where it is partly stored and thus excluded from the natural circulation for hundreds of years, helping to reduce the effects of global warming. However, nature can not remain indifferent to our actions. Sea level rise, extreme weather events, ocean de-oxygenation, ocean acidification, spreading of tropical diseases, species extinctions and ecosystems changes are a consequence of the human impacts on the natural carbon cycle (Millero, 2007). How much more carbon dioxide can sink in the ocean abyss? Which are the underlying processes and how will they change in the future? An accurate understanding of the ocean carbon cycle will allow to respond to the many questions posed by scientists, politicians, economists, manufacturers...and will help them understand, predict, mitigate and even manage climate change. This is not an easy task because the carbon cycle in the ocean depends on many factors: the oceanic circulation, the presence of phytoplankton, and thus theirs access to light and macro- and micronutrients (phosphorus, nitrogen, silicium, iron…). Moreover, to observe and monitor the carbon biogeochemical cycle, we have to face a difficult ocean environment which is harsh, dark, difficult to access, and characterized by large pressure, temperature, and ionic strength variations.

Oxygen Minimum Zones (OMZs) are oceanic areas which have concentrated much interest recently. They are characterized by low oxygen concentrations (even less than 1 μmol L^{-1}) and thus have a strong influence on biogeochemical cycles, greenhouse gases emission and life in the ocean. Denitrification is a common bacterial process occurring only in O_2- deficient regions. Due to this process, nitrate is converted into radiatively active gaseous nitrogen oxide which is released to the atmosphere (Cornejo and Farijas, 2012). This has a strong influence on nitrate to phosphate ratio which is lower than the canonical Redfield ratio of 16. Consequently, the phosphorus cycle is also influenced by the deoxygenation process. Lower ratios than Redfield of nitrate to phosphate have a strong impact on the carbon uptake by photosynthese processed and thus on the biological carbon pump.

Much of what we currently know about the temporal variability of biogeochemical processes comes primarily from *in situ* observations either ship-based, or from time series stations which give us just a limited understanding of how ocean biogeochemistry is changing in response to natural climate variations. The advent of satellite technology and the availability of satellite ocean colour allowed us to shed some more light on ocean biogeochemistry changes in response to El Niño for instance, or to anthropogenic climate changes driven by the accumulation of greenhouse gases in the atmosphere. The development of multi-disciplinary oceanic observatories for a long-time monitoring will help to increase the observing capacities in the constantly changing marine environment. This monitoring requires *in situ* miniaturized autonomous instrumentation able to achieve excellent figures of merit: long lifetime, high precision, low detection limit, fast response time, good reproducibility, resistance to biofouling and high pressure, able of stable long-term operation, and have low energy consumption. Within the past few years, sensor technologies for oxygen, chlorophyll, particles and nitrate have been refined (Johnson et al., 2009). These sensors are capable of deployment on long-endurance missions on autonomous platforms such as profiling floats and gliders.

For a large number of analytical methods, electrochemistry provides promising reagentless methods capable of miniaturization, have a decrease in response time with low energy requirements. In aquatic systems, electrochemical methods are used routinely for monitoring of pH by potentiometry, dissolved oxygen by amperometry (Revsbech et al., 2009), trace metals and speciation by voltammetry (Luther et al., 2001; Tercier-Waeber et al., 2005), conductivity and therefore salinity by impedimetry. Electrochemistry offers also a wide range of possibilities for achieving an excellent phosphate determination in seawater but

no autonomous electrochemical sensor for *in situ* phosphate determination currently exintsts. Generally, the use of electrochemical *in situ* sensors in the ocean is not well developed but the opportunities provided by some teams show an increasing interest in this research field.

My PhD thesis has two objectives:

A) Construction of an electrochemical sensor for *in situ* determination of **phosphate** in sea water,

B) Improvement of the STOX sensor for the determination of dissolved **oxygen** in the Oxygen Minimum Zones (OMZ).

The first part of the PhD thesis was performed in Toulouse, France in close cooperation with two laboratories: LEGOS (Laboratoire d'Etudes en Géophysique et Océanographie Spatiales) and LGC (Laboratoire de Génie Chimique).

The second part was carried out during a stage at Aarhus University and UNISENSE Company in Aarhus, Denmark.

This project is situated at the border of several fields: analytical chemistry, oceanography and biogeochemistry of the open ocean. Fundamentals of each of these disciplines must be presented here.

The first chapter is divided in two parts. The first part describes the biogeochemical cycles in the oceans related to the biological and physical carbon pumps. The phosphate chemistry and its special place in the biological carbon pump are also presented in this chapter. The second part is focused on the Oxygen Minimum Zone problem with a special attention on the influence of OMZs on the greenhouse gases budget and on biogeochemical cycles of nitrogen and phosphorus.

The second chapter is an overview of electrochemical techniques and is dedicated to non-specialists in this field. Firstly, principles of electrochemistry are described. Then electrochemical kinetics are presented with possible solutions of Fick's diffusion law which is the basis of electroanalytical chemistry. Electrochemical techniques used in this work are recalled and finally the influence of adsorption and coupled chemical reactions on electrochemical signals is investigated.

The third chapter is a summary of the observing systems and autonomous *in situ* sensors deployed for phosphate and oxygen measurements in the ocean. It also includes the

various electroanalytical techniques used for phosphate detection in laboratory conditions. The crucial problem of corrosion and biofouling for deployments at sea is also addressed.

Chapter IV is a presentation of the work done during the secondment at Aarhus University. The work was focused on improvement of STOX sensor for detection of ultra-low oxygen concentrations by changing the method for front gold cathode formation. Firstly, the wet chemical method for gold plating on silicon membrane is described. Then a comparison of figures of merit for the traditional and improved STOX sensors is discussed.

Chapter V presents an additional work done on elucidation of complicated electrochemistry of isopoly- and heteropolyoxomolybdates formed during anodic oxidation of molybdenum in seawater. This work uncovers the chemical formulas of silico- and phosphomolybdate complexes and explains complicated electrode reactions. It thus helps to understand the difficulty of phosphate detection by electrochemistry.

Chapter VI is a presentation of the work done on development of phosphate sensor. The method is based on oxidation of molybdenum electrode in seawater in order to form phosphomolybdate complex, electrochemically detectable by means of amperometry or voltammetry. The construction of an electrochemical cell based on membrane technology done during this work gives the possibility to detect phosphate in presence of silicate without addition of any liquid reagents.

The final chapter is a description of work done on preliminary analysis of Peruvian water masses using data obtained during an oceanographic cruise offshore Peru. The CTD (Conductivity, Temperature, and Depth) data are supported by phosphate concentration profiles obtained by electrochemical measurements (as described in Chapter VI).

INTRODUCTION GENERALE (français)

L'eau a des propriétés « extraordinaires » qui jouent un rôle important dans le façonnement du climat sur Terre. La circulation océanique contribue à la répartition de la chaleur depuis les zones tropicales vers les pôles. De plus, les océans absorbent de grandes quantités de dioxyde de carbone de l'atmosphère. Environ un quart du dioxyde de carbone émis par les activités humaines se retrouve dans les océans (Balino et al., 2001; Denman et al., 2007), où il est en partie stocké et donc exclus de la circulation naturelle pendant plusieurs centaines d'années, contribuant ainsi à la réduction des effets du réchauffement climatique. Cependant, la nature ne reste pas indifférente à nos actions. L'élévation du niveau de la mer, les phénomènes météorologiques extrêmes, la désoxygénation et l'acidification des océans, la propagation des maladies tropicales, l'extinction d'espèces et les changements de structure et de fonctionnement des écosystèmes marins sont autant de conséquences des impacts des activités humaines sur le cycle naturel du carbone (Millero, 2007). Combien de dioxyde de carbone peut se dissoudre dans l'océan ? Quels sont les facteurs qui contrôlent ce processus et comment vont-ils changer dans le futur ? Une compréhension précise du cycle du carbone océanique permettra de répondre aux nombreuses questions posées par les scientifiques, les politiciens, les économistes, les industriels ... et permettra de les aider à comprendre, prédire, atténuer et même peut être « gérer » le changement climatique. Ceci ne représente pas une tâche facile parce que le cycle du carbone dans l'océan dépend de nombreux facteurs : la circulation océanique, les mécanismes biologiques de photosynthèse, de respiration et reminéralisation de la matière organique et les processus chimiques. La pompe biologique de carbone via le phytoplancton est contrôlée par la lumière et la disponibilité en macro- et micronutriments (phosphore, azote, silice et fer, etc.). Afin de mieux comprendre les

mécanismes inhérents à cette pompe, il convient d'établir une surveillance à long terme de cet environnement marin, environnement difficile d'accès car sombre et lointain, caractérisé par de fortes pressions, une grande variabilité de la température et de la salinité.

Les zones de minimum d'oxygène (OMZ) sont des régions océaniques où l'intérêt des oceanographes s'est concentré récemment. Elles sont caractérisées par des concentrations faibles en oxygène (moins de 1 µmol L^{-1}) et ont donc une forte influence sur les cycles biogéochimiques, les émissions de gaz à effet de serre et la vie dans l'océan. La dénitrification est un processus bactérien qui apparaît seulement dans les OMZ. En raison de ce processus, le nitrate est transformé en protoxyde d'azote, puissanr gaz à effet de serre qui est libéré dans l'atmosphère (Cornejo et Farijas, 2012). Le processus de désoxygénation a donc une forte influence sur le rapport N/P qui devient inférieur à la valeur canonique de 16 de Redfield. En conséquence, le cycle biogéochimique du phosphore est aussi influencé par la désoxygénation. Les rapports nitrate sur phosphate inférieurs à la valeur de Redfield ont un fort impact sur l'absorption du carbone par le processus de photosynthèse et donc sur la pompe biologique de carbone.

Une grande partie de ce que nous savons actuellement sur la variabilité temporelle des processus biogéochimiques provient principalement d'observations *in situ*, soit à partir de navires, soit à partir de stations de séries temporelles qui nous donnent cependant une compréhension limitée de la façon dont la biogéochimie des océans évolue en réponse aux variations naturelles du climat. L'avènement des missions satellitaires et de la disponibilité des données couleur de l'eau par satellite a permis une meilleure compréhension des changements biogéochimiques des océans en réponse au phénomène El Niño par exemple ou aux changements climatiques d'origine anthropique entraînés par l'accumulation de gaz à effet de serre dans l'atmosphère. Le développement des observatoires océaniques pour une surveillance continue de l'océan permettra d'accroître les capacités d'observation de l'environnement marin. Cette surveillance nécessite une instrumentation *in situ* miniaturisée, autonome, capable d'atteindre de hautes performances en terme de durée de vie, de précision de la mesure, de limite de détection, couplée avec un temps de réponse rapide, une faible consommation d'énergie, une bonne reproductibilité, une résistance aux biosalissures et aux hautes pressions. Ces dernières années, les technologies pour les capteurs d'oxygène, de nitrate, de chlorophylle, et du carbone particulaire ont été affinées (Johnson et al., 2009). Ces capteurs sont capables d'être délpoyé sur des missions longues sur des plateformes autonomes tels que les flotteurs profileurs et les planeurs.

Parmi le grand nombre de méthodes d'analyse, l'électrochimie permet d'aller plus loin dans la miniaturisation, de diminuer le temps de réponse et les besoins énergétiques, et donc dans le développement de méthodes prometteuses sans ajout de réactifs liquides. En milieu aquatique, les méthodes électrochimiques sont utilisées en routine pour la surveillance du pH par potentiométrie, l'oxygène dissous par ampérométrie (Revsbech et al., 2009), les métaux traces et leur spéciation par voltampérométrie (Luther et al., 2001 ; Tercier-Waeber et al., 2005), la conductivité et la salinité par impédance. L'électrochimie offre également un large éventail de possibilités pour parvenir à une excellente détermination du phosphate dans l'eau de mer, mais aucun capteur autonome pour la détermination électrochimique *in situ* des phosphates n'existe à ce jour. Globalement, l'utilisation de capteurs électrochimiques *in situ* dans l'océan n'est pas bien développée, cependant les possibilités offertes par certaines équipes montrent un intérêt croissant dans ce domaine de recherche.

Les travaux de ma thèse ont deux objectifs:
A) la construction d'un capteur électrochimique pour la détermination *in situ* de phosphate dans l'eau de mer,
B) l'amélioration de la sonde STOX pour la détermination de l'oxygène dissous dans les zones de minimum d'oxygène (OMZ).

La première partie de ma thèse a été réalisée à Toulouse, en France, en étroite coopération entre: le LEGOS (Laboratoire d'Etudes en Géophysique et Océanographie Spatiales) et le LGC (Laboratoire de Génie Chimique).

La deuxième partie a été réalisée au cours d'un stage de 3 mois à l'Université d'Aarhus et dans la compagnie Unisense à Aarhus au Danemark.

Ce projet de recherche est situé à la frontière de plusieurs champs disciplinaires : la chimie analytique, l'océanographie et la biogéochimie de l'océan ouvert. Les principes de base de chacune de ces disciplines seront présentés dans ce manuscript.

Le premier chapitre est divisé en deux parties. La première partie décrit les grands cycles biogéochimiques dans les océans en lien avec les pompes biologique et physique du carbone. La chimie des phosphates et sa place particulière dans la pompe biologique du carbone sont également présentées dans ce chapitre. La deuxième partie se concentre sur le problème des Zones de Minimum d'Oxygène avec une attention particulière sur l'influence des OMZs sur le budget des gaz à effet de serre et sur les cycles biogéochimiques.

Le deuxième chapitre est un aperçu des techniques électrochimiques et est plutôt dédié aux non-spécialistes dans ce domaine. Tout d'abord, les principes de l'électrochimie sont

décrits. Puis la cinétique électrochimique qui consitue la base de la chimie électroanalytique est présentée. Les techniques électrochimiques utilisées dans ce travail sont rappelées et nous discuterons enfin des problèmes d'adsorption et des réactions chimiques couplées.

Le troisième chapitre est un résumé des systèmes d'observation et des capteurs *in situ* autonomes déployés pour les mesures du phosphate et de l'oxygène dissous dans l'océan. Ce chapitre inclut une description des différentes méthodes d'analyse utilisées pour la détection de phosphates et d'oxygène dans des condtions de laboratoire, avec une attention particulière aux techniques électroanalytiques. Le problème crucial de corrosion et des biosalissures sera mentionné.

Le chapitre IV est une présentation du travail effectué pendant le stage à l'Université d'Aarhus. Ce travail a été axé sur l'amélioration du capteur STOX pour la détection d'oxygène à faible concentration. Cette amélioration a été effectuée par un changement dans la construction du capteur. Au lieu d'électrodéposer de l'or sur du platine, un dépôt d'or a été réalisé sur une membrane silicium afin de créer la cathode d'or. La comparaison entre le capteur STOX traditionnel et la version améliorée est discutée en fin de chapitre.

Le chapitre V présente un travail supplémentaire effectué sur l'électrochimie des complexes isopoly- et hétéropolyoxomolibdiques formés via l'oxydation du molybdène métal dans l'eau de mer. Ce travail a révélé la structure chimique des différents complexes silico- et phosphomolibdiques et a illustré la complexité des réactions électrochimiques et par conséquent la difficulté d'interprétation des signaux pour la détection des phosphates.

Le chapitre VI présente le travail effectué sur le développement du capteur de phosphate. Le procédé développé est basé sur l'oxydation d'une électrode de molybdène dans l'eau de mer pour former le complexe phosphomolibdique qui est ensuite détecté par ampérométrie ou voltammétrie. La réalisation d'une cellule électrochimique utilisant des membranes a permis de détecter les phosphates en présence de silicates sans addition de réactifs liquides.

Le dernier chapitre est une description du travail effectué sur l'analyse préliminaire des masses d'eaux péruviennes en utilisant les données obtenues au cours de la campagne océanographique au large du Pérou. Les données de CTD (Conductivité, Température, Profondeur) sont compilées avec les profils de concentration en phosphate obtenus par mesures électrochimiques (tel que décrits dans le chapitre VI).

CHAPTER I:

INTRODUCTION ON OCEAN BIOGEOCHEMISTRY AND ON OXYGEN MINIMUM ZONES

The goals of this work were to develop an electrochemical sensor for phosphate detection in seawater and to improve an existing sensor for detection of ultra-low oxygen concentrations. A good understanding on ocean biogeochemical cycles in general and on the deoxygenation process is crucial for marine sensors development since it will help in finding solutions which respond to the needs of marine biogeochemists.

The basics of the ocean carbon cycle are firstly described. Both physical and biological pumps are discussed with a special attention to the factors controlling the biological CO_2 uptake. Then the cycle of phosphate and its influence on the biological carbon pump are discussed. The purpose of this part is to explain the importance of phosphate measurements in the general context of this project.

In the second section the deoxygenation issue associated to the Oxygen Minimum Zones is discussed and its impact on biogeochemical cycles and greenhouses emissions is mentioned. The biotic response to the Oxygen Minimum Zones is briefly presented. The purpose of this part is to explain the critical importance of oxygen ultra-low detection in the Oxygen Minimum Zones.

Contents:

1. Introduction on ocean biogeochemistry

Many closely related geological, physical, chemical, biological and biogeochemical processes take place in the ocean on a variety of spatio-temporal scales. The study of biogeochemical cycles of chemical elements (C, N, Si, P, Fe,...) requires taking into account the origins (sources), sinks and changes within each of the reservoirs (ocean, continent, atmosphere ...) of each element constituting them.

The carbon cycle in the global ocean includes the CO_2 exchange at the ocean-atmosphere interface, the general oceanic circulation, the riverine and eolian inputs of nutrients and inputs of nutrients by submarine volcanism. CO_2 is one of the major greenhouse gases with nitrous oxide and methane. The study of the carbon cycle is essential for understanding and predicting evolution of the climate. During photosynthesis, algae use energy from sunlight to convert CO_2 and dissolved nutrients (nitrate, phosphate, silicate…) to organic carbon. Monitoring levels of nutrients over time, as key elements of the marine food chain but also as tracers of water masses, is therefore a critical factor to ulimately monitor climate change.

1. 1. The role of the ocean in the global carbon cycle

The carbon cycle is the exchange of carbon among three reservoirs or storage places: land, oceans and the atmosphere (Figure I. 1.1). The atmosphere is the smallest pool of actively cycling carbon, that is, carbon which stays in a reservoir less than a thousand years or so. The land and its plants and animals, which are called the terrestrial biosphere, constitute the next largest reservoir of carbon and the oceans are the earth's largest carbon active reservoir by far (Denman et al., 2007).

The processes by which carbon moves through the earth's reservoirs take place on different time scales. The short-term carbon cycle includes processes that transfer carbon from one reservoir to another in a matter of years, including photosynthesis, plant and animal respiration, and the movement of CO_2 across the air-sea interface. Other processes, such as transformation of carbon into limestone and its subsequent release as the rock weathered, occur very slowly (thousands to millions of years). We call these processes the long-term carbon cycle.

Recent interest in the global carbon cycle corresponds to increasing levels of carbon containing gases like carbon dioxide (CO_2), methane (CH_4), carbon monoxide (CO), and chlorofluorocarbons (CFCs). These gases are all radiatively active, that is, they trap the heat near the surface of the earth causing elevation of the average temperature. So, they are considered greenhouse gases (Millero, 2007).
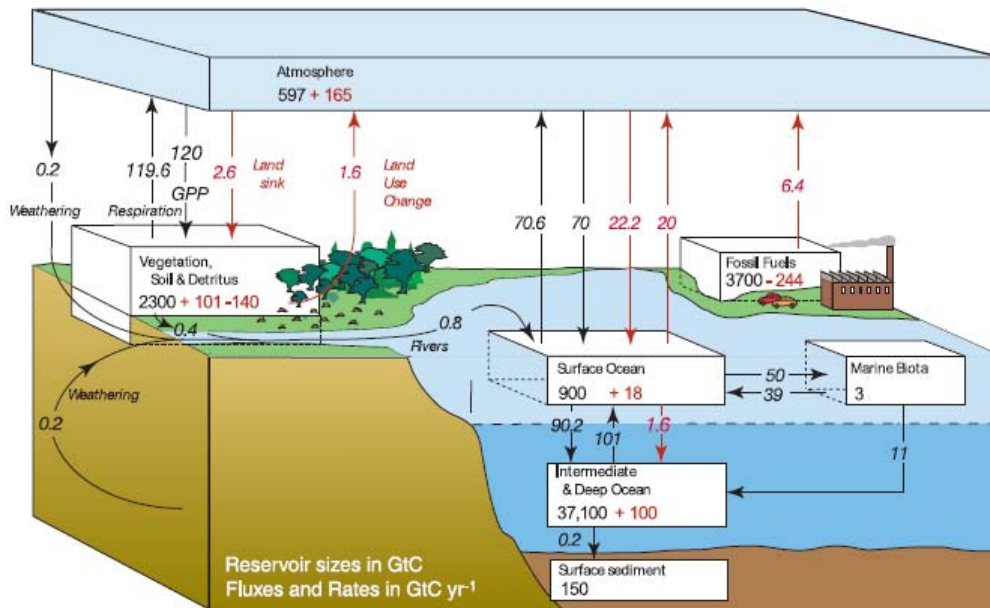
Fig. I. 1.1. The global carbon cycle taken from the 4th IPCC Assessment Report, 2007. In the figure the carbon fluxes are shown in Gt C/yr with natural fluxes depicted by black arrows and the anthropogenic fluxes by red arrows (Denman et al., 2007).

The most important greenhouse gas is carbon dioxide (CO_2). The amount of this gas is increasing due to human activity. The pre-industrial level of this gas was 280 ppmV and has increased to the current levels of 370 ppmV (Figure I. 1.2). The levels of CO_2 in the past varied between 200 ppmV (glacial times) and 300 ppmV (interglacial times). More recent ice core measurements indicate that these levels have been similar for 600 ky (ky=1000 years) (Figure I. 1.3). These results indicate that the present level of CO_2 in the atmosphere is 23% higher than 280 ppmV in the past 600 ky (Siegenthaler et al., 2005). Thanks to its ability to buffer CO_2, the oceans play a crucial role in regulation of the atmospheric level of this gas and thus, have a great impact on greenhouse effect and climate. This has led to an increasing

interest in understanding the cycling of CO_2 between the atmosphere and the oceans. The influence of increasing CO_2 levels on climate will be discussed later.
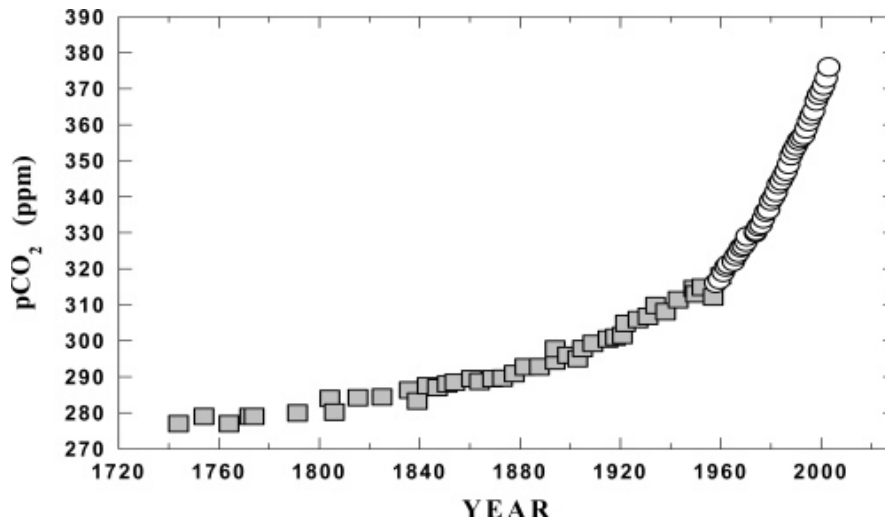
Fig. I. 1.2. The increase of carbon dioxide in the atmosphere at Hawaii from atmospheric sources and trapped in ice cores (Millero, 2007).
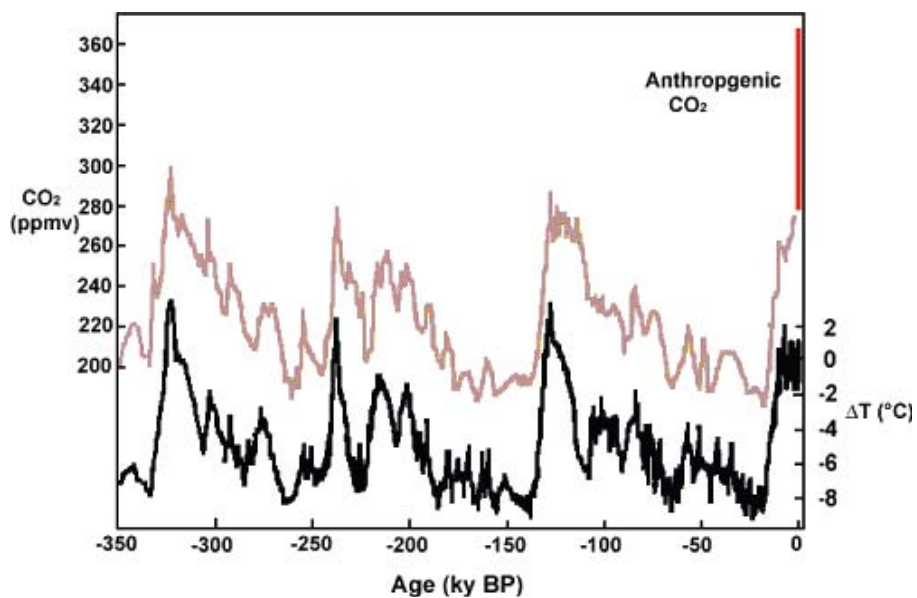
Fig. I. 1.3. The variations of carbon dioxide and temperature as recorded in the Vostok ice core during the last climate cycle (Millero, 2007).

Our present understanding of the temporal and spatial distribution of the net CO_2 flux into and out of the ocean is derived from a combination of field data, which is limited by sparse temporal and spatial coverage, and models, which are validated by comparisons with the observed distributions of tracers, like natural carbon-14 (^{14}C), and anthropogenic chlorofluorocarbons, tritium (^3H) and bomb ^{14}C. With the additional data from global surveys of CO_2 in the ocean (1991-1998), carried out during the Joint Global Ocean Flux Study (JGOFS), the World Ocean Circulation Experiment (WOCE) Hydrographic Program, and during IMBER (Integrated Marine Biogeochemistry and Ecosystem Research) and SOLAS (Surface Ocean Lower Atmosphere Study) international cruises, it is now possible to characterize in a quantitative way the regional uptake and release of CO_2 and its transport in the ocean.

1.1.1. The physical and biological carbon pumps

The ocean plays an important part in both the organic and inorganic components of the carbon cycle. The ocean contains about fifty times more carbon than the atmosphere, but only 1 % of this carbon is in the form of CO_2, most of the carbon is found as bicarbonate (HCO_3^-) or carbonate (CO_3^{2-}). CO_2 dissolves in the ocean and reacts with water to form carbonic acid, which rapidly dissociates into bicarbonate and carbonate ions according to the following equilibrium reactions (I. 1.1-1.3):

$$CO_2(g) \Leftrightarrow CO_2(aq) \tag{I. 1.1}$$

$$CO_2(aq) + H_2O \Leftrightarrow H^+ + HCO_3^- \tag{I. 1.2}$$

$$HCO_3^- \Leftrightarrow H^+ + CO_3^{2-} \tag{I. 1.3}$$

The sum of CO_2, HCO_3^- and CO_3^{2-} is called Dissolved Inorganic Carbon (DIC); 91 % of DIC is in the form of HCO_3^-, 8% in CO_3^{2-} and only 1% in CO_2 (Sarmiento and Gruber, 2001). Only CO_2 is exchanged with the atmosphere due to physical and biological processes known as physical and biological pumps presented in Figure I. 1.4.

The physical pump is driven by gas exchange at the air-sea interface and the physical processes that transport CO_2 to the deep ocean. Atmospheric CO_2 enters the ocean by gas exchange depending on wind speed and the difference in partial pressure across the air-sea

interface. The amount of CO_2 absorbed by seawater is also a function of temperature through its effect on solubility: solubility increases as temperature falls so that cold surface waters absorb more CO_2 than warm waters. Generally speaking, cold and dense water masses in high latitude oceans, particularly of the North Atlantic and Southern Oceans, absorb atmospheric CO_2 before they sink to the ocean interior. The sinking is balanced by an upwelling in other regions. Upwelled water warms when it reaches the surface where CO_2 becomes less soluble and some is released back to the atmosphere. The net effect is to pump CO_2 into the ocean interior (Maier-Reimer et al., 1996; Sarmiento and Gruber, 2002).
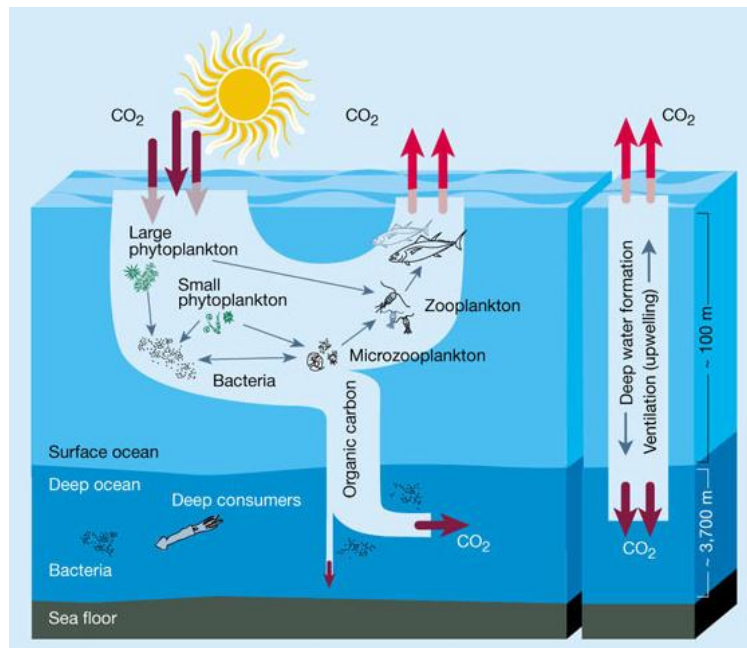
Fig. I. 1.4. The schematics of the biological and physical pumps (Chisholm, 2000).

Once CO_2 is pumped to the ocean due to physical processes, the DIC is absorbed by phytoplankton during photosynthesis. Using sunlight for energy and dissolved inorganic nutrients, phytoplankton convert DIC to organic carbon, which forms the base of the marine food web. When phytoplankton die or are eaten by zooplankton and higher trophic organisms, the part of the organic carbon from dead tissues can remain in the water as Dissolved Organic Carbon (DOC). The DOC can be transported by currents to deeper waters. Finally, another fraction of the organic carbon is transformed into aggregates called Particulate Organic Carbon (POC), which sink to greater depths. The carbon entrained in POC is remineralized by bacteria at depth and stored in the intermediate deep waters rich in carbon and transported back to the surface by ocean currents and vertical mixing (Chisholm, 2000). The food web's

structure and the relative abundance of species influence how much CO_2 will be pumped to the deep ocean. This structure is dictated also by the availability of inorganic nutrients such as nitrogen, phosphorus, silicon and iron. The influence of dissolved nutrients will be discussed in detail later.

Some marine organisms grow their shells out of calcium carbonate ($CaCO_3$), changing the surface water carbon chemistry. Shells sink in the deep water and the concentration of CO_3^{2-} at the ocean surface decreases moving the equilibrium of reaction I. 1.4 towards the right.

$$CO_3^{2-} + Ca^{2+} \Leftrightarrow CaCO_3(s) \tag{I. 1.4}$$
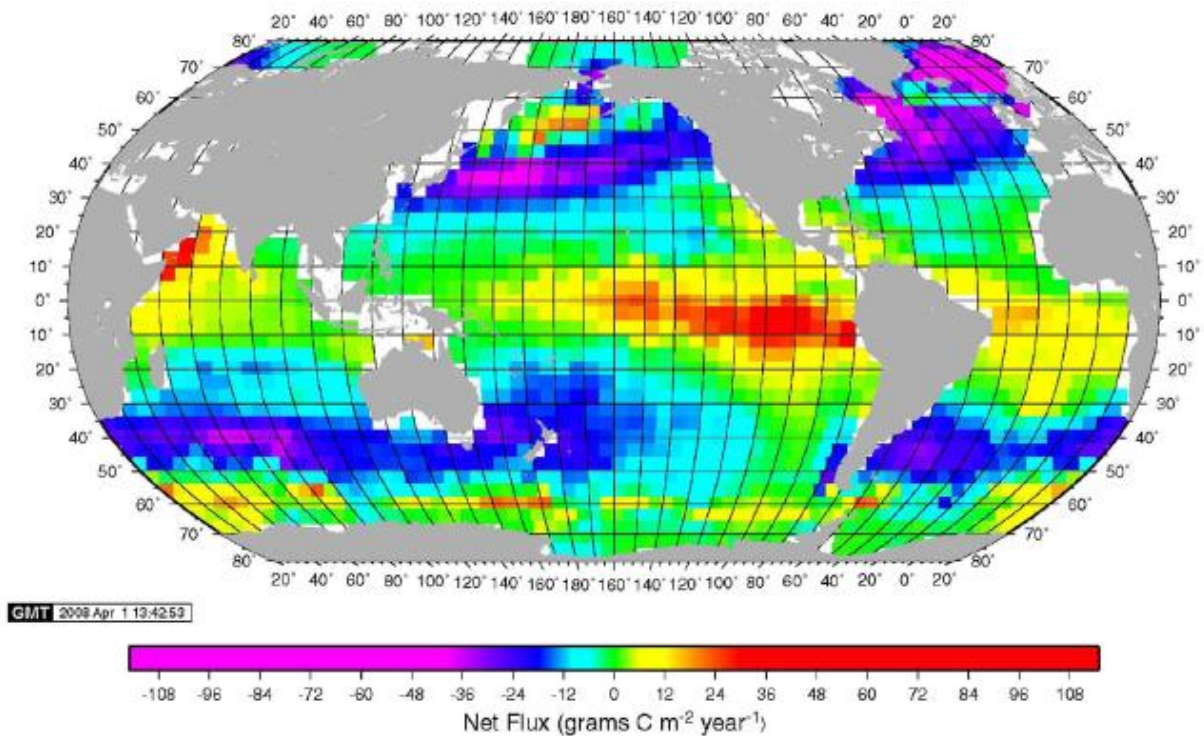
Fig. I. 1.5. Annual exchange of CO_2 across the sea surface (Takahashi et al., 2009).

Together with the solubility pump, the biological pump maintains a sharp gradient of CO_2 between the atmosphere and the deep ocean. The annual CO_2 exchange is presented in Fig. I. 1.5. The blue and purple colours denote regions in which the ocean takes up large amounts of CO_2, red and yellow colours mark regions in which large amounts of CO_2 are emitted into the atmosphere. The map shows that the Equatorial Pacific is the largest source of CO_2. This is due to the combination of strong upwelling of CO_2-rich waters and low

26

biological activity. The North Atlantic, on the other hand, is the most intense region of CO_2 uptake in the global ocean. As the Gulf Stream and the North Atlantic Drift transport water northwards, it cools and absorbs CO_2 from the atmosphere (Takahashi et al., 2009).

1.1.2. Human impact on ocean CO_2 uptake

More than seven billion people burn fuel to keep warm, to provide electricity to light their homes, to run industry, and to use cars, buses, boats, trains, and airplanes. The burning of fuels adds about 6 gigatons of carbon to the atmosphere each year (Balino et al., 2001; Denman et al., 2007). The CO_2 emitted into the atmosphere by human activities is taken up by the ocean at a rate which depends primarily on the rate of increasing atmospheric CO_2 as compared with the rate of the ocean mixing. Nowadays, the ocean takes up about 2.2 PgC/yr (Denman et al., 2007, Gruber et al., 2009). However in the past 20 years models and observations suggest that the rate of growth of this sink may have slowed down (Canadell et al., 2007). Measurements show that the oceans have absorbed 29 % of the total CO_2 emitted since pre-industrial times (Sabine et al., 2004, Lee et al., 2003), but at present the ocean uptake is only 15% of the potential uptake level for an atmospheric concentration of 385 ppmV (Greenblatt and Sarmiento, 2004). Potential variations in the oceans' sink efficiency due to climate change are extremely important because of the size of this sink. Several examples of influence of carbon dioxide increase on climate are discussed below.

The increase in the concentration of CO_2 in the atmosphere will increase its flux across the air-sea interface. This will result in a decrease in the pH of about 0.3-0.4 units if atmospheric CO_2 concentrations reach 800 ppmv (Doney et al., 2009). The decrease in the pH is expected to cause large changes in the carbonate system in the ocean. For example, organisms like pteropods, foraminifera, and cocolithophores will have difficulty with precipitating $CaCO_3$; coastal corals may have difficulty in growing and may dissolve (Beaufort et al., 2011). The constantly increasing carbon dioxide concentration in the atmosphere is causing the global increase of temperature. The carbon dioxide dissolves better in cold waters, thus increasing the temperature will cause the oceans to absorb less carbon dioxide than now, and this will result in strengthening the greenhouse gases effect. Moreover, higher temperatures will cause ice melting and greater inflows of freshwater into the oceans. In addition, higher temperatures, in accordance with the laws of physics, will lead to increased water volume. As an effect, this will lead to sea level rise and thus to intense flooding

(Millero, 2007). These are only a few examples of the effects of global warming. To understand, stop or mitigate these changes, we need to know first how the ocean machinery is functioning.

1.1.3. Oceanic circulation and global warming

The main forces driving oceanic circulation are the difference in density of different water masses and the winds. The density of seawater is controlled by its salinity and temperature. The salinity of the surface water is controlled mostly by the balance between evaporation and precipitation. As a result the highest salinities are found at low latitudes where evaporation is high and precipitation low. The temperature of the oceans depends mostly on the heat exchange with the atmosphere. In general the heat is transferred for low latitudes to high latitudes via the winds in the atmosphere and by the currents in the ocean (Wunsch, 2002; Colling, 2004). The thermohaline circulation known as the oceanic conveyor belt is a key regulator for climate (Figure I. 1.6). This circulation emphasises the interconnections among the waters of the world ocean.
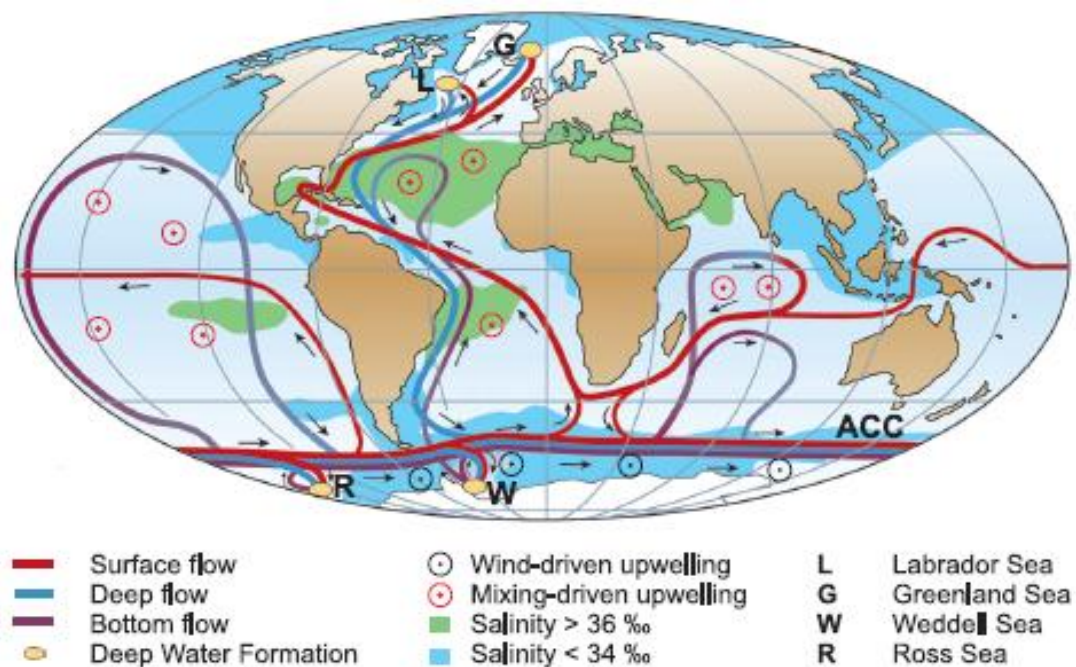
*Fig. I. 1.6. The thermohaline circulation of the oceans. Surface currents are shown in red, deep waters in light blue and bottom waters in dark blue. The main deep water formation sites are shown in orange (*Rahmstorf, *2006).*

Salty and warm surface waters reaching the high latitudes of the North Atlantic with the Gulf Stream are cooled in winter and sink to great depths and release heat. This heat helps to mitigate the climate in northern Europe. Deep waters being formed that way start their journey southwards where they join newly formed cold deep waters in Antarctica. Some then flow outward at the bottom of the ocean in the Atlantic, Indian and Pacific basins. These waters return to the North Atlantic as a surface flow, primarily through upwelling in the Pacific and Indian Oceans. The deep waters become enriched with essential nutrients and CO_2 as they circulate, from organic matter decomposition in the water and sediments. A complete cycle of the conveyor belt takes about 1000 years.

There are evidences that the thermohaline circulation has changed regularly in the past (Rahmstorf, 2003, Toggweiler and Russell, 2008). The variation of climate due to changes in the circulation has been large, abrupt and global (Denton and Hendy, 1994; Clement and Peterson, 2008). One of the consequences of global warming will be an increase of sea surface temperature and the alteration of the hydrological cycle, both factors will make the formation of the salty deep water, which is the main driver of the ocean circulation, more difficult. Models used by the IPCC AR4 (Intergovernmental Panel on Climate Change, 4th Assessment Report: Climate Change 2007) show a reduction in the circulation by 15% to 50% in 2100 (Meehl et al., 2007).

1.2. The components of the biological carbon pump

If we wish to understand all the factors controlling the biological carbon pump in the ocean, both now and in the future as the ocean responds to global warming, then we must survey the oceanic biogeochemical cycles of phosphates, nitrate, iron and silicate. Generally, the access to carbon dioxide and sunlight is sufficient to start the photosynthesis process, but nutrients and iron concentrations are not similar in every region of the ocean and they play a main role in the biological carbon pump.

1.2.1. Phytoplankton and primary production

Phytoplankton are comprised of microscopic plants that live in the euphotic layer of the oceans. Most of them are simply drifting with the currents, but some may also move

independently. They use sunlight, micro- and macronutrients, carbon dioxide (CO_2) in sea water in a process called photosynthesis to produce organic matter, which they use as a building material for their own cells. In addition, during the photosynthesis process, phytoplankton release oxygen as a by-product (equation I. 1.5). Phytoplankton remove almost as much carbon dioxide from the atmosphere as terrestrial plants, and thus defines the Earth's climate.

$$6 H_2O + 6CO_2 + hv \text{ (energy)} \rightarrow C_6H_{12}O_6 + 6 O_2 \qquad\qquad (I. 1.5)$$
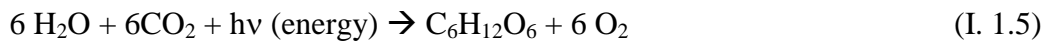
Both the amount and the rate at which phytoplankton are produced are important to consider with respect to the availability of organic carbon in the food chain. The standing crop is the amount of living phytoplankton at a given time and a given amount of seawater (mg C m^{-3} of seawater) or at given surface of seawater (mg C m^{-2}). The rate of *primary production (*P) is defined as the weight of inorganic carbon fixed photosynthetically per unit time per unit volume (mg C m^{-3} h^{-1}) or under unit surface area (mg C m^{-2} day^{-1}) (Millero, 2006). The *new production* is the *primary production* associated with newly available nitrogen (NO_2^-, NO_3^-, and NH_3). The *new production* plus the *regenerated production* (the *primary production* associated with recycled nitrogen) are equal to the total *primary production*. These definitions are based on a system being in steady state. The ratio of the *new production* to the total production is called the "f" ratio. This ratio is useful in describing the fraction of organic nitrogen and carbon exported from the surface waters to the deep ocean. It also represents the capacity of the system to sustain secondary and high levels of production.

A number of factors can affect the growth of phytoplankton in the ocean. One of the most important is light and thus, the sun's altitude, cloud cover, and then reflection, absorption and scattering of light in water have a great influence on phytoplankton growth. The other important factor is salinity. Marine phytoplankton will grow at salinities as low as 15, some more successfully than at 35. Stenhaline organisms will only thrive in a limited range of salinity, for example Peridinium bacterium at salinity of 8-12 (Baltic Sea). Euryhaline organisms can live over a wide range of salinities. The temperature range in the ocean is -2° to 30°C. Phytoplankton are rapidly killed at temperatures 10° to 15°C above the temperature at which they are adapted to live. A slow decrease of the temperature has less of an effect (Millero, 2006).

Additionally, phytoplankton need nitrogen, phosphorus, iron and silicon for growth. This problem will be discussed later. Some organics are necessary as well: vitamin B_{12} and B_1

are growth promoters, ascorbic acid and cysteine may also be needed. The limitation in vitamin B_{12} inhibits the rates of photosynthesis by stopping cell division, causing a loss of pigmentation and cell size (Millero, 2006).

Regional differences make it a challenge to measure *primary production* of the ocean basins. Traditional techniques, based on discrete bottle samples, cannot give an accurate global picture. Recent advances in remote-sensing technologies have vastly improved estimates of primary production based on phytoplankton pigment levels. For instance, the Sea-viewing Wide Field-of-view Sensor (SeaWiFS), a satellite, mounted ocean colour instrument, measures chlorophyll (algal pigment) in every part of the global ocean. With these data now, it is possible to derive global seasonal to annual estimates of primary production (Fig. I. 1.7).
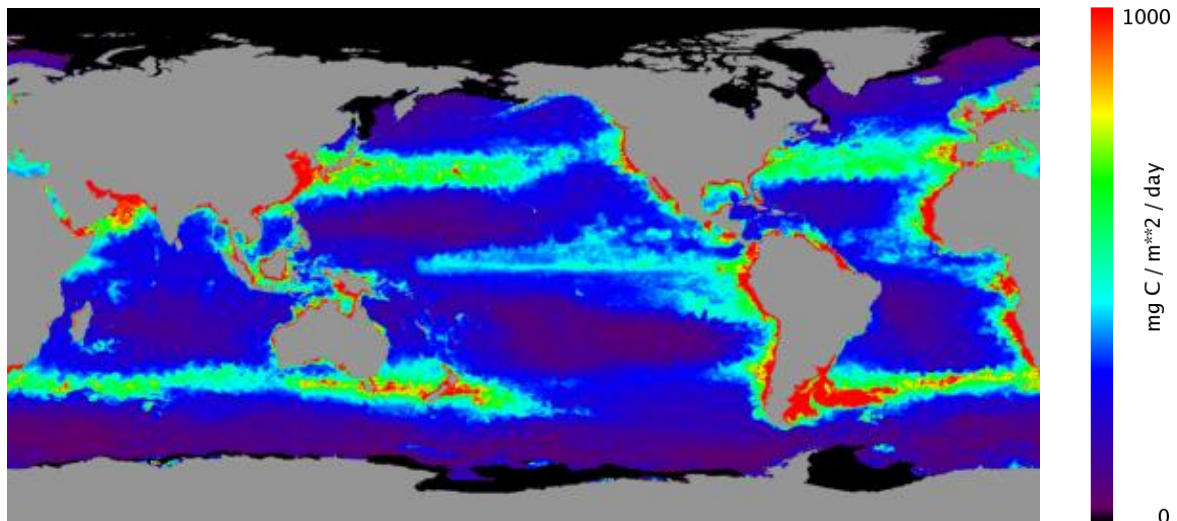
Fig. I. 1.7. Global ocean primary production estimated from chlorophyll a distribution derived from SeaWiFS data (www.science.oregonstate.edu/ocean.productivity).

The estimation shows very low primary production in the subtropical gyre regions of Pacific, Atlantic and Indian Ocean. These regions are called oligotrophic regions and are characterized by low nutrient concentrations. Eastern boundary regions (offshore Africa and Peru-Chile, for instance) are very productive due to upwelling phenomena which bring water masses rich in nutrients to the surface. Finally, there are the HNLC (High Nutrient Low Chlorophyll) zones characterized by high nutrient concentrations but low primary production due to limitation in iron and/or high rate of consumption of phytoplankton by zooplankton.

The HNLC regions are located in the Southern Ocean, in the equatorial band and in the subarctic Pacific Ocean.

1.2.2. Role of nutrients and iron in the biological pump

Phytoplankton need macronutrients, mainly nitrogen and phosphorus. Phytoplankton need nutrients in certain proportions according to the following reaction (Paytan and McLaughlin, 2007):

106 CO_2 + 16 HNO_3+ H_3PO_4 + 122 H_2O + photons $\rightarrow$ $(CH_2O)_{106}(NH_3)_{16}(H_3PO_4)$ + 138 O_2

(I. 1.6)
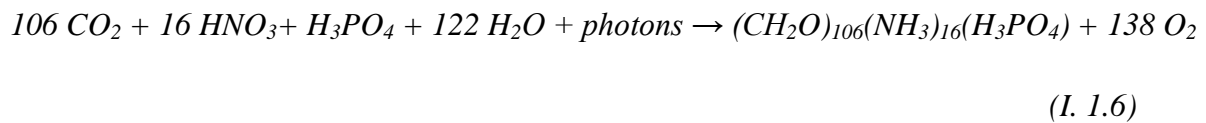
For every 106 carbon atoms, which are processed in organic matter, it is necessary to use 16 nitrogen atoms and one phosphorus atom. These proportions are known as Redfield ratios (Redfield, 1958). Atmospheric nitrogen (N_2) is usually not directly absorbed by phytoplankton, although it can be by nitrogen fixers. Nitrate (NO_3^-) and ammonia (NH_4^+) are the chemical substances being mostly uptaken by phytoplankton. In most areas of the ocean, nitrogen is lacking and we can say that the growth of phytoplankton is dependent on the availability of nitrogen. However, for example, in some oceanic areas, for instance in the eastern Mediterranean, it is the availability of phosphorus which determines the growth of phytoplankton. Natural sources of these nutrients are weathering of rocks (Paytan and McLaughlin, 2007) but also eolian and riverine inputs. Human activity also constitutes a source of nutrients. The main anthropogenic sources of phosphorus are detergents and sewage. The occurrence of nitrogen in waters is mainly due to intensive agricultural activities (Brandes et al., 2007) and coming from the excessive use of fertilizers containing nitrates and ammonia.

Another important nutrient is silicate, which is derived mainly from the weathering of rocks. The ratio of silicate over carbon varies from 0.06 and 0.45. Lack of silicate prevents the growth of certain species of phytoplankton, diatoms, which use this nutrient to build their skeletons. When running low on nitrogen or phosphorus, phytoplankton cease to grow. When running out of silicon, phytoplankton may continue growing, but a change in species composition may occur.

Phytoplankton also need a small amount of metal particles such as iron, copper, zinc and cobalt. The HNLC regions mentioned above do not have enough iron for phytoplankton to develop. These regions account for about 20% of the total area of the oceans. From the oceanographic point of view, these regions should be biologically active because they are located in upwelling regions. However, these regions are distant from the desert areas and very limited amounts of dust (and iron) reach the surface ocean (Sunda et al., 2010).

The so called iron limitation hypothesis has been tested by carring out *in situ* iron fertilization experiments for instance in the Southern Ocean (SOIREE, Jan '99), similar to those carried out earlier in the eastern Pacific (IronEx I, 1993, and IronEx II, 1995). The experiments showed enhanced phytoplankton growth and uptake of atmospheric CO_2, but at the same time a shift in the planktonic community was noticed (Balino et al., 2001; de Baar et al., 2005).

1.3. The phosphate in the ocean

As mentioned before, phosphate availability can impact primary production rates in the ocean as well as species distribution and ecosystem structure. Thus, the availability of phosphates in marine systems can strongly influence the marine carbon cycle and the sequestration of atmospheric carbon dioxide.

1.3.1. Chemistry of phosphate

From a chemical point of view, phosphates are the salts of phosphoric acid. In dilute aqueous solution, phosphate exists in four forms. In strongly-basic conditions, the orthophosphate ion (PO_4^{3-}) predominates, whereas in weakly-basic conditions, the hydrogen phosphate ion (HPO_4^{2-}) is prevalent. In weakly-acid conditions, the dihydrogen phosphate ion ($H_2PO_4^-$) is the most common. In strongly-acid conditions, aqueous phosphoric acid (H_3PO_4) is the main form. More precisely, considering the following three equilibrium reactions:

$$H_2PO_4 \Leftrightarrow H^+ + H_2PO_4^- \tag{I. 1.7}$$

$$H_2PO_4^- \Leftrightarrow H^+ + HPO_4^{2-} \tag{I. 1.8}$$

$$HPO_4^{2-} \Leftrightarrow H^+ + PO_4^{3-} \tag{I. 1.9}$$

the corresponding constants at 25°C (in mol/L) are:

$$K_{a1} = \frac{[H^+][H_2PO_4^-]}{[H_3PO_4]} \approx 7.5 \cdot 10^{-3}, pK_{a1} = 2.12 \tag{I. 1.10}$$

$$K_{a2} = \frac{[H^+][HPO_4^{2-}]}{[H_2PO_4^-]} \approx 6.2 \cdot 10^{-8}, pK_2 = 7.21 \tag{I. 1.11}$$

$$K_{a3} = \frac{[H^+][PO_4^{3-}]}{[HPO_4^{2-}]} \approx 2.14 \cdot 10^{-13}, pK_{a3} = 12.67 \tag{I. 1.12}$$

1.3.2. The cycle of phosphate in the ocean

The phosphorus content on both oceans and land is very small. The main reservoir of phosphorus on land is rocks formed in ancient geological epochs. These rocks gradually ventilate and release phosphorus compounds into marine ecosystems. Continental weathering is the primary source of phosphorus to the oceanic phosphorus cycle. Most of this phosphorus is delivered via rivers with a smaller portion delivered via dust deposition. In recent times, anthropogenic sources of phosphorus have become a large fraction of the phosphorus delivered to the marine environment, effectively doubling the pre-antrophogenic flux. The main anthropogenic sources of phosphorus are detergents and sewage. The primary sink for phosphorus in the marine environment is the loss to sediments. Much of the particulate flux from rivers is lost to sediments on the continental shelves, and a smaller portion is lost to deep-sea sediments. In surface waters, certain phosphate forms (PO_4^{3-}) are taken up by phytoplankton during photosynthesis. Subsequently, the phosphate travels up through the food chain to zooplankton, fish and other top marine organisms. Much of organic-P is converted back to PO_4^{3-} in surface waters as phytoplankton die but some of it finds its way to the deep ocean (via downwelling and sinking of organic matter) where it is remineralized back to inorganic-P. It may return to the surface waters (via upwelling) or be bound by the widely prevalent cations (Al^{3+}, Ca^{2+}, Fe^{2+}, Fe^{3+}) and stored as minerals for a long time in the rocks and sediments. In that case, only geological processes can bring them back to cycle. The processes described above are presented in Fig. I. 1.8 as the marine phosphorus cycle with a special attention to different phosphorus fluxes.

The transformations between the various phosphate (DIP, DOP, PIP, POP) forms in the water column and sediments, shown in Fig. I. 1.9, allow a better understanding of the oceanic phosphate cycle.
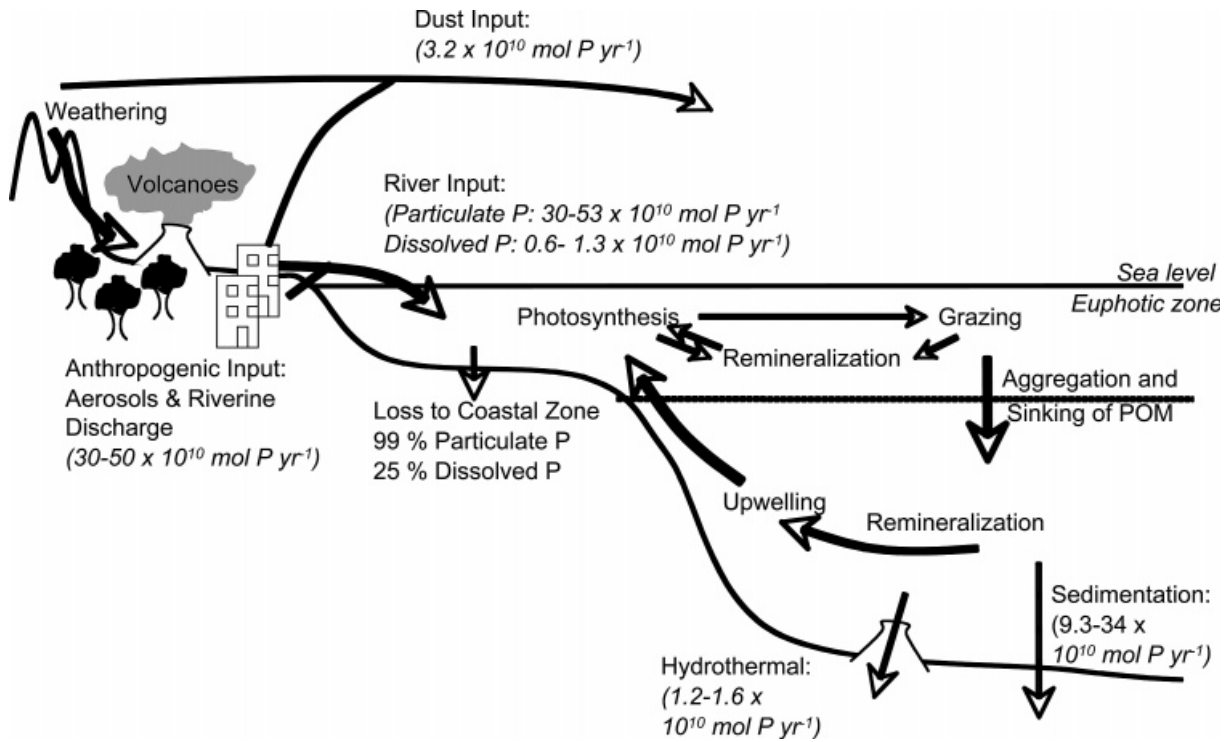
Fig. I. 1.8. The marine phosphorus cycle (Paytan and McLaughlin, 2007).
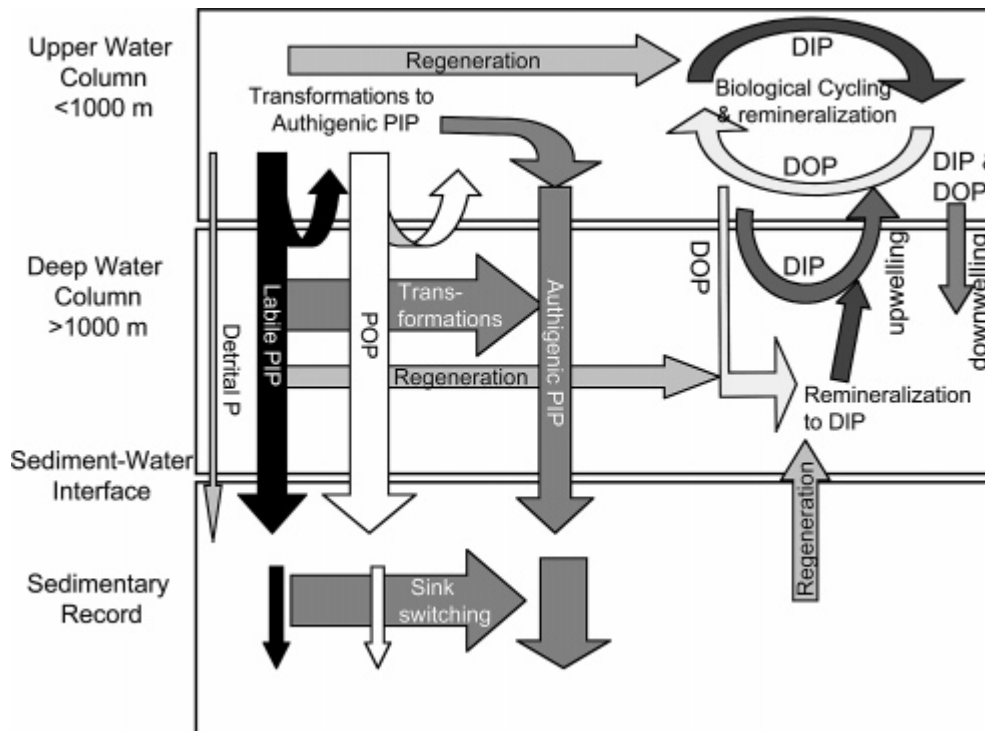
Fig. I. 1.9. Transformation between phosphorus forms in the water column and sediments. (Paytan and McLaughlin, 2007) (DIP-dissolved inorganic phosphorus, DOP-dissolved organic phosphorus, PIP-particulate inorganic phosphorus, POP-particulate organic phosphorus).

Vertical sections for phosphate concentrations in sea water are presented in Fig. I. 1.10 for the Atlantic, Pacific and Indian Oceans. As phytoplankton and other organisms die, PO_4^{3-} is regenerated in the water column. A maximum regeneration occurs near 1000 m, which is the same depth as the oxygen minimum layer. The maximum values of phosphate concentration in the Atlantic are about 2.5 μM, while in the Pacific values around 3.25 μM occur. The higher values observed in the Pacific (and Indian) oceans as compared to the Atlantic are due to the age of the water masses (older in the Pacific thus accumulating more oxidized plant material). Generally, knowledge of the phosphate concentration in the ocean surface allows us to deduce information on the biological activity in the ocean. Secondly, phosphate is one of the chemical tracers (along with temperature, salinity, other nutrients concentration…) which allows us to analyse water mass mixing and determine the origin of the water masses.
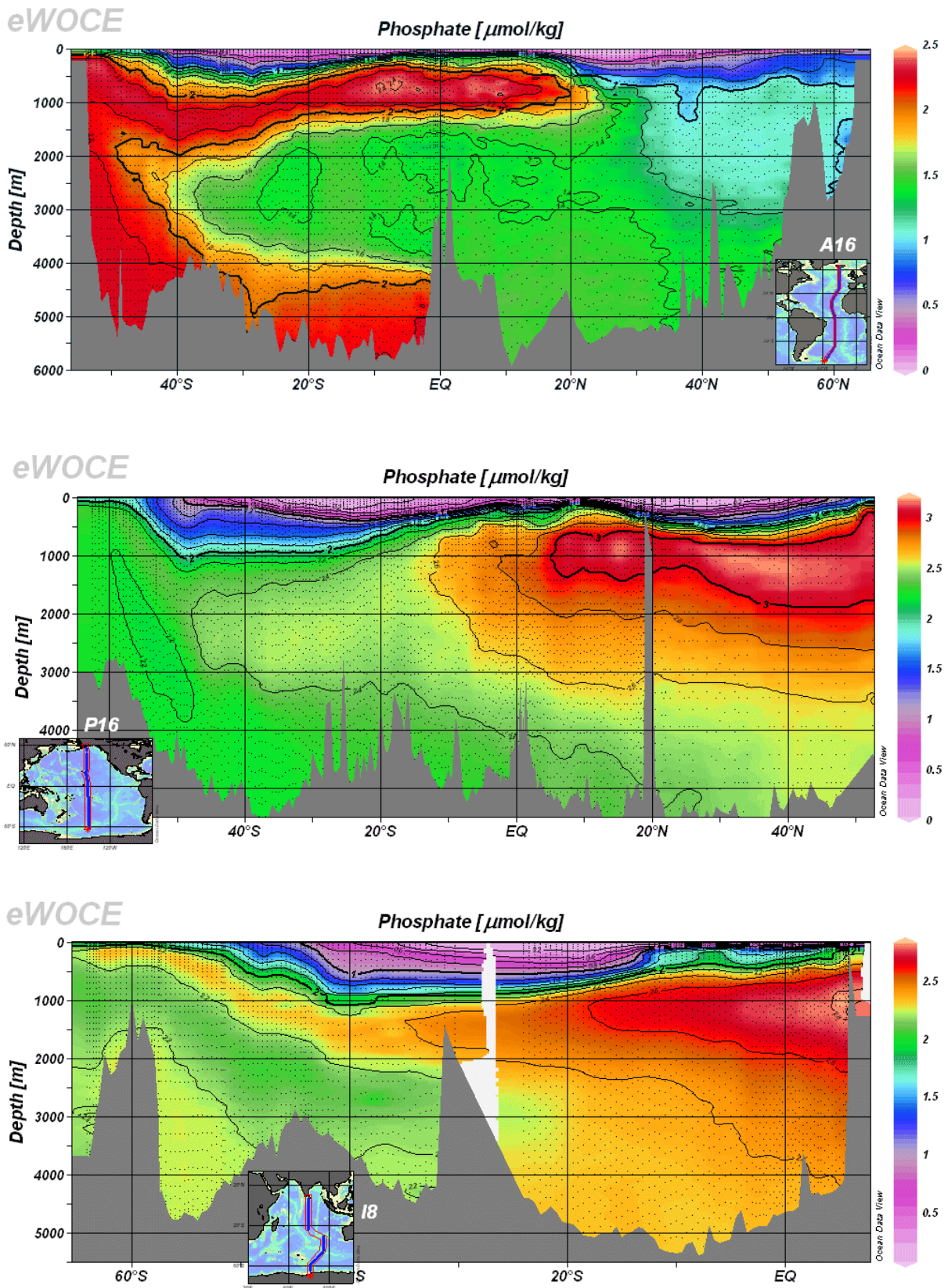
Fig.I. 1.10. Vertical section of phosphate concentrations obtained during the campaign WOCE A16, P16 and Indian Ocean 18.

2. Introduction on the Oxygen Minimum Zones (OMZs)

For various reasons, the content of the global ocean dissolved oxygen is far from uniform. In some places, hypoxia (oxygen deficiency) occurs and strongly affects the biological activity in the first few hundred meters depth. These regions are called the Oxygen Minimum Zones (OMZ) and are found in tropical regions, in the eastern Pacific and northern Indian Ocean. They are usually associated with upwelling systems and their extent increases in summer and reduces in winter. Global warming is expected to help expand the OMZ and to increase the hypoxia (Oschlies et al., 2008; Stramma et al., 2008; Keeling et al., 2010). Models indicate that the average concentration of oxygen should decrease as well (Stramma et al., 2012). These regions are still rather poorly understood despite much recent interest. A better understanding of biological, biogeochemical and physical processes in these regions will help us to answer many questions about the OMZ's formation and expansion, and its influence on ocean's life, biogeochemical cycles of phosphorus, nitrogen and carbon and emission of greenhouse gases to the atmosphere.

2.1. Oxygen in the ocean

The most studied gas (other than CO_2) is dissolved oxygen. The oxygen cycle is very complicated due to the fact that it participates in the composition of many compounds. Sources of oxygen in natural waters are the process of absorption of oxygen from the atmosphere, the formation of oxygen as a result of the photosynthesis and the entering oxygen from rain and snow water. The distribution of oxygen in the oceans is the net result of (Millero, 2006):

- Near equilibrium of atmospheric oxygen in the surface mixed layer

- Biological production in subsurface waters caused by photosynthesis

- Biological use of oxygen in respiration in all waters and oxidation of plant material in intermediate waters

- Increases in oxygen in deep waters caused by the sinking of cold water rich in oxygen.
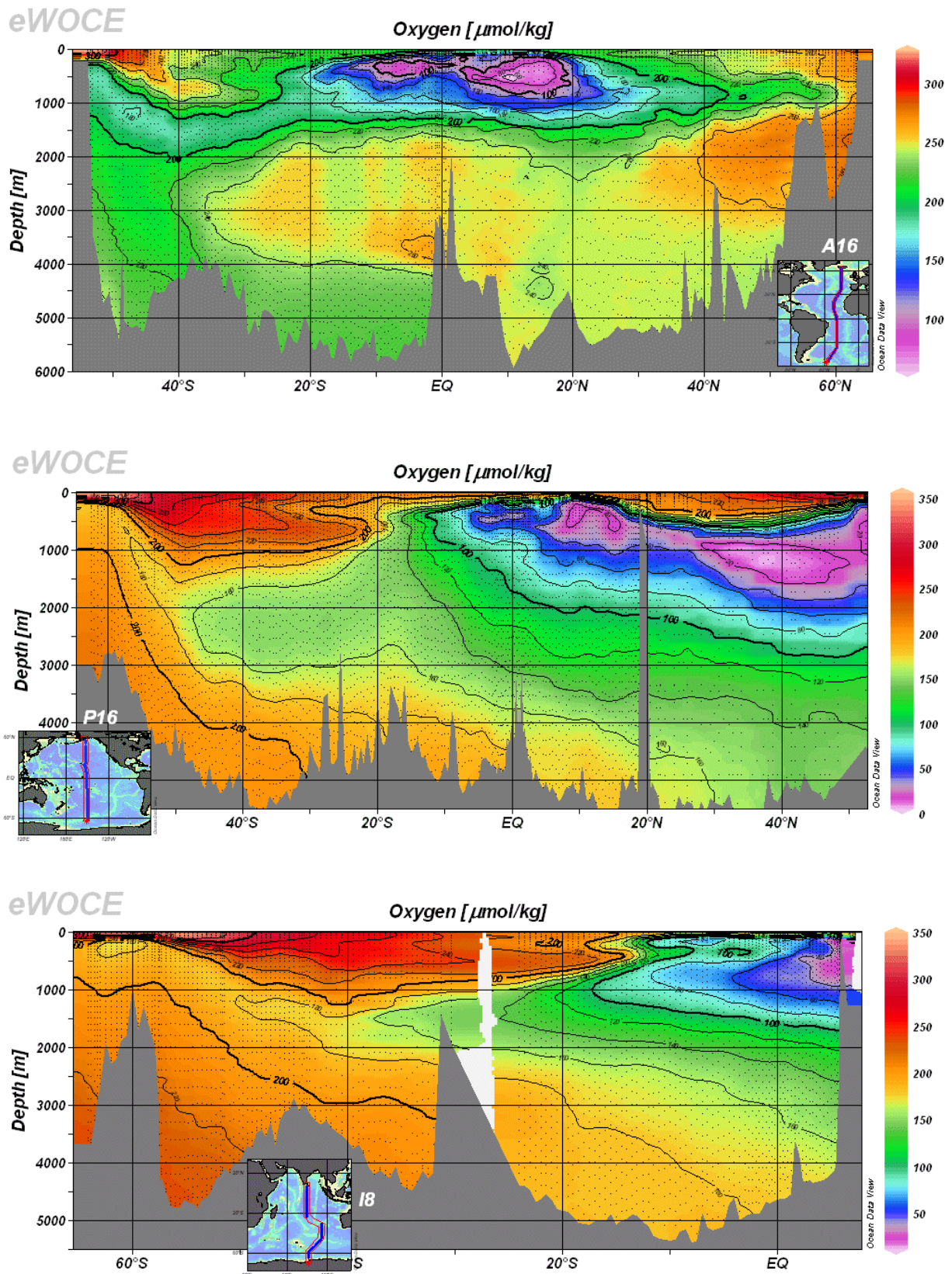
Fig.I. 2.1. Vertical section of oxygen concentrations obtained during the campaigns WOCE A16, P16 and Indian Ocean 18.

The dissolved oxygen concentrations decrease with depth in the ocean (to reach minimum values at depth of about 1000 m) due to utilization of oxygen for oxidation of organic substances and respiration of aquatic organisms. At greater depths the concentrations of oxygen increase slightly again as presented in Figure I. 2.1. Normally, the concentration of oxygen is sufficient for sustaining life of marine organisms. However, in Oxygen Minimum Zones a severe reduction or in extreme cases the complete loss of animal life may occur.

2.2. Formation, distribution and stability of the OMZ

Oxygen Minimum Zones are the regions in aquatic systems where concentrations of oxygen are as low as a few μM. Oxygen Minimum Zones constitute primarily a problem in Eastern Boundary Upwelling Systems (EBUS), some coastal waters and enclosed seas (Fig. I. 2.2), although it can also be an issue in freshwater lakes. Vertical oxygen profiles in the OMZs are different from the classical O_2 minimum profiles (Fig. I. 2.2). The oxygen minimum is 5 times shallower up to 100-200 m than in the oxygenated ocean including a marked gradient, the oxycline (Paulmier and Ruiz-Pino, 2009) and it is also 50 times more intense. The total area of permanent OMZs is 8% of the global oceanic area and these include mainly: the Eastern South Pacific, Eastern Tropical North Pacific, the Black Sea, the Arabian Sea and Bay of Bengal. Oxygen Minimum Zones result from the combination of complex ecological phenomena that arise from the convergence of several factors:

- Physical environment: In these oceanic areas, ventilation is very weak due to a sluggish circulation and in EBUS undercurrents usually advect low oxygen waters. Wind strength and direction also affect the rate of mixing. Poorly-mixed waters increase the chance that an OMZ might develop.

- Nutrient enrichment**:** An overabundance of nutrients, combined with enough light and warm, slow-moving, and poorly-mixed water, can result in algae blooms and eutrophication. This is a prerequisite for the chain of reactions leading to OMZ formation. These overabundant nutrients may come from both natural sources (upwelling) and human activities.
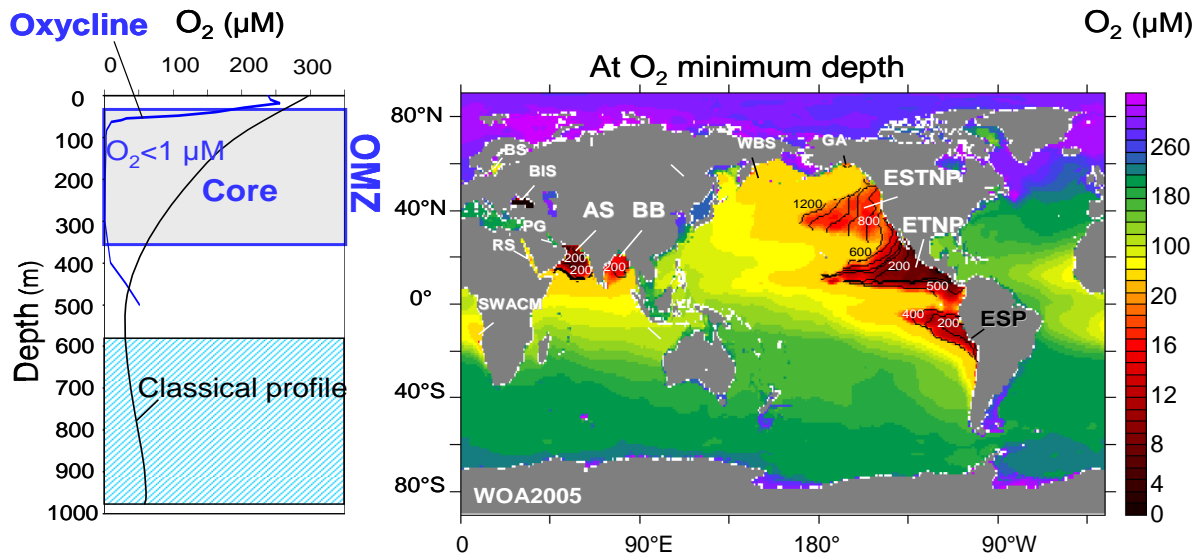
Fig. I. 2.2. The global ocean oxygen concentration at depth where it is minimal from World Ocean Atlas 2009 (right panel); The OMZs oxygen profile vs. the classical oxygen profile in the ocean (left panel) (Paulmier and Ruiz-Pino, 2009).
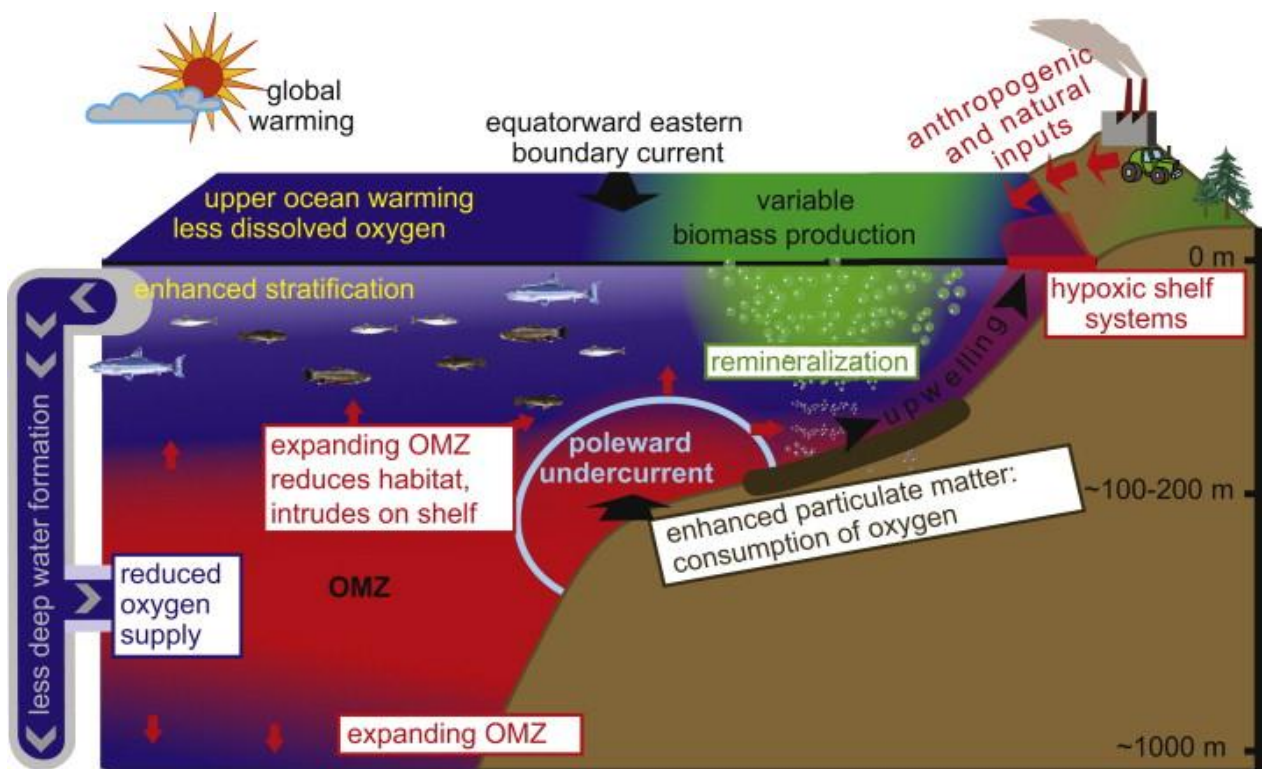
Fig. I. 2.3. Schematic of interactions of open ocean oxygen minimum zones (OMZ, red) with hypoxic shelf systems and dead zones (Diaz and Rosenberg, 2008) on continental shelves of eastern ocean boundaries.

Figure I. 2.3 presents behaviour of ecosystems associated with Oxygen Minimum Zones and explains the formation, functioning and the future predictions about the spreading of these regions. Global warming and eutrophication reduce oxygenation of the world ocean and spread the hypoxia vertically and horizontally (Stramma, et al., 2010). Thus, there is a pressing need to understand the functional consequences of oxygen depletion on biogeochemical cycles and marine biota.

2.3. The role of OMZ in the global climate change

It was reported that OMZs are the main areas of nitrogen loss (under N_2, N_2O forms) to the atmosphere (Naqvi and Noronha, 1991; Farias et al., 2007; Paulmier et al., 2008). This loss is driven mainly by denitrification and anammox (ammonium anaerobic oxidation) processes which appear in oxygen deficit waters. In this way, OMZs can affect the nitrogen (and indirectly phosphorus) and carbon ocean cycles.

2.3.1. Influence of OMZ on the biogeochemical cycles and greenhouse gases budget

OMZs have been mainly known for playing an essential role in the global nitrogen cycle. The comparison of nitrogen involved processes in oxic and anoxic waters is presented in Fig. I. 2.4 together with the oxidation states. Under oxic conditions, nitrification transforms NH_4^+ into NO_3^-. Denitrification is a bacterial process occurring in O_2-deficient regions (Paulmier and Ruiz-Pino, 2008) and is present in all OMZs. Denitrification converts NO_3^-, one of the main limiting nutrients in the ocean, into gaseous nitrogen (for example, N_2O, N_2) (Paulmier et al., 2008) which is lost to the atmosphere and contributes to the oceanic nitrate deficit (Cornejo and Farijas, 2012). Moreover, recently, an unknown process in the ocean has been observed, first in anoxic sediments and then in the water column in the OMZs: the anaerobic oxidation of NH_4^+ using NO_2^- (anammox); this imposed a complete revision of the global nitrogen cycle (Kuypers et al., 2005; Brandes et al., 2007). Denitrification and anammox both represent large sinks of inorganic fixed nitrogen in anoxic or suboxic waters close to the shelves, thereby lowering N:P stoichiometry and driving the autotrophic system ultimately into N limitation (Glessmer et al. 2011; Franz et al. 2012). Furthermore, anoxic conditions in shelf sediments and shelf bottom waters enhance the release of reactive

phosphate into the water column formerly associated to iron hydroxides, further enhancing the negative deviation from the Redfield N:P ratio of 16:1 (Ingall and Jahnke, 1994).
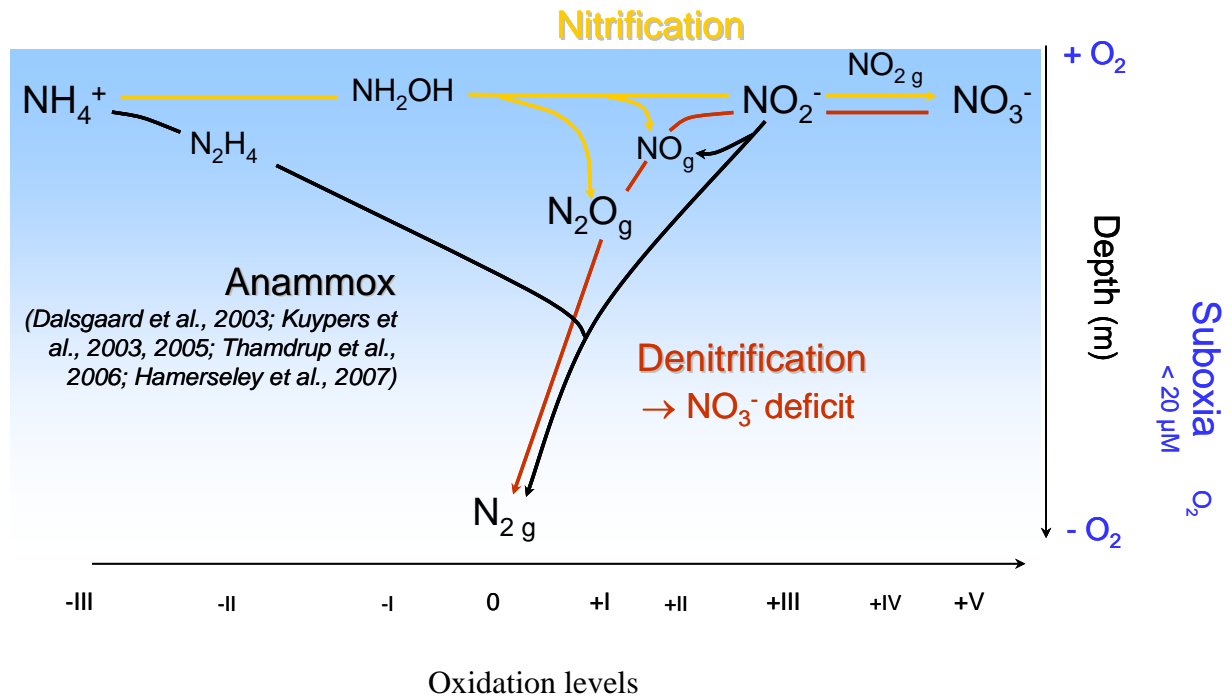
Fig. I. 2.4. Influence of OMZs on the nitrogen cycle. Comparison of nitrogen involved processes in oxic and anoxic waters (Paulmier, com. pers.).

The OMZ role on CO_2 is unknown, but we can presume a different behaviour than in oxygenated areas, contributing to a redistribution of the oceanic DIC, fixed into organic carbon by photosynthesis and then remineralized and ventilated to the atmosphere above the OMZs. Indeed, a remineralization, up to 5 times higher than in the oxygenated ocean, has been estimated for the OMZ off Chile (Paulmier et al., 2006), producing locally potential high CO_2 concentrations in the OMZs. This was already suggested for the OMZ region of the Arabian Sea (Naqvi et al., 1993).

2.3.2. Biotic response to OMZ

OMZ conditions lead to major loss in biodiversity and impact the surviving organisms through sublethal stress (Levin, 2003), such as reduced growth and reproduction,

physiological stress, forced migration, reduction of suitable habitat, increased vulnerability to predation, and disruption of life cycles (Vaquer-Sunyer and Duarte, 2008).

A drastic example of the OMZ influence on ocean life can be related to major events which occurred in North Carolina: two separate hypoxic events in the Neuse River Estuary in 1995 killed millions of fish. Additional events in 1998 and 1999 killed tens of thousands of fish. These fish kills were closely linked to hypoxia in the estuary. Another example is the Chesapeake Bay, where low oxygen levels have killed many blue crabs, one of the most popular local menu items (Chesapeake Bay Foundation, 2008). Off the coast of Cape Perpetua, Oregon, there is also a dead zone due to hypoxia with a 2006 reported size of 300 square miles (780 km²) (Chan et al., 2008). This dead zone only exists during the summer, perhaps due to wind patterns. This event causes death of starfish, mussels and rockfish.

However, some organisms demonstrated adaptation skills to hypoxia (Levin, 2003) like body size change (*Foraminifera* in the Oxygen Minimum Zones can facilitate respiration by enhancing surface area to volume ratios), migration (*Orchomene obtusus* appears to migrate into the anoxic bottom waters of Saanich Inlet, Britich Columbia to exploit abundant food and escape from predators and competitors, but will migrate upward into oxygenated waters to recover oxygen debt), or development of respiratory pigments (a fish *Sebastolobus alascanus* developed respiratory pigments with an affinity for oxygen).

3. Summary

With 50 times more carbon dioxide than in the atmosphere, the oceans contain the largest reservoir of carbon actively circulating in the biosphere. In the long term, the ocean plays a dominant role in the natural regulation of CO_2 in the atmosphere and thus exerts a powerful influence on the climate. A comprehensive and quantitative understanding of the way the ocean carbon cycle functions is fundamental to predict the consequences of rising levels of carbon dioxide and other greenhouse gases in the atmosphere.

The Ocean removes CO_2 due to both physical and biological pumps. Many factors can influence carbon dioxide uptake: temperature, salinity, availability of light and nutrients. Phosphate is one of the main components of the biological carbon pump. Moreover, by monitoring the phosphate concentration and other factors (like temperature, salinity…) we can deduce information on the biological activity and on water mass mixing. It is thus critical

to monitor properly phosphate concentration in the ocean, if we are to understand climate regulation.

This chapter has described the OMZs problem in the ocean which can result both from natural and anthropogenic processes. Oxygen Minimum Zones are locations where oxygen sensitive processes may influence both the marine nitrogen budget and the formation of climatically relevant gases (e.g. nitrous oxide, carbon dioxide), with possible consequences on climate, marine ecosystems, biological production and associated marine carbon uptake. The OMZs will probably expand in the coming decades as a consequence of global climate change. Therefore, an accurate knowledge of causes of these processes in these areas is so very interesting and crucial.

CHAPTER II:

FUNDAMENTALS OF ELECTROCHEMICAL METHODS

Electrochemical methods in this work were used for oxygen and phosphate detection by amperometry and voltammetry. Moreover, electrochemical techniques were applied to study the electrochemical properties of isopoly- and heteropolyoxomolybdates. This chapter aims to present the principles of electrochemistry and electroanalytical methods for a better understanding of results presented in Chapters IV, V and VI. Thus, this chapter is intended for non-subject specialists.

Firstly, principles of electrochemistry are described with a special attention to the electrochemical kinetics problem. After an overview of the experimental devices, the electrochemical methods are presented. Here, a particular attention is paid to the voltammetric and amperometric methods. The problem of rotating disk electrode is also discussed. The problem of absorption and chemical coupled reactions are briefly described. This approach allows the systematic study of electrochemical properties of molecules of interest and the determination of analytes.

Contents

1. Basic concepts

Electrochemistry studies chemical reactions which take place at the interface between an electronic conductor (a metal or a semiconductor) and an ionic conductor (the electrolyte), and sometimes involve electron transfer between the electrode and the electrolyte or species in electrolytic solution.

1.1. Electrolytes and the electrode-solution interface

Electrolytes are molecules dissociating in a polar solvent to ions, which act as charge-carriers and provide an ionic type of conductance in solution. Typical electrolytes are salts, acids and bases. The driving force for the dissociation is an energy gain due to solvation of the ions formed by the molecules of the solvent. The most frequently used polar solvent is water. Electrodes are the systems consisting of two kinds of conductive phases, metal and electrolyte. When a metal is introduced into an electrolyte solution, an electron exchange between the electrode and the ions in solution will take place. This leads to a potential difference over the metal-electrolyte interface, i.e. an electrical field is generated. As a consequence, the electrical field will lead to the redistribution of mobile ions and water dipole molecules in the region near the electrode. This electrode-solution interface is also known as "electric double layer" which is illustrated in Figure II. 1.1. It is a representation of electrode-solution interface derived from Helmholtz and Gouy-Chapman models which show the interface as a single capacitor and as a Boltzman distribution of ions, respectively. The electrical double layer consists of an inner layer (Inner Helmholtz Plane-IHP), an outer layer (Outer Helmholtz Plane-OHP) and the diffuse or Gouy layer. The inner layer is the area closest to the electrode where absorbed ions and solvent are found. The outer layer is the imaginary plane passing through the solvated cations. The solvated cations undergo nonspecific adsorption and are pulled towards the electrode surface by long range coulombic forces. The distance from the electrode to the IHP is equivalent to the radius of cation and the distance to the OHP is approximately two solvent molecules and the radius of the ion. These two layers are strongly held on the electrode and they remain at the surface even if the electrode is removed from the solution. The most outer plane is the diffuse or Guoy layer where ions can move due to electrostatic attractive and repulsive forces from the electrode surface. The presence of the electrode cannot be felt by ions beyond this region.
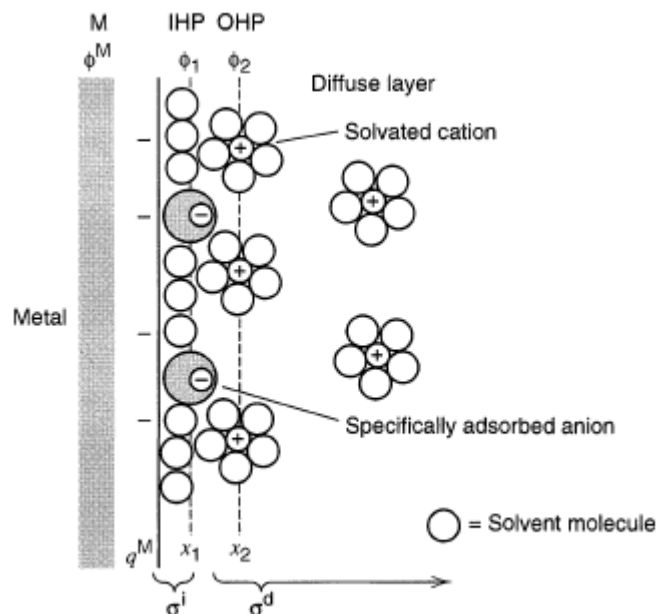
Fig. II. 1.1. Proposed model of the double-layer region (Bard and Faulkner, 2001).

1.2. The electrode reactions

Oxidation-reduction reactions (redox) involve transfer of electrons between the species of different systems:

$$Ox_1 + Red_2 \leftrightarrow Red_1 + Ox_2 \qquad\qquad (II.\ 1.1)$$

where Ox and Red are the oxidized and the reduced forms of reactants forming a redox couple. In electrochemical systems, the oxidation and reduction are spatially separated and an actual exchange of electrons occurs via the electrodes. Thus the whole reaction can be split into half-reactions:

$$Ox_1 + n_1e^- \rightarrow Red_1 \text{ (reduction on cathode)} \qquad\qquad (II.\ 1.2)$$

$$Red_2 \rightarrow Ox_2 + n_2e^- \text{ (oxidation on anode)} \qquad\qquad (II.\ 1.3)$$

The current response is deduced from the transfer of electrons during the redox process of the target analyte. The current that arises from the oxidation or reduction of the analyte species is called the Faradic current. Non Faradic currents are a result of those processes that do not

involve the transfer of electrons across the electrode-solution interface and they stern from the capacitance present at the interface. The capacitance (C) of the electrical double layer can be defined using equation (II. 1.4):

C=q/E   (II. 1.4)

Where q and E represent charge and potential, respectively.

1.3. Galvanic cell and Nernst equation

Galvanic cell (Volta cell) presented in Figure II. 1.2 is an electrochemical cell that derives electrical energy from spontaneous redox reactions taking place within the cell. It generally consists of two different metals connected by a salt bridge, or individual half-cells separated by a porous membrane.
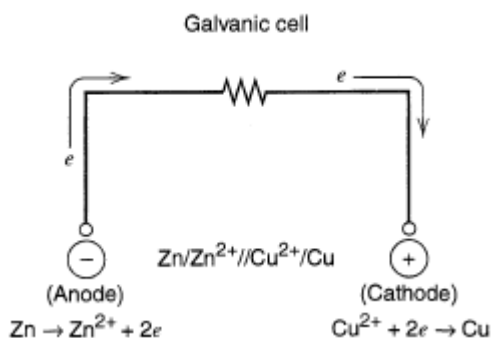
Fig. II. 1.2. Galvanic cell (Bard and Faulkner, 2001)

There is a math between the open circuit potential (E [V]) and the change in Gibbs free energy (ΔG [J]) for spontaneous reactions in the cell:

ΔG = -zEF   (II. 1.5)

Where z is the number of electrons, F-Faraday's constant (F = 96,485 C/mol).

For chemical reactions ΔG value is in the range of 0-300 kJ meaning that the open circuit potential for galvanic cells based on simple spontaneous reactions should be in the range of 0-2 V.

The galvanic cells are used in potentiometry (Compton and Sanders, 1996) and the equilibrium electrode potential (E_{eq}) can be described using the Nernst equation:

$$E_{eq} = E^\circ + \frac{RT}{nF}\ln\left(\frac{a_{ox}}{a_{red}}\right)$$ (II. 1.6)

Where E° is the standard half-cell reduction potential (the potential difference measured between the electrode and the Standard Hydrogen Electrode-SHE), R is the universal gas constant: $R = 8.314$ J K^{-1} mol^{-1}, T is the absolute temperature, F is the Faraday constant, n is the number of moles of electrons transferred in the cell reaction or half-reaction and a is the chemical activity for the relevant species, where a_{Red} is the reductant and a_{Ox} is the oxidant.

If we consider that the ionic force remains stable during the experiment and that the compounds behave ideally in the solution, we can change the chemical activities to concentrations $(C_{ox}^{sol}, C_{red}^{sol})$ in the Nernst equation:

$$E_{eq} = E^\circ + \frac{RT}{nF}\ln\left(\frac{C_{ox}^{sol}}{C_{red}^{sol}}\right)$$ (II. 1.7)

For equation involving protons Ox + mH$^+$ + ne$^-$ ↔ Red, the equilibrium potential can be described by the following equation:

$$E_{eq} = E^\circ + \frac{RT}{nF}\ln\left(\frac{a_{ox}a_{H^+}^m}{a_{red}}\right)$$ (II. 1.8)

or at 298 K: $E_{eq} = E^\circ - \frac{m}{n}0.0595\,pH + \frac{RT}{nF}\ln\left(\frac{a_{ox}}{a_{red}}\right)$ (II. 1.9)

and the standard potential of the reaction presented above can be described by:

$$E^{\circ'} = E^\circ - \frac{m}{n}0.0595\,pH$$ (II. 1.10)

The ratio $\frac{m}{n}$ is the number of protons divided by the number of electrons.

1.4. Electrolysis cell and non-equilibrium processes

If a chemical reaction is driven by an external applied current, the measured potential will be different than the equilibrium potential. The electron transfer from redox species to electrodes (or reverse) appears and thus, the electrode is polarized with a characteristic overpotential applied to the electrode (η), where $\eta = E - E_{eq}$. This potential difference creates an imbalance in the system, causes a change (more or less rapid) for the restoration of a new equilibrium state. This implies a change in the composition of the solution:

- for $\eta > 0$ the oxidation reaction appears and thus the ratio of Ox over Red increases,

- for $\eta < 0$ the reduction reaction appears and thus the ratio of Ox over Red decreases.

The electrolysis cell presented in Figure II. 1.3 is used in voltammetry, polarography, amperometry, etc.
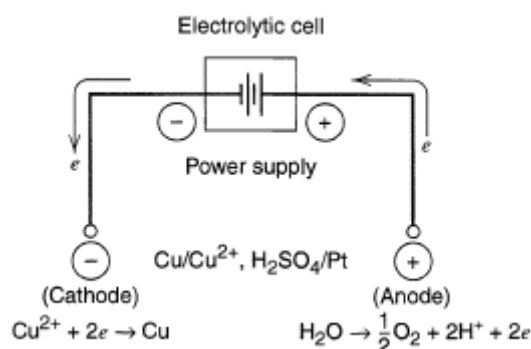
Fig. II. 1.3. Electrolysis cell (Bard and Faulkner, 2001)

1.5. Electrochemical methods and apparatus

Electrochemical methods can be divided in several categories depending on which aspects of the cell are controlled and which are measured. The three main categories are potentiometry (the difference in electrode potentials is measured), amperometry and voltammetry (the cell's current is measured while actively altering the cell's potential), coulometry (the cell's current is measured over time). Table II. 1.1 presents a summary of the

control parameters and signals measured for typical electroanalytical methods (Denuault, 2009).

Table II. 1.1. Overview of electrochemical techniques. E is the potential, i is the current flowing between electrodes, Q the charge passed (the integral of the current over time), Z the electrical impedance of the electrochemical circuit, f and t are the frequency and time of the potential perturbation respectively, c and a are the concentration and activity of the analyte of interest, respectively (Denuault, 2009).

Method	Control parameter	Signal measured	Relation to analyte	Driving circuitry required
Amperometry or voltammetry	$E =$ fixed, stepped, ramped	i	$i \propto c$	Yes
Coulometry	E	Q	$Q \propto c$	Yes
Impedimetry – Conductimetric sensing – Capacitive sensing	i or $E = \sin(2\pi\ ft)$	Z	$Z \propto (\sum c)^{-1}$	Yes
Potentiometry	$i = 0$	E	$E \propto \ln(a)$	No
Self-powered electrochemical cells	Chemistry, electrode material	i	$i \propto c$	No

Depending on the technique, the electrochemical cell involves a number of electrodes as presented in Table II. 1.2 (Denuault, 2009). The most important one is the working electrode (WE) where the electrochemical reaction is studied. The reference electrode (RE) allows the potential of the working electrode to be determined and the counter electrode (CE) completes the electric circuit. The best reference electrode is one whose potential does not shift from equilibrium, meaning non polarizable electrode. In order to minimize the potential shift, a reference electrode with large area is often used. Potentiostats based on operational amplifiers are often used for the complete elimination of the reference electrode polarization. A potentiostat adequate for voltammetric/amperometric techniques is presented in Figure II. 1.4. As shown on this figure the potentiostat maintains the potential difference, ΔE, between the RE and WE and collects the current, I, occurring during changes at WE.

Table II. 1.2. Overview of typical electrode configurations found in electrochemical systems, WE-working electrode, CE-counter electrode, RE-reference electrode, CE/RE-counter electrode also acting as reference electrode, WE/CE-working electrode alternatively acting as counter electrode (Denuault, 2009).

Technique	Number of electrodes	Electrode configurations
Potentiometry	2	Indicator electrode+RE
	3	Indicator electrode+RE +common electrode
Amperometry or voltammetry	2	WE+CE/RE
	3	WE+CE+RE
	4	2 WE+1 CE+1 RE
	Arrays	n WE+1 CE+1 RE
Impedimetry	2	WE+CE or 2 WE/CE
	3	WE+CE+RE
	4	2 WE+2 indicator electrodes
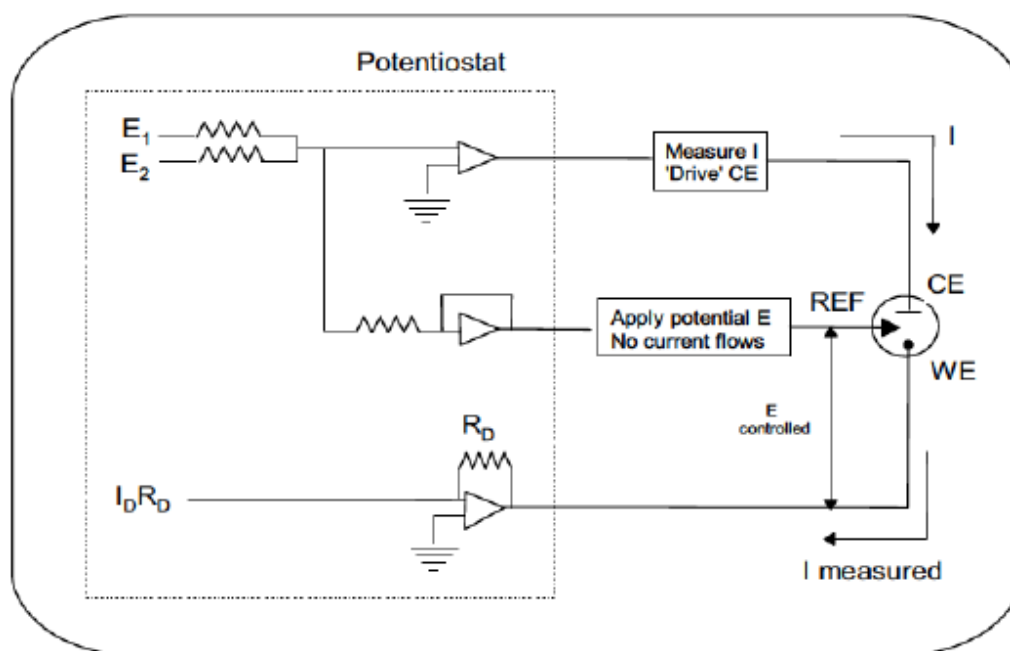
Fig. II. 1.4. Graphical representation of a convectional three-electrode cell (Compton and Banks, 2007).

There are numerous reference electrodes employed in electroanalytical experiments, but the most common is the silver/silver chloride one (Ag/AgCl, 3 mol L^{-1} KCl). It is a piece of silver wire covered by silver chloride which is immersed in potassium chloride solution encased in a glass tube. The electrode is protected from the bulk solution by a salt-bridge. Platinum rods, wire, loops, gauze or foil are usually used as counter electrodes. Commonly used working electrodes include mercury, carbon and inert materials such as gold and platinum. The modification of working electrodes with conducting polymers (Dhawan et al., 1997), gels (Tercier-Weaber et al., 1999), polymers loaded with enzymes or redox mediators (Grundig et al., 1995), doped polymers (Trojanowicz et al., 1996) are also common.

2. Electrochemical kinetics

The electronic transfer is located at the surface of the electrode, at the interface between the electronic conductor (electrode) and the ionic conductor (the solution). The electrochemical reaction can take place if the electroactive substance is present on the surface of the electrode. Overall an electrochemical reaction can be described according to Figure II. 2.1. In addition to the charge transfer, the transport of matter should also be considered for the establishment of a relation between the current (I), the potential (E) and concentrations in solution of Red and Ox.

The fundamental movement of charged or neutral species in an electrochemical cell to the electrode surface is facilitated by three processes namely: diffusion, migration and convection:

- diffusion: spontaneous movement caused by the establishment of a concentration gradient, due to the consumption and/or production of species in the vicinity of the electrode,
- convection: movement of species under the effect of a velocity gradient of the fluid (stirring the solution, rotating electrode),
- migration: displacement of the charged species under the effect of an electric field created by applying a potential difference between electrodes.

Like in any global process involved in consecutive steps, the overall rate is equal to the rate of the slowest step. Any quick step before a slow step is assumed to be in a state of near

equilibrium. We must therefore consider the rate of charge transfer and the kinetics of transport of matter and determine the slowest step.
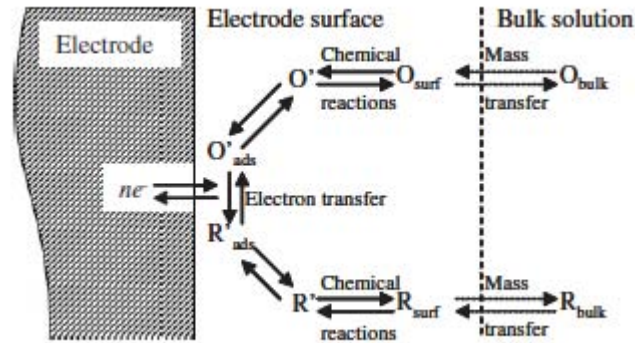
Fig. II. 2.1. Processes involved in an electrode reaction (Zoski, 2007, adapted from Bard and Fauklner, 2001)

2.1. Faraday's law and Butler-Volmer's law

Faraday's law links the quantitative number of moles of electroactive species produced or consumed Ox and Red (denoted N_{Red} and N_{Ox}, respectively) and the total electric charge (Q) passed through the electrode-electrolyte interface. For an electrochemical reaction of the form:

$$\mathrm{Re}\,d \overset{k_a}{\underset{k_c}{\longleftrightarrow}} Ox + ne^- \tag{II. 2.1}$$

where k_a and k_c represent the rate constants for the oxidation reaction (k_a-anodic) and reduction (k_c-cathodic), respectively, Faraday's law is expressed by:

$$\boxed{N_{\mathrm{Re}\,d} = N_{Ox} = \frac{Q}{nF}} \tag{II. 2.2}$$

From Faraday's law, it is possible to establish the relationship between the electric current passing through the electrochemical interface and the velocity (*v*) of the electrochemical process:

$$I = \frac{dQ}{dt}, \tag{II. 2.3}$$

so $v(mol \cdot s^{-1}) = \dfrac{dN}{dt} = \dfrac{I}{nF}$ (II. 2.4)

and so $v(mol \cdot s^{-1} cm^{-2}) = \dfrac{I}{nFA} = \dfrac{j}{nF}$ (II. 2.4')

where I-current (A), A-electrode surface (cm^2) and j-current density (A cm^{-2}).

The current density in the simplest case, where both oxidation and reduction reactions are first order reactions, can be expressed by:

$$j = j_a + j_c = nF\left(k_a C_{\text{Re}d}^{el} - k_c C_{Ox}^{el}\right)$$ (II. 2.5)

where j_a and j_c are density currents for oxidation and reduction reactions, respectively.

The rate constants of charge transfers k_a and k_c depend on transfer coefficients α and β for anodic and cathode reactions, respectively and on electrode potential E:

$$k_a = k^\circ \exp\left(\frac{\alpha F}{RT}\left(E - E^{\circ'}\right)\right)$$ (II. 2.6)

$$k_c = k^\circ \exp\left(-\frac{\beta F}{RT}\left(E - E^{\circ'}\right)\right)$$ (II. 2.7)

where k° is the standard heterogenous rate constant of the electrochemical system and E °' the apparent standard potential of a couple Ox / Red.

If we combine the equations II. 2.5-II. 2.7, the current density can be described by:

$$j = Fk^\circ \left\langle C_{\text{Re}d}^{el} \exp\left[\frac{\alpha F}{RT}\left(E - E^{\circ'}\right)\right] - C_{Ox}^{el} \exp\left[-\frac{\beta F}{RT}\left(E - E^{\circ'}\right)\right]\right\rangle$$ (II. 2.8)

At equilibrium the current density is null, so:

$$C_{\text{Re}d}^{el} \exp\left[\frac{\alpha F}{RT}\left(E - E^{\circ'}\right)\right] = C_{Ox}^{el} \exp\left[-\frac{\beta F}{RT}\left(E - E^{\circ'}\right)\right]$$ (II. 2.9)

When the concentrations on the electrode and in the solutions are the same and in ideal conditions of elementary reaction: $\alpha + \beta = 1$, the equation can be written:

$$\frac{C_{Ox}^{sol}}{C_{\mathrm{Re}d}^{sol}} = \exp\left[\frac{F}{RT}\left(E_{eq} - E^{\circ'}\right)\right] \tag{II. 2.10}$$

This equation is in fact the Nernst equation:

$$E_{eq} = E^{\circ'} + \frac{RT}{nF}\ln\left(\frac{C_{ox}^{sol}}{C_{red}^{sol}}\right) \tag{II. 2.11}$$

At equilibrium, it is possible to define the exchange current density j °, equal in fact to the anodic and cathodic components of the current (j_a and j_c):

$$j^{\circ} = Fk^{\circ}C_{\mathrm{Re}d}^{sol}\exp\left[\frac{\alpha F}{RT}\left(E - E^{\circ'}\right)\right] = Fk^{\circ}C_{Ox}^{sol}\exp\left[-\frac{\beta F}{RT}\left(E - E^{\circ'}\right)\right] \tag{II. 2.12}$$

If we combine the equations II. 2.10 and II. 2.12 and raise to the power α, we obtain:

$$j^{\circ} = k^{\circ}F\left(C_{\mathrm{Re}d}^{sol}\right)^{1-\alpha}\left(C_{Ox}^{sol}\right)^{\alpha} \tag{II. 2.13}$$

And in the special cases: $C_{\mathrm{Re}d}^{sol} = C_{Ox}^{sol} = C$:

$$j^{\circ} = k^{\circ}FC \tag{II. 2.14}$$

The current-voltage presented below is obtained by introducing the voltage in the expression of the current density in order to overcome the term E ° '.

$$j = j^{\circ}\left[\frac{C_{\mathrm{Re}d}^{el}}{C_{\mathrm{Re}d}^{sol}}\exp\left(\frac{\alpha F}{RT}\eta\right) - \frac{C_{Ox}^{el}}{C_{Ox}^{sol}}\exp\left(\frac{(1-\alpha)F}{RT}\eta\right)\right] \tag{II. 2.15}$$

This equation is composed of two terms related to anode and cathode components of the current. When the applied voltage is positive and large, the cathodic component is considered negligible; the total current is the only anode current. Conversely, when the overpotential is very negative, only the cathodic component is to be considered.

Considering that the concentrations of Ox and Red at the electrode surface are equal to concentrations in solution, the equation becomes the equation of Butler-Volmer:

$$\boxed{j = j^{\circ}\left[\exp\left(\frac{\alpha F}{RT}\eta\right) - \exp\left(\frac{(1-\alpha)F}{RT}\eta\right)\right]} \tag{II. 2.16}$$

The kinetic parameters of this equation can be determined experimentally from the Tafel curves which give the decimal logarithm of the current density in absolute value depending on the voltage (Figure II. 2.2).
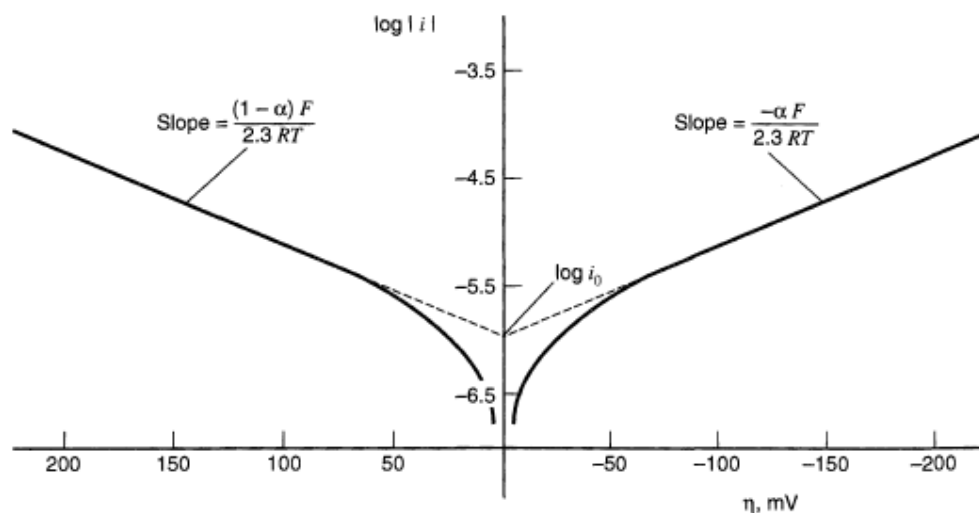
Fig. II. 2.2. Tafel plots for anodic and cathodic branches of the current-overpotential curve (Bard and Faulkner, 2001).

2.2. Fick's diffusion law

The use of a supporting electrolyte in large excess eliminates the effect of migration of the electroactive species and ensures the charge transport in the electrolytic solution. It remains to consider two modes: pure diffusion (where the electrode and the solution are immobile) and the convective diffusion (controlled agitation of the solution). In both cases, the natural convection is negligible due to the use of large scan rates, or by performing measurements on short times, or by the establishment of a controlled and forced stirring of the solution. Subsequently, the particular case of a planar electrode is considered to be the phenomenon of diffusion in a single direction perpendicular to the surface of the electrode.

The flux density (J), expressed as mol cm^{-2} s^{-1}, defines the number of electroactive molecules per unit time which passes through a plane parallel to the surface of the electrode, located at a distance "x". According to Fick's first law, the flux of species "i" is directly proportional to its concentration gradient:

$$J_i(x,t) = -D_i \frac{\partial C_i(x,t)}{\partial t}$$ (II. 2.17)

where D_i is the diffusion coefficient of species "i", expressed as $cm^2 \, s^{-1}$. Applying the law of conservation of mass, and considering the correlation between flux and current density, it appears that the flow of Red is equal in value and opposite in sign to the flux of Ox, and we have:

$$\frac{i}{nF} = D_R \left(\frac{\partial C_{Red}}{\partial x} \right)_{x=0} = -D_{Ox} \left(\frac{\partial C_{Ox}}{\partial x} \right)_{x=0}$$ (II. 2.18)

Fick's second law determines the variation of the concentration of the species "i" in question in space and time:

$$\frac{\partial C_i(x,t)}{\partial t} = D_i \frac{\partial^2 C_i(x,t)}{\partial x^2}$$ (II. 2.19)

Solutions of Fick's law depend on the initial and boundary conditions at infinity and the surface of the electrode.

2.2.1. First case: transport by pure diffusion

If the electrolytic solution is not stirred, the single transport phenomenon is diffusion. The present system is then in terms of a pure diffusion regime. Figure II. 2.3 shows the concentration profiles over time, depending on the distance "x" to the electrode, for a species "i' consumed during electrolysis at fixed potential, with a zero interfacial concentration. As illustrated in this figure, the thickness of the diffusion layer δ increases over time.

The calculation of the limiting current density distribution (j_{diff}) and the concentration profile C_i (x, t) requires solving Fick's second law with the following boundary conditions:

$$C_i(x,t) = C_i^{sol}$$

$$C_i(\infty,0) = C_i^{sol}$$

$$C_i(0,t) = 0, \text{ for } t > 0$$
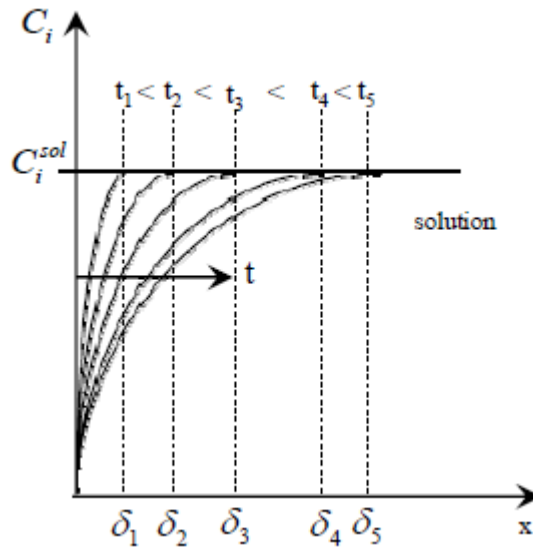
Fig. II. 2.3. Concentration profiles in function of distance from electrode for species "i" at different times (Bockris and Reddy, 1970)

The initial condition means that the solution is homogeneous at $t = 0$ and the semi-infinite condition that there are no perturbations during the experience, at a sufficient distance from the electrode. The third condition corresponds to the situation on the surface of the electrode after the application of a potential. By using the Laplace transformation, the expression of the concentration profile is:

$$C(x,t) = C_i^{sol} erf\left[\frac{x}{2\sqrt{Dt}} \right]$$
(II. 2.20)

The current density is proportional to the flow to the surface of the electrode:

$$j_{diff} = nFD_i \left(\frac{\partial C_i(x,t)}{\partial x} \right)_{x=0}$$
(II. 2.21)

The calculation of the derivative $\left(\frac{\partial C}{\partial x} \right)_{x=0}$, from equation (II-20), leads to Cotrell's equation:

$$\boxed{j(t) = \frac{nFD^{1/2}C_i^{sol}}{\pi t^{1/2}}}$$
(II. 2.22)

2.2.2. Second case: transport by convective diffusion

The intervention of convection by stirring the solution or rotating the electrode increases the rate of mass transport. The system is then under the condition of a convective diffusion regime. A simplified theoretical approach is based on the hypothesis of the formation of the diffusion layer. Two cases can be considered (Figure II. 2.4) depending on whether one is in the diffusion layer or in homogeneous solution:

- for x<δ: material transport is controlled only by diffusion
- for x>δ: the agitation of the solution is sufficient to maintain a constant concentration of species i, C_i^{sol}
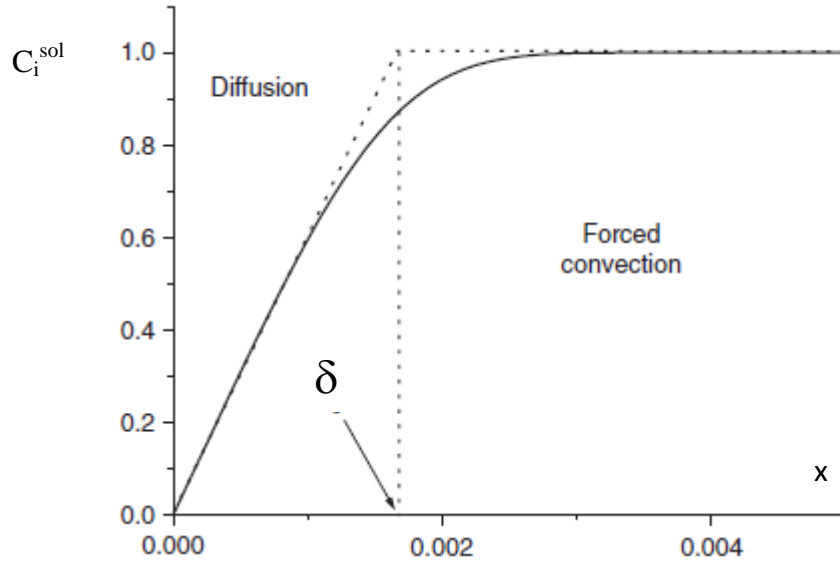
Fig. II. 2.4. Concentration profile of species "i" in function of distance from the electrode.

The system is in steady state condition, so:

$$\frac{\partial C_i(x,t)}{\partial t} = D_i \frac{\partial^2 C_i(x,t)}{\partial x^2} = 0 \text{ and the expression of the diffusion flux is:}$$

$$J_i = -D_i \frac{1}{\delta}\left(C_i^{sol} - C_i^{el}\right) \tag{II. 2.23}$$

The current density is a function of the difference in concentration of species "i" (Ox or Red) in solution and the species "i" (Ox or Red) presented on the surface of the electrode. The terms of the anodic and cathodic current density are given below:

$$j_a = \frac{nFD_{\text{Re}d}}{\delta}\left(C_{\text{Re}d}^{sol} - C_{\text{Re}d}^{el}\right)$$ (II.2.24

$$j_c = \frac{nFD_{\text{Re}d}}{\delta}\left(C_{Ox}^{sol} - C_{Ox}^{el}\right)$$ (II. 2.25)

When the diffusion rate is much lower than that of the electron transfer at the surface of the electrode $C_i^{el} = 0$, the diffusion limiting current density is proportional to the concentration of the species in solution.

$$j_{\lim,a} = \frac{nFD_{\text{Re}d}C_{\text{Re}d}^{sol}}{\delta}$$ (II. 2.26)

$$j_{\lim,c} = -\frac{nFD_{Ox}C_{Ox}^{sol}}{\delta}$$ (II. 2.27)

3. Electrochemical methods used in this work

3.1. Diffusion controlled methods: Cyclic voltammetry

Cyclic voltammetry is the most extensively used electrochemical technique and is used to study electrochemical reactions as well as to provide information on the reversibility and kinetics of such reactions. During a cyclic voltammetry experiment, the potential of an electrode is scanned linearly from an initial potential to a final potential and then back to the initial potential. The potential is a function of scan rate (r) and time (t):

$$E = E_i \pm rt$$ (II. 3.1)

Where E_i indicates the initial potential and usually the potential at zero current ($E_{I=0}$) is chosen to ensure that there is no reaction when starting the recording of the current-potential curve.

The potential at which the peak current occurs is known as the peak potential (E_p) where the redox species has been depleted at the electrode surface and the current is diffusion limited. The magnitude of the Faradic current (I_{pa}-anodic peak current or I_{pc}-cathodic peak current) gives an indication of the rate at which electrons are being transferred between the

redox species and the electrode. Cyclic voltammogram can be reversible, quasi-reversible or irreversible as presented in Figure II. 3.1.
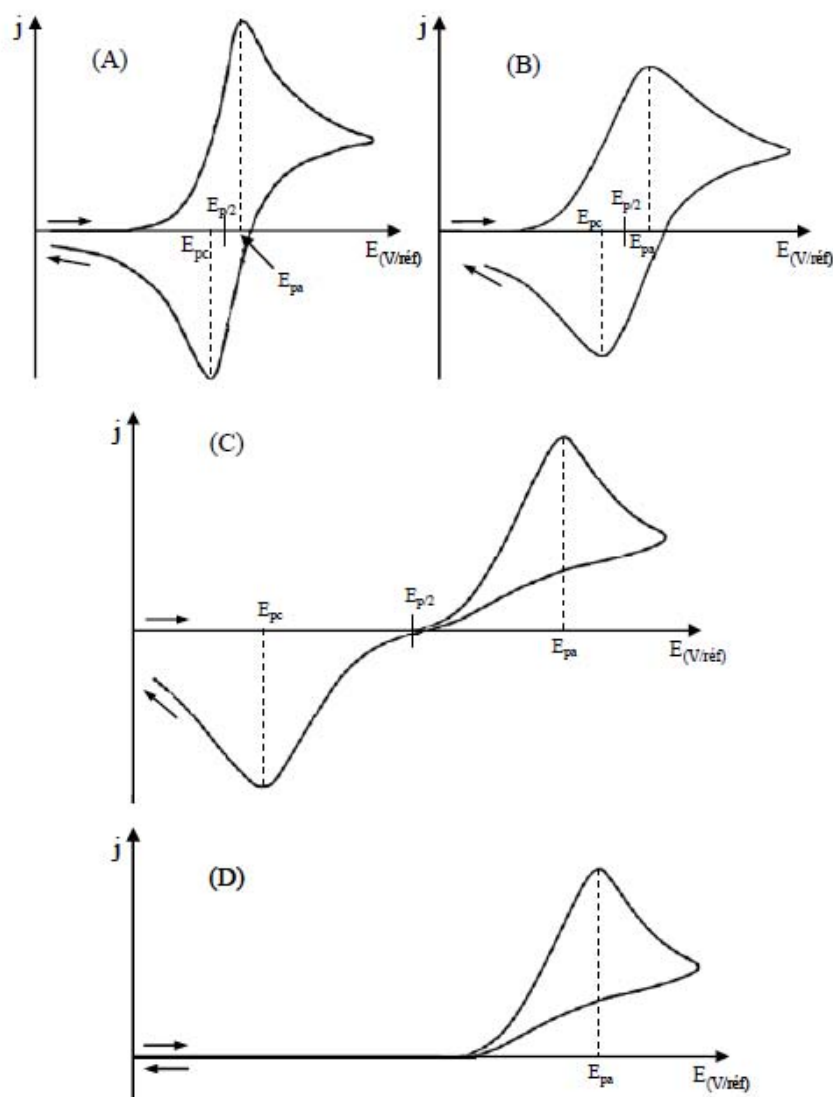
Fig. II. 3.1. Cyclic voltammetry for different systems: A-reversible, B-quasi-reversible, C, D-irreversible (Barus, 2008, adapted from Bard and Faulkner, 2001).

The experimental conditions of implementation of this technique are the use of a device with three electrodes and an electrolyte of sufficient concentration and not being agitated. Only diffusive transport semi-infinite is then considered. Natural convection is negligible during the relatively short time of measurement.

When applying the potential, the electroactive species present on the surface of the electrode can be oxidized (or reduced) and the anodic current (or cathodic) increases until it

reaches a maximum. Current-potential curves have therefore the form of peaks. Indeed, the concentration of species consumed at the interface electrode / electrolyte solution decreases and, in conditions of semi-infinite linear diffusion, the current then decreases as predicted by Cottrell's law $\left(\dfrac{1}{(\pi t)^{1/2}}\right)$. The intensity of the peak obtained is proportional to the concentration of the species concerned.

3.1.1. First case: reversible system

A reversible process is one in which the electron transfer process is rapid, and the electroactive oxidized (or reduced) species in the forward scan is in equilibrium with the electroactive reduced (oxidized) species in the reverse scan. The electroactive species are stable and so the magnitudes of I_{pc} and I_{pa} are equal and proportional to the concentration of the active species. The current density of the peak (j_p) can be determined by a Randles-Sevcik law:

$$\boxed{j_p = (2.69 \cdot 10^5) n^{3/2} D_i^{1/2} C_i^{sol} v^{1/2}}$$
(II. 3.2)

E_p is not dependent on scan rate (v), but current increases with $\sqrt{v}$ and indicates that the current is controlled by diffusion to the electrode surface. ΔE_p (E_{pa}-E_{pc}) should be independent on the scan rate (v) but in practice it increases slightly with increasing v due to the solution resistance (R_s) between the reference and working electrodes. The potential difference between the oxidation and reduction peaks is 59 mV for a one electron reversible redox reaction. However, in practice, ΔE_p is sometimes found in the 60-100 mV range. The separation between peaks can be used for calculation of electron numbers:

$$\Delta E = E_{pa} - E_{pc} = 2.303 \frac{RT}{nF}$$
(II. 3.2)

And at room temperature:

$$\Delta E = \frac{0.059V}{n}$$
(II. 3.3)

3.1.2. Second case: irreversible system

For an irreversible system, only the forward oxidation (reduction) peak is observed. A weak reverse reduction (oxidation) peak is a result of slow electron exchange or slow chemical reactions at the electrode surface. The peak current density, j_p, for an irreversible process is given by equation II. 3.4.

$$\boxed{j_p = (2.69 \cdot 10^5)\alpha^{1/2} D_i^{1/2} C_i^{sol} v^{1/2}}$$ (II. 3.4)

Where α is the coefficient of electron transfer.

For a totally irreversible system, ΔE_p is calculated from the following equation:

$$\Delta E_p = E^{\circ'} - \frac{RT}{\alpha F}\left[0.78 + \ln\frac{D_i^{1/2}}{k_0} + \ln\left(\frac{\alpha F v}{RT}\right)^{1/2} \right]$$ (II. 3.5)

The potential peak for an irreversible system shifts by $0.048/\alpha n$ at 25°C.

3.1.3 Third case: quasi-reversible system

Unlike the reversible process in which the current is purely mass-transport controlled, currents due to a quasi-reversible process are controlled by a mixture of mass transport and charge transfer kinetics. The process occurs when the relative rate of electron transfer with respect to that of mass transport is insufficient to maintain Nernst equilibrium at the electrode surface. For a quasi-reversible process, i_p increases with $v^{1/2}$, the peak potential shifts and ΔE increases when increasing v and $\Delta E > 0.059/n$.

3.2. Modulated voltammetric techniques-differential pulse voltammetry

Advanced voltammetric techniques have been developed to increase the sensitivity and selectivity of the voltammetric signal. In most cases this requires minimizing the current from non-faradic processes such as that due to the charging and discharging of the double layer (Bard and Faulkner, 2001). These techniques rely on combinations of sweeps and steps

(Table II. 3.1) and have names such as staircase voltammetry, normal pulse voltammetry, differential pulse voltammetry, and square wave voltammetry (Whitfield and Jagner, 1981). A classic example of the power of sweep and step combinations is anodic stripping voltammetry where a step to low concentrations is used to pre-concentrate metallic species by reducing them on the electrode while subsequent sweep towards high potentials is used to oxidize them sequentially.

In the differential pulse voltammetry, pulses of constant height are imposed on a linear sweep of the voltage. Current is sampled twice-before the pulse and on the end of the pulse and the difference is recorded. Differential pulse technique is one of the most sensitive techniques and allows acheving low limits of quantification. The curves take a shape of the peak with a maximum which corresponds to the half wave potential from classical cyclic voltammetry. The width of the peak at half height, $W_{1/2}$ increases as the pulse height grows larger, because differential behaviour can be seen over a greater range of base potential. Normally, one refrains from increasing pulse amplitude (ΔE) much past 100 mV, because resolution is unacceptably degraded. The precise form of $W_{1/2}$ as a function of ΔE is complicated and is of no real use. However, it is of interest to note the limiting width as ΔE approaches zero:
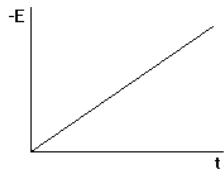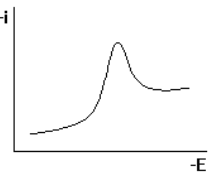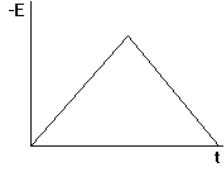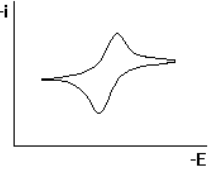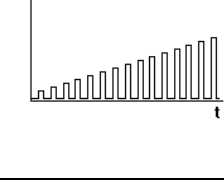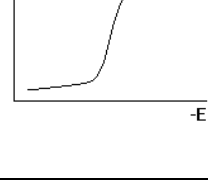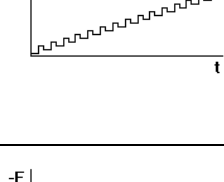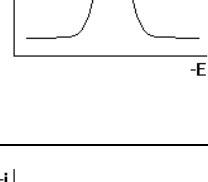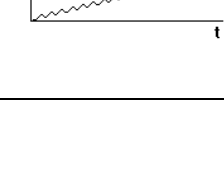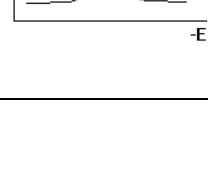
$$W_{1/2} = 3.52 \ RT/nF \tag{II. 3.6}$$

In this method, there is total elimination of the capacitive current and the magnitude of the Faraday's diffusion current is measured. The height of peak $(\delta_i)_{max}$ is given by the equation:

$$(\delta_i)_{max} = \frac{nFAD_i^{sol}C_i^{sol}}{\pi^{1/2}(\tau-\tau')^{1/2}}\left(\frac{1-\sigma}{1+\sigma}\right) \tag{II. 3.7}$$

Where $\tau - \tau'$ is pulse duration, $\sigma=nFv/RT$. The quotient $(1-\sigma)(1+\sigma)$ decreases monotonically with diminishing potential amplitude (ΔE) and reaches zero for $\Delta E=0$. When ΔE is negative δ_i is positive (or cathodic), and vice versa.

Table II. 3.1. Voltammetric and modulated voltammetric techniques

Technique	Driving waveform	Response	Equation
Linear sweep voltammetry			$i_p = kn^{3/2}AD^{1/2}V^{1/2}C$ [Randles-Sevcik]
Cyclic voltammetry			$i_p = kn^{3/2}AD^{1/2}V^{1/2}C$ [Randles-Sevcik]
Normal pulse voltammetry			$i_l = \dfrac{nFAD^{1/2}C}{\pi^{1/2}t^{1/2}}$ [Cottrell]
Differental pulse voltammetry			$i_p = \dfrac{nFAD^{1/2}C}{\pi^{1/2}t^{1/2}}\left(\dfrac{1-\sigma}{1+\sigma}\right)$ $\sigma = \exp\left(\dfrac{nF}{RT}\cdot\dfrac{\Delta E}{2}\right)$
Square wave voltammetry			$i_p = kn^2ACD^{1/2}\Delta E\omega^{1/2}$ $k = F^2/4RT$

3.3. Methods controlled by forced convection: hydrodynamic methods

Hydrodynamic methods are characterized by convection of the solution, forced and controlled through the use of a rotating electrode. These methods give a possibility to achieve quickly steady state conditions. The working electrode, controlled by the attached electric

motor, actually rotates, and in so doing provides an influx of the analyte species at the electrode surface. As it turns it pulls the solution closest to the surface (hydrodynamic boundary layer) creating a whirlpool effect. Thus the solution from the center of the electrode is displaced as a result of centrifugal force. Solution from the bulk now flows up, perpendicular to the electrode, to replace the boundary solution. The sum result is a laminar flow across and towards the electrode surface. The rate of the rotating disk controls the solution flow which in turn controls the steady-state current. This method is different to unstirred techniques where the steady-state current is controlled by diffusion. Indeed, the mass transport is faster and independent of time. In addition, the thickness of the diffusion layer (δ) can be controlled and δ is directly proportional to the inverse of the square root of the speed of rotation of the electrode ($\omega^{-1/2}$) according to the following relationship:

$$\delta = 1.62 v^{1/6} D_i^{sol} \omega^{-1/2}$$ (II. 3.7)

3.3.1. Levich's equation

The voltammograms obtained in conditions of steady state have the form of sigmoid of the limiting current density, in the case of a rotating disk electrode, is defined by the Levich's equation:

$$\boxed{j_{\lim} = 0.62 nFD_i^{2/3} \omega^{1/2} v^{-1/6} C_i^{sol}}$$ (II. 3.8)

3.3.2. Koutecky-Levich's equation

For more complex systems, a linear correlation is observed between the inverse of the current density and the inverse of the square root of the rotation speed of the electrode. This relationship, known as the Koutecky-Levich equation reveals the existence of a coupled chemical reaction or the presence of a reaction intermediate in the oxidation mechanism:

$$\boxed{\frac{1}{j} = \frac{1}{j_k} + \frac{1}{j_{\lim}}}, \quad j_k = FCk^\circ \exp\left[\frac{\alpha F}{RT}\left(E - E^{\circ\prime}\right)\right] \text{ and } j_{\lim} = 0.62 nFD_i^{2/3} \omega^{1/2} v^{-1/6} C_i^{sol}$$ (II. 3.9)

Where j, j_k, $j_{\lim}$ are the measured current, kinetic and diffusion-limited current, respectively.

3.5. Chronoamperometry

Chronoamperometry is based on applying a constant potential on the working electrode immersed in a solution and the registration of the current variation over time. If an electroactive species is oxidized or reduced at the applied potential, a decrease in the current density with time is observed. In the case of a pure diffusion regime and for the first tens of seconds of the experiments, this decrease in current obeys the Cottrell law. In this case, the solution concentration of the oxidized or reduced species is invariable (micro-electrolysis). Instead, the application of a potential for a long period (macro-electrolysis) causes a change in the composition of the solution. The concentration of the species in solution decreases with time, the law of Cottrell is no longer applicable.

4. Influence of adsorption of electroinactive species

The adsorption phenomena play an important role in the electrochemical processes. If an electroactive species is adsorbed on the electrode surface, it is necessary to modify the theoretical treatment of the electrochemical method and consider then the concentration of reactive species at the electrode surface is relatively higher than at the beginning of the experiment. On the contrary, the adsorption of a non-electroactive species causes the fall of the electrochemical signal by forming an insulating layer on the surface of the electrode.

Generally, there are two types of adsorption: specific and non-specific.

Non-specific adsorption is characterized by electrostatic interactions of long distance which modify the distribution of ions in the vicinity of the surface of the electrode. The non-specific adsorption of an electroactive species affects the electrochemical response because it alters the concentration of the species and the potential distribution in the vicinity of the electrode.

In the case of specific adsorption, a strong interaction between the adsorbate and the electrode material causes the formation of a layer (partial or complete) on the surface of the electrode.

As described above, electroactive and non-electroactive species can be adsorbed on electrode surface. Generally, the first one causes the increase of the measured signal whereas the second one decreases the signal due to formation of blocking layer on the electrode

surface. Here, only the second one will be described in detail since the problem of adorption of electroinactive species is discussed in Chapter V when dealing with reduction of isopolyoxomolybdates on a gold electrode.

The adsorption of electroinactive species occurs frequently. Such adsorption can inhibit (or poison) an electrode reaction. Indeed, in many studies with solid electrodes, one observes a slow change in the electrochemical response with time, which can be ascribed to the build up of asorbed impurities on the electrode surface at a rate limited by their diffusion from the bulk solution. An adsorbed film may inhibit an electrode reaction by completely blocking the electrode surface so that reaction occurs only at the uncovered fraction $(1 - \theta)$. Alternatively, the reaction may occur also at the covered part of the electrode, for example, by penetration of the reactive species or by transfer of electrons through the film but at reduced rate as compared to the free surface.

If we consider that the film has a porous structure and that, the species can pass through to the active sites of the electrode surface, so that the sites behave as a collection of UMEs (ultramicroelectrodes). The expression for the total limiting density current registered at rotating disk electrode is:

$$j_l = FD_i^{Sol}C_i^{Sol}(1-\theta)^{1/2} / \gamma R_0 \qquad\qquad \text{(II. 4.11)}$$

where γ is a factor which depends upon the site type and distribution. For the disk array the following equation has been proposed:

$$\boxed{j_l = FD_i^{Sol}C_i^{Sol}(1-\theta)^{1/2} / 0.6R_0} \qquad\qquad \text{(II. 4.12)}$$

θ is the fractional coverage of the electrode by the blocking film and $2R_0$ is the spacing between the sites.

5. Electrochemical reactions coupled with chemical reaction

The heterogeneous electron transfer is often accompanied by homogeneous chemical reactions that involve species Ox and/or Red. The presence of coupled chemical reactions affects the electrochemical response and complicates the elucidation of the mechanism. There

are several possible types of coupling with effects on the electrochemical signal. A coupled chemical reaction leads to changes in peak height, changes in the shape of the curves (peak symmetry, absence of the return peak, variation in the ratio $\frac{j_{pa}}{j_{pc}}$). The relationship between the potential and concentrations of electroactive species is still governed by the Butler-Volmer's law in the case of limiting charge transfer, but concentrations of oxidizing and reducing species to the electrode surface are dependent this time upon the speed of the processes associated with the electronic transfer. The integration of differential equations takes into account the kinetic characteristics of these phenomena and considers:

- The speed of electron transfer

- The rate of chemical reactions associated

- Nature of the system (reversible, quasi-reversible, irreversible)

Electrochemical methods most commonly used to study such processes are:
- Voltammetry in steady state convective diffusion regime which is suitable for studying thermodynamics of reactions in solution,

- Voltammetry in pure diffusion regime, including cyclic voltammetry, which allows the detection of reaction intermediates.

The consequences of different chemical couplings of the electrochemical responses obtained by cyclic voltammetry are detailed below.

The effect of a chemical reaction on the parameters coupled to an electrode reaction depends on the progress of this reaction compared to the duration of the whole electrochemical experiment. So $t_{1/2}$: half-reaction for a chemical coupled reaction and the τ-duration of electrochemical experiment:

-   if $\tau \ll t_{1/2}$: no change in the electron transfer is observed,

-   if $\tau \gg t_{1/2}$: there is a coupled chemical reaction, leading to possible variations of current – voltage curves.

Investigation of chemical coupled reactions is based on varying several parameters such as the scan rate, the speed of rotation of the electrode, etc… and studying the variations obtained on the characteristic intensity-potential curves.

The theory was developed for numerous mechanisms involving different combinations of reversible, quasi-reversible, and irreversible heterogenous electron transfer and homogenous steps. In this chapter, two well known mechanisms will be considered.

5.1. C_rE_r mechanism

In the C_rE_r mechanism, an electroactive species X is converted into the oxidized species O via reversible chemical reaction (II. 5.1) preceding reversible electron transfer reaction (II. 5.2):

$$X \leftrightarrow_{k_b}^{k_f} O \qquad \text{(II. 5.1)}$$

$$O + ne^- \leftrightarrow R \qquad \text{(II. 5.2)}$$

The appropriate dimensionless parameters are $K=k_f/k_b$ and $\lambda=(RT/nF)[(k_f + k_b)/v]$. Using these parameters, the voltammetric behaviour of a C_rE_r mechanism can be summarized in a zone diagram (Figure II. 5.1). The small log λ, $\lambda < 0.1$ (large v) values correspond to the pure diffusion regime (DP). In this zone, reaction is slow on a short experiment time scale and does not significantly affect the concentrations of the redox species in the electrode proximity. The chemical kinetics is too slow to be measured. At higher λ ($0.1< \lambda<1$) values the process shifts to the intermediate kinetic zone (KI), where the response is under mixed diffusion/kinetic control. By further decreasing the sweep rate, one can reach the pure kinetic zone, ($1< \lambda<100$) (KP). The current is independent of v, and at extreme potentials it reaches a plateau value.

$$\boxed{i_L = nFAD^{1/2}C_i^{sol}K(k_b+k_f)^{1/2}} \qquad \text{(II. 5.3)}$$

The half – plateau potential of such voltammogram (the potential at which $i=0.5i_L$) is:

$$\boxed{E_{1/2} = E^{\circ\prime} - \frac{RT}{nF}(\ln \lambda + 0.554)} \qquad \text{(II. 5.4)}$$
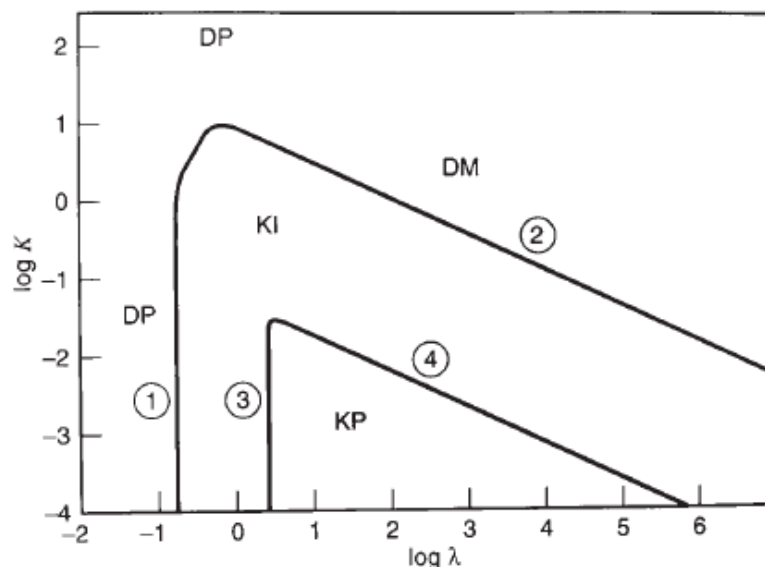
Fig. II. 5.1. Zone diagram for C_rE_r process (Zoski, 2007)

5.2. E_rC_i mechanism

The kinetic behavior of a E_rC_i process can be presented as:

$$O + ne^- \leftrightarrow R \qquad\qquad\qquad\qquad (II.\,5.5)$$

$$R \xleftarrow{\quad k \quad} X \qquad\qquad\qquad\qquad (II.\,5.6)$$

and is determined by the single dimensionless parameter $\lambda = (RT/nF)[(k)/v]$, and the corresponding zones are: KP-pure kinetic control ($\lambda > 5$), KI-intermediate zone ($5 > \lambda > 0.1$), DP-pure diffusion zone ($\lambda < 0.1$).

In the DP zone, the following reaction is too slow to be detected, and the corresponding voltammogram is essentially indistinguishable from CVs of a simple, diffusion controlled electron-transfer. In the KI zone, the reaction (II. 5.6) becomes sufficiently fast to compete with diffusion. A significant fraction of species R is converted to electroinactive X before being re-oxidized at the electrode surface during the potential sweep in reverse (anodic) direction. Hence, height of the reverse peak is decreased. The disappearance of the reverse peak at slower v (KP zone) is typical of an irreversible chemical reaction following the electron transfer step. The value of λ, and subsequently the rate constant of reaction (k),

can be obtained by measuring the difference between the peak potential and $E_{1/2}$. The following equation shows that in KP region this quantity is a linear function of ln v.

$$E_p - E_{1/2} = \frac{RT}{2nF}(\ln \lambda - 1.56)$$

(II. 5.7)

6. Summary

The basic concepts of electrochemistry are explained and two electrochemical cells are presented. In the Galvanic cell, a spontaneous redox reaction is taking place within the cell, due to Nernst's law. In the electrolysis cell, a chemical reaction is driven by an external applied current and the forced reduction (or oxidation) processes can be registered. A galvanic cell is used in an electrochemical method called potentiometry and this cell usually consists of a working and reference electrode. The electrolysis cell is used in many methods: amperometry, voltammetry and this cell has an additional electrode-counter electrode.

Electrochemical kinetics is based on Fick's diffusion law and describes transport of species to the electrode surface. Two cases are possible: transport by pure diffusion where current density can be described by Cotrell's equation or transport by convective diffusion.

Electoanalytical methods used in this work (Chapters IV, V, and VI) are described as well. Cyclic voltammetry is a well known and often used method and is dependent on reaction rate. Three cases are considered: reversible, quasi-reversible and non reversible reactions. A large ratio of capacitive over faradic current is sometimes a severe problem when using cyclic voltammetry, especially if the analyte is at low concentrations. To solve this problem, different modulated voltammetric techniques were developed. Differential pulse voltammetry is one of these methods. In the differential pulse voltammetry, pulses of constant height are imposed on a linearly changing voltage. Current is sampled twice-before the pulse and on the pulse and the difference is recorded. The measured current difference is only the faradic current. Cyclic voltammetry was used in this work for characterizing isopoly- and heteropolyoxomolybdates formed during anodic oxidation of molybdenum in seawater (Chapter V). Differential pulse voltammetry was used for phosphate detection (Chapter VI).

Chronoamperometry (or amperometry) is based on applying a constant potential on the working electrode immersed in a solution and the recording of the current variation over time is obtained. This method was also used for phosphate (Chapter VI) and dissolved oxygen (Chapter IV) detection.

Methods involving rotating electrodes are called hydrodynamic methods or methods controlled by forced diffusion. The current density can be described by Levich or Koutecky-Levich's equation. Linear sweep voltammetry at rotating disc electrode was used in this work for characterizing isopoly- and heteropolyoxomolybdates formed during anodic oxidation of molybdenum in seawater (Chapter V).

The adsorption of electroinactive species blocks the electrode and the measured currents are lower than expected or the potential-current curves behave unexpectedly. Adsorption of electroinactive species was observed in this work (Chapter V) during reduction of isopolyoxomolybdates on rotating disk electrode and caused deviation of traditional signals with limiting current.

Electron transfer is sometimes associated with homogenous chemical reactions which can have a great influence on voltammograms. This problem was observed for silico- and phosphomolybdate complex (Chapter V). The reduction of complexes is preceded by a chemical step, protonation, which is much slower for phosphomolybdate complex than for the silicomolybdate one.

This chapter has provided a general overwiew on electrochemistry and electroanalytical methods and will help to understand the work described in the following chapters.

CHAPTER III:

IN SITU PHOSPHATE AND OXYGEN MONITORING

If we are to understand the factors controlling the biological carbon pump in the ocean, both now and in the future as the ocean responds to global warming, then we must survey the oceanic biogeochemistry at proper spatial and temporal scales. Long term monitoring of marine environments requires in situ platforms and miniaturized autonomous sensors with long lifetime, high precision, low detection limit, fast response time, good reproducibility, resistance to biofouling and high pressure and low energy consumption.

This chapter provides a description of the state of the art of in situ sensors for phosphate and oxygen monitoring. Firstly, amperometric sensors for oxygen detection are described with a special attention to the STOX sensor. Thus, the chapter is focused mainly on amperometric sensors but a comparison of amperometric sensors with optodes is also provided. Both methods, amperometric and optodes sensors, seem to be the future of in situ oxygen monitoring. Secondly, in situ analyzers for phosphate monitoring are presented with a special attention to the ANAIS one. Finally, the future of in situ phosphate monitoring is discussed focussing mainly on electrochemical sensors.

Contents

1. Ocean observing systems

The processes involved in the ocean, shown in Figure III. 1.1, cover very wide spatial and temporal scales ranging from molecular processes (below the millimeters and seconds) to climate change on a global scale over several decades (Dickey, 2001; Prien, 2007).
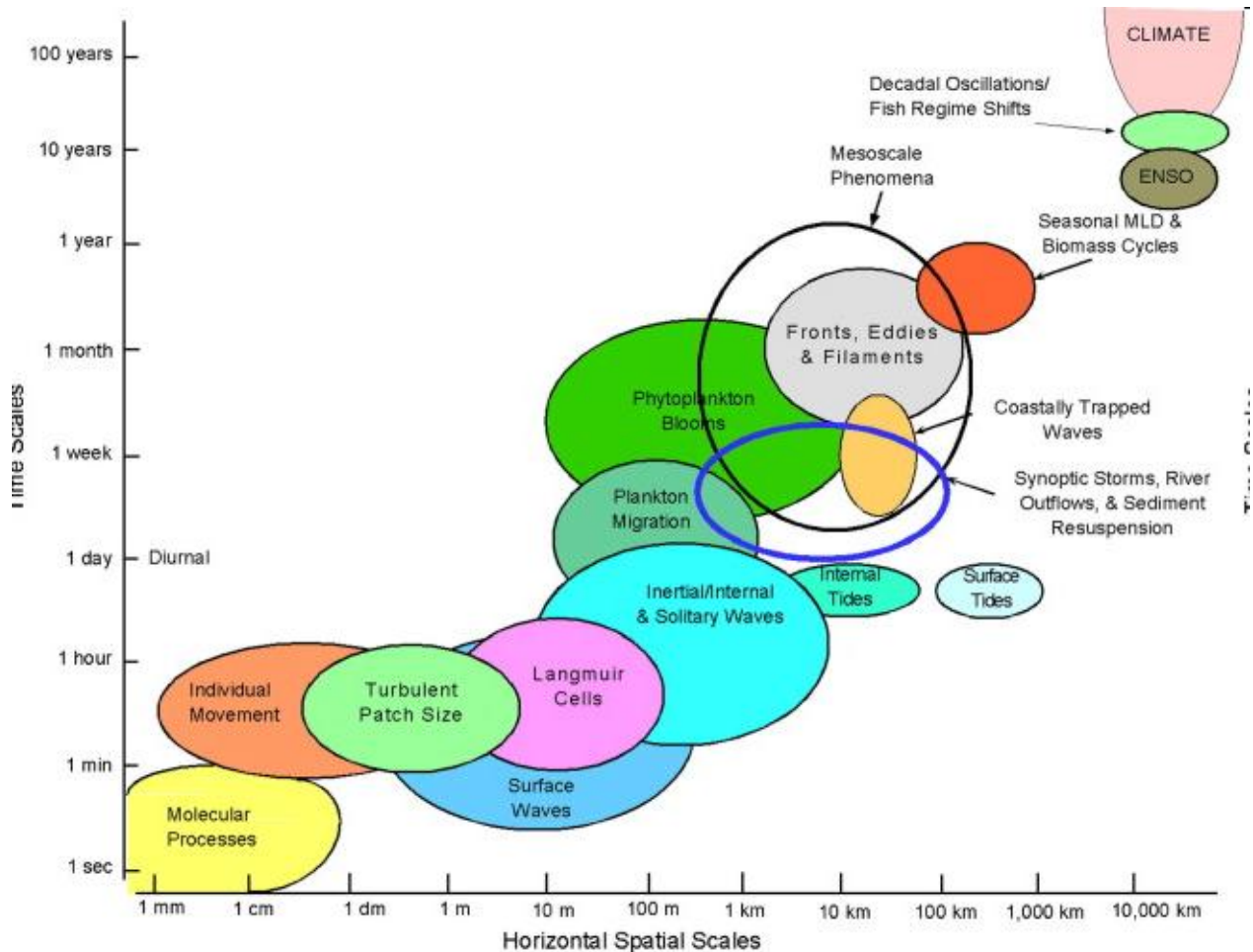
Fig. III. 1.1. Spatial and temporal scales of ocean processes (Dickey, 2001).

Much of what we currently know on spatial and temporal variability of oceanic processes is based on satellite measurements and several, primarily ship-based, time series programs, for example: Hawaii Ocean Time series-HOT (23°N, 158°W), Bermuda Atlantic Time series Study-BATS (31-32°N, 64°W), European Station of Time-Series in the Ocean Canary Islands-ESTOC (29°N, 15°W). Data from these observatories showed for the first time the increase of dissolved CO_2 associated with decreased pH of the ocean (Bindoff et al., 2007), the so-called ocean acidification issue.

Ship-based sampling can provide information about mesoscale processes but it is very time-consuming and extremely expensive. Satellite observations can overcome this problem giving access easily to meso-and submesoscale features on a global world ocean scale. With respect to biogeochemistry, the suite of observable parameters comprises: chlorophyll a concentration, particle load (or particulate organic carbon), qualitative nature of the particles (size, composition), dissolved/detrital material. However, they can be retrieved only during cloud-free periods. Consequently, we have limited information about ocean biogeochemistry. Observing ocean biogeochemistry at the proper spatial and temporal scales requires a revolution in observing technology (Johnson at al., 2009). Rapid progress is being made in the development of a suite of chemical and biological sensors that are low power, small in size, precise and accurate, and have long-term stability. Within the last few years, sensors adaptable on platforms for oxygen, chlorophyll or nitrate have been refined. They represent the enabling technology for a global observing system that might operate on a scale comparable to the physically oriented ARGO array (Fig. III. 1.2).
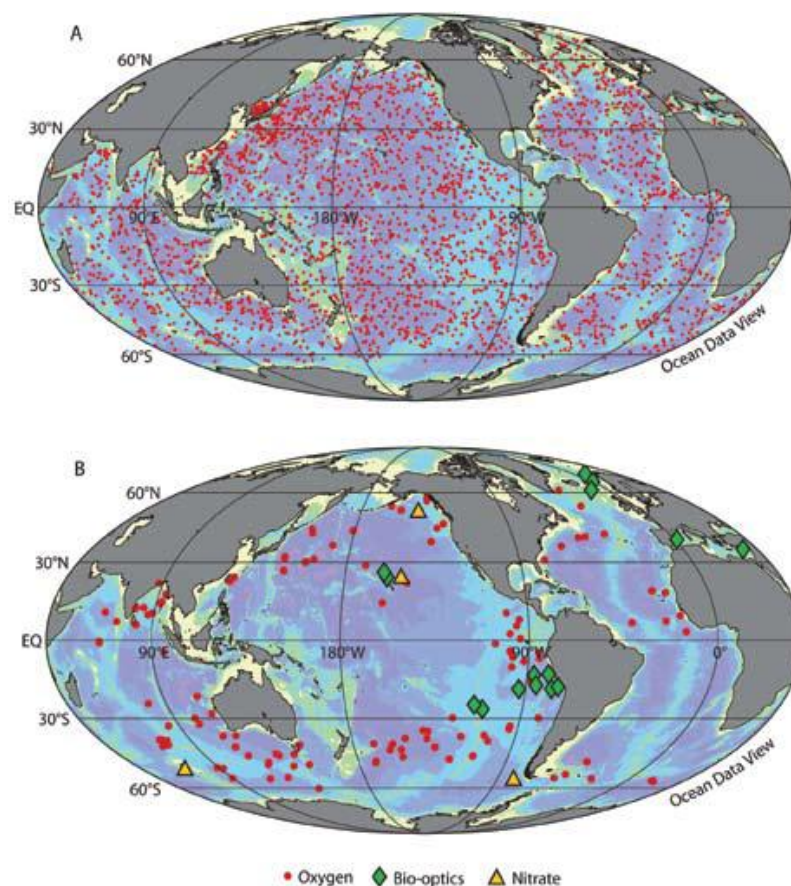
Fig. III. 1.2. a) ARGO floats from June 9-16, 2009 equipped with CTD, b) ARGO floats, from the same period, equipped with biogeochemical sensors (Johnson et al., 2009).

ARGO is a major contributor to the WCRP's Climate Variability and Predictability Experiment (CLIVAR) project and to the Global Ocean Data Assimilation Experiment (GODAE). The ARGO array is part of the Global Climate Observing System/Global Ocean Observing System GCOS/ GOOS. There are about 3000 of these floats in the ocean (Roemmich et al., 2004, 2009, 2012) equipped with typical physical sensors whereas the same floats equipped with biogeochemical sensors (to measure oxygen, chlorophyll and nitrate) are a few hundred in number. The next step will be to increase the number of biogeochemical sensors adapted on ARGO floats.

Other observation systems are developed intensively as well: autonomous vehicles, permanent stations situated at ocean bottom (landers), moorings, drifters, profiling floats (gliders). Together, satellite and ship-based data gives us the possibility of ocean monitoring at different spatial and temporal scales (Figure III. 1.3).
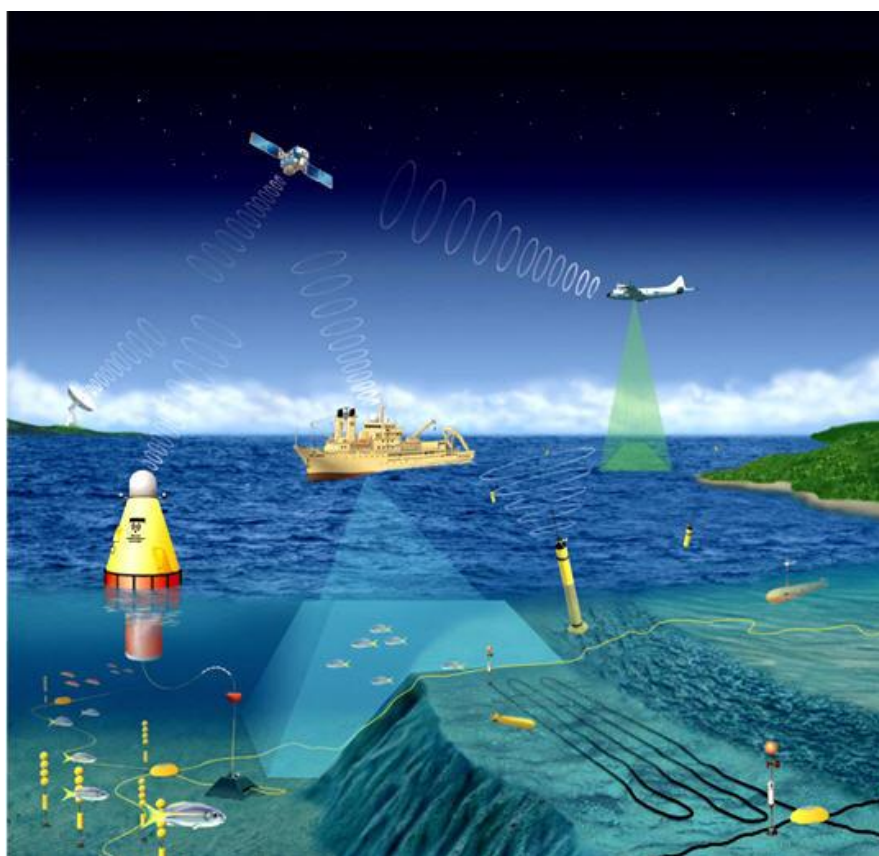
Fig. III. 1.3. The integrated ocean observations (www.oceanleadership.org).

2. Sensor characteristics for long term ocean monitoring

Ocean observing systems require development of a new generation of sensors that can be deployed on underwater vehicles, on moorings or landers equipped with communication systems to facilitate the collection of oceanographic data. An important step was taken in the last ten years in the development of autonomous sensor networks by the community of chemists and marine environmentalists. The number of the biogeochemical sensors remain below the physical ones but some biogeochemical sensors are now continuously deployed in rivers, lakes, estuaries and in the open ocean. And thanks to networks and modern communication systems, data can be transmitted directly to research centers and then disseminated in near real time via the Internet.

Following the booming development of new sensors and chemical analyzers *in situ* over the past decade, two major works on chemical sensors in aquatic environments have been published (Varney, 2000; Buffle and Horvai, 2000). More recently Johnson et al. (2007) brought together the various networks of chemical sensors in the aquatic environment in a review. Some of the sensors have already been deployed for at least several months and years.

The development of autonomous chemical sensors suitable for the *in situ* measurements in the long term will have to meet a set of rigorous specifications. Indeed, the instrument must be deployed for several months without human intervention. These key features are listed below (Johnson, 2003; Prien, 2007):

- Strength (mechanical, electronic, corrosion resistance ...),

- Protection or strong resistance against biofouling,

- Low power consumption,

- Low cost (when investing and during maintenance),

- High accuracy measurements,

- Low detection limit (adapted to the needs of the study),

- Fast response time (if the device is fitted to a profiling vehicle),

- Lack of reagents or stability of reagents over time (and low consumption of reagents),

- Methods of self-calibration and stability over time,

- Presence of other essentials, such as temperature, conductivity and pressure,

- Reliability, critical factor in field deployments,

- Data transfer (sometimes adapted in real time).

There are a lot of sensors which detect analytes directly, without addition of liquid reagents. Among them, the most often used ones are oxygen and pH sensors. Clark-type sensors are essential to study primary production and metabolism of organisms. They are also essential for oxygen measurement of special ecosystems like the Oxygen Minimum Zones. There are many examples of applications of these sensors on CTD profilers or floats (Figure III. 2.1). pH sensors are essential for measurements of growing acidification of the oceans and its impact on the carbon pump and life of marine organisms.

However, there are many species which are undetectable by direct measurement (ammonium, phosphate, silicate,…). Analyzers have been developed to measure these elements *in situ* but these methods require a set of elements for measuring samples where the detection is done after a chemical reaction (pump, valves, sensors, electronics ...).
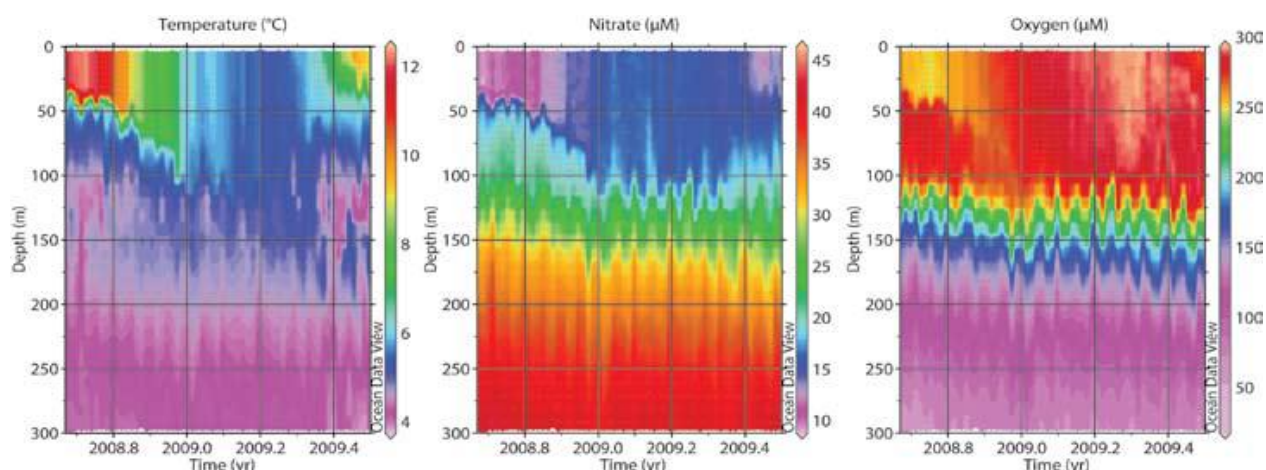
Figure III. 2.1. Temperature, nitrate, and oxygen measured at Ocean Station Papa in the North Pacific (50°N, 145°W) by Apex profiling float 5143, which is equipped with an ISUS nitrate sensor and Aanderaa oxygen optode (Johnson et al., 2009).

3. Sensors for oxygen *in situ* monitoring

The iodometric titration technique (Winkler, 1888) probably represents the oldest and most widely used method for O_2 determination and it is still used with some modifications since the original description (Horstkotte et al., 2010). Techniques such as gasometry, mass spectrometry, and gas chromatography have been employed, but have never become widely

used, and they were not well suited for *in situ* applications. Various polarographic and voltammetric measuring principles have been applied for oxygen sensing (Glazer et al., 2004; Luther III et al., 2008). However amperometric sensors have probably been the most successful within the aquatic sciences and most certainly the most widely applied for *in situ* studies.

Next to the electrochemical sensors, a new generation of sensors was introduced: optodes. The basic principle of O_2 optodes is dynamic fluorescence quenching. In the absence of O_2, the fluorophore absorbs light at a given wavelength and releases the absorbed energy by emitting fluorescence with a defined intensity and lifetime. In the presence of O_2, quenching of the fluorophore appears and results in a decrease of the fluorescence light as well as in the fluorescence lifetime (Fisher and Wenzhofer, 2010).

Generally, two types of amperometric oxygen sensors have been applied *in situ:* Clark-type and gold plated cathode-type microsensors, but the so called Needle-type sensors were also used in the aquatic environment (Figure III. 3.1). The scheme of the sensors is presented in Figure III. 3.2 A-C. The working principle of these sensors is based on measurement of current that is proportional to the oxygen concentration reduced on metal surface kept at fixed potential of -0.8V. The measurement principle is presented in Figure III. 3.2 D.

Characteristics of the amperometric sensors are presented in Table III. 3.1. The main advantage of the Clark-type and gold plated cathode-type microsensors is the small size of their sensing tip. This allows measurements at small spatial and temporal scales. Besides, microscale sensors improve the signal stability as compared to macroscale sensors, and reduce the response time and analyte consumption rates. However, the gold plated cathode-type microsensors are generally more sensitive to stirring than Clark-type ones, because of their close distance between the cathode and the bulk water (the gold cathode is plated on membrane). Additionally the gold plated cathode-type and Clark-type microsensors are fragile to mechanical shocks. The tip size can be increased like in the needle-type sensors. This leads also to an increase of the signal size, but the sensor consumes an important quantity of oxygen (thus it requires a stable flux of this analyte to the tip). Therefore, the sensor is sensitive to stirring and gives a longer time response. The choice of the most appropriate sensor depends on its properties for a given task. For example, in benthic studies, stirring sensitivity and low

analyte consumption rate will be crucial for data interpretation and thus rather small tip size sensors will be preferred.

It is worth noticing that all discussed amperometric sensors have a membrane to provide chemical and physical shielding from the environment. The membrane allows oxygen to penetrate but also some ions can pass through it to make the sensor electrically conducting and this can cause several interferences. Many membranes have been used (silicone, DPX, cellulose acetate, acrylic polymers etc.) with different parameters (adhesion, mechanical stability, permeability towards oxygen and various electrolytes) and the optimal membrane for a given application has to be carefully evaluated and selected.

Fig. III. 3.1. Clark-type (up) and needle-type (dawn) amperometric sensors from UNISENSE (www.unisense.com)

Table III. 3.1: Characteristics of three types of oxygen amperometric sensors applied for in situ interface studies (In situ monitoring of aquatic systems, edited by Buffle and Horvai, 2000).

	Sensor		
	Micro-cathode*	Micro-Clark	Needle-type
Tip size (μm)	0.2–5	1–10	600–800
Stirring sensitivity (%)	2–50	0–2	5–50
90% Response time (s)	0.1–2	0.5–2	60–120
Detection limit (μmol L^{-1})	0.1	0.1	1
Signal size at air saturation (pA)	100–200	50–200	5000
Main interference	Mg^{2+}, Ca^{2+}, H_2S	H_2S	Mg^{2+}, Ca^{2+},
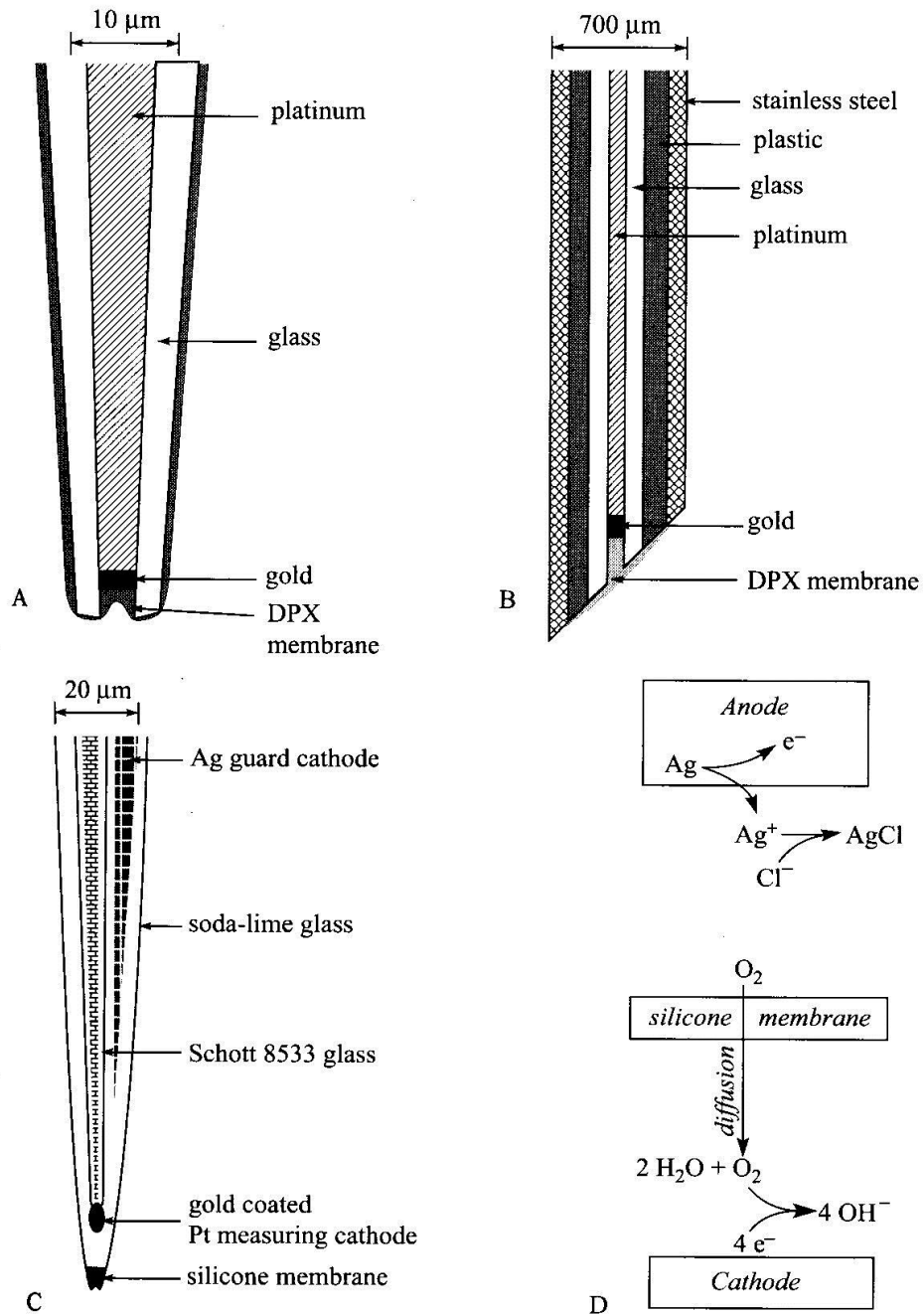
Fig. III. 3.2. The basic structure of gold plated and DPX-coated cathode-type sensor (A), The tip zone of the needl-type DPX-coated cathode sensor (B), The tip of the Clark-type oxygen microelectrode (C), Schematic drawing of the measurement principle (Buffle and Horvai, 2000).

3.1. Clark-type oxygen microsensor

In the following pages, the characteristics of the Clark-type microsensor will be discussed. This discussion is important, if we are to understand the function of the STOX sensor, which is in fact an improved Clark-type microsensor.

3.1.1. Construction and functioning

The Clark-type microsensor consists of a metal cathode and Ag/AgCl anode which acts like a reference electrode. The electrodes are immersed in an electrolyte containing KCl. The sensor is separated from the environment by a membrane. An additional improvement was achieved by an addition of a guard cathode behind the sensing cathode (Revsbech, 1989). This additional electrode reduces oxygen diffused deep inside the sensor from the tip. The sensing and guard electrodes are polarized at -0.8V against Ag/AgCl electrode. The oxygen reduction leads to OH^- formation with an intermediate H_2O_2 (Bucher, 1983). The porous sensing cathode has a large catalytic area which ensures total oxygen reduction and thus a stable signal. At the anode, solid Ag is oxidized (to Ag^+) and precipitates as AgCl (in presence of KCl from the electrolyte solution). The Clark-type microsensor is presented in Figure III. 3.2 C with a principle of measurement in Figure III. 3.2 D.

The signal measured at the sensing electrode depends on many parameters: the geometry of the sensor, solubility, diffusion coefficient (and thus temperature and salinity), and membrane permeability. Therefore, the signal measured (Si) on the sensing electrode can be described by diffusion theory (equation III. 3.1) (Gundersen et al., 1998, Crank, 1989). In this theory, a few assumptions were made: a) the sensor tip is conical and it can be described by three radii, the length of silicone membrane, and the distance between membrane and cathode surface, b) the oxygen concentration at the outer silicone membrane surface is equal to the concentration in the bulk water phase (true only for the sensor with low stirring sensitivity) c) the oxygen concentration on cathode is zero (as it is the case after short polarization period).

$$\text{Si} = \Phi \pi r_1 p_w \left(\frac{Z_m}{r_2 \Psi} + \frac{Z_e}{r_0 D_e S_e} \right)^{-1} \qquad \text{(III. 3.1)}$$
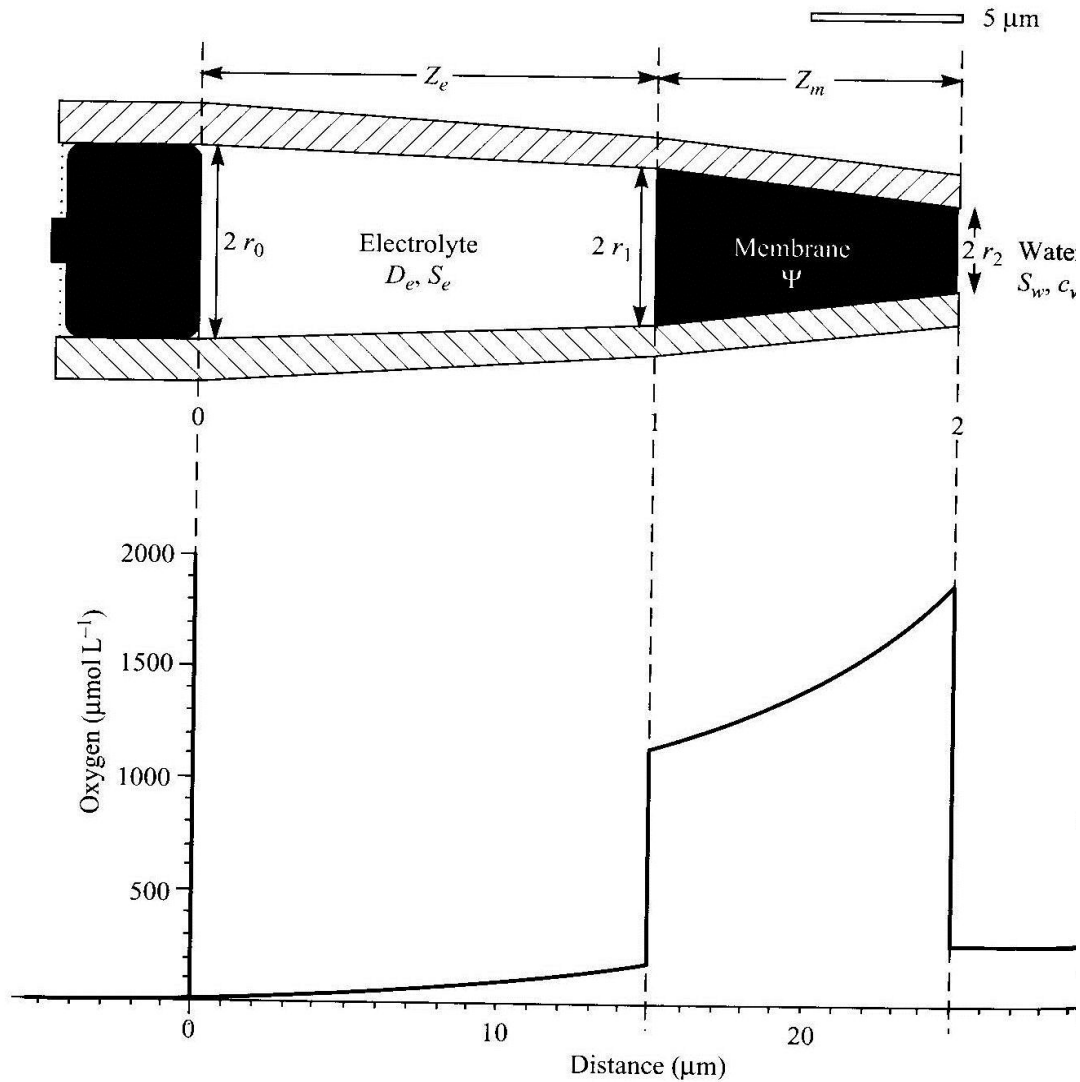
Fig. III. 3.3. The tip of a Clark-type microelectrode described like in equation III. 3.1. (Gundersen et al., 1998)

The geometry of the sensor is given by r_0, r_1, r_2, Z_m and Z_e (Figure III. 3.3.) and can be determined by microscopy. Thus r_0, r_1, r_2 are the internal sensor radii at the cathode, inner and outer position of the silicone membrane, respectively (m), Z_m and Z_e are the lengths of the silicone membrane and electrolyte distance respectively (m), p_w is the partial oxygen pressure in the ambient water (Pa), D_e is the oxygen diffusion coefficient in the electrolyte ($m^2 s^{-1}$), S_e, S_w is the oxygen solubility in the electrolyte or in the water sample (mol L^{-1} Pa^{-1}), Φ is the current generated per mole of oxygen reduced (3.86×10^{-5} A s mol^{-1}), Ψ is the oxygen permeability of the silicone membrane (11.2×10^{-15} mol m^{-1} Pa^{-1} s^{-1}). The S_e and D_e can be

found in gas tables and recalculated for different temperature and salinity conditions. The parameter p_w (partial pressure) is determined by the oxygen concentration and other environmental parameters (temperature, salinity etc.). The model was experimentally validated by comparing the signal from 23 different O_2 microsensors to signals predicted by equation (III. 3.1) and presented in Figure III. 3.4.
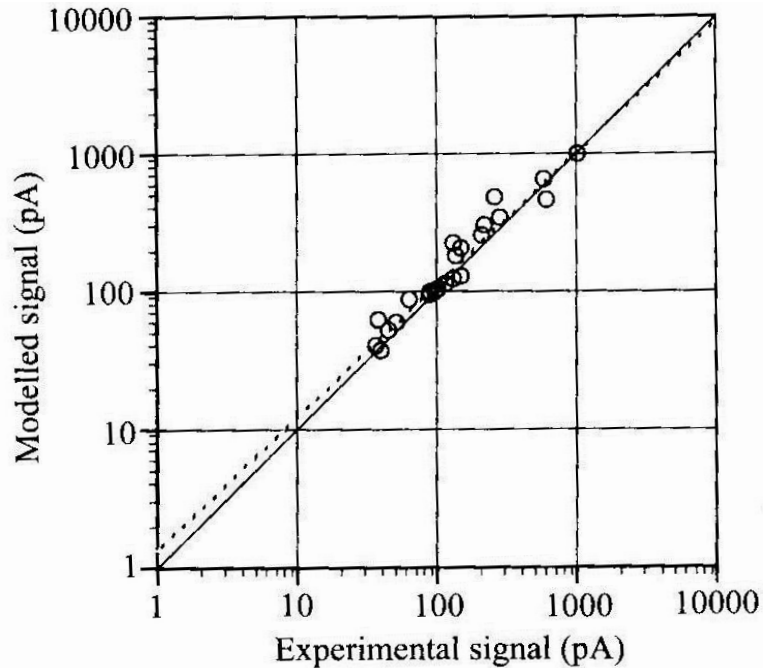
Fig. III. 3.4. The signals of 23 Clark-type sensors as calculated using equation 1 versus experimentally determined values. (Gundersen et al., 1998)

3.1.2. Characteristics of Clark-type sensors

Temperature and salinity effect

The model described above (Section 3.1.1.) predicts sensor behaviour in different conditions. For example the increase of salinity will cause an increase of partial pressure. Since partial pressure is the only parameter affected by salinity, the sensor signal will increase with salinity (Figure III. 3.5 A). The increase of temperature will affect more parameters: partial pressure, membrane permeability and diffusion coefficient will increase whereas the oxygen solubility will decrease. The combined effect will lead to an increase of the signal with temperature (Figure III. 3.5 B). Increasing the relative membrane thickness determined as $(Z_m/Z_e)+Z_m$ will lead to an increase of the signal since the solubility of oxygen is higher in silicone membrane than in water (Figure III. 3.5 C).
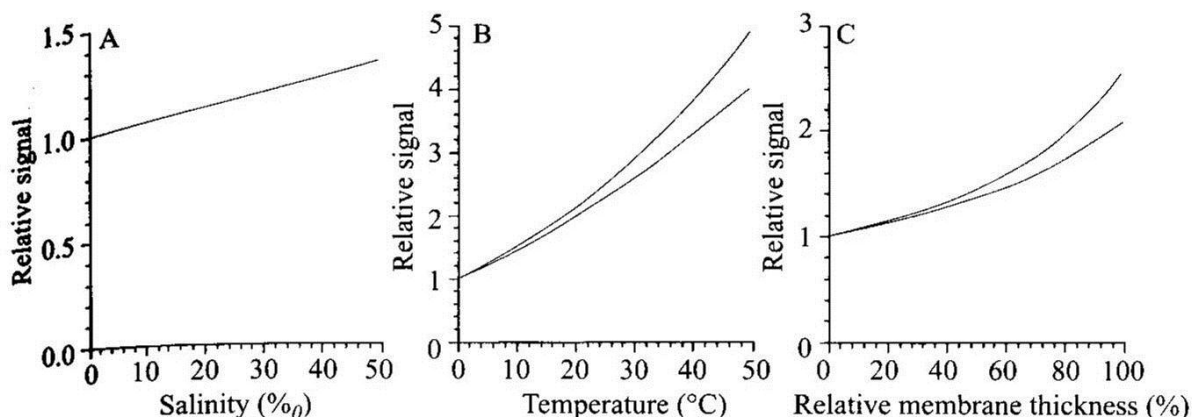
Fig. III. 3.5. Relative signal change as a function of salinity (A), temperature (B) (for relative membrane thickness of 99.9 %-upper line and 0.1%-lower line), relative membrane thickness (C) (in temperature of 50°C-upper line and 0°C-lower line) (Gundersen et al., 1998).

Stirring sensitivity

The Clark-type microsensor consumes oxygen, and thus requires a steady flux of analyte into the sensing tip. This means that the sensor will be affected by the transport of analyte in the surrounding medium-the so-called "stirring sensitivity". It is a very important parameter, since the moving of the tip sensor from the free flowing water to the stagnant interstitial water of the sediments will cause a signal decrease due to the decrease of oxygen transport rate.

The model predicts that a low stirring sensitivity can be achieved by using relatively thick membranes and a small sensor opening and pulling the cathode back from the sensor opening. This will increase the response time. Some commercially available sensors are equipped with stirred measuring chambers or flow-through systems.

Stability and lifetime

The drift of the Clark-type microsensors was found to be 2% over 25 days (Buffle and Horvai, 2000). It is due to changes in temperature and pressure. It can be calculated from equation (III. 3.1) that a signal change of 2% can be the result of 1°C temperature change.

The lifetime of the microsensor is from months to years unless they are mechanically damaged or poisoned by interfering species (Kühl and Revsbech, 2000).

Possible interference

For the Clark-type microsensors with hydrophobic membranes (like silicone) the only major interfering species is hydrogen sulphide, H_2S, which can pass the gas-permeable membrane and interfere with the electrochemical reactions of the sensor. The result is usually the increase of the signal at the beginning of the measurements but after some time sulphur-metal complexes may be formed and precipitated on the membrane and cathode and thus they may decrease the signal (Hale, 1983). It is worth noticing that, in the oldest cathode-type micosensors, a hydrophilic membrane was used and sensors were poisoned also by Ca^{2+} and Mg^{2+} due to precipitation of hydroxides and carbonates on the cathode and membrane (Revsbech and Jorgensen, 1986). The result is a non-linear and a drifting calibration curve.

Spatial and temporal resolution

Spatial resolution is highly dependent on the sensor tip size. It is assumed that the spatial resolution of a sensor is of the order of twice the outside tip diameter. Since the Clark-type microsensor tip can be made small, down to 1-10 μm, the spatial resolution is more than sufficient for many practical purposes (Revsbech and Jorgensen, 1986). On the other hand, sensors of greater size like the needle-type one with big tip diameters (600-800 μm) will have lower spatial resolution and their high oxygen consumption rates will cause local distortion of the oxygen gradient.

The response time of Clark-type sensor can be as fast as 0.5s and this guarantees sufficient temporal resolution. To achieve a sensor with such a short response time, the distance between the cathode and the bulk water should be limited but we should consider also the fact that this modification will increase the stirring sensitivity. Thus, construction of such a sensor requires a very skillful constructor.

3.2. STOX sensor as an improved Clark -type sensor

The modifications of Clark-type microsensors led to develop the STOX (**S**witchable **T**race amount **OX**ygen) sensor where oxygen can be determined at very low (nM)

concentrations (Revsbech et al., 2009). Thus characteristics of Clark-type microsensors presented above are applicable for the STOX sensor.

3.2.1. Construction and principle of functioning

The STOX sensor construction is based on Clark-type microsensors; one inside the other as presented in Figure III. 3.6.
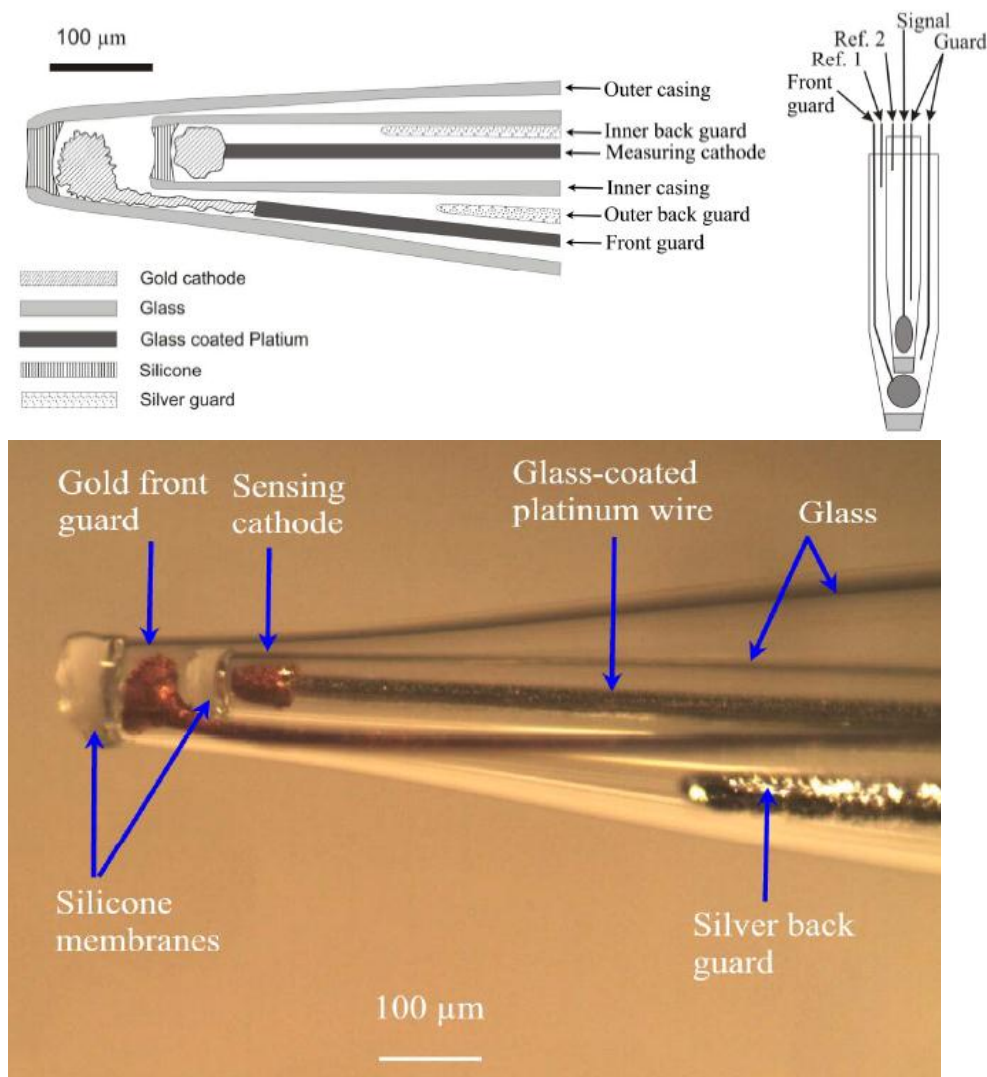
Figure III. 3.6. Schematic drawing of STOX microsensor tip with a diagram on the right showing all anodes and cathodes in a STOX sensor (up), For clarity of the drawing, reference electrodes do not appear on the left schematic. They are shown on the right schematic. Photography of the microsensor tip made under microscope (down) (Revsbech et al., 2009).

94

There are 6 electrodes: two gold cathodes (one sensing electrode called inner cathode and one front guard electrode called outer cathode), two anodes which act as reference electrodes Ag/AgCl/KCl 1M and two silver back guard cathodes. The electrodes are immersed in glass casings with thin tip and protected from the environment by silicone membrane. The outer cathode is made porous, so that oxygen can pass through a gold matrix into the inner cathode when the gold matrix is depolarized. When polarized at about -0.8V, the gold matrix of outer cathode will reduce the incoming oxygen and very little of the oxygen will reach the sensing cathode. This arrangement enables *in situ* zero determination.

On the anodes which act like reference electrodes, oxidation of silver to silver cations is present in buffer containing KCl solution and thus the precipitation of AgCl salt appears.

The non-reduced oxygen (which diffuses deep to the sensor from the tip area) is eliminated by silver back guard cathodes which are kept at a stable potential of -0.8V.

3.2.2. Sensor characteristics

Sensor signals achieved during calibration are presented in Figure III. 3.7. The low signals at the beginning are due to a small amount of oxygen being present in spite of deoxygenation of water under nitrogen. Typical STOX sensor signals are due to repetitive changing polarization of the outer gold cathode. When the outer gold cathode is polarized, the current reading on the sensing cathode is close to zero. When the cathode is depolarized, the oxygen can pass through the outer gold cathode to be reduced on the inner. The current is proportional to the amount of diffusing oxygen.

It is worth noting that the current on the sensing electrode is never zero pA when the front guard cathode is polarized. This means that some oxygen can pass to the sensing cathode. It was found that a front guard electrode consumes only 98.3 % of incoming oxygen. Thus the useful signal can be achieved by calculation of the difference between the signal on the inner gold cathode measured when the front guard electrode is off and then on.

The detection limit was found to be as low as 1-2 nmol L^{-1}, the sensor gives a linear response in the concentration range of 2-1000 nmol L^{-1}. The response time is about 1-2 minutes and a signal drift of 2% was noticed during the first day of sensors working. This sensor was validated during a number of oceanographic cruises offshore Peru and showed

excellent improvement on sensitivity for low oxygen concentrations in the Oxygen Minimum Zone layer as compared to other amperometric sensors. The sensors are currently used for analysis of oxygen consumption rates (Revsbech, com. pers.).
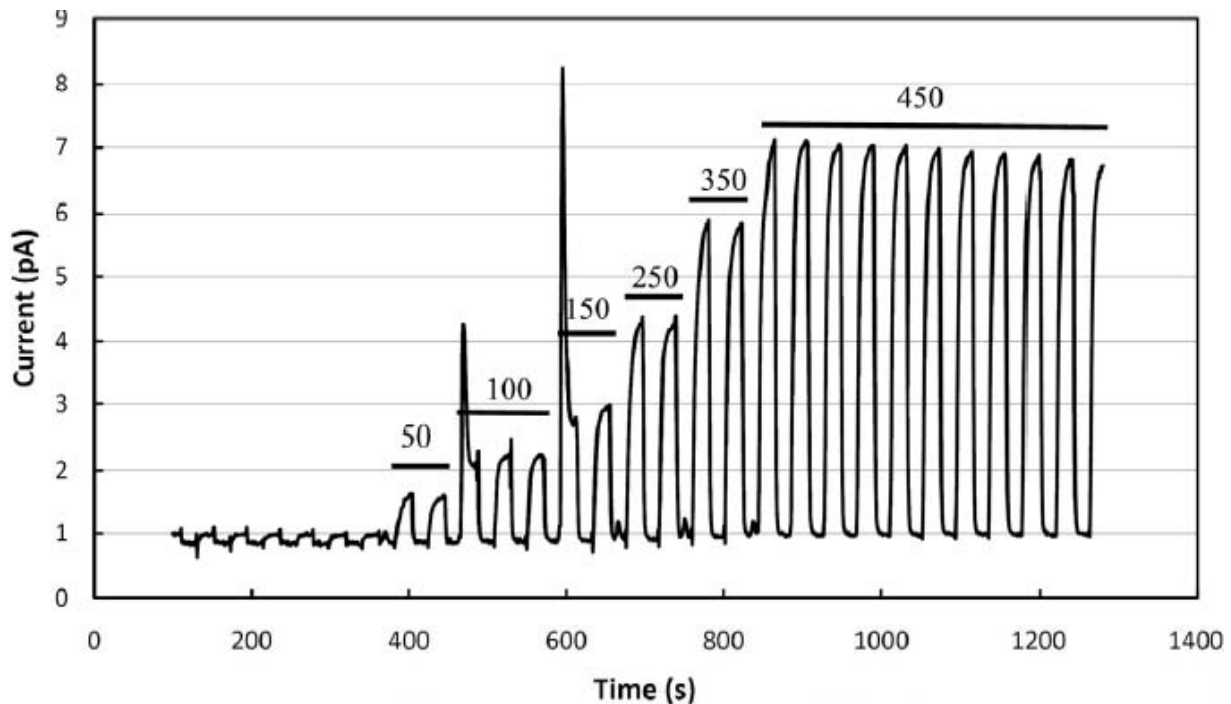
Fig. III. 3.7. Sensor signals during calibration of a STOX sensor (Revsbech et al., 2009).

3.2.3. *In situ* applications of STOX sensor

One of the first *in situ* uses of the STOX sensor took place in the Oxygen Minimium Zone off shore Peru and Chile (Revsbech et al., 2009) during the Danish Galathea 3 Expedition in February 2007. For *in situ* use, the STOX sensor has to be protected from the environment. Thus, electronics were housed into a light metal alloy cylinder that was designed to resist external pressure of 600 atm. The cylinder also housed a timer that could be programmed for continous shifts between front guard polarization/depolarization with variable intervals. The rear end of the electronics cylinder was equipped with a cable that allowed interfacing with the Seabird CTD (Figure III. 3.8). The STOX sensors were interfaced with the electronics cylinder by use of a custom-built Plexiglas sensor holder with oil pressure compensation as described by Reimers and Glud (2000) (Figure III. 3.9, III. 3.10).
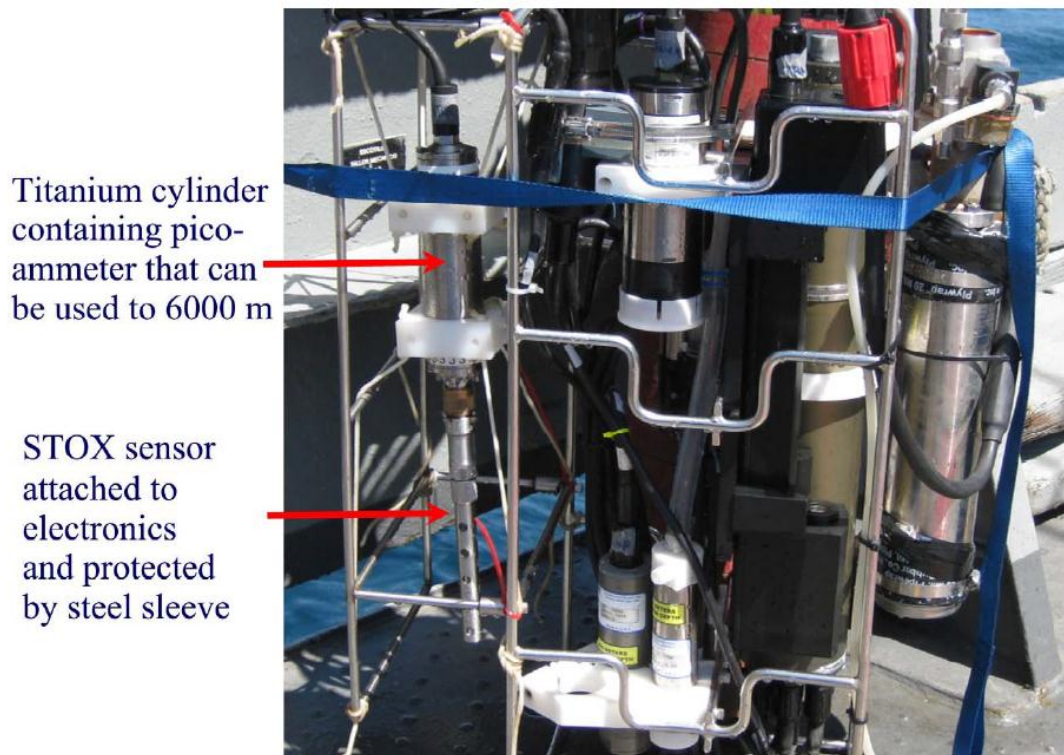
Fig. III. 3.8. In situ application of the STOX sensor (Revsbech, com. pers.)
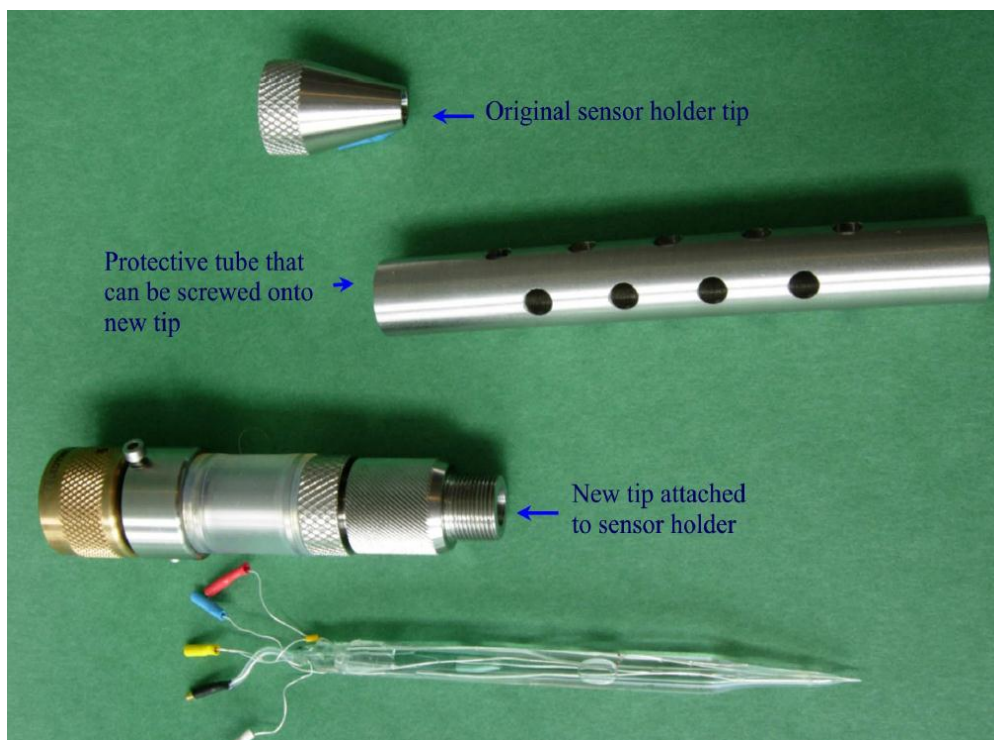
Fig. III. 3.9. STOX sensor, sensor folder and protective tube for in situ applications (Revsbech, com. pers.)
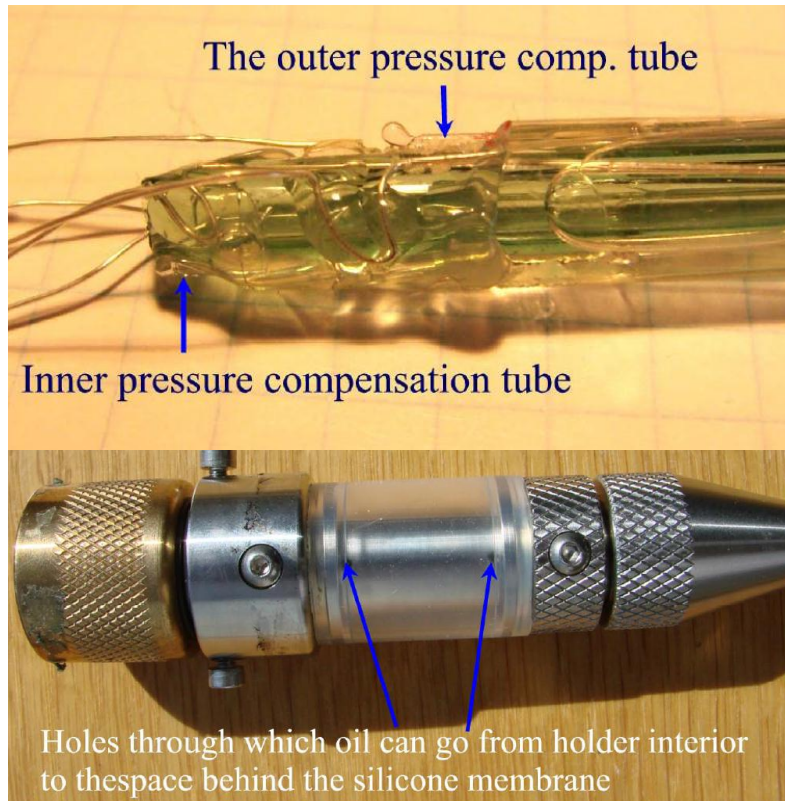
Fig. III. 3.10. (upper) STOX sensor with compensation tubes, (down) sensor holder (Revsbech, com. pers.).
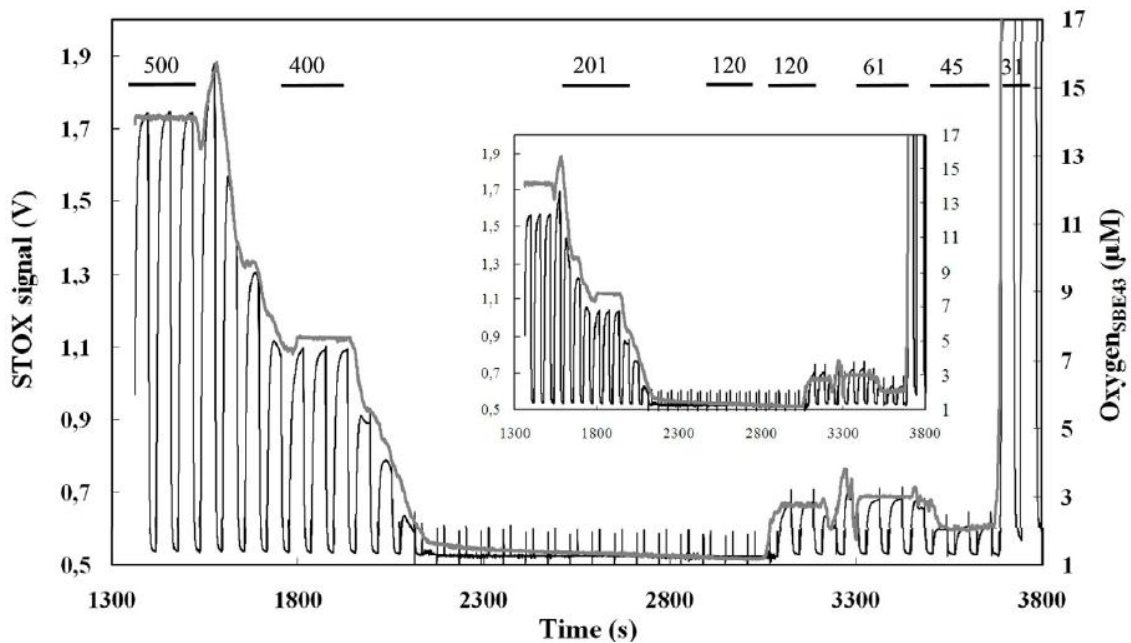
Fig. III. 3.11. STOX microsensor (black line) and Seabird oxygen sensor (grey line) signals in the OMZ off Peruvian cost at depths varying from 500 to 31 m (Revsbech et al., 2009).

Oxygen profiles were measured by the STOX sensor at 26 OMZ CTD stations with a maximum deployment depth of 1000 m. Data from one CTD station are presented in Figure III. 3.11. There is a good corelation between the Seabird oxygen signals and STOX signals.

3.2.4. Advantages and disadvantages

The traditional STOX sensor for measurements of ultra-low oxygen concentration has a lot of advantages. The sensor has very low detection limit (1-2 nmol L^{-1}) which makes it very suitable for measurements of ultra-low oxygen concentrations in Oxygen Minimum Zones. The sensor is thus essential to scientific questions like respiration rates, anoxia, and denitrification. Thanks to *in situ* zero calibration there is no need of frequent sensor calibration. The sensor is also small and thus has small area for colonization (biofouling). Besides, the sensor is easy to operate; it has a high degree of signal stability and extremely high resolution (2-1000 nmol L^{-1}). However, the sensor has some disadvantages (fragility and quite long response time). To overcome some disadvantages, work through a new method for gold electrode production was done within my PhD programme.

Nowadays, electrochemical deposition of gold on the platinum electrode is used to form porous gold electrodes as described by Revsbech et al. (2009). The method is fast and simple but sometimes the outer gold cathode collapses and pushes the membrane out. Plating of gold on the silicone membrane can overcome this problem. Besides, a thin layer of gold on the membrane instead of a gold ball will give us the possibility to place the inner casing closer to the outer cathode and consequently, make the sensor work faster and increase its sensitivity (but in the same time, the sensor can be more sensitive to stirring). The technique has been already applied. For example a porous film of Pt was deposited on a Nafion membrane by reduction of $PtCl_6^{2-}$ with hydrazine (Bard and Fauklner, 2001).

A faster response can be achieved also by having thin silicone membranes and also by having the outer back guard electrode very close to the tip of the inner sensing electrode. A smaller opening of the sensor will also result in a faster response time and a lower stirring sensitivity, but it can result in a decrease of the signal.

3.3. Optical vs. amperometric microsensors

A range of oxygen sensors is now available for *in situ* applications (Table III. 3.2). For water column studies instrument packages such as CTD capable of carrying electrochemical oxygen sensors, like the SBE 43 (Sea-Bird Electronics, Inc.), have been used from many years. For *in situ* monitoring of oxygen in the sediments, microprofilers with mounted sensors are used. Clark-type electrodes are widely used (www.unisense.com), but optodes have potential advantages for *in situ* research (Fischer and Wenzhofer, 2010). In both cases, the oxygen detection is possible thanks to two-point calibration (0% and 100% air saturation). The fluorescence signal to oxygen ratio is not linear, and an optode is most sensitive at low oxygen concentration meaning the sensitivity decreases as oxygen concentration increases following the Stern-Volmer relationship. On another hand, no oxygen is consumed and hence the fluorescence sensor is insensitive to stirring. The problem of stirring does not exist in electrochemical sensors today. Clark-type sensors can be made very small with a tip size of 10 μm. The oxygen consumption of such a microsensor is so small that it is practically insensitive to stirring. However, small and thin glassy tips of the Clark sensor are very fragile and it is quite easy to destroy them during monitoring of sediments or in highly pressure characterized deep waters. In addition, the hydrophobic membrane is sensitive to H_2S, which can pass though the gas-permeable membrane and interfere with the electrochemical reactions in the sensor. The result is usually a drift of the signal. This problem does not appear in the optode sensors. The oxygen quenching is extremely specific for $Ru(diph)_3$-PS-based optodes and interferences from for example CO_2, pH, H_2S and heavy metals have not been detected. The electrochemical sensors are relatively cheap, small, and simple and give a linear response in a wide range of concentrations. Even now the oxygen detection in the Oxygen Minimum Zones is no longer a critical issue thanks to the very sensitive STOX sensor (Revsbech et al., 2009).

Table III. 3.2. In situ amperometric sensors and optodes for oxygen monitoring in seawater

Name/ Sensor type	Laboratory/ Society	Outside tip Diameter, μm	Stirring Sensitivity, %	Response time, t^{90}	Primary Applications	Literature
Needle – DPX coated cathode sensor	Netherlands Institute for Sea Research	700	5-50	60-120s	Marine sediments	Helder and Bakker, 1985
DPX – coated cathode sensor	Aarhus Univeristy	0.2-2	2-50	0.1-2s	Microbial ecosystems	Revsbech and Jorgensen, 1986
Clark – type microelectrode	UNISENSE, Aarhus University	10	0 – 2	0.3-3s	Sediments, biofilms, microrespiration, wastewaters, cell and tissue analysis	Revsbech, 1989 www.unisense.com
STOX sensor	UNISENSE, Aarhus University	100	7	15s (60s full cycle)	Ultra – low oxygen detection in Oxygen Miniumu Zones, respiration rates	Revsbech et al., 2009 www.unisense.com
Needle – type minioptode	PyroSciense	1100	None	10s (in stirred solution)	Non – précised	www.pyro-science.com
Needle – type microoptode	PreSens	50	None	2s	Sediments, biofilms, microrespiration, cell and tissue analysis	www.presens.de
Planar optode	Max Planck Institut, MPI	-	None	5-10s	Sediments, mats, biofilms, photosynthesis	Fischer and Wenzhofer, 2010

101

4. Methods for phosphate monitoring in seawater

Although only phosphate interests us directly in this study, the three major nutrients (silicate, phosphate and nitrate) used in oceanography have been the subject of this literature search. These three anions are often inseparable and usually analyzed at the same time (Adornato et al., 2009).

4.1. Autonomous phosphate analyzers based on wet chemistry and spectrophotometry

Phosphate analysis in the ocean is generally based on traditional shipboard sampling techniques with subsequent analysis either on board or in a shore-based facility. Most *in situ* analyzers use wet chemistry like ANAIS (Thouron et al., 2003) or NAS 3-X (www.n-virotech.cim), etc. They are able to work 1-2 months without human intervention and are capable of the simultaneous determination of phosphate, silicate, nitrate and nitrite. Such analyzers provide also a good accuracy but require addition of reagents. The drawback of these techniques is also their large size and weight. New technologies are developed now, but no autonomous, reagentless sensor for phosphate detection exists nowadays. Within a wide range of techniques, electrochemistry can be a promising tool to go further in miniaturization, decrease in response time and energy requirements. The purpose of my PhD project was to use electrochemical methods for the development of *in situ* sensor for phosphate detection in sea water.

4.1.1. Principle of phosphate measurements

The analysis is performed using the method of Murphy and Riley (1962) adapted by (Strickland and Parsons, 1972). Molybdic acid is formed by conversion of ammonium heptamolybdate in acidic medium (reaction III. 4.1). The phosphate in reaction with molybdic acid forms a phosphomolybdate complex which absorbs yellow in the UV (reaction III. 4.2):

$$(NH_4)_6Mo_7O_{24}, 4H_2O + 6H^+ \rightarrow 7(MoO_3, H_2O) + 6NH_4^+ \qquad \text{(III. 4.1)}$$

$$PO_4^{3-} + 12MoO_3 + 3H^+ \rightarrow H_3PMo_{12}O_{40} \qquad \text{(III. 4.2)}$$

$$PMo^{VI}_{12}O_{40}{}^{3-} + 4e \rightleftharpoons PMo^{V}_{4}Mo^{VI}_{8}O_{40}{}^{7-} \qquad \text{(III. 4.3)}$$
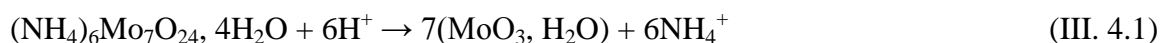
The phosphomolybdate complex (the oxidation state of molybdenum is VI) is reduced using ascorbic acid (III. 4.3). This gives a blue complex with molybdenum in an oxidation state between V and VI. This complex has an absorption maximum at 882 nm. The measurement is also possible at 715 nm but with a loss of sensitivity. The concentration can be found by measurements of absorbance which is directly proportional to the concentration as described by Lambert-Beer's law:

$$I = I_0 \, e^{-\alpha \, l \, C} \qquad \text{(III. 4.4)}$$

$$A_\lambda = -\log_{10} \frac{I}{I_0} = \varepsilon_\lambda \, l \, C \qquad \text{(III. 4.5)}$$

With I_0-intensity of excitation light, I-intensity of light output, I / I_0-transmittance of the solution, A-absorbance or optical density at a wavelength λ, ε-molar extinction coefficient (in mol^{-1} cm^{-1}); l-optical path length traversed in the solution, it corresponds to the thickness of the vessel used (cm); C-molar concentration of the solution (mol L^{-1}), α-absorption coefficient (m^2 mol^{-1} or m^3 mol^{-1} cm^{-1}).

The absorption measurements required the use of spectrophotometers. The very simple schematic of a spectrophotometer is presented in Fig. III. 4.1. Today, spectrophotometers with simple measurements using cuvettes are still performed but methods coupled with flow-injection apparatus are preferable.
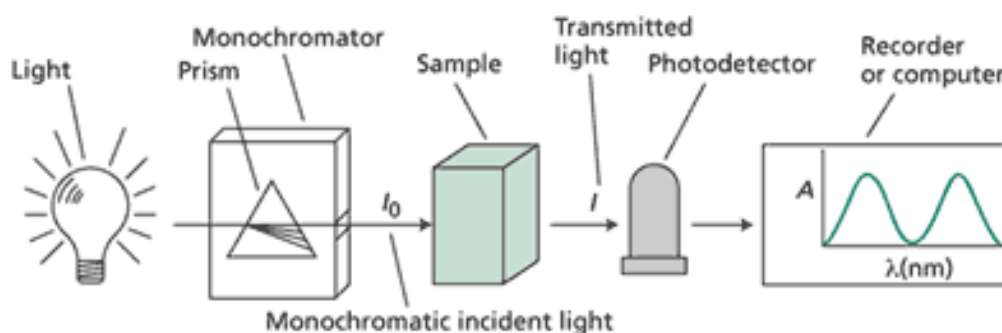
Fig. III. 4.1 . The schematics of spectrophotometer.

Arsenate and silicate form the same type of complex which can be a source of interferences. However, normally arsenate concentrations are very small as compared to phosphate and do not exceed 0.03 μM in seawater. Thus, the influence of arsenate on phosphate detection is negligible. On the other hand, silicate concentration is much higher in the ocean and without special treatment can cause a significant interference. To avoid silicate interferences, the ratio of protons over molybdates H^+/Mo and pH of solution should be in range 60-80 and 0.4-0.9, respectively (Drummond and Maher, 1995).

Some fractions of particulate phosphorus (included in phytoplankton or mineral) react like dissolved phosphate. For this reason, the procedure of analysis for nutrient rich coastal waters must be preceded with the removal of particles by filtration or centrifugation (Kérouel and Aminot, 1987). Another problem during phosphate sampling is associated with adsorption of phosphate on plastic and glass bottles (especially in brackish waters) and contamination in contact with the skin (Kérouel and Aminot, 1987).

4.1.2. ANAIS-Autonomous Nutrient Analyzer *In Situ*

The chemical analyzer ANAIS developed at LEGOS allows simultaneous measurement of nitrate, phosphate and silicate. This instrument is suitable for autonomous vehicle YOYO, profiler developed by the LODYC (Laboratory of Dynamic Oceanography and Climatology, now LOCEAN laboratory) in the framework of the European MAST III "YOYO 2001: The Voyage of the ocean. The YOYO vehicle passes along a cable stretched between 1000 meters and the surface with a range of 400 up-down cycles. This vehicle is also equipped with several other bio - optical, biological, physical and chemical sensors.

This instrument is autonomous and capable of *in situ* measurements in pressure between 0 and 1000 m depth (Vuillemin et al., 1999; Thouron et al., 2003).

The analyzer ANAIS represented in Figure III. 4.2 is a set of:

1. Three chemical sensors (nitrate, silicate, phosphate) which contain:

   - A manifold where the chemical reaction takes place at a constant temperature maintained between 20 ° and 25 ° C by a heating resistor integrated into the manifold,

   - A colorimeter, integrated into the manifold with characteristic wavelength for the studied analyte,

   - Two clamping plates sealing the manifold and the fixing of pumps (pumps solenoids Lee Co.).

2. A container in which the three sensors mentioned above are fixed.

3. A set of bags for storing reagents and standard solutions.

4. An electronic card for the sensors' control and data storage (1 card for each salt), receiving control commands transmitted by a central brain outside (the YOYO) and data transmission to a central brain outside (one card called master card).

The device offers an analytical measurement reproducibility of about 1%, and very good calibration results similar to those obtained with a Technicon colorimetric chain (conventional laboratory equipment) (Thouron et al., 2003).
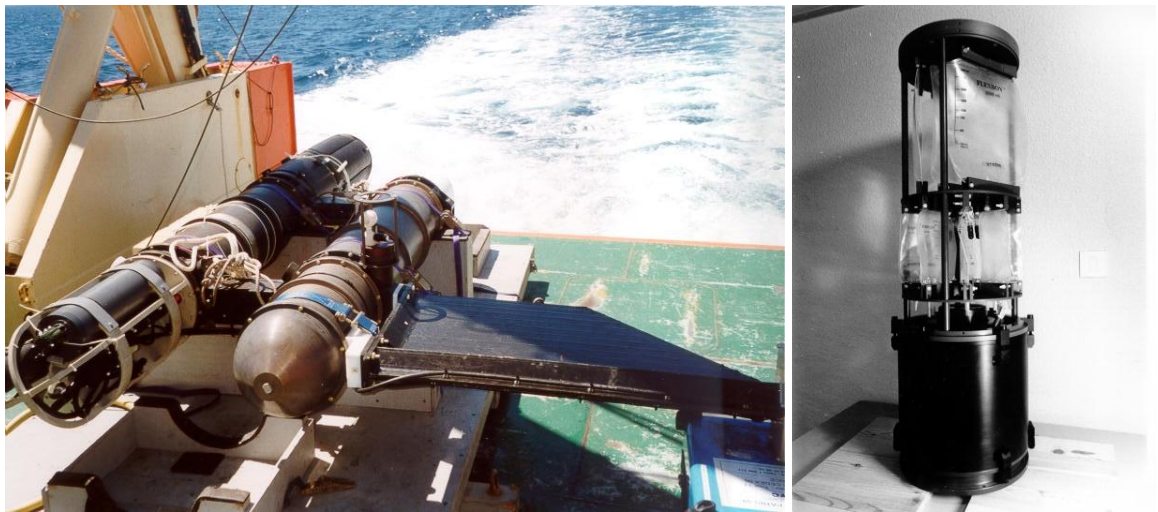
Fig. III. 4.2. ANAIS applied on YOYO vehicle (left), and the container with reagents bags and spectrophotometer (right).

This analyzer (only nitrate) was tested in 2003 off shore Argentina as part of the CLIVAR programme. The scientific objectives were articulated along two axes: 1) to monitor the Malvinas Current transport at 41 °S with a line of current meters on moorings under a track of the satellite altimeter JASON, 2) to study variations and characteristics of Antarctic Intermediate Water in the Argentine Basin. This deployment has yielded a total of 28 profiles of nitrate concentration with two calibrations per profile (80 m and 800 m depth). These results are the first profiles of nitrate concentrations obtained independently at these depths (Figure III. 4.3).
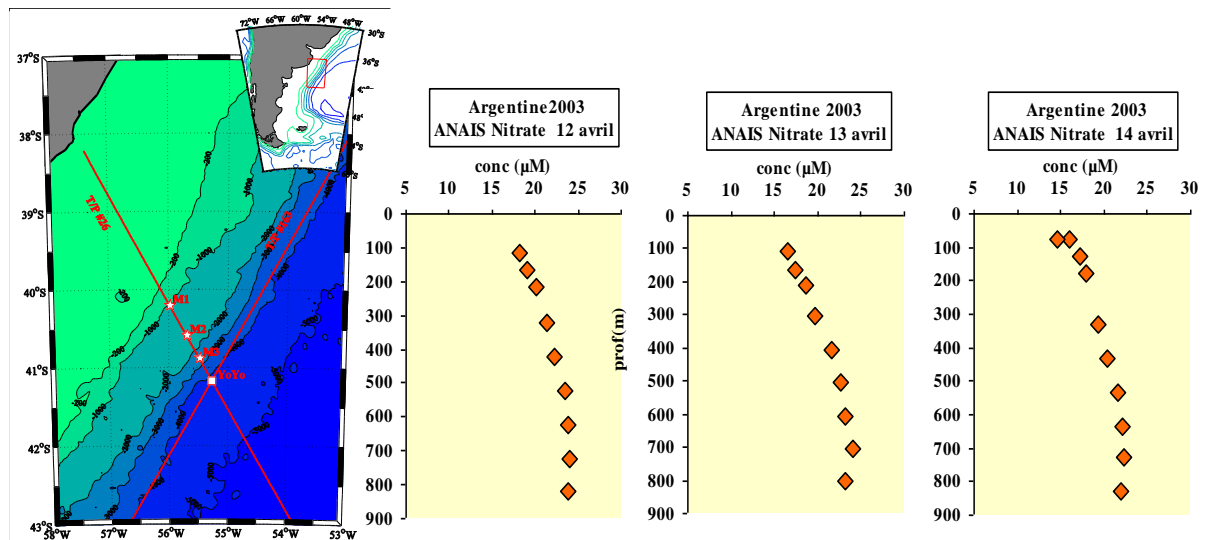
Fig. III. 4.3. Nitrate profiles done in 2003 offshore Argentina (Thouron et al., 2006; Thouron and Garçon, 2006).

The sensor was also deployed at the station SOLA (Service Observing Laboratory Arago) of Banyuls sur Mer in the Mediterranean Sea from 2003 to 2005. The measurements obtained (4 analyses per day) helped to describe the diurnal variability of very low concentrations of nitrate in the area (Figure III. 4.4).
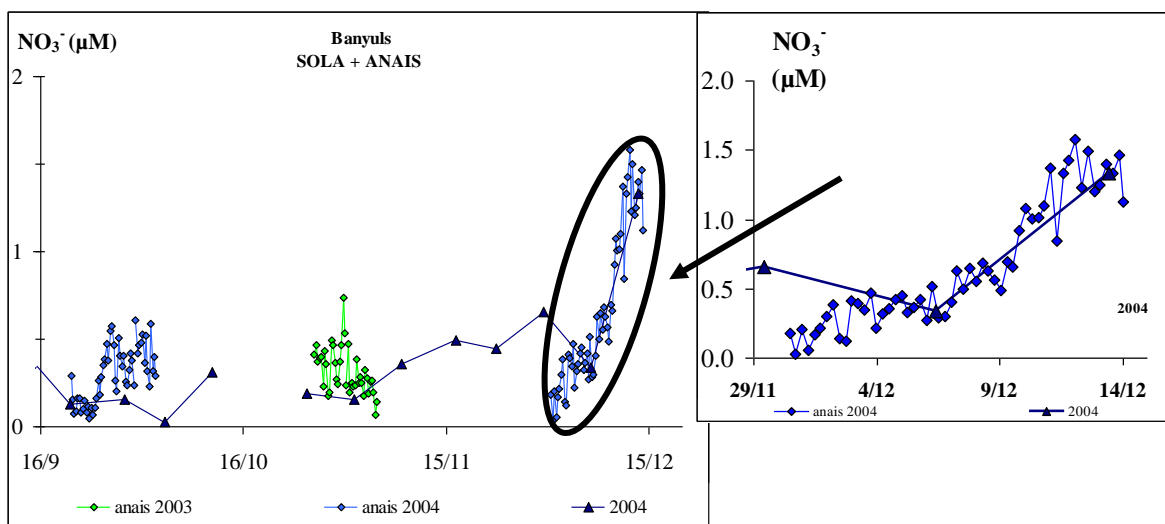
Fig. III. 4.4. Nitrate variability at SOLA station obtained with ANAIS analyser in 2003 and 2004 (Thouron et al., 2006).

4.1.3. Other spectrophotometric analyzers

Many adaptations of classic colorimetric methods for the measurement of phosphate (silicate and nitrate) have been developed for *in situ* analysis. Many of these instruments are now commercially available. The basic principle is an assembly of pumps, valves, manifolds and colorimetric detectors that can be combined to measure multiple analytes simultaneously. The calibration has to be done regulary and thus, bags with standards are needed. Characterization of some phosphate analyzers is presented in Table III. 4.1. The characterization is based on a few parameters like: range of measured chemicals, detection limit for phosphates, size and weight, and application of analyzer.

Both commercial and experimental analyzers are characterized by a good precision (1-3%) and high sensitivity. Detection limit is in the range of 10 to 100 nM. The analyzers can measure simultaneously all salts. Some of them have a possibility of additional measurement of iron or sulphur (CHEMINI, SubChemPak Analyzer). Cycle-PO_4 analyzer is dedicated to phosphate measurements. Most of the analyzers are not resistant to high pressure (except ANAIS and CHEMINI) and can not go deeper than 10-200 m. Most of the analyzers can work autonomously for a few months, but require addition of reagents which can be unstable (ascorbic acid). Globally, they are large and heavy.

The analyzers were deployed in natural waters. However, there are not many examples of phosphate monitoring using these analyzers. Nitrate is the most commonly measured. For example, the *SubChemPak Analyzer* was installed on a winch-deployable, electronic profiling package. The profiling package also included a Sea Bird Electronics Model 25 Sea Logger CTD with modular sensors for the measurement of conductivity, temperature, pressure, dissolved oxygen, pH, chlorophyll fluorescence, and light transmission and irradiance. The analyzer measured iron (II) and nitrate concentration at Providence River (Figure III. 4.5).

The Wet Labs Cycle-PO_4 was succesfully used at three different fixed mooring stations. The field tests were performed during 4 weeks at fixed depth in coastal freshwaters (Clinton River), brackish waters (Chesapeake Bay), and saltwater (Resurrection Bay). Phosphate concentrations at Chesapeake Bay were found in the range of 0.039-0.092 μmol L^{-1}, despite a significant contribution of river water to the site. Phosphate concentrations were higher at the Resurrection Bay (even 0.701 μmol L^{-1}) and the highest in the Clinton River (0.09-3.77 μmol L^{-1}) (Figure III. 4.6). The same analyzer was used on CHARM (**CHA**nnel Island **R**elocatable **M**ooring) mooring at Hawai Ocean Time Series (HOTS)

station in February- March 2004 at depth of 22 m. The phosphate there varied from 0.1 to 0.9 $\mu mol\ L^{-1}$.
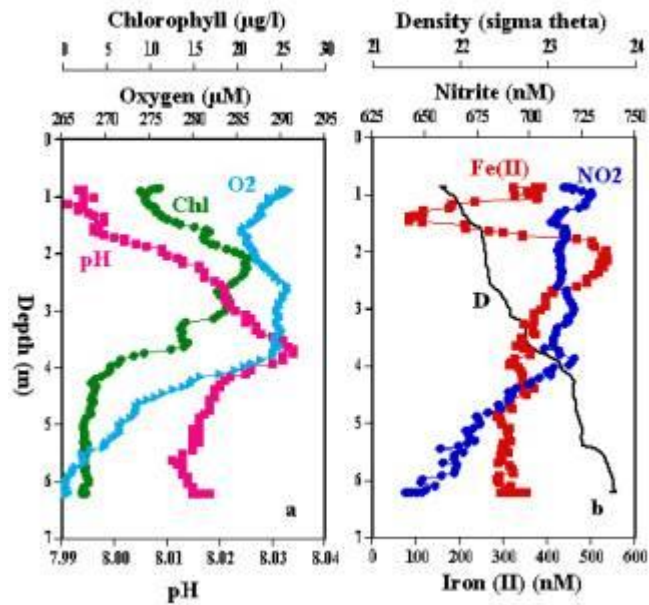
Fig. III. 4.5. Vertical profiles obtained at Station 6 located in the Providence River (http://www.subchem.com/Oceans2000Paper.htm).
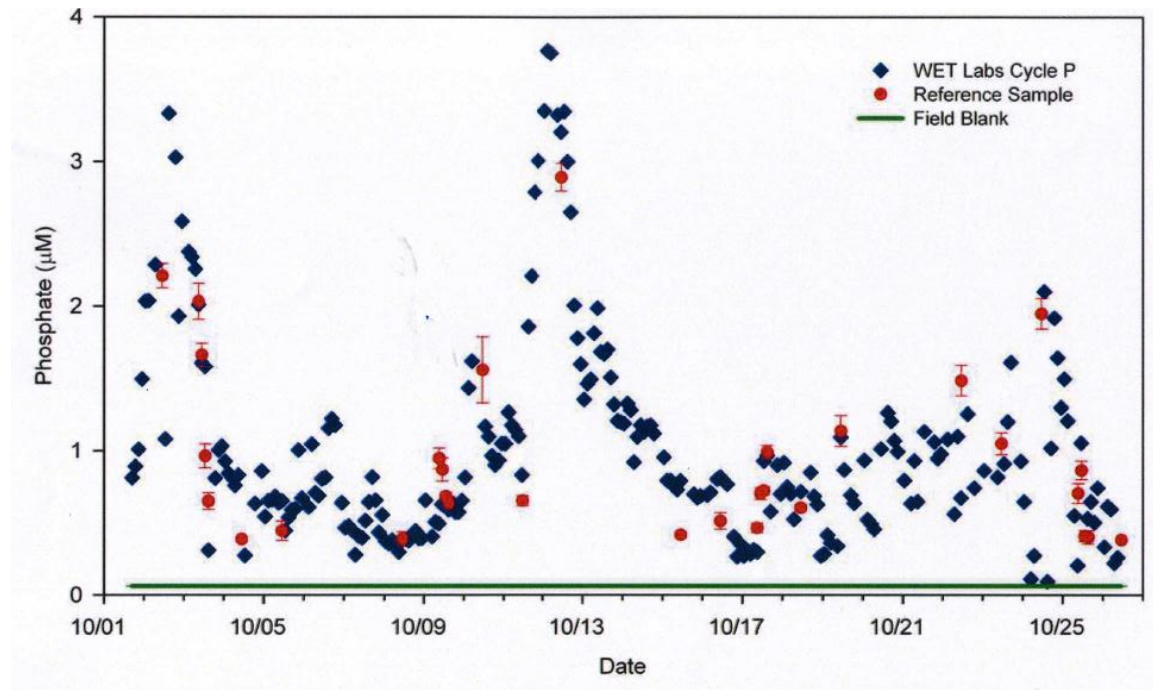
Fig. III. 4.6. Time series comparison of WET Labs Cycle-PO₄ measured phosphate concentrations against laboratory measured reference samples and field trip blanks for the Clinton River, MI moored deployment test (www.wetlabs.com).

Table III. 4.1. In situ analyzers for phosphate detection in seawater, detection limits only for phosphates.

Name	Laboratory/ Society	Detection method	Detected Chemicals	Detection limit	Autonomy	Size, mm	Weight in air, kg	Depth max. m	Applications	Literature
ANAIS (Autonomous Nutrient Analyzer In Situ	LEGOS	FIA colorimetry	$Si(OH)_4$, PO_4^{3-}, $NO_3^-+NO_2^-$,	100 nmol L^{-1}	1 month	320(d)x1000	50	1000	Open ocean, coastal waters	Vuillemin, 1999, Thouron et al., 2003
NAS – 3X MicroLab EcoLab	EnviroTech LLC	FIA colorimetry	$Si(OH)_4$, PO_4^{3-}, $NO_3^- + NO_2^-$,	50 nmol L^{-1}	1-3 months	246(d)x799	27	250	Bays, coastal waters	www.n-virotech.com
DPA/NPA (Deep – sea/ Nutrient Probe Analyer	Systea	colorimetry	$Si(OH)_4$, PO_4^{3-}, $NO_3^-+NO_2^-$,	1 ppb (10 nmol L^{-1})	1 month	320(d)1220	36	10-4500	Open ocean, coastal waters	www.systea.it
APP 4004	Me Grisard Gmbh	colorimetry	$Si(OH)_4$, PO_4^{3-}, $NO_3^-+NO_2^-$,	np	1-2 months	-	8	7	Bays, coastal waters	www.me-grisard.de
SubChemPak Analyzer	SubChemSystems, Inc. /Wet Labs	FIA colorimetry	$Si(OH)_4$, PO_4^{3-}, $NO_3^-+NO_2^-$, Fe	20-50 nmol L^{-1}	-	12(d)x635	6	200	Bays, costal waters	www.subchem.com/ prod0.1.htm
CHEMINI (Chemical Miniutarized Analyzer)	IFREMER	FIA colorimetry	$Si(OH)_4$, PO_4^{3-}, Fe, H_2S, $NO_3^- + NO_2$	np	-	120x140+ 140(d)x264	4	6000	Coastal waters, hydrothermal vents	www.ifremer.fr Vuillemin et al. 2007
Cycle – PO_4	Wet Labs	FIA colorimetry	PO_4^{3-},	75 nmol L^{-1}	1 month	560x180	6.8	200	Bays, coastal waters	www.wetlabs.com

4.2. Alternative phosphate sensing techniques

Other alternative methods for phosphate-spectrofluorimetry do not require addition of molybdate. Some very selective membranes, dyes etc. in contact with phosphates create or change the luminescence signal and thus can be used for quantitative analysis (Nakamura et al., 1997; Lin et al., 2006; Saeed et al., 2010).

The potentiometric analysis of phosphate requires application of ion-selective electrodes (ISE). In these conditions, the water sample does not have to be pretreated. Numerous membranes are being used and are presented in Table III. 4.2. Some of them are dedicated to environmental water analysis but so far no *in situ* application of potentiometric sensors in seawater is described. Several issues affect potentiometric methods: the electrode response is often slow, interferences from other species are very common, and miniaturization is tricky especially because the potential is unstable when the electrode approaches micrometre dimensions. Finally, electrodes require very often calibration, sometimes before and after the measurement of interest.

As an alternative to spectrophotometry, methods based on electrochemistry have also been proposed. Amperometric procedures have been reported for the determination of phosphate as phosphomolybdate complex (Fogg and Bsebsu, 1981; Harden and Nonidez, 1984; Quintana, 2004). Phosphate has been also determined by using voltammetric methods with carbon paste electrode (Guanghan et al., 1999), gold microdisk electrode (Carpenter et al., 1997) and glassy carbon electrode (Matsunaga et al., 1986). Different modifications were proposed to increase the sensitivity or eliminate the interferences from other coexisting molecules. Applications of these methods are proposed in Table III. 4.3 but only a few of them were used for natural analysis of seawater in laboratory conditions. In spite of many advantages of voltammetric or amperometric methods, some serious problems may appear. In particular, electrode surface fouling by absorbing compounds, or oxidation by oxygen are the most important of issues.

Table III. 4.2. Examples of potentiometric sensors for phosphate detection

Literature	Technique	Figures of Merit	Comments
Chen et al. 1998	Potentiometric flow injection detection using a cobalt wire electrode (Co/CoO)	**LOD:** 1 μM **Slope:** 41 mV/decade **R:** 10 μM-5m M	+ The method works the best in neutral pH - Interferences from CO_3^{2-} and HCO_3^- in neutral pH +The interference can be reduced by working in pH 4
Ganjali et al. 2006	Selective membrane based on molybdenum bis (2-hydroxyanil) acetylacetonate complex (MAA) is used	**LOD:** 60 nM **Slope:** 29.5 mV/decade **R:** $0.1-1.0*10^5$ μM	+ The electrode can be used for at least 10 weeks without any considerable divergence in its slope and detection limit + Sensor works the best in pH 8.2 - The silicate interferences are not described
Jain et al. 2006	Polyvinyl chloride (PVC) based membrane with macrocyclic dithioxamide receptor (I) derived from isophtaloyl dichloride and dithiooxamide	**LOD:** 2 nM (0.2 ppm) **Slope:** 29.6 mV/decade **R:** 1.7-1000 μM Response time: 8s	+ The electrode can be used 2 months without showing any significant change in the value of slope or concentration range + Sensor works the best in pH 8 - The silicate interferences are not described
Kivlehan et al. 2007	PVC membrane-based ion-selective electrodes doped with urea- and thiourea-calix(4) arene ionophores	**LOD:** non determined **Slope:**28or33 mV/decade **R:** 50 μM-0.1 M Operation time: 2 months	- The silicate interferences are not described
Zou et al. 2007	On-chip sensor with planar cobalt (Co/CoO) microelectrode on polymer substrate	**LOD:** about 10 μM **R:** 10 μM-10 mM Response time 30-60s	+ Sensor can be mass-produced with very low-cost - The possible interferences are not discussed
Lawal and Adeloju, 2009	Two phosphate biosensors are compared. Purine nucleoside phosphorylase and xantine oxidase were co-immobilised by: a) chemical cross-linking with glutaraldehyde and bovin serim albumin (BSA-GLA-PNP-XOD) b) via entrapment into polypyrrole films by galvanostatic polymerisation (PPy-PNP-XOD-Fe(CN)$_6^{4-}$)	**LOD:** 1 μM (b) 20 μM (a) **Slope:** 46.5 mV/decade **R:** 5 - 25 μM (b) 40-120 μM (a)	The PPy-PNP-XOD-Fe(CN)$_6^{4-}$ is notably superior - The interferences from common water anions and cations were not investigated
Ejhieh et al. 2010	Selective electrode based on surfactant-modified zeolite (SMZ) particles into carbon paste	**LOD:** 12.8 μM **Slope:** 29.9 mV/decade **R:** 15.8-10000 μM Operation time: 3 months	+ The sensor can work in different pH 4-12 - Significant interference from AsO_4^{3-} - The silicate interferences are not described

Figures of merit: LOD-detection limit, R-concentration ranges

Table III. 4.3. Examples of voltammetric and amperometric sensors for phosphate detection

Literature	Technique	Figures of Merit	Comments
Fogg and Bsebsu 1981	**Differential pulse voltammetry** at carbon electrode for determination of phosphate as molybdovanadophosphate at carbon electrode	Detection at 10^{-7} M levels	The work described also procedures for silicate, arsenate and germanate analysis but no interferences study was done
Carpenter et al. 1997	**Voltammetric** methods for phosphate detection as a phosphomolybdic complex at gold microelectrode	**LOD:** - **R:** 1-1000 μM	+The work described also procedure for silicate + The possibilities for avoidance of silicate interference are discussed - Method was not applied in seawater analysis
Tanaka et al. 2001	**Adsorptive voltammetric** at a glassy carbon electrode (reoxidised of the preadsorbet heteropoly blue)	**LOD:** 0.3 μg/L **R:** 0.3-30 μg/L	-Interferences from arsenates
Yao et al. 2003	**Bioamperometric** flow-injection analysis	**LOD:** 0.25 μM **R:** 0.5-800 μM	+ 30 samples/h + Simultaneous determination of orthophosphate and total phosphates + Highly selective to sulphate, nitrate, chlorate etc. but no description about silicate interferences -The method was not applied for natural samples
Quintana et al. 2004	Reduction of phosphomolybdic complex at carbon electrode at 0.3 V (**amperometric**)	**LOD:** 0.3 μM **R:** 1-20 μM	+ Interferences from silicates were eliminated appropriate selection of H^+/MoO_4^{2-} ratio + The method was applied for seawater and cyanobacterial biofilm analysis
Udnan et al. 2005	Flow injection **amperometric** detection at carbon electrode (with on-line pre-concentration on ion-exchange column)	**LOD:** 0.18 μg/L **R:** 0.1-10 μg/L	+70 samples/h + Method was investigated with and without preconcentration step + No silicates interferences +applied for tap water
Cheng et al. 2010	Activated nickel platform for **amperometric** flow injection detection	**LOD:** 0.3 μM	+ Highly selective to sulphate, nitrate, chlorate etc. but no description about silicate
Jonca et al., 2011	Amperometric reduction of phosphomolybdate complex created during oxidation of molybdenum in seawater	**LOD:** 0.22 μM **R:** 0.49-3.33 μM	+ no interferences from silicate +method applied for seawater analysis

Figures of merit: LOD-detection limit, R-concentration ranges

5. Corrosion and biofouling problem

Corrosion is the disintegration of an engineered material into its constituent atoms due to chemical reactions with its surroundings. In the most common use of the word, this means electrochemical oxidation of metals in reaction with an oxidant such as oxygen. This type of damage typically produces oxide(s) and/or salt(s) of the original metal. Corrosion control and protection are based on the use of high corrosion resistance materials, protective coating surfaces or corrosion inhibitors. The corrosion of a metal can be used to provide required electrical current in the process called cathodic protection with galvanic anodes or impressed current cathodic protection. In most cases, effective corrosion control is obtained by combining two or more of these methods. The methods selected must be appropriate for the materials used, for the configurations, and for the types and forms of corrosion which must be controlled.

Biofouling is the undesirable accumulation of microorganisms, plants, algae, and/or animals on wetted structures (Figure III. 5.1.). Biofouling greatly reduces the efficiency of materials and equipment. Biofouling can also accelerate corrosion and bio-deterioration problems (Little et al., 2008). The old methods for preventing corrosion are based on mechanical cleaning or air/sun drying, but those do not completely remove biofouling. Among the most recent methods, we can find biological control using grazers, new materials (silicone based fouling-release coatings), and electrical antifouling, new cage designs and spraying with an antifouling solution such as acetic acid (Delauney et al., 2010).

The corrosion and biofouling problem is inherent in development of sensors. Biofouling can disrupt the quality of measurements, sometimes in less than a week. Without proper prevention, our sensors are useless. Thus, it is very important to follow new techniques for avoidance of this serious problem.
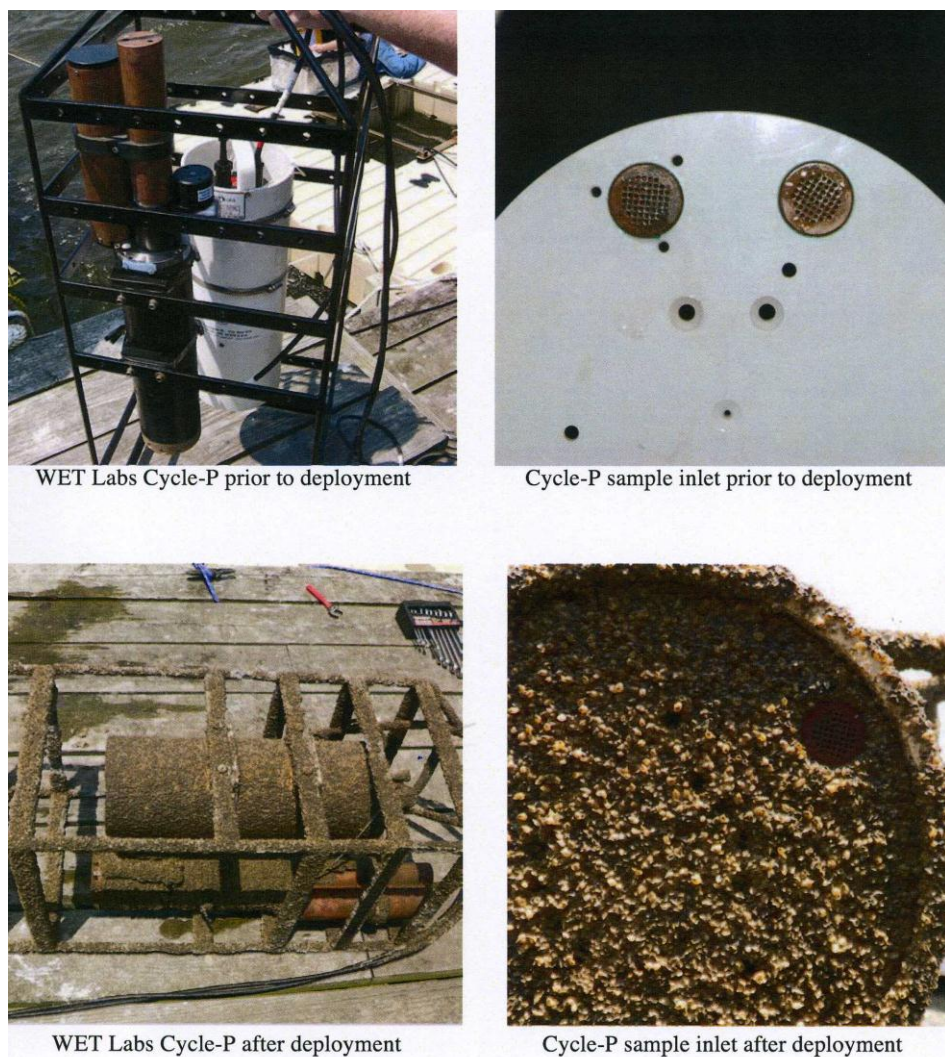
Fig. III. 5.1. Photographs of the WET Labs Cycle-PO₄ before and after deployement in Chesapeake Bay (www.wetlabs.com).

6. Summary

Monitoring of oceanic biogeochemical cycles at proper spatial and temporal scale requires miniaturized *in situ* sensors with excellent figures of merit: fast response time, low detection limit, low energy consumption, resistance to mechanical shocks etc. Development of the marine sensors is even more complicated due to harsh and difficult access to oceanic environment. In spite of all these large number of requirements, some very good sensors actually exist and new onces are still being developed.

Here only sensors for oxygen detection and analyzers for nutrient (phosphate) monitoring are discussed. A wide range of amperometric, polarographic and voltammetric

sensors for oxygen detection exists nowadays; whereas the Winkler's colorimetric detection of oxygen still prospers quite well. Optodes based on fluorescence quenching are widely used and together with amperometric sensors are the future of *in situ* oxygen monitoring. A special attention was paid on the STOX sensor for ultra-low oxygen detection. This sensor is essential for scientific questions like hypoxia, respiration rates, denitrification and anammox processes. The STOX sensor was improved during my PhD project and preliminary results are presented in Chapter IV.

Phosphate monitoring is based on wet chemical analyzers. Analyzers have good accuracy, reliability and can measure a few analytes at the same time. However, phosphate detection is based on addition of liquid reagents to the sample and thus analyzers contain reagents and standards bags which make them large and heavy. There is also the issue of stability of the reagents and of high energy consumption of the analyzers. Actually, many teams work on electrochemical sensors for phosphate detection. There are a few voltammetric and amperometric sensors for phosphate detection but none of them have been applied *in situ.* Moreover, they still require addition of liquid reagents to transform electroinactive phosphate species into active phosphomolybdate complex. During this PhD, a method for phosphate detection, based on molybdenum oxidation, in order to form phosphomolybdate complex electrochemically detectable by amperometry or voltammetry, was developed. The method does not require addition of any liquid reagents and is free from silicate interferences (Chapter VI).

Even the best sensors without proper protection against corrosion and biofouling are useless. This problem was briefly presented and the existing anticorrosion and antibiofouling methods were shortly mentioned.

CHAPTER IV:

IMPROVEMENT OF THE STOX SENSOR FOR ULTRA-LOW OXYGEN CONCENTRATIONS

This chapter describes the improvement of an amperometric STOX sensor for detection of ultra-low oxygen concentrations. This improvement is based on the change of the sensor construction. Instead of electrodeposition of gold on platinum to form the front gold cathode, a wet chemical method was developed. The method requires reduction of gold chloride to gold with hydrazine by gold plating on silicon membrane.

Firstly, the best conditions to form a gold layer on silicon membrane were found. Thus, concentrations of hydrazine hydrate and gold chloride were optimized and used to form the front gold cathode. In this way, the inner part of the sensor can be pushed closer to the outer membrane.

Secondly, the improved sensor was compared with traditional STOX sensor and preliminary data showed a better sensitivity (about 2-3 times higher than for traditional sensor), a shorter response time (t^{90} about 7s instead of 16s) but similar detection limit and temperature dependence (loss of signal 2.36%/°C). These results showed great potential in STOX sensors with the new gold electrodes.

Contents

1. Introduction

Determination of oxygen in both the water column and at the sediment-water interface is extremely important for oceanographers. At the sediment-water interface oxygen gradients are very steep and the characteristic depth scales are on the order of mm to μm (Archer and Devol, 1992). Moreover, the oxygen concentration can change within seconds due to changes in hydrodynamics, faunal activity, or photosynthesis. Great care must be taken on the sensor to be used in terms of size, response time, and stirring sensitivity.

The temporal and spatial variability in the water column is usually several orders of magnitude smaller than the variability found across the sediment-water interface. The vertical oxygen gradient in the water column extends over depth scales of meters to hundreds of meters and the oxygen concentration is stable for hours or days. The dissolved oxygen concentrations in the water column decrease with depth due to the decline of photosynthesis and utilization of oxygen for respiration and decomposition processes. At greater depths the concentrations of oxygen increase slightly again. The concentration of oxygen is sufficient for sustaining life of marine organisms. However some areas of coastal waters and open ocean are characterized by low oxygen concentration of 1 μmol L^{-1} or less (Oxygen Minimum Zones-Paulmier and Ruiz-Pino, 2009) which causes a severe reduction or in extreme cases the complete loss of animal life in these regions (Levin, 2003). Thus very sensitive oxygen sensors are required for adequate monitoring of these important ocean areas.

Among the many techniques dedicated to oxygen determination in seawater (Winkler method, gasometry, gas chromatography, mass spectrometry, polarography), the amperometric oxygen sensors are the most used within the aquatic sciences. Recently, a very sensitive STOX sensor was developed (Revsbech et al., 2009). The detection limit of this sensor is as low as 1-2 nmol L^{-1} and thus provides ideal conditions for oxygen measurements in Oxygen Minimum Zones. The sensor has other advantages like small size, easy to operate, *in situ* zero calibration. From the other hand some disadvantages are noticed as well: fragility, signal drift and quite long response time.

In this work, an improvement of the STOX sensor was achieved by changing the construction of the front gold electrode. Instead of using electrodeposition of gold on platinum wire, a wet chemical method was chosen for gold plating on silicon membrane. This change, due to Fick's law, should give faster response time and increase sensitivity of the sensor.

The work is structured as follows: at the beginning optimization of gold plating on membrane is performed and then the comparison of traditional and new STOX sensor is presented. Finally, future possible improvements of the sensors are discussed.

2. Sensors preparation

The traditional STOX sensor construction can be described shortly as follows (Revsbech et al., 2009):

- Preparation of casings

The outer casing was constructed using Schott AR glass with an outer diameter (OD) of 8 mm and inner diameter of (ID) of 7 mm. The inner casing was prepared using Schott AR glass with outer and inner diameter of 6 and 5 mm, respectively. The glasses were formed under heat with the use of microscope. The diameter of the formed tips should be as small as 50 – 100 μm. The silicon membranes were made by inserting the tip of the casing into acetic acid-curing silicon rubber (Wacker Elastosil E43, Wacker Chemie) and letting the capillary force suck in the silicone membrane.

- Preparation of gold electrodes

The central cathode of the inner sensor was made from Schott 8512 glass with an OD of 4mm and ID of 2.5mm. A 5cm piece of tapered 0.05 mm platinum wire was melted into the glass capillary. This action causes the glass closure. Thus the outermost 200-400 μm glass coating was removed by immersion into hydrofluoric acid-HF (a drop of 30% HF covered by mineral oil and contained in a plastic spectrophotometer cuvette).

The front guard cathode was made from 0.6-0.8 mm thick glass capillary made from either Schott 8533 or AR glass. A piece of platinum wire was immersed into the glass capillary but the tapered part was uncovered with glass.

The tips of the tapered wires (10-20 μm) were plated with 50 % saturated gold chloride under microscope and using an applied potential of -0.7V (versus a platinum wire inserted into the plating solution). For the outer gold electrode, after achieving a gold ball diameter of 70 % of the inner cathode diameter, the voltage was increased subsequently until it reaches a potential of -2.3 V. The final plating resulted in a porous gold matrix. The

electrical connections to the gold electrodes were made with Teflon coated silver wire from which the Teflon was removed from both ends and then the wires were pushed into the capillaries until they touched the platinum part of the sensing or front guard electrodes.

- Preparation of guard and reference electrodes

The back guard electrodes and reference electrodes were made from Teflon-coated silver wire (diameter 250 μm) from which the Teflon was removed from the tip region. The wires dedicated to serve as reference electrodes were coated with AgCl. The wires dedicated to serve as back guard electrodes were tapered using an applied voltage in (potassium cyanate) KCN solution.

To permanently fix the cables and casings were glued using UV-curing cement (Loctite 190672, Loctite Corp.) and fixed onto the glass shaft. The sensor in both parts (inner and outer casing) was filled with phosphate buffer (pH 7.4) containing 1M of KCl.

It is worth noting that the Teflon-coated wires (reference and guard electrodes) or glass protection around the outer and inner cathodes were used to avoid any kind of soldering or other fusion of conductors near the sensor, as it is a general experience that soldering near humid glass surfaces may result in erratic currents.

For laboratory use, a PA2000 picoammeter (Unisense) was applied. Polarization and depolarization of the front guard were mediated by inserting a banana jack with connection to the front guard into either the guard or reference socket. For subsequent land-based work, a custom-built picoammeter with timer-controlled switching between front guard on and off was used. The signal was recorded by a Unisense ADC816 16-bit A/D converter.

The improved STOX sensor was prepared in the same way except for the front guard cathode. This electrode was created by electroplating of gold on the silicon membrane. The method is based on gold chloride hydrate (Sigma Aldrich) or potassium dicyanoaurate (Sigma Aldrich) reduction by hydroxylamine (50% in water solution, Bie and Berntsen) or hydrazine hydrate (50-60% in water solution, Sigma Aldrich) with some ammonium hydroxide addition (25% in water solution, Merck). Optimization of this method is presented below.

3. Results and discussion

3.1. Optimization of gold plating on silicon membrane

The gold chloride $AuCl_4^-$ or gold cyanide complex $Au(CN)_2^-$ was reduced by hydroxylamine or hydrazine in order to form a gold layer on the silicon membrane. The gold chloride (or gold cyanide) complex was added into the tips with membranes and the whole tip was immersed into a plastic tube containing a solution of reducing agent. The hydroxylamine (or hydrazine) passed through a membrane and reduced gold chloride (or gold cyanide) complex to gold. The process depends on the concentration of gold chloride (or gold cyanide) complex, reducing agent and addition of other composites. The method does not require high temperature, strong acid or addition of organic composites. The hydroxylamine and hydrazine were used because they are small molecules but strong reducing agents and thus they can pass through the silicon membrane.

The results showed that hydrazine and hydroxylamine will not reduce gold cyanide. Thus it is not a good source of gold for our purposes.

Gold chloride seems to be a good source to produce gold particles. The effects of reducing the gold chloride with 0.015 % hydroxylamine are visible after one week, so the reaction is very slow. It was not possible to increase the concentration of hydroxylamine since it can destroy the silicon membrane. The reduction with hydrazine gives better and faster results since we obtained a well defined gold layer after a few hours. Moreover, ammonia increases the reducing capability of gold chloride but the optimal concentration is about 1-2 %. Larger ammonia concentrations will lead to the formation of a red polymer into the tip. We also optimized the gold concentration and the results showed that the larger the gold chloride concentration is, the thicker the gold layer is achieved. Increasing the concentration of gold chloride to 10 % will lead to the change in color of the membrane into red. The hydrazine concentration was optimized at the end and it seems that the higher the hydrazine concentration is, the thicker the layer of gold is achieved. To summarize, the best conditions to form the gold layer on the silicon membrane is to use 3-5 % gold chloride, and to immerse it into 12 mL of aquatic solution containing 1 mL of hydrazine, and 0.5 mL of ammonia for 8-12h.

After optimization of gold plating on membrane, the porous gold outer cathode was created. First, gold was electrodeposited on platinum wire by applying a low potential of

0.6 V to form a small gold ball of 20 μm diameter. This gold plated wire was immersed into the outer glass tip (together with the inner glass tip). The outer casing is filled with gold chloride complex and then the whole tip is placed in hydrazine/ammonia solution for 8-12 h. After, the construction of the sensor is continued as for the traditional STOX sensor.

3.2. Comparison of traditional and improved STOX sensor

To characterize the new STOX sensor, a few experiments were carried out. We determined figures of merit such as: detection limit, reproducibility in short (1-2 h) and longer time of utilization (12-15 h), sensitivity, behavior of the sensor in different temperatures, etc. To compare the traditional and new STOX sensors, we carried out the experiments in the conditions where both types of sensors were utilized simultaneously.

3.2.1. Calibration curves and sensitivity

Calibration curves were made in low oxygen concentration solutions (100-400 nmol L^{-1}) for traditional and new STOX sensors (Figure IV. 3.1).
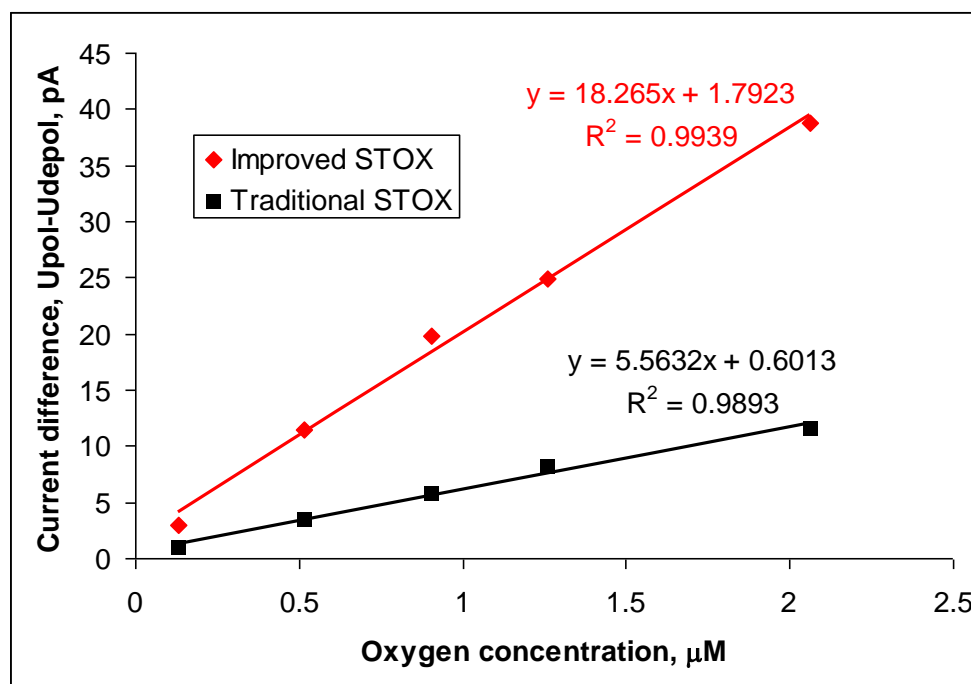
Fig. IV. 3.1. Calibration curves achieved for different STOX sensors. Traditional one: STOX 173 and STOX sensor with new gold outer cathode: STOX 179.

It is clear that the new sensors give higher signals. This is due to the decrease of the distance between sensing electrode and the outer membrane. Table IV. 3.1 presents all sensitivity values achieved for both types of sensors. To summarize, the new STOX sensor presents a 2-3 higher sensitivity than the traditional ones. Sensitivity is defined as the slope taken from the calibration curves. It seems that it is difficult to obtain two sensors with the same sensitivity. The signal can be further increased by increasing the tip opening, but this will also lead to the increase of the stirring sensitivity.

Table IV. 3.1. Sensitivity for traditional (*) and new STOX sensors:

Sensor number	Sensitivity pA/μmol L^{-1}
STOX 173*	5.27
STOX 177*	2.66
STOX 179	18.3
STOX 180	13.7
STOX 181	10.0

3.2.2. Signal stability

Stability tests for short and long term utilization of the sensors were made. The stability of the sensors was performed by repetition of signal measurements at given oxygen concentrations on a short period of time (few repetitions; 1 hour) or on a longer period of time (overnight; 12-15 h). From these data, precision was calculated as a standard deviation divided by the average value of the signal achieved at given oxygen concentrations (and multiplied by 100 to obtain values in %). On short time scales, the drift of the signal is very small for both types of sensors (Table IV. 3.2). On longer time scales (Table IV. 3.3), we can notice a drift: the signal value decreases for all sensors. It is presently dificult to conclude that this drift problem is more serious for the new STOX sensor than it is for the traditional one. It was noticed before that a drift can appear due to the presence of oxygen in the electrolyte solution but pre-polarization of the sensor will remove it by the guard electrode. However, in our case the drift was still present after 12 h (or more in some cases) of pre-polarization. The

other possibility can be the presence of impurities in the sensor which are difficult to remove or changes in temperature and pressure.

Table IV. 3.2. Precision (%) achieved in different oxygen concentrations (μmol L⁻¹) by different STOX sensors (*traditional STOX sensors). Precision was calculated from about 7-10 measurements of signal for each oxygen concentration.

	Oxygen concentration, (μmol L^{-1})					
Sensor number	0.129	0.516	0.903	1.29	2.06	3.61
STOX 173*	0.83	1.31	1.1	2.84	1.02	5.35
STOX 177*	1.23	1.5	2.3	3.06	1.56	6.03
STOX 178	3.0	1.4	1.35	1.3	1.04	-
STOX 179	3.7	1.0	0.77	0.74	0.69	-
STOX 180	0.79	1.08	-	2.0	2.19	4.2
STOX 181	0.48	0.97	-	1.95	2.21	4.5

Table IV. 3.3. The drift of the signal for the same oxygen concentration presented as a precision calculated from 86-100 measurements performed overnight at a given oxygen concentration of 2.1 μmol L⁻¹.

Sensor number	Precision (signal drift)
STOX 173*	2.5%
STOX 177*	6.5 %
STOX 178	4.0 %
STOX 179	8.4 %
STOX 180	3.0 %
STOX 181	2.6 %

3.2.3. Detection limit

Since it is difficult to fully remove oxygen from the water, we were looking for the detection limit as the smallest signal for oxygen achieved by addition of ascorbic acid to oxygenated water. Ascorbic acid will reduce oxygen in the solution, thus the signal given by the STOX sensor will be reduced as well. The amount of ascorbic acid has to be low enough to not reduce oxygen too fast. By careful addition of ascorbic acid, we were able to reduce oxygen to very small levels and to register the corresponding signal. Table IV. 3.4 presents detection limits found for traditional and new STOX sensors. It is dificult to conclude which type of sensors has the lowest detection limit. For the time being, it seems that the traditional STOX sensors have slightly lower detection limits than the new STOX sensor.

Table IV. 3.4. Detection limits achieved by different STOX sensors (*traditional STOX sensors):

Sensor number	Detection limit, nmol L^{-1}
STOX 173*	1.7
STOX 177*	4.14
STOX 178	19.4
STOX 179	11.3
STOX 180	7.6
STOX 181	10.9

3.2.4. Temperature dependence

The sensor response in different temperature conditions was checked for traditional and new STOX sensors. The signals were measured for milliQ water in temperature range of $2.5 - 25°C$. We started the measurements at the highest temperature conditions and then we cooled down the system. The temperature calibrations waves are presented in Figure IV. 3.2.
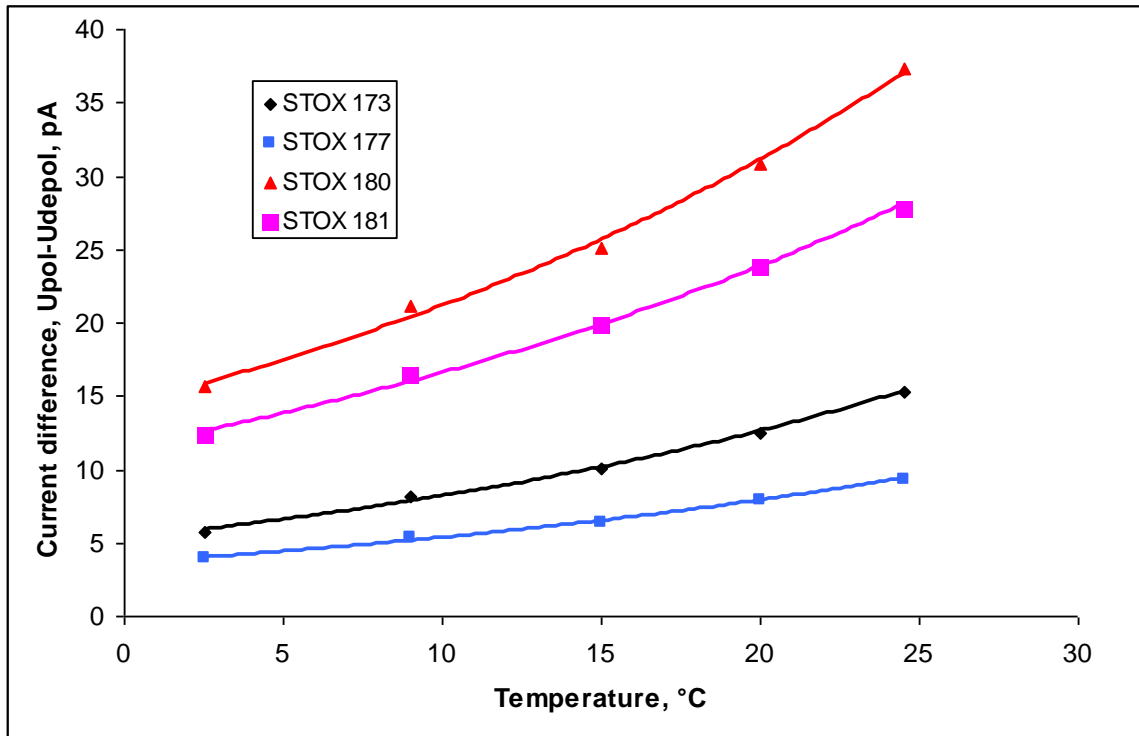
Fig; IV. 3.2. Temperature calibrations for different sensors: STOX 173 and STOX 177 (traditional STOX sensors), STOX 180 and STOX 181 (STOX sensor with gold plating on membrane).
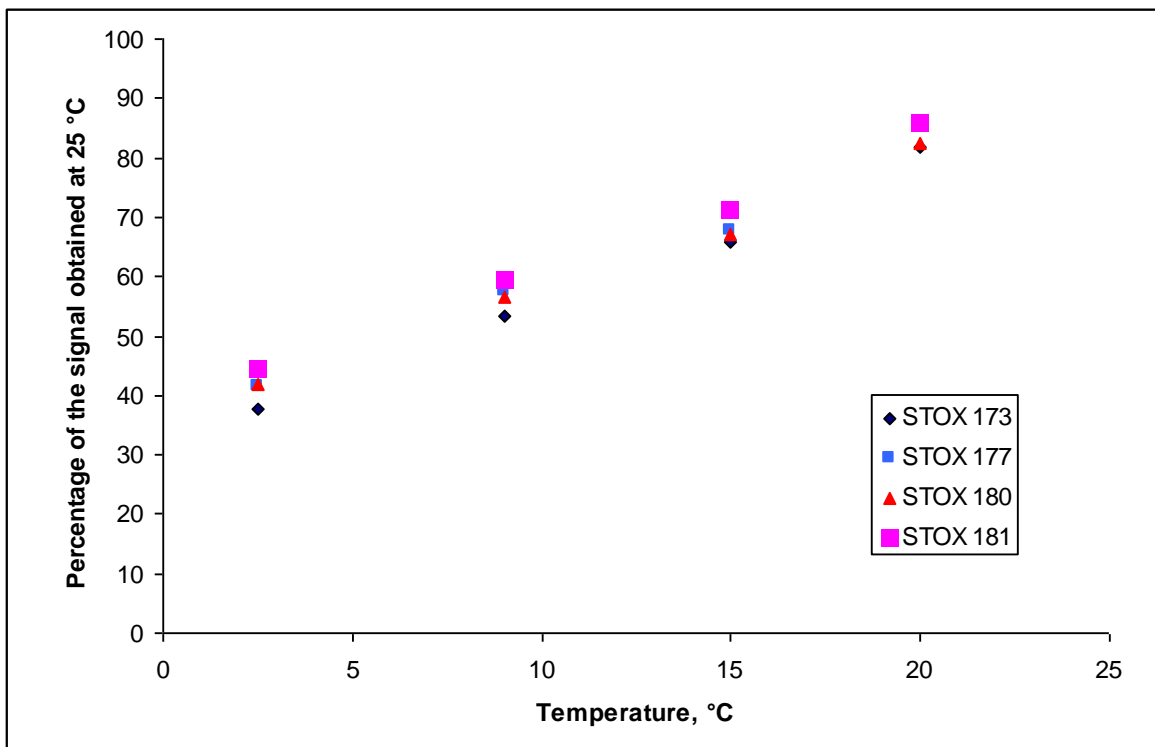
Fig. IV. 3.3. Percentage of the highest signal registered for 25 °C.

We also examined the loss of signal sensitivity with temperature as compared with the highest signal achieved here at 25 °C. We present data (in %) as the ratio of the signal at a given temperature over the signal at 25 °C (Figure IV. 3.3.). The average slope of this dependency is 2.36 %/°C.

The similar behavior of the sensors can be explained using the Fick's diffusion theory. Temperature changes will affect parameters like partial pressure, membrane permeability and diffusion coefficient and they are not dependent upon the construction of the sensor. Thus a change of the front gold cathode formation method will have no influence on the sensor behavior at different temperatures.

3.2.5. Response time

A very useful parameter to compare the response time of different sensors is the time calculation over which the sensor will achieve 90% of the total signal value-t^{90}. The response time depends strongly on the sensor construction. One way to achieve fast working sensors is to decrease the distance between the inner and the outer membrane which was the objective of this work. The values of t^{90} are presented in Table IV. 3.5.

*Table IV. 3.5. Values of t^{90} achieved for different sensors (*traditional STOX sensor):*

Sensor	t^{90} (s)
STOX 173*	12.96
STOX 177*	16.67
STOX 178	155.7
STOX 179	16.5
STOX 180	7.3
STOX 181	18.4

The longest response time that we achieved was for the STOX sensor 178. This sensor 178 was characterized by a large distance between the inner and the outer membrane (around 120 μm).

The shortest response time was obtained for the STOX 180 where the distance between the inner and the outer membrane was the smallest (around 25 μm). This sensor 180 had also small casings openings which also leads to a decrease in response time. However, the other sensors with the new outer cathode didn't show short response times because it was difficult manually to construct a sensor with such a short distance between the inner and outer membranes. Indeed, their response time is comparable with traditional STOX sensors. However, the example of the sensor STOX 180 confirms that it is possible to achieve a very short response time sensor with the new method for gold cathode formation.

4. Conclusions and perspectives

STOX sensors with new gold electrodes show higher signals as compared with traditional STOX sensors, leading to an improved sensitivity. This is due to the decrease of the distance between the inner and outer membranes. Detection limit for both sensors' types is similar; both sensors are characterized by an excellent precision (when we repeat measurement 7-10 times on the same concentration). However, after 12-15 h of measurements with the same oxygen concentration, both sensors show a drift; the signal decreases with time. For the time being, it is difficult to asses whether the drift is more significant for the traditional or for the new sensor type. The temperature calibrations show an increasing signal with temperature (2.36 %/°C). The parameter t^{90} (time for which the sensor will achieve the 90% of the total signal value) confirmed that by decreasing the distance between the inner cathode and the outer membrane, we can obtain a sensor with a shorter response time than the traditional STOX sensor.

These preliminary studies showed a great potential in STOX sensors with the new gold electrodes. However, construction of the sensor with such a short distance between the inner and outer membranes is quite difficult. Thus, more sensors of this type should be constructed and tested to confirm the results achieved in this work. Future work should be focused on working on the drift problem. To increase further sensitivity, we could also increase the tip size but this will lead to an increase of the stirring sensitivity.

CHAPTER V:

ELUCIDATION OF MOLYBDATE'S COMPLEX CHEMISTRY

Chapter V presents additional work on electrochemical behaviour of isopoly- and heteropolyoxomolybdates formed during anodic oxidation of molybdenum in seawater. Recognition of these complexes has never been done before. Thus, our knowledge about different forms of molybdates produced during molybdenum oxidation is very limited. This work helps to discover which kind of silico- and phosphomolybdate complex are formed, explains complicated electrode reactions and thus helps to understand the difficulty of phosphate detection by electrochemistry. Thus, these results will help us to develop a first electrochemical sensor for in situ detection of phosphate and silicate in the ocean. For this purpose different analytical methods were used: electrochemistry, spectrophotometry and equilibrium analysis. Electrochemical behaviour of isopoly- and heteropolyoxomolybdates formed during simple addition of liquid reagents was used in this work for comparison.

Contents

Article 1: Jońca, J., Barus, C., Giraud, W., Thouron, D., Garçon, V., Comtat, M., 2012, ***Electrochemical Behaviour of Isopoly- and Heteropolyoxomolybdates Formed During Anodic Oxidation of Molybdenum in Seawater***, International Journal of Electrochemical Sciences, 7, 7325-7348

Electrochemical Behaviour of Isopoly- and Heteropolyoxomolybdates Formed During Anodic Oxidation of Molybdenum in Seawater

Justyna Jońca[1,*], Carole Barus[1], William Giraud[1], Danièle Thouron[1], Véronique Garçon[1], Maurice Comtat[2]

[1] Laboratoire d'Etudes en Géophysique et Océanographie Spatiales, UMR 5566, 18 Avenue Edouard Belin, 31401 Toulouse Cedex 9, France
[2] Laboratoire de Génie Chimique, UMR 5503, Université Paul Sabatier, 118 Route de Narbonne, 31062 Toulouse Cedex, France
*E-mail: justyna.jonca@legos.obs-mip.fr

The electrochemical behaviour of isopoly- and heteropolyoxomolybdates formed during anodic oxidation of molybdenum in seawater at constant current intensity was investigated in this work. The results supported by spectrophotometry clearly indicate the formation of mixed valence molybdates (V/VI) during this process. The electrochemical behaviour of isopolyoxomolybdates shows a typical quasi-reversible mass-transport limited system coupled with an adsorption of reduced species and under some kinetic limitations. For heteropolyoxomolybdates a reversible mass-transport limited system coupled with an homogeneous chemical reaction was found. The coupled reaction, probably protonation, prevents a rapid heterogeneous electron transfer for heteropolyoxomolybdate complex. The phenomenon is more noticeable for the phosphomolybdate complex since the protonation step has a greater influence on the registered voltammograms. The presented results have a great importance in research areas where molybdate chemistry is used in detection of silicate and phosphate, namely in seawater.

Keywords: isopolyoxomolybdates, heteropolyoxomolybdates, molybdenum oxidation, voltammetry

1. INTRODUCTION

Polyoxomolybdates have long been applied for detection, separation and quantification, based on properties such as high molecular mass, electrochemical activity, reducibility, and variety of elements that can be incorporated. One of the most widely used application has been the spectrophotometric determination of phosphate and silicate in seawater after reduction of $[XMo_{12}O_{40}]^{n-}$

135

(X=Si, P) to "heteropoly blues" by ascorbic acid [1-3]. The determination of P, Si, Ge and As has been also performed by differential pulse anodic voltammetry [4], cyclic voltammetry [5, 6] and amperometry [7, 8]. Recently, a totally new electrochemical method was developed in our group for determination of silicate [9, 10] and phosphate [11] without addition of any liquid reagents. The method is based on the anodic oxidation of molybdenum in seawater in order to form silico- or phosphomolybdate complex electrochemically detectable either by means of cyclic voltammetry or amperometry. This method offers a great possibility for the *in situ* phosphate and silicate monitoring in seawater, but our knowledge about different forms of molybdates produced during molybdenum oxidation is limited. The purpose of this work is to find what kind of isopoly- and heteropolyoxomolybdates complexes are formed during electrochemical oxidation of molybdenum electrode in seawater. These results will help us to develop a first electrochemical sensor for the *in situ* detection of phosphate and silicate in the ocean and to elucidate the complex chemistry of isopoly- and heteropolyoxomolybdates.

Oxidation of molybdenum has been performed in several solutions. The polarization curve for molybdenum in acidic medium was divided in three regions: cathodic, passive and transpassive [12, 13]. In the first region hydrogen evolution proceeds on the electrode; in the middle zone a layer of MoO_2 leads to passivity; in the high potential region, the MoO_2 layer is transformed to MoO_3 and Mo dissolves to form molybdate. Bojinov et al. [14, 15] suggested that the final soluble product of the molybdenum oxidation in acid solution is Mo(VI) which can exist according to Hull [16] as molybdate or polymolybdate species (depending on pH). However, Itagaki et al. [13] claimed coexistence of Mo(V) and Mo(VI) in the solution after oxidation of molybdenum at high anodic potentials. Chukalovskaya et al. [17] stated that the final soluble product in this region was molybdenum blue. The Mo(VI)/Mo(V) ratio of molybdenum blue composition was 0.5.

The electrochemical behaviour of molybdenum in basic solutions was also investigated but to a lesser extent. However, the molybdenum electrode in this medium was covered with a film consisting mainly of $Mo(OH)_3$, MoO_2 and MoO_3 [16]. The soluble product of anodic oxidation at higher potentials (0.2 – 1.0 V) was Mo(VI) as monomeric MoO_4^{2-} species since the pH was basic. Moreover some Mo(III) species were reported but at much lower concentrations than when oxidizing molybdenum at low potentials (-0.3V – 0.2 V). At very high potentials > 1.0 V the molybdate (V) species were also found in the solution.

There are only a few publications about the oxidation of molybdenum in neutral medium like seawater [10] or 0.15 mol L^{-1} NaCl solution [18]. Wang et al. [18] stated that molybdate oxides film consists of MoO_2 and Mo_2O_3, but the final soluble product is Mo(VI). Lacombe et al. [10] supposed also that the produced soluble Mo(VI) can exist in different forms depending on the pH of the solution.

It is worth noticing also that the produced anodic layers of molybdenum oxides were conductive [19]. This is very important for our purposes since the molybdenum electrode could not be cleaned *in situ* after oxidation.

As it was mentioned above, polyoxomolybdate form depends strongly on pH and concentration. It was found that, at very low concentrations (<10^{-4} mol L^{-1}), mononuclear species predominate. At higher concentrations (>10^{-3} mol L^{-1}), the polynuclear species appear [20]. Additionally, it was found that in the pH 7-12 the main species is MoO_4^{2-} and its protonated forms:

136

$HMoO_4^-$ and H_2MoO_4, but at pH 3-5 the $Mo_7O_{24}^{6-}$, $HMo_7O_{24}^{5-}$, $H_2Mo_7O_{24}^{4-}$, $H_3Mo_7O_{24}^{3-}$ are predominant. Finally at pH 2 and below, the $Mo_8O_{26}^{4-}$ [21] appears and $[Mo_{36}O_{112}(H_2O)_{16}]^{8-}$ was also found [22]. Future acidification might lead to more and more complicated polyoxomolybdates due to a polymerization process. In the aqueous solutions lower oxidation state molybdates are not very well defined. The aqua ions of Mo(V) and Mo(IV) are $[Mo_2O_4]^{2+}$ and $[Mo_3O_4]^{4+}$. The aqueous chemistry of Mo(III) suggests monomeric $MoO(H_2O)_5^+$ or $Mo(H_2O)_6^{3+}$ and dimer $[(H_2O)_5Mo-O-Mo(H_2O)_5]^{4+}$ [21, 23].

Polyoxomolybdates can incorporate other ions into their structure, forming heteropolyoxomolybdates. The major silicomolybdate is $SiMo_{12}O_{40}^{4-}$. The α– and β– isomers are known, but the α– isomer is more stable. Both appear in acidic medium, but the first one corresponds to a pH range about 3.5-4.5, the second one to a pH about 0.8-2.5 [24]. In pH higher than 4 the $SiMo_{11}O_{40}^{4-}$ is formed but upon simple acidification or excess of MoO_4^{2-} the $SiMo_{12}O_{40}^{4-}$ form is predominant [25]. The major phosphomolybdate are α– and β– $PMo_{12}O_{40}^{3-}$, $P_2Mo_{18}O_{62}^{6-}$, $PMo_{11}O_{37}^{3-}$, $PMo_{10}O_{34}^{3-}$, $PMo_9O_{31}(OH_2)_3^{3-}$, $P_2Mo_5O_{23}^{6-}$ [26]. The Keggin anion $PMo_{12}O_{40}^{3-}$ is the most known complex of phosphomolybdates which appears in very acidic aqueous solutions. The β– isomer as any β– Keggin anion is less stable in aqueus solutions than the α– one [25].

The study of molybdate complexes in this work was performed by electrochemistry, spectrophotometry and equilibrium analysis. It is a first paper describing in details the electrochemical behavior of isopoly- and heteropolyoxomolybdates formed during molybdenum oxidation in seawater.

2. REAGENTS AND SOLUTIONS

Molybdate solution (1 mol L^{-1}) was prepared by dilution of 2.42 g of sodium molybdate (VI) (Merck) in 10 mL of milliQ water.

Sulphuric acid solutions (0.5 mol L^{-1} and 5 mol L^{-1}) were prepared by dilution of concentrated sulphuric acid (Merck) in milliQ water.

Phosphate and silicate solutions were prepared with sodium silicofluoride (Na_2SiF_6, Merck) and potassium dihydrogen phosphate (KH_2PO_4, Merck).

The ascorbic acid for spectrophotometrical analysis was prepared by dissolution of 7.5 g of ascorbic acid (Sigma) in 250 mL milliQ water.

All experiments were performed in artificial sea water at salinity 35.4.

3. METHODS

3.1. Electrochemistry

The reference electrode was an Ag/AgCl/3 mol L^{-1} KCl electrode (Metrohm). All the following potentials are given relative to this electrode. Electrochemical measurements were carried out with a potentiostat μ-Autolab III (Metrohm).

Voltammograms at a stationary or rotating disk electrode were recorded in a three electrode cell with a platinum counter electrode. Working electrode was in gold (Metrohm, area 0.07 cm^2). The

electrode was polished with lapping film sheet (3 mol L^{-1} Aluminium Oxide, 1 µm) and electrochemically cleaned in 0.5 mol L^{-1} sulphuric acid solution (5 scans, from 0.0 to 1.5 V, 200 mV s^{-1}) before each measurement.

The molybdenum electrode (Good Fellow Metals, purity: 99.9%) has an area of 0.20 cm^2 (or $7.85*10^{-3}$ cm^2). The intensity potential curves for molybdenum oxidation were obtained with small electrode ($7.85*10^{-3}$ cm^2). The oxidation of molybdenum at constant current was done with a bigger one (0.20 cm^2).

The production of isopoly- and heteropolyoxomolybdates without addition of any liquid reagents in our conditions is based on the use of a 20 mL cell divided in two by a membrane (N117 DuPont^{TM} Nafion^{R} PFSA Membranes); the first part of the cell was filled with 3 mL of the solution, the second with 17 mL of solution. Molybdenum, reference and working electrodes were in the anodic compartment while the counter electrode was in the cathodic one. Molybdates were produced by molybdenum anodic oxidation performed in artificial seawater at a constant current electrolysis (50 mA) during different times.

3.2. Spectrophotometry

The measurements were carried out on a UV-Vis spectrophotometer (Varian Inc. Cary 50, Australia) using 10 mm 100-QS quartz cuve (Hellma Analytics, Germany). The spectrograms for isopoly- and heteropolyoxomolybdates were registered at different pH and concentrations of molybdate. The final solution was treated with ascorbic acid to reduce heteropolyoxomolybdates (VI) to molybdenum blue which gives a spectrum in visible (400-900 nm). Spectrograms for isopoly- and heteropolyoxomolybdates created without addition of any liquid reagents were performed after different oxidation times of the molybdenum electrode in artificial seawater. The spectrograms (400-900 nm) were registered in presence and absence of ascorbic acid.

3.3. Equilibrium analysis

Artificial sea water solutions at different initial pH were prepared and the 1 mol L^{-1} molybdate solution was added to obtain different final concentrations. The pH was measured before and after addition of molybdate.

The pH was also measured after different times of the molybdenum electrode oxidation and the concentration of protons was compared with theoretical values obtained from Faraday's law.

The pH was controlled using the pH meter Metrohm 744.

4. RESULTS AND DISCUSSION

4.1. Molybdenum oxidation

Molybdate and protons were produced by anodic oxidation of molybdenum in the electrochemical cell according to reaction (1). By separation of the anode from the cathode with a

138

Nafion diaphragm, we eliminate the consumption of the protons on the platinum cathode. This allows us to achieve the desired pH in the anodic compartment.

$$Mo + 4H_2O \rightarrow MoO_4^{2-} + 8\ H^+ + 6e^- \qquad (1)$$

The intensity potential curves for molybdate oxidation in natural seawater at different pH and in 0.6 mol L^{-1} NaCl solution are presented on Fig. 1a. The anodic parts of the Tafel plots (Fig. 1b) can be described by a general equation (2).

$$\eta = \frac{2.3RT}{\alpha F} \log j_0 - \frac{2.3RT}{\alpha F} \log j \qquad (2)$$

Where j is the current density (A cm^{-2}), j_0 is the exchange current density (A cm^{-2}), α is the anodic transfer coefficient, η is the overpotential (V), F is the Faraday constant (C mol^{-1}) and R is the molar gas constant (J mol^{-1} K^{-1}).
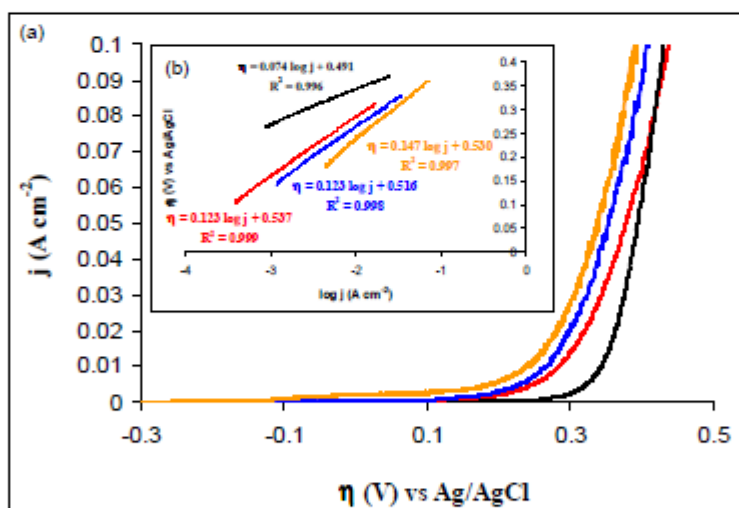
Figure 1. (a) Linear sweep voltammograms (5 mV s^{-1}) for molybdenum oxidation in 0.6 mol L^{-1} NaCl solution (red line) and in natural seawater at pH 7.8 (blue line), pH 1.0 (black line) and pH 10 (orange line); (b) corresponding Tafel plots.

The Tafel plot slopes in 0.6 mol L^{-1} NaCl and in natural seawater (pH 7.8) are the same and equal to 0.123. The exchange current density was $10^{-4.1}$ A cm^{-2} for seawater and $10^{-4.3}$ A cm^{-2} for the NaCl solution. The determined transfer coefficient α from equation (2) was equal to about 0.46 for both media. Acidification of seawater to pH 1.0 by sulphuric acid caused a decrease of the Tafel plot slope to 0.074 and the exchange current density is decreasing to $10^{-6.7}$ A cm^{-2}. The alkalinisation of

seawater with sodium hydroxide to pH 10 results in the increase of the Tafel plot slope to 0.147 and an increase of exchange current density to $10^{-3.6}$ A cm^{-2}. The transfer coefficient was 0.39 for seawater at pH 10 and 0.79 for seawater at pH 1.0. The obtained results showed similar order of magnitude that those obtained by Wang et al. [18] in different solutions and clearly indicate that the passivation of molybdenum can be achieved more easily in acidic medium than in basic one. The following experiments may be done in artificial seawater because the electrochemical behaviour of molybdenum electrode in 0.6 mol L^{-1} NaCl solution is very similar to the one in natural seawater (pH 7.8).

For further analysis a constant current intensity is chosen for the molybdenum oxidation in order to control the quantity of molybdate formed, according to the Faraday's law. We chose a current of 50 mA corresponding to potentials between 0.8 – 1.0 V and thus, we are in the transpassive region where active dissolution of molybdenum to molybdate occurs.

The concentration of molybdate and protons increases with oxidation time. A longer oxidation time of molybdenum leads to a higher molybdate concentration in the solution and the percentage of polynuclear species increases.
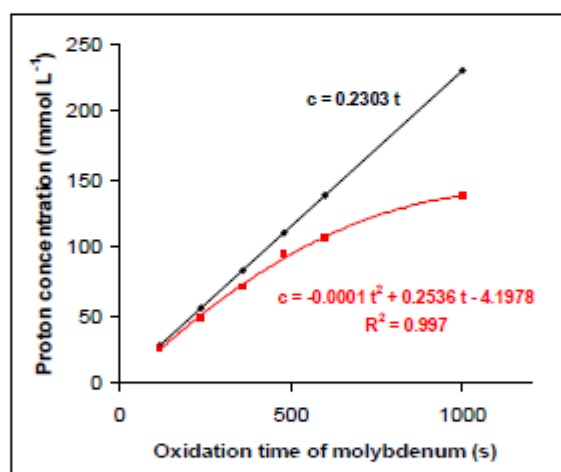
Figure 2. Comparison of (black line) expected value of proton concentration (calculated from Faraday's law) with (red line) experimental measurements of pH.

Besides, the formation of polyoxomolybdates consumes some protons and more and more complex polyoxomolybdates are created with an increase of acidification. Having all this in mind, we assume that equation (1) will change with time during the molybdenum oxidation. Fig. 2 presents the comparison between the expected value of protons and that calculated from measured pH after different oxidation times. The results show that the measured concentration of protons is lower than the theoretical one. This may be due to mentioned protonation process of molybdates. Some protons are used for the formation of polyoxomolybdates and thus the measured pH for the solution is higher than expected.

In spite of the complexity of the reactions occurring during the molybdenum dissolution, the measured pH in the solution is repeatable with a precision of 1.7% for 500s of oxidation [11]. The colour of the solution after molybdenum dissolution is blue and its intensity increases with time of oxidation. This fact clearly indicates the presence of isopolyoxomolybdate complexes containing Mo(V) and Mo(VI) known as molybdenum blues. Moreover, the blue colour appears in both 0.6 mol L^{-1} NaCl solutions: in presence and absence of phosphate (or silicate). Additionally, the surface of the oxidized molybdenum electrode is covered with a dark blue oxide layer which is conductive as it had been noticed before [19].

4.2. Electrochemical behavior of isopolyoxomolybdates

4.2.1. Cyclic voltammetry

Cyclic voltammetry was performed on a 3 mm gold disk electrode (200 mV s^{-1}) after each oxidation time of molybdenum in 0.6 mol L^{-1} NaCl solution and presented on Fig. 3a. For comparison cyclic voltammograms made with isopolyoxomolybdates created by addition of sodium molybdate (VI) and sulphuric acid are presented on Fig. 3b where the value of molybdate concentration and pH were the same as those achieved during the oxidation of molybdenum. For clarity only selected curves are presented.

Cyclic voltammetry of isopolyoxomolybdates created by addition of sodium molybdate (VI) to an acidified solution was investigated before by Krishnan et al. [21]. The work shows clearly that the shape of the curves depends strongly on pH since different molybdate species might be formed from simple MoO_4^{2-} to protonated species of $Mo_8O_{26}^{4+}$. Similar conclusions were made in this work but the situation is even more delicate since the pH of medium was lower (pH 1-2) and diverse isopolyoxomolybdates can be formed as it is suggested by different shapes of voltammograms. Calculation of parameter "z" –the number of protons consumed by one molecule of MoO_4^{2-} is a proper equilibrium method to indicate the isopolyoxomolybdates formed at different conditions (Table 1.). The method is based on pH measurements of an acidified solution before and after addition of sodium molybdate at adequate concentration. The difference in proton concentrations is divided by the molybdate concentration giving a value of parameter "z" characteristic for each created molybdate species. Moreover, total formation reaction can be proposed for each species (equations 3a-e). It is clear from these results that with growing acidification and molybdate concentration more and more complicated isopolyoxomolybdates are formed due to protonation and condensation reactions. The proposed forms of isopolyoxomolybdates are in good agreement with a reaction model of the equilibrium system for molybdate described by Cruywagen et al. [27].

$$8\ MoO_4^{2-} + 12\ H^+ \rightarrow Mo_8O_{26}^{4+} + 6\ H_2O \tag{3a}$$

$$13\ MoO_4^{2-} + 22\ H^+ \rightarrow H_2Mo_{13}O_{42}^{+} + 10\ H_2O \tag{3b}$$

$$13\ MoO_4^{2-} + 21\ H^+ \rightarrow HMo_{13}O_{42}^{5-} + 10\ H_2O \tag{3c}$$

$$12\,MoO_4^{2-} + 17\,H^+ \rightarrow HMo_{12}O_{40}^{7-} + 8\,H_2O \tag{3d}$$

$$36\,MoO_4^{2-} + 65\,H^+ \rightarrow HMo_{36}O_{112}^{7-} + 32\,H_2O \tag{3e}$$
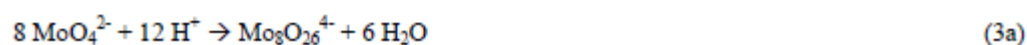
The cyclic voltammetry for isopolyoxomolybdates formed during oxidation of molybdenum differs from the characteristics described above. The shapes of the curves registered after each oxidation times are similar to each other, the signal peak is more or less at the same potential and the reduction peak current density is proportional to the molybdate concentration calculated from Faraday's law (j_{pc}=-0.323c-0.664, R^2=0.995). These results suggest that during the oxidation of molybdenum in seawater only one species of molybdate is formed and it is rather different than those achieved during simple addition of sulphuric acid and sodium molybdate (VI). However, it is not possible at this step to propose a chemical formula for this species.

Figure 3. Cyclic voltammograms recorded on a gold disk electrode (3 mm, 200 mV s^{-1}) for isopolyoxomolybdates created by: (a) oxidation of molybdenum at constant current of 50 mA in 0.6 mol L^{-1} NaCl solution at several times; (b) simple addition of sulphuric acid and sodium molybdate (VI) to 0.6 mol L^{-1} NaCl solution to achieve appropriate pH and molybdate concentrations.

142

Table 1. Parameter « z » - the number of protons consumed by one molecule of MoO_4^{2-} calculated for different pH and molybdate concentrations with some proposition of chemical formula for the created isopolyoxomolybdates.

$[MoO_4^{2-}]$ (mmol L^{-1})	Initial pH*	Final pH**	Parameter « z »	Proposed form of isopolyoxomolybdate	Eq.
1.73	1.93	2.04	1.52 (σ=0.021)	$Mo_8O_{26}^{4-}$ (8, 12)	3a
3.45	1.65	1.78	1.69 (σ=0.015)	$H_2Mo_{13}O_{42}^{4-}$ (13, 22)	3b
6.91	1.31	1.42	1.61 (σ=0.014)	$HMo_{13}O_{42}^{5-}$ (13, 21)	3c
10.0	1.21	1.32	1.40 (σ=0.017)	$HMo_{12}O_{40}^{7-}$ (12, 17)	3d
13.8	1.08	1.23	1.80 (σ=0.007)	$HMo_{36}O_{112}^{7-}$ (36, 65)	3e
17.3	0.87	0.98	1.80 (σ=0.010)	$HMo_{36}O_{112}^{7-}$ (36, 65)	3e

* pH of acidified NaCl solution before addition of molybdate
** pH of acidified NaCl solution after addition of molybdate
σ-standard deviation

Figure 4. Cyclic voltammograms recorded on a gold disk electrode (3 mm) at different scan rates for isopolyoxomolybdates created by: (a) oxidation of molybdenum in 0.6 mol L^{-1} NaCl solution during 240 s at constant current of 50 mA (pH 1.45, [Mo]=6.91 mmol L^{-1}); (b) simple addition of sulphuric acid and sodium molybdate (VI) to 0.6 mol L^{-1} NaCl solution (pH 1.42, [Mo]=6.83 mmol L^{-1}).

In spite of many differences between isopolyoxomolybdates formed during molybdenum oxidation and by simple addition of sodium molybdate (VI) to sulphuric acid solution, the cyclic voltammograms show some similarities. In both methods, the reduction current density (j_{pc}) is proportional to the square root of the scan rate (Fig. 4), as it is indicated by equations: j_{pc}=-105.3 $\upsilon^{-1/2}$+ 45.5; R^2=0.993 (isopolyoxomolybdates created by simple addition of reagents), j_{pc}=-106.5 $\upsilon^{-1/2}$+ 44.5; R^2=0.992 (isopolyoxomolybdates created by molybdenum oxidation). However, the reverse oxidation peaks (j_{pa}) are less pronounced (the ratio j_{pa} over j_{pc} is smaller than 1) which is indicative of a very slow rate of electron transfer. Reduction potential peak (E_{pc}) shifts to higher potentials as scan rate (υ) increases as it is indicated by equations: E_{pc}=-1.34 υ-0.141; R^2=0.992 (isopolyoxomolybdates created by simple addition of reagents), E_{pc}=-1.62υ-0.10; R^2=0.983 (isopolyoxomolybdates created by molybdenum oxidation). Moreover, the peaks are broader and the peak separation (E_{pa}-E_{pc}) increases with scan rate (υ) as described by equations: (E_{pa}-E_{pc})=0.902υ-0.054; R^2=0.985 (isopolyoxomolybdates created by simple addition of reagents), (E_{pa}-E_{pc})=1.19υ-0.137; R^2=0.985 (isopolyoxomolybdates created by molybdenum oxidation). These results indicate a typical quasi-reversible mass-transfer limited process.

4.2.2. Linear sweep voltammetry

Measurements were performed on a 3mm rotating disk gold electrode (1000 rpm, 5 mV s^{-1}) after each oxidation time of molybdenum in 0.6 mol L^{-1} NaCl solution and presented on Fig. 5a. For comparison a linear sweep voltammetry made for isopolyoxomolybdates created by addition of molybdate and sulphuric acid is presented on Fig. 5b where the value of molybdate concentration and pH were the same as those achieved during oxidation of molybdenum. For clarity only selected curves are presented.

The comparison of both conditions showed some similarities. After experiments, the surface of the gold electrode was covered with a thin dark layer. It has been noticed before by Kuznestov et al. [28] for isopolyoxomolybdates created by simple addition of acid to molybdate (VI) ions. He stated that the thin layer consists of compounds of Mo of lower valences. The reduced solution becomes blue after reduction of isopolyoxomolybdates created by simple addition of sulphuric acid and sodium molybdate which indicates the presence of mixed valence (VI/V) molybdates. Similar results could not be observed for isopolyoxomolybdates created by oxidation of molybdenum since the solution after this process was already blue.

For both methods, the voltammograms presented on Fig. 5 show two waves. The wave at less negative potentials which becomes a peak at higher molybdate concentrations is characteristic of an electrochemical process coupled with adsorption of reduced species or coupled with a homogenous reaction. Additionally, the limiting current density (j_{lim}) for this wave is independent on rotation rate (ω) as it is shown on Fig. 6. These results might suggest that the wave indicates a process with adsorption of the reduced species.
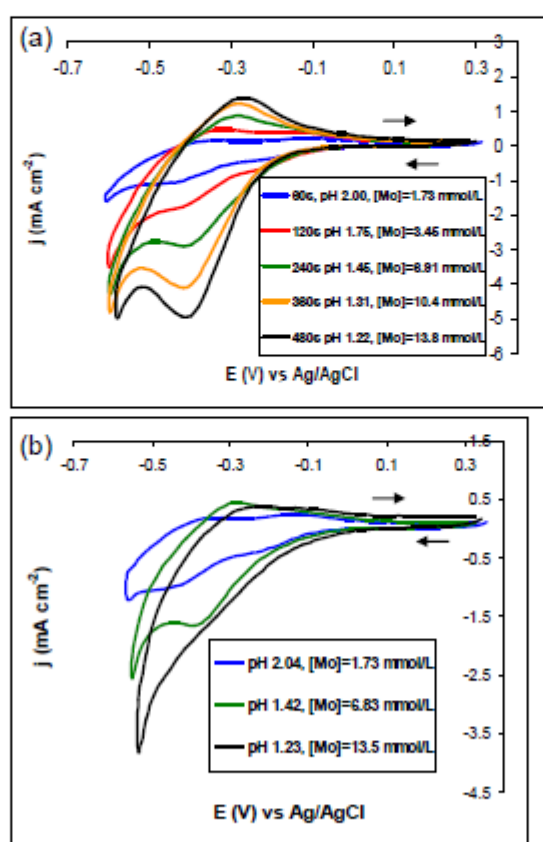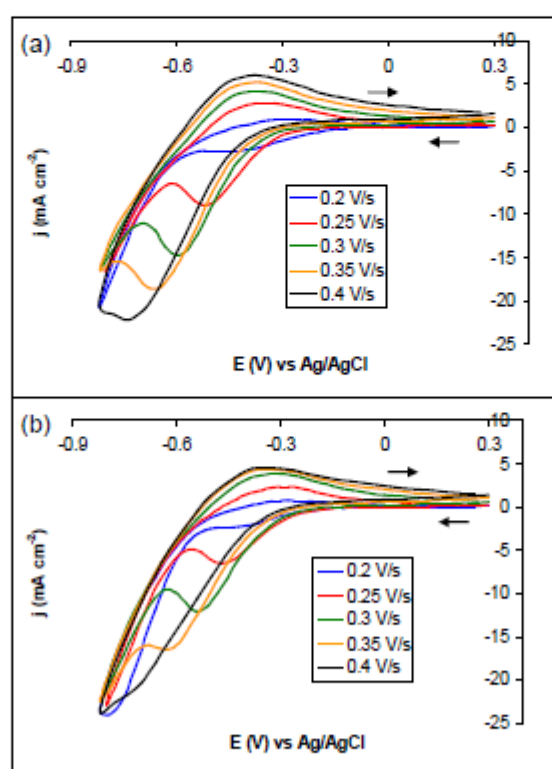
Figure 5. Linear sweep voltammograms recorded on a rotating gold disk electrode (3 mm, 1000 rpm, 5 mV s^{-1}) for isopolyoxomolybdates created by: (a) oxidation of molybdenum at constant current of 50 mA in 0.6 mol L^{-1} NaCl solution at several times; (b) simple addition of sulphuric acid and sodium molybdate (VI) to 0.6 mol L^{-1} NaCl solution to achieve appropriate pH and molybdate concentrations.

The second wave occurring at more negative potentials is more dependent on the rotation rate. However, for the greater rotation rates (up to 3000 rpm) the limiting current density (j_{lim}) becomes constant. A deviation of a plot $j_{lim}=f(\omega^{1/2})$ from a straight line intersecting the origin suggests that a kinetic limitation is involved in the electron-transfer reaction [29]. In this case, one can measure the

145

limiting current density in the absence of any mass transport effects (j_k). There is a well-defined point where the limiting current density starts to be kinetically limited (Fig. 7).
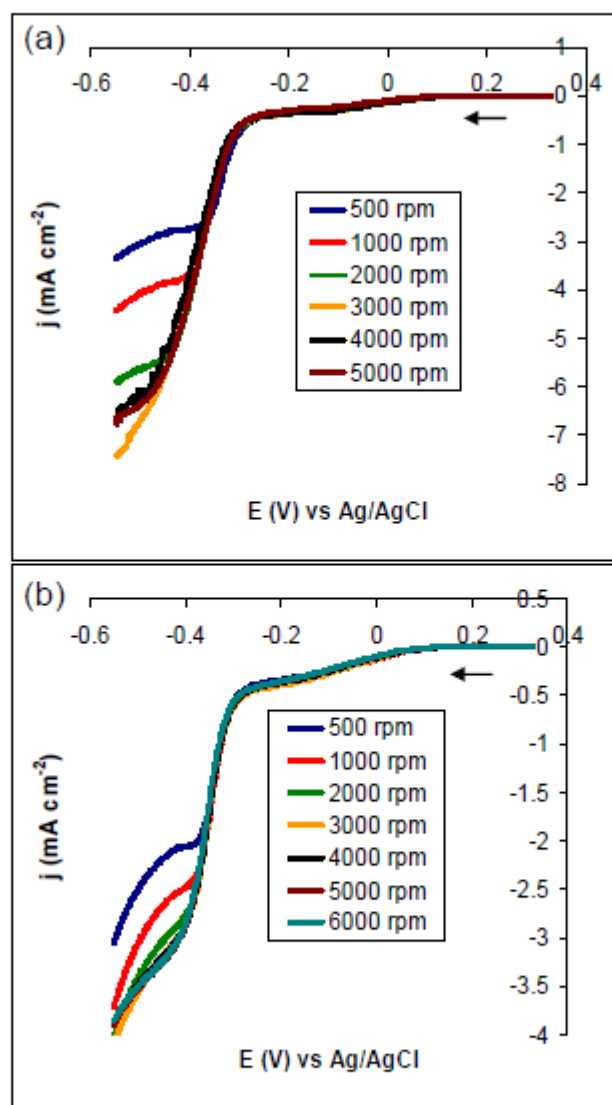
Figure 6. Linear sweep voltammograms recorded on a rotating gold disk electrode (3 mm, 5 mV s^{-1}) at different rotation rates for isopolyoxomolybdates created by: (a) oxidation of molybdenum in 0.6 mol L^{-1} NaCl solution during 240 s at constant current of 50 mA (pH 1.45, [Mo]=6.91 mmol L^{-1}); (b) simple addition of sulphuric acid and sodium molybdate (VI) to 0.6 mol L^{-1} NaCl (pH 1.42, [Mo]=6.83 mmol L^{-1}).
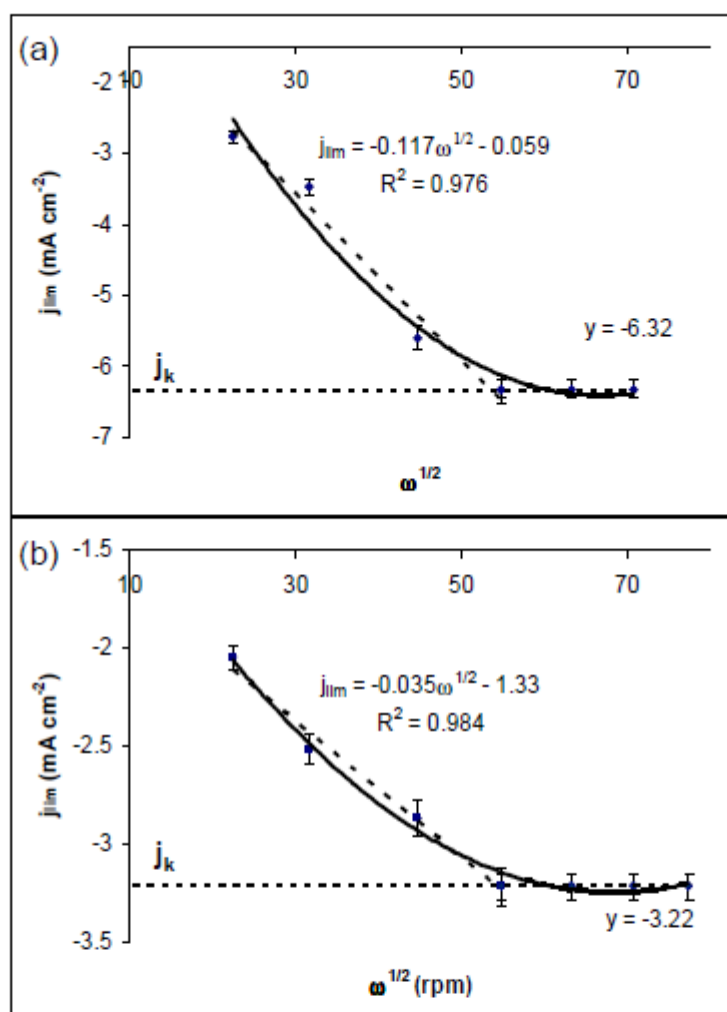
Figure 7. Limiting current density vs. square root of the electrode rotation rate for isopolyoxomolybdates created by: (a) oxidation of molybdenum in 0.6 mol L^{-1} NaCl solution during 240 s at constant current of 50 mA (pH 1.45, [Mo] =6.91 mmol L^{-1}); (b) simple addition of sulphuric acid and sodium molybdate (VI) to 0.6 mol L^{-1} NaCl (pH 1.42, [Mo] =6.83 mmol L^{-1}).

Thus, the j_k for isopolyoxomolybdates created by addition of liquid reagents is equal to -3.22 mA cm^{-2}, whereas for isopolyoxomolybdates created by oxidation of molybdenum is equal to about -6.32 mA cm^{-2}. This allows to calculate the heterogeneous rate constant (k_f) due to equation (4):

$$k_f = \frac{j_k}{FAC_0^*} \tag{4}$$

Where F is the Faraday's constant (C mol^{-1}), A is the electrode surface (cm^2), C_0^* is the concentration of reduced species (mol cm^{-3}), k_f is the heterogeneous rate constant (cm s^{-1}), j_k is the kinetically limited current density (A cm^{-2}).

The calculated heterogeneous rate constant is equal to 4.7 * 10^{-3} cm s^{-1} (for isopolyoxomolybdates created by addition of liquid reagents) and 9.3 * 10^{-3} cm s^{-1} (for isopolyoxomolybdates created by oxidation of molybdenum).

When comparing both methods, some differences indicate the formation of more complicated species during molybdenum oxidation, than in the conditions were isopolyoxomolybdates are created by simple addition of acid to molybdate (VI) solution. For instance the potentials of the waves on Fig. 5a are shifted to more negative values than those corresponding to Fig. 5b.
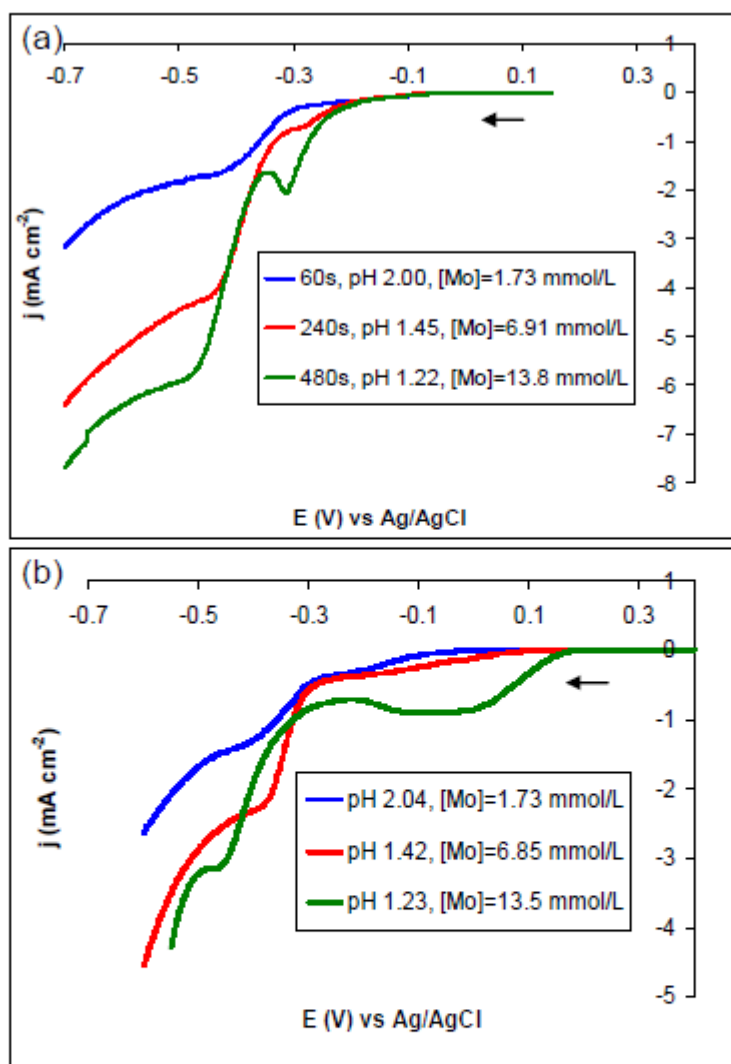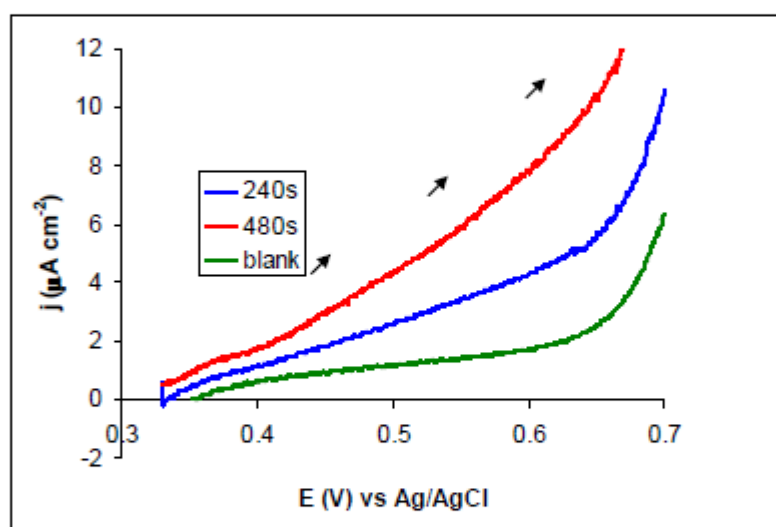

Figure 8. Linear sweep voltammograms recorded on a rotating gold disk electrode (3 mm, 5 mV s^{-1}, 1000 rpm) for isopolyoxomolybdates created by oxidation of molybdenum in 0.6 mol L^{-1} NaCl solution during 240s and 480s at constant current of 50 mA.

It was mentioned above that isopolyoxomolybdates containing Mo(V) and Mo(VI) can be formed during molybdenum oxidation. A linear sweep voltammetry was performed on a gold electrode (1000 rpm, 5 mV s^{-1}) after molybdenum oxidation in order to find molybdates at lower valences. The presence of a wave at more positive potentials than +0.3 V (Fig. 8) clearly indicates the presence of Mo (V) in the solution. Moreover, spectrophotometry in visible was performed after oxidation of molybdenum and presented on Fig. 9. The data showed peaks at wavelengths corresponding to molybdenum blue spectrum with a maximum at 800 nm. This kind of spectrum did not appear when only Mo (VI) is present in the solution.

148
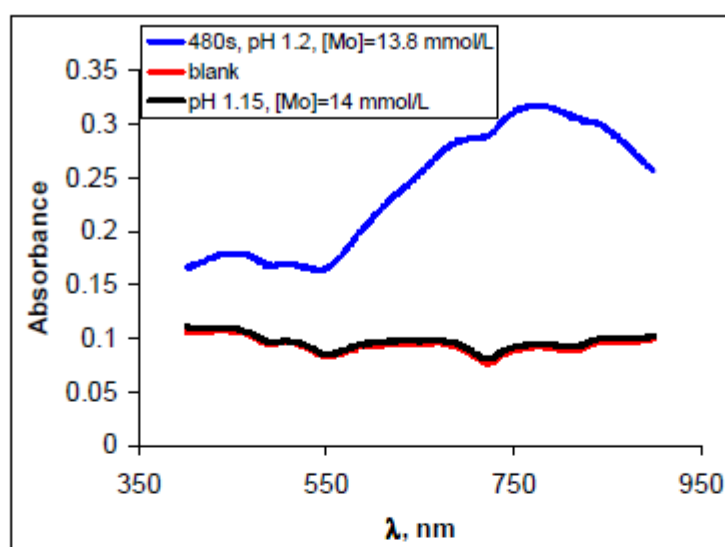
Figure 9. Absorbance as a function of wavelength for isopolyoxomolybdates created by: (black line) simple addition of sulphuric acid and sodium molybdate (VI) to 0.6 mol L^{-1} NaCl; (blue line) oxidation of molybdenum in 0.6 mol L^{-1} NaCl solution during 480 s at constant current of 50 mA.

4.3. Electrochemical behaviour of heteropolyoxomolybdates

4.3.1. Cyclic voltammetry

Cyclic voltammetry for hereropolyoxomolybdates was performed on a 3 mm disk gold electrode (50 mV s^{-1}) after oxidation of molybdenum in 0.6 mol L^{-1} NaCl solution containing phosphate or silicate at a concentration of about 100 µmol L^{-1}. For comparison, a cyclic voltammetry was made for heteropolyoxomolybdates created by addition of sodium molybdate (VI) and sulphuric acid to the 0.6 mol L^{-1} NaCl solution containing phosphate or silicate at a concentration of about 100 µmol L^{-1}, where the value of molybdate concentration and pH were the same as those achieved during oxidation of molybdenum. The resulting voltammograms are presented on Fig. 10 and show four peaks: two oxidation and two reduction ones. The reduction peaks are at 0.32 V and 0.45 V for phosphomolybdate complex and at 0.26 V and 0.37 V for silicomolybdate one. The oxidation peaks are at 0.40 V, 0.53 V and 0.32 V, 0.43 V, respectively.

Comparison of both conditions shows a great agreement between voltammograms for heteropolyoxomolybdates created by oxidation of molybdenum and by simple addition of sulphuric acid and sodium molybdate (VI) to the sample containing phosphate or silicate. This suggests that the formed types of heteropolyoxomolybdates are the same. However, the voltammograms for phosphomolybdate species differ from that of the silicomolybdate complex in several ways. The peaks are broader and not as well defined. The peaks separation (E_{pa}-E_{pc}) is bigger on phosphomolybdate voltamograms (80 mV) than for silicomolybdate ones (60 mV). The peak currents densities for the

149

phosphomolybdate complex are lower than for the silicomolybdate one. These results clearly indicate that the electrode reactions are limited by a homogeneous chemical step which prevents rapid electron transfer for phosphomolybdate complex. It was concluded by Carpenter et al. [15] that the electrode reactions of both phosphomolybdate and silicomolybdate complexes are preceded by a pH dependent chemical reaction, probably protonation. This chemical step is faster for the silicomolybdate than for phosphomolybdate complex (equation 6) and thus has a small influence on the registered voltammograms.

$$SiMo_{12}O_{40}^{4-} + H^+ \leftrightarrow HSiMo_{12}O_{40}^{3-} \qquad (6)$$
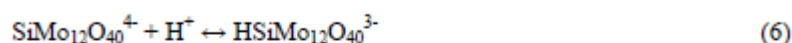
The change in pH or molybdate concentration does not influence the potential or shape peak, but it has a strong influence on peak current density for both silicomolybdate and phosphomolybdate complexes. Thus optimization of these parameters gives a possibility to find the best conditions for electrochemical quantitive analysis of silicate and phosphate. This optimization was done before [9-11] and it was found that the best pH to form the silicomolybdate complex is equal to 1.4, whereas to form the phosphomolybdate complex it is necessary to acidify the solution to pH 1.0. To achieve appropriate pH, the oxidation time of molybdenum has to be conducted during 240s and 600s, respectively. Additionally, the formation of silicomolybdate complex takes about 5 min, whereas formation of phosphomolybdate complex 1 min only.
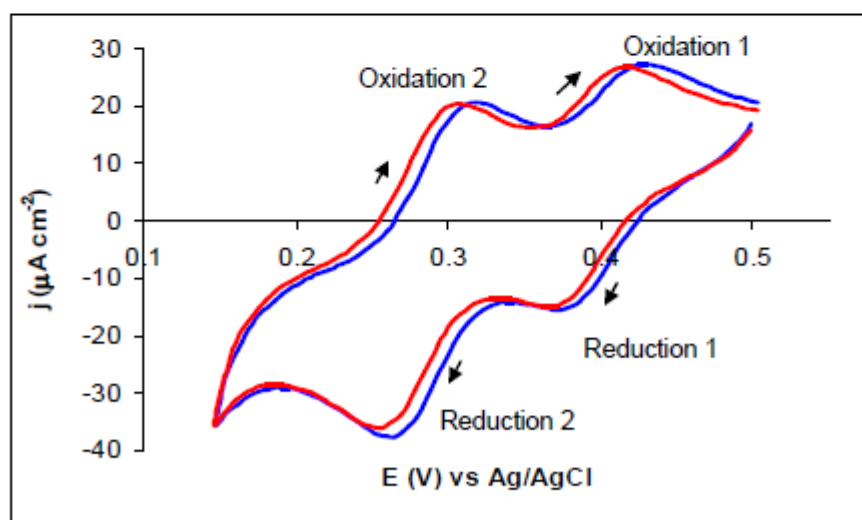
Figure 10a. Cyclic voltammograms recorded on a gold disk electrode (3 mm, 50 mV s^{-1}) for silicomolybdate complex (100 µmol L^{-1}) created by: (blue line) simple addition of sulphuric acid and sodium molybdate (VI) (pH 1.42, [MoO$_4^{2-}$] =6.83 mmol L^{-1}); (red line) oxidation of molybdenum at constant current of 50 mA during 240s.

150

Figure 10b. Cyclic voltammograms recorded on a gold disk electrode (3 mm, 50 mV s^{-1}) for phosphomolybdate complex (100 µmol L^{-1}) created by: (blue line) simple addition of sulphuric acid and sodium molybdate (VI) (pH 1.0, [MoO$_4^{2-}$]=16.7 mmol L^{-1}); (red line) oxidation of molybdenum at constant current of 50 mA during 600s.

Cyclic voltammograms at different scan rates for both complexes are presented on Fig. 11. Since the voltammograms for heteropolyoxomolybdates created by both methods are very similar, only those created by oxidation of molybdenum in the sample containing phosphate or silicate are presented. The results show that the peak potential is not dependent on scan rate whereas the peak current density (j$_p$) is proportional to the square root of scan rate ($\upsilon^{-1/2}$) and the oxidation peaks are as well pronounced as the reduction ones. These results are clearly indicative of a reversible mass-transport limited system. For clarity the slopes j$_p$=f($\upsilon^{-1/2}$) are gathered in Table 2.

Table 2. Peak current density vs. square root of the scan rate, j$_p$=f($\upsilon^{-1/2}$) for silicomolybdate and phosphomolybdate complexes created by both methods.

Peak	Phosphomolybdate complex created by :	Silicomolybdate complex created by :
simple addition of sulphuric acid and sodium molybdate		
Oxidation 1	j$_p$=16.4$\upsilon^{-1/2}$ + 5.90, R^2=0.978	j$_p$=32.2$\upsilon^{-1/2}$ + 4.59, R^2=0.982
Oxidation 2	j$_p$=56.3$\upsilon^{-1/2}$ − 2.68, R^2=0.996	j$_p$=81.2$\upsilon^{-1/2}$ + 2.55, R^2=0.994
Reduction 1	j$_p$=-32.6$\upsilon^{-1/2}$ − 2.95, R^2=0.998	j$_p$=-49.3$\upsilon^{-1/2}$ − 4.94, R^2=0.991
Reduction 2	j$_p$=-49.1 $\upsilon^{-1/2}$ + 1.46, R^2=0.997	j$_p$=-93.9$\upsilon^{-1/2}$ + 7.08, R^2=0.993
oxidation of molybdenum at constant current of 50 mA		
Oxidation 1	j$_p$=27.86$\upsilon^{-1/2}$ + 6.57, R^2=0.987	j$_p$=37.6$\upsilon^{-1/2}$ +3.36, R^2=0.972
Oxidation 2	j$_p$=65.3$\upsilon^{-1/2}$ − 2.25, R^2=0.993	j$_p$=84.5$\upsilon^{-1/2}$ +1.47, R^2=0.993
Reduction 1	j$_p$=-57.4$\upsilon^{-1/2}$ + 2.82, R^2=0.998	j$_p$=-47.5$\upsilon^{-1/2}$ − 4.96, R^2=0.996
Reduction 2	j$_p$=-43.1$\upsilon^{-1/2}$ − 4.21, R^2=0.995	j$_p$=-94.2$\upsilon^{-1/2}$ +5.35, R^2=0.999
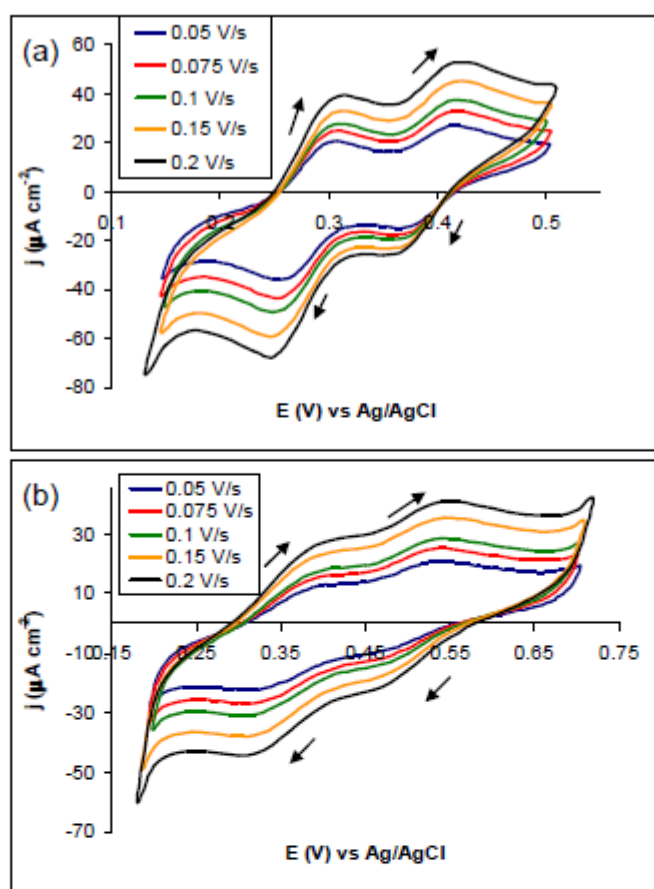
Figure 11. Cyclic voltammograms recorded on a gold disk electrode (3 mm) at different scan rates for 100 μmol L^{-1} of silicomolybdate complex (a) and phosphomolybdate (b) created by oxidation of molybdenum during 240 s (silicomolybdate complex) or 600 s (phosphomolybdate complex) at constant current of 50 mA.

4.3.2. Linear sweep voltammetry

Linear sweep voltammetry for heteropolyoxomolybdate was performed on a 3 mm rotating disk gold electrode (5 mV s^{-1}, 1000 rpm) after oxidation of molybdenum in 0.6 mol L^{-1} NaCl solution containing phosphate or silicate at a concentration of about 100 μmol L^{-1}. For comparison, a linear sweep voltammetry was made for heteropolyoxomolybdates created by addition of sodium molybdate (VI) and sulphuric acid to the 0.6 mol L^{-1} NaCl solution containing phosphate or silicate at a concentration of about 100 μmol L^{-1}, where the value of molybdate concentration and pH were the same as those achieved during oxidation of molybdenum. The resulting voltammograms are presented on Fig 12. The voltammograms for heteropolymolybdates created by oxidation of molybdenum were performed firstly from zero-current potential (E$_{I=0}$) to increasing potentials and then to decreasing ones. Finally, both curves were plotted on the same figure.

Linear sweep voltammetry for silico- and phosphomolybdate created by simple addition of acid and sodium molybdate (VI) to the sample containing phosphate or silicate was already done by Carpenter et al. [5]. Similar curves were achieved in this work and present two waves. It can be seen that the first wave shows reduction of complexes in a $2e^-$ process followed by a further $3e^-$ step. According to the results presented above we can propose the following electrode reduction reactions (7 a-d):

$$PMo_{12}O_{40}^{3-} + 2e^- + 2H^+ \leftrightarrow H_2PMo_2^VMo_{10}^{VI}O_{40}^{3-} \tag{7a}$$

$$H_2PMo_2^VMo_{10}^{VI}O_{40}^{3-} + 3e^- + 3H^+ \leftrightarrow H_5PMo_5^VMo_7^{VI}O_{40}^{3-} \tag{7b}$$

$$SiMo_{12}O_{40}^{4-} + 2e^- + 2H^+ \leftrightarrow H_2SiMo_2^VMo_{10}^{VI}O_{40}^{4-} \tag{7c}$$

$$H_2SiMo_2^VMo_{10}^{VI}O_{40}^{4-} + 3e^- + 3H^+ \leftrightarrow H_5SiMo_5^VMo_7^{VI}O_{40}^{4-} \tag{7d}$$
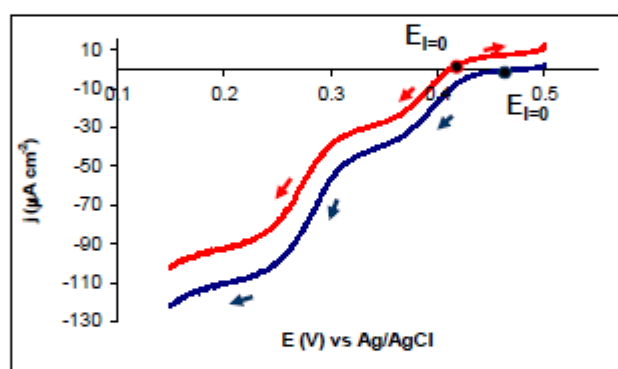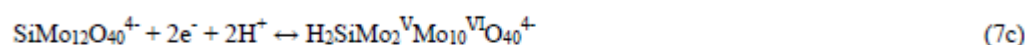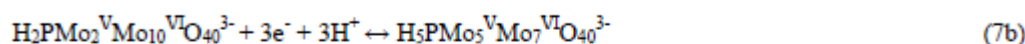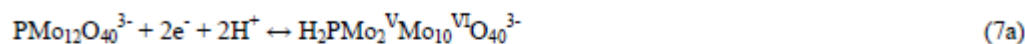
Figure 12a. Linear sweep voltammograms recorded on a rotating gold disk electrode (3 mm, 5 mV s^{-1}, 1000 rpm) for silicomolybdate complex (100 µmol L^{-1}) created by: (blue line) simple addition of sulphuric acid and sodium molybdate (VI) (pH 1.42, $[MoO_4^{2-}]$=6.83 mmol L^{-1}); (red line) oxidation of molybdenum at constant current of 50 mA for 240s.

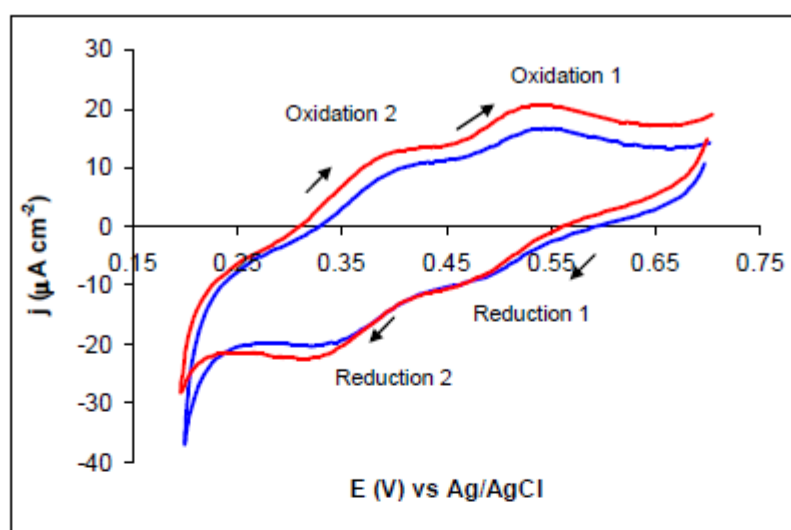However, linear sweep voltammograms for heteropolyoxomolybdates created by oxidation of molybdenum differ from those achieved by simple addition of sulphuric acid and sodium molybdate (VI) to the sample containing phosphate or silicate. Voltammograms for heteropolyoxomolybdates formed by oxidation of molybdenum show an oxidation wave which is not present on voltammograms for heteropolyoxomolybdates formed by simple addition of sodium molybdate and sulphuric acid. Besides, the zero current potential ($E_{I=0}$) reaches a constant value a long time after immersing the electrode and is shifted toward less positive potentials. These results suggest that during oxidation of molybdenum mixed valence heteropolyoxomolybdates (V, VI) are formed. Moreover, the ratio of current density of oxidation over current density of reduction waves gives a possibility to calculate the percentage content of Mo(V) and Mo(VI). The oxidation wave represents the oxidation of Mo(V) to (VI) and the reduction wave the reduction of Mo(VI) to Mo(V). Presuming that the only form of

153

heteropolymolybdate species formed in this work is Keggin anion, the proposed forms of silicomolybdate are: $Si(Mo_2^V Mo_{10}^{VI} O_{40})^{4-}$ – 60% and $Si(Mo_3^V Mo_9^{VI} O_{40})^{4-}$ – 40% , whereas the main form of phosphomolybdate is $P(Mo_6^V Mo_6^{VI} O_{40})^{3-}$.
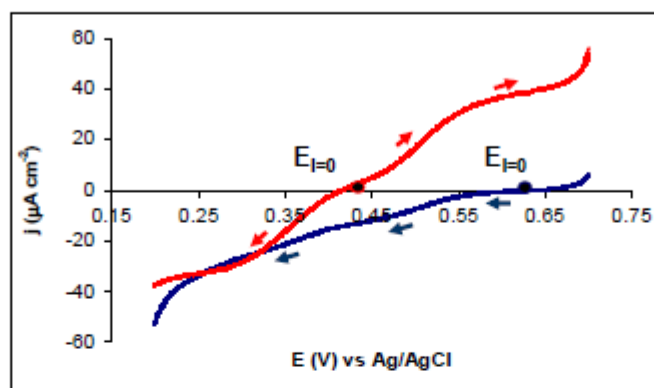
Figure 12b. Linear sweep voltammograms recorded on a rotating gold disk electrode (3 mm, 5 mV s^{-1}, 1000 rpm) for phosphomolybdate complex (100 µmol L^{-1}) created by: (blue line) simple addition of sulphuric acid and sodium molybdate (VI) (pH 1, $[MoO_4^{2-}]$=17.3 mmol L^{-1}); (red line) oxidation of molybdenum at constant current of 50 mA for 600s.
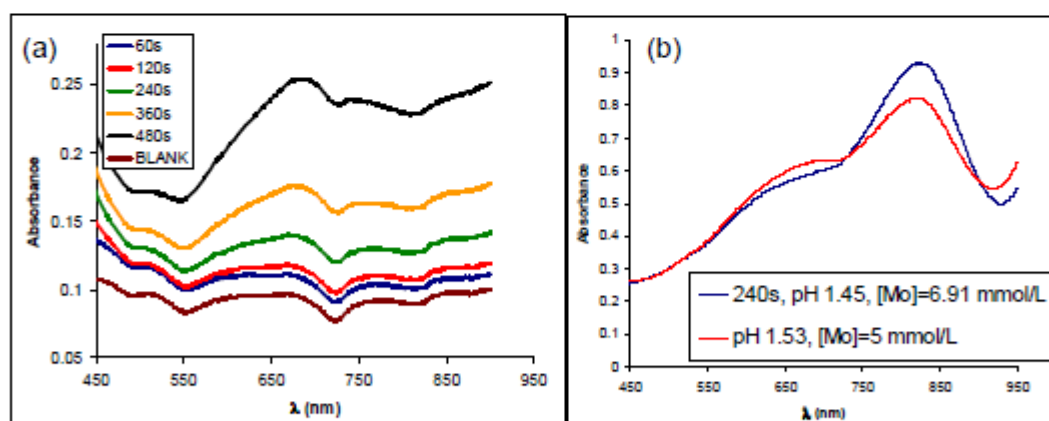
Figure 13. (a) Absorbance as a function of wavelength for molybdates created by oxidation of molybdenum in 0.6 mol L^{-1} NaCl solution containing silicate at concentration of 140 µM at constant current of 50 mA during different times. (b) Absorbance as a function of wavelength for molybdates created by both methods and treated by ascorbic acid.

The existence of mixed valence heteropolymolybdates can be confirmed by spectrophotometry. The data shows peaks at wavelengths corresponding to molybdenum blue spectrum with a maximum at 800 nm (Fig. 13a). This kind of spectrum did not appear if only Mo (VI) is present in the solution.

154

Moreover, addition of ascorbic acid after the oxidation of molybdenum increases the absorbance value and the shape of the spectrograms remains typical of those obtained by simple addition of sodium molybdate and sulphuric acid to the sample containing phosphate or silicate (Fig. 13b).

Linear sweep voltammograms registered at different rotation rates for both complexes formed by both methods are presented on Fig 14. The results show that the potential half wave (E_p) is not dependent on rotation rate whereas current density (j_{lim}) is proportional to the square root of rotation rate ($\omega^{-1/2}$). This characteristic indicates a mass-transport controlled system. For clarity the plots (j_{lim})=f($\omega^{-1/2}$) are gathered in Table 3
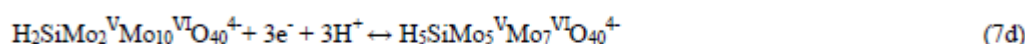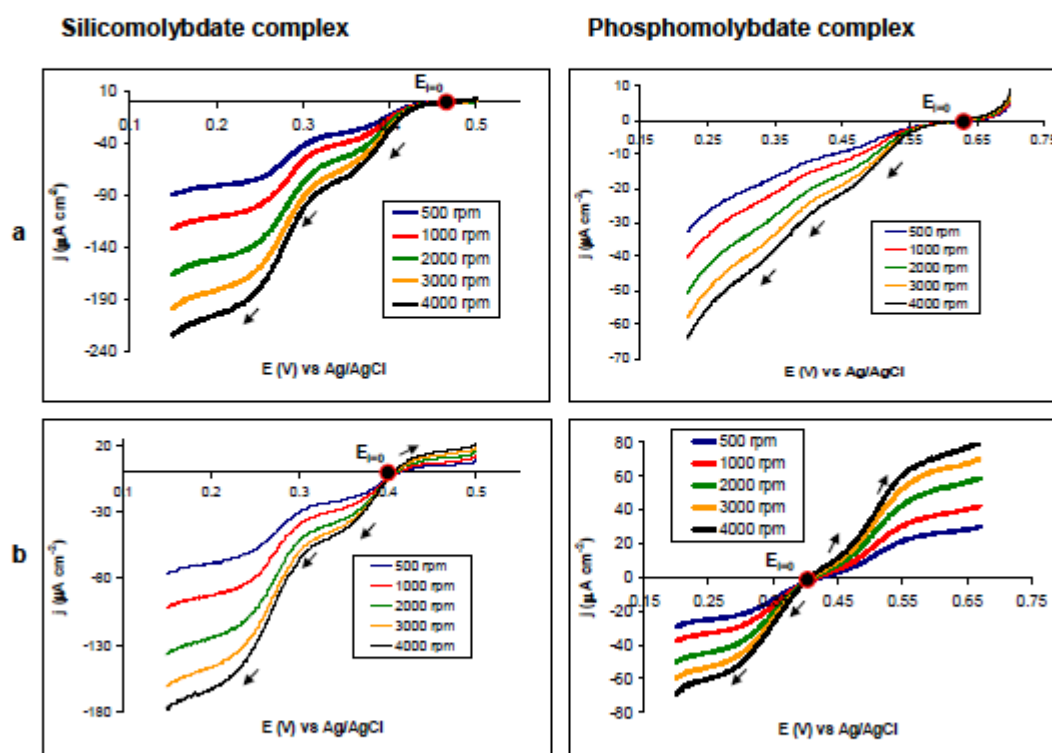

Figure 14. Linear sweep voltammogram recorded on a rotating gold disk electrode (3 mm, 5 mV s^{-1}) at different rotation rates for 100 µmol L^{-1} of silicomolybdate complex (left insets) and phosphomolybdate (right insets) created by: (a) simple addition of sulphuric acid and sodium molybdate (VI) [for silicomolybdate complex: pH 1.42, MoO_4^{2-} = 6.83 mmol L^{-1}; for phosphomolybdate complex: pH 1, MoO_4^{2-} = 16.7 mmol L^{-1}]; (b) oxidation of molybdenum during 240 s (silicomolybdate complex) or 600 s (phosphomolybdate complex) at constant current of 50 mA.

Table 3. Limiting current density vs. square root of rotation rate, $j_{lim}=f(\omega^{-1/2})$ for silicomolybdate and phosphomolybdate complexes created by both methods.

Wave	Phosphomolybdate complex created by :	Silicomolybdate complex created by :
a) simple addition of sulphuric acid and sodium molybdate		
Reduction 1	$j_{lim}=-0.61\,\omega^{-1/2}-7.16,\ R^2=0.999$	$j_{lim}=-3.06\omega^{-1/2}-12,\ R^2=0.999$
Reduction 2	$j_{lim}=-0.30\ \omega^{-1/2}-2.56,\ R^2=0.999$	$j_{lim}=-1.17\ \omega^{-1/2}-5.61,\ R^2=0.999$
b) oxidation of molybdenum at constant current of 50 mA		
Oxidation	$j_{lim}=1.11\ \omega^{-1/2}+1.52,\ R^2=0.999$	$j_{lim}=0.27\ \omega^{-1/2}-0.85,\ R^2=0.997$
Reduction 1	$j_{lim}=-0.86\ \omega^{-1/2}-6.02,\ R^2=0.999$	$j_{lim}=-2.32\ \omega^{-1/2}-18.9,\ R^2=0.997$
Reduction 2	-	$j_{lim}=-0.67\ \omega^{-1/2}-8.55,\ R^2=0.995$

The linear sweep voltammograms for the reduction of the phosphomolybdate species differ from those of the silicomolybdate complex. The waves are not as well formed; they are less steep and they overlap to a greater extent. The limiting currents densities for the phosphomolybdate complex are lower than for the silicomolybdate one. They are not proportional to the radii of the microdisks, being less than the expected ones. These results confirm that the electrode reactions are preceded by a reaction of protonation; this chemical step is faster for the silicomolybdate than for phosphomolybdate complex.

5. CONCLUSION

The purpose of this work was to unravel which kinds of molybdates are formed during anodic oxidation of molybdenum in seawater. The molybdenum oxidation in seawater and in 0.6 mol L^{-1} NaCl solution show similar behaviour as demonstrated by calculations from Tafel plot slopes where the determined anodic transfer coefficient and exchange current density were almost identical for both solutions and equal to about 0.46 and 10^{-4}, respectively.

Electrochemical behaviour of isopoly- and heteropolyoxomolybdates was investigated. The complexes were formed by two methods: one based on oxidation of molybdenum in artificial seawater and the second based on classical addition of sulphuric acid and sodium molybdate which served as a reference method. The investigation shows that the isopolyoxomolybdates formed by oxidation of molybdenum differs from those created by simple addition of reagents. However, it seems that the heteropolyoxomolybdates created by both methods have similar forms. Additionally, the results supported by spectrophotometry indicate formation of mixed valence molybdates (V/VI) during molybdenum oxidation in seawater in presence and absence of phosphate or silicate.

The formed isopolyoxomolybdate shows complicated electrode reactions. Cyclic voltammograms clearly indicate a mass-transport controlled quasi-reversible system, but the linear sweep voltammetry uncovers also the adsorption of reduced species and a kinetically limited reaction. The electrochemical behaviour of molybdate complexes change if phosphate or silicate is present in the solution. The cyclic voltammograms represent a typical reversible mass-transport controlled

system with coupled homogeneous reaction, probably protonation, which prevents rapid electron transfer and influences current magnitude. The protonation step is slower for phosphomolybdate complex and it has greater influence on voltammograms. The cyclic voltammograms for phosphomolybdate species show peaks which are not as well formed as those for silicomolybdate complex. The peaks separation ($E_{pa}-E_{pc}$) is bigger on the phosphomolybdate voltammograms (80 mV) than for silicomolybdate ones (60 mV). Finally, the peak currents densities for the phosphomolybdate complex are lower than for the silicomolybdate. These results explain how delicate the problem of phosphate detection by electrochemistry is. The problem intensifies at low phosphate concentrations (which is the case in the seawater) since complicated electrode reactions coupled with high capacity current lead to disappearance of the characteristic reduction and oxidation peaks [11] and thus, the detection of phosphate by cyclic voltammetry is very difficult.

References

1. W. V. Truesdale, J. S. Smith, *Analyst*, 101 (1976) 19.
2. L. I. Gordon, J. C. Jennings, A. A. Ross, J. M. Krest, WOCE, Method Manual. W. H. P. Office Report (1993) 68.
3. D. Thouron, R. Vuillemin, X. Philippon, A. Laurenço, C. Provost, A. Gruzado, V. Garçon, *Anal. Chem.*, 75, (2003) 2601.
4. A. G. Fogg, N. K. Bsebsu, *Analyst* 106 (1981) 1288.
5. N. Carpenter, A. W. E. Hodgson, D. Pletcher, *Electroanalysis* 9 (1997) 1311.
6. L. Guanghan, W. Xiaogang, L. Yanhua, Y. Shenlai, *Talanta* 49 (1999) 511.
7. S. M. Harden, W. K. Nonidez, *Anal. Chem.* 56 (1984) 2218.
8. J. C. Quintana, L. Idrissi, G. Palleschi, P. Albertano, A. Amine, M. El Rhazi, D. Moscone, *Talanta* 63 (2004) 567.
9. M. Lacombe, V. Garçon, M. Comtat, L. Oriol, J. Sudre, D. Thouron, N. Le Bris, C. Provost, *Mar. Chem.* 106 (2007) 489.
10. M. Lacombe, V. Garçon, D. Thouron, N. Le Bris, M. Comtat, 2008. *Talanta* 77 (2008) 744.
11. J. Jońca, V. León- Fernàndez, D. Thouron, A. Paulmier, M Graco, V. Garçon, *Talanta* 87 (2011) 161.
12. M. Koening, H. Goehr, *Ber. Bunsenges. Phys. Chem.*, 67 (1963) 837.
13. M. Itagaki, T. Suzuki, K. Watanabe, *Electrochim. Acta*, 42 (1997) 1081.
14. M. Bojinov, I. Betova, R. Raicheff, *J. Electroanal. Chem.* 381 (1995) 123.
15. M. Bojinov, I. Betova, R. Raicheff, *Electrochim. Acta*, 41 (1996) 1173.
16. M. N. Hull, *J. Electroanal. Chem.*, 38 (1972) 143.
17. T. V. Chukalovskaya, N. D. Tomashov, V. D. Manaskaya, *Zashchita Metallov* 20 (1984) 864.
18. K. Wang, Y.-S. Li, P. He, *Electrochim. Acta* 43 (1998) 2459.
19. R. D. Armstrong, M. F. Bell, A. A. Metcalfe, *J. Electroanal. Chem.*, 84 (1977) 62.
20. S. Himeno, N. Niiya, T. Ueda, *Bull. Chem. Soc. Jpn.* 70 (1997) 631.

21. C. V. Krishnan, M. Garnett, B. Hsiao, B. Chu, *Int. J. Electrochem. Sci.* 2 (2007) 29.
22. K. H. Tytko, B. Schonfeld, B. Buss, O. Glemnser, *Angew. Chem. Int. Ed.*, 12 (1973) 330.
23. P. Chalilopyil, F. C. Anson, *Inorg. Chem.*, 17 (1978) 2418.
24. A. K. Pettersson, B. Karlberg, *Anal. Chim. Acta* 378 (1999) 183.
25. M. T. Pope (1983) *Heteropoly and Isopoly Oxometalates*, Springer-Verlag, New York.
26. C. E. Easterly, D. M. Hercules, M. Houalla, *Applied Spectroscopy* 55 (2001) 1671.
27. J. J. Cruywagen, A. G. Draaijer, J. B. B. Heyns, E. A. Rohwer, *Inorg. Chim. Acta* 331 (2002) 322.
28. V. V. Kuzenstov, M. R. Pavlov, D. I. Zimakov, S. A. Chepeleva, V. N. Kudryavtsev, *Rus. J. Electrochem.*, 40 (2004) 711.
29. A. J. Bard and L. R. Faulkner: *Electrochemical methods: Foundamentals and applications "*, John Wiley and Sons, INC. (2001), New York, 341.

SUMMARY OF ARTICLE 1

The purpose of this work was to discover which kinds of isopoly- and heteropolyoxomolybdates complexes are formed during the electrochemical oxidation of molybdenum electrode in seawater. These results will help us to develop a first electrochemical sensor for *in situ* detection of phosphate and silicate in the ocean having elucidated the complex chemistry of isopoly- and heteropolyoxomolybdates.

The complexes were formed by two methods. The first one was based on oxidation of molybdenum in artificial seawater. The second was based on classical addition of sulphuric acid and sodium molybdate and serve as a reference method. The results supported by spectrophotometry indicate formation of mixed valence molybdates (V/VI) during molybdenum oxidation in seawater in presence and absence of phosphate or silicate. The chemical formula for silicomolybdate and phosphomolybdate complexes was proposed: $H_4Si(Mo_2^{V}Mo_{10}^{VI}O_{40})$-60%, $H_4Si(Mo_3^{V}Mo_9^{VI}O_{40})$-40% and $H_3P(Mo_6^{V}Mo_6^{VI}O_{40})$.

The formed isopolyoxomolybdate represent complicated electrode reactions. Cyclic voltammograms clearly indicate a mass-transport controlled quasi-reversible system, but the linear sweep voltammetry uncovers also some absorption and kinetically limited reactions. The electrochemical behaviour of molybdate complexes changes if phosphate or silicate is present in the solution. The cyclic voltammograms represent a typical reversible mass controlled system with coupled homogenous reaction, probably protonation, which prevents rapid electron transfer and influences current magnitude. The protonation step is slower for phosphomolybdate than silicomolybdates complex and it has a greater influence of registered voltammograms.

These results explain how delicate the problem of phosphate detection by electrochemistry is. Because of the slow rate of the protonation step the voltammograms for phosphomolybdate species show peaks which are not as well formed as those for the silicomolybdate complex (Figure V. 1.1). The peaks separation (E_{pa} - E_{pc}) is larger on the phosphomolybdate voltammograms (80 mV) than for the silicomolybdate ones (60 mV). Finally, the peak currents for the phosphomolybdate complex are lower than for the silicomolybdate one.
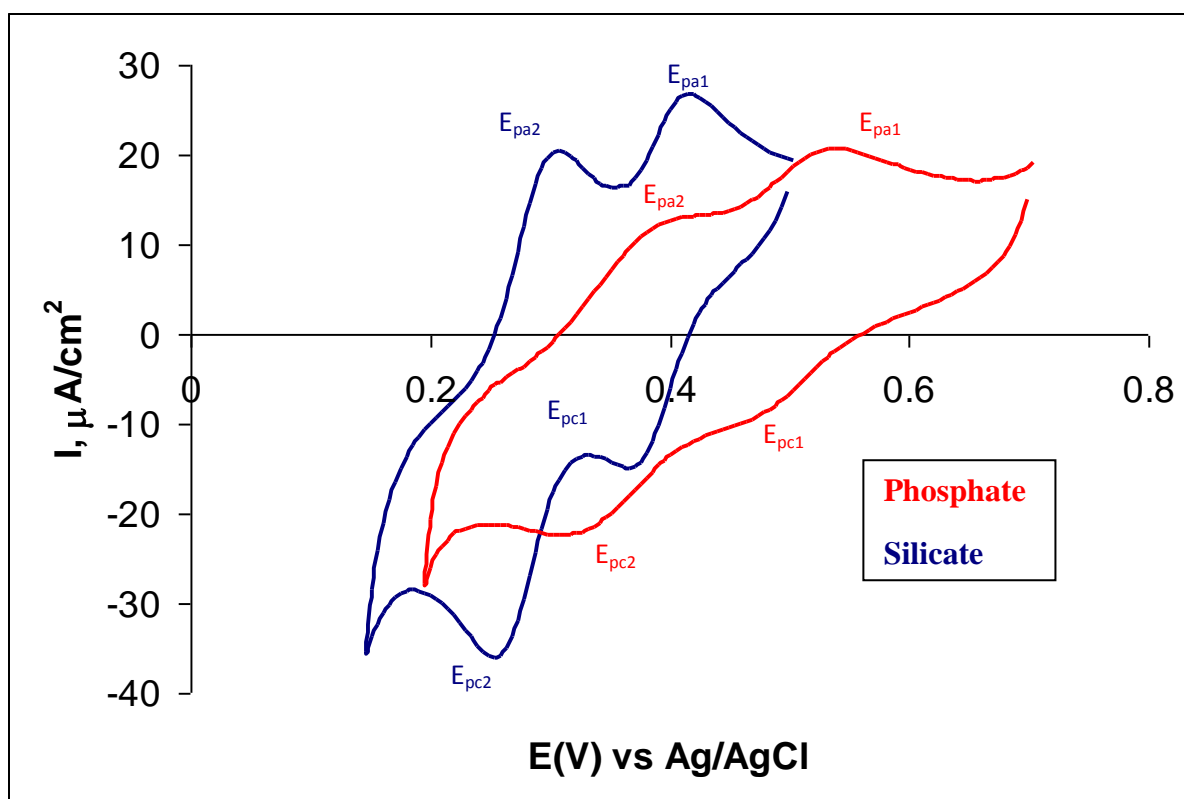
Figure V. 1.1. Cyclic voltammetry performed on gold electrode (3mm, 50 mV/s) for silicomolybdate (blue line) and phosphomolybdate (red line) formed by oxidation of molybdenum in artificial seawater containing silicate or phosphate

CHAPTER VI:

ELECTROCHEMICAL METHODS FOR PHOSPHATE DETECTION IN SEAWATER

The long term objective is to obtain an electrochemical sensor which will be able to measure phosphate in the concentration range found in the ocean (below 3.5 μM). This sensor has to work autonomously meaning without reagents and standard calibration. The sensor has to be highly selective to avoid interferences from other species found in the ocean, especially from silicates. The final sensor should be characterized by a short time response (shorter than a few minutes), low power consumption and long operation time (minimum 3 months). The instrument will remain in the ocean for a long time so pressure, temperature and salinity have to be considered, because these parameters have an influence on the electrochemical signals. The appropriate steps must be taken to avoid biofouling and corrosion problems. The sensor should be adaptable on eulerian or lagrangian platforms for biogeochemical monitoring of the oceans.

The two publications (Articles 2 and 3) presented below show the current state of the phosphate sensor development. Future work required for this sensor is discussed as well.

Contents:

Article 2: Jońca, J., Leon-Fernandez, V., Thouron, D., Paulmier, A., Graco, M., Garçon, V., 2011, *Phosphate determination in seawater: Towards an autonomous electrochemical method,* Talanta 87, 161-167

Contents lists available at SciVerse ScienceDirect

Talanta

Phosphate determination in seawater: Toward an autonomous electrochemical method

Justyna Jońca [a,b,*], Violeta León Fernández [c], Danièle Thouron [a], Aurélien Paulmier [a,c], Michelle Graco [c], Véronique Garçon [a]

[a] *Laboratoire d'Etudes en Géophysique et Océanographie Spatiales, UMR 5566, 18 Avenue Edouard Belin, 31401 Toulouse Cedex 9, France*
[b] *Laboratoire de Génie Chimique, UMR 5503, Université Paul Sabatier, 118 Route de Narbonne, 31062 Toulouse Cedex, France*
[c] *Instituto del Mar del Perú IMARPE Esquina Gamarra y General Valle S/N Chucuito, Lima, Peru*

ARTICLE INFO

ABSTRACT

Initial steps to create an autonomous *in situ* electrochemical sensor for orthophosphate determination in seawater are presented. First, the optimal conditions to form the molybdophosphate complex in artificial seawater medium were determined by addition of sulphuric acid and sodium molybdate to the solution containing orthophosphate. Secondly, the anodic oxidation of molybdenum to form molybdate ions and protons was used to create the molybdophosphate complex without addition of any liquid reagents. The molybdophosphate complex is detectable by amperometry with an average precision of 2.2% for the concentration range found in the open ocean and the detection limit is 0.12 μM.

Three solutions are proposed to address the silicate interferences issue and one of these methods is used for the natural samples collected in the coastal waters offshore Peru during the Pelagico 1011-12-BIC OLAYA cruise in November–December 2010. Results showed a good precision with an average of 2.5% and a reasonable deviation of the amperometric analysis as compared with colorimetric measurements (4.9%).

1. Introduction

Phosphorus is an essential nutrient element for organisms in the marine environment and may be sometimes a limiting factor for primary production [1]. The phosphorus cycle still remains one of the important research topics in biogeochemical oceanography [2]. Thus, rapid and selective methods for the determination of orthophosphate, the major form of phosphorus in the open ocean, constitute an important target. The common analytical method to measure phosphate in natural waters is spectrophotometry which is now frequently carried out in an automated continuous flow system [3,4]. The method requires the addition to the sample of an acidic molybdate solution to convert phosphate into the Keggin anion, $PMo_{12}O_{40}{}^{3-}$ which is intensely blue after reduction by ascorbic acid with a maximum of absorption at 810 nm. Alternate methods based on electrochemistry have also been proposed. Amperometric procedures have been reported for the determination of phosphate as molybdophosphate complex [5,6]. Phosphate has been also determined by using voltammetric methods with carbon paste electrode [7], gold microdisk electrode [8] and glassy carbon electrode [9]. The obtained voltammetric signals are based on the reduction of the molybdophosphate complex and the detection limit was a few micromoles per liter. Other electrochemical phosphate sensors include: liquid–membrane electrodes with organotin carriers [10], coated-wire electrode [11], heterogeneous membrane electrodes [12] and a large number of biosensors [13–15]. The latter usually require more than one enzyme and a rigorous control of the activity and stability of the used enzymes. Electrochemistry offers a wide range of possibilities for achieving an excellent phosphate determination in seawater with the following figures of merit: long lifetime, high precision, low detection limit, fast response time, good reproducibility but no autonomous electrochemical sensor for *in situ* phosphate determination exists nowadays.

Our team developed an electrochemical method for silicate determination in seawater based on anodic oxidation of molybdenum [16,17]. The aim of the present work is to adopt this method to phosphate detection in seawater and to create an electrochemical cell where molybdate ions and protons will be produced in order to create molybdophosphate complex electrochemically detected either by means of cyclic voltammetry or amperometry. The situation is more delicate because of cross interference in the natural seawater samples which contain both silicate and phosphate.

* Corresponding author at: Laboratoire d'Etudes en Géophysique et Océanographie Spatiales, UMR 5566, 18 Avenue Edouard Belin, 31401 Toulouse Cedex 9, France. Tel.: +33 05 61 33 29 13; fax: +33 05 61 25 32 05.
E-mail address: justyna.jonca@legos.obs-mip.fr (J. Jońca).

165

This work is a first step to develop an autonomous *in situ* sensor for electrochemical detection of phosphate in seawater. First, the method with the addition of sodium molybdate and sulphuric acid solutions to the phosphate artificial samples is described. Then the electrochemical oxidation of molybdenum to form molybdate and protons is presented. The silicate interference problem is discussed and a comparison with classical phosphate detection (colorimetry) is provided. Finally, an application of our method to natural seawater samples collected during an oceanographic cruise off Peru is presented.

2. Methods

2.1. Reagents and calibration standards

All solutions are prepared in Milli-Q water (Milli-pore Milli-Q water system) with reagent grade salts.

Artificial sea water for standards calibration, phosphate and silicate samples is prepared at a salinity of 34.4.

Working calibration standards are prepared as described in the WOCE operation and method manual [4] with potassium dihydrogen phosphate (KH_2PO_4, Merck) and sodium silicofluoride (Na_2SiF_6, Merck).

The reagents used for electrochemical phosphate detection are sulphuric acid (H_2SO_4, 5 N, Merck) and sodium molybdate solution ($Na_2MoO_4 \cdot 2H_2O$, Merck).

Phosphate artificial samples determinations by colorimetry are performed using:

- an acidified ammonium heptamolybdate solution (6 g of ammonium heptamolybdate, 0.15 g potassium antimonyl tartrate, 40 mL of sulphuric acid, H_2SO_4 0.051 M in 1000 mL of Milli-Q water),
- an ascorbic solution (7.58 g of L-ascorbic acid in 250 mL of Milli-Q water and 0.5 mL of Aerosol 22).

Phosphate natural samples determinations by colorimetry are performed using:

- an ammonium heptamolybdate solution (15 g of ammonium heptamolybdate in 500 mL of Milli-Q water),
- an acidic solution (140 mL of sulphuric acid, H_2SO_4 in 900 mL of Milli-Q water),
- an ascorbic acid solution (27 g of ascorbic acid in 500 mL of Milli-Q water),
- an antimonyl potassium tartrate solution (0.34 g of antimonyl potassium tartrate in 250 mL of Milli-Q water).

These solutions are mixed together (100 mL ammonium heptamolybdate, 250 mL sulphuric acid, 100 mL ascorbic acid and 50 mL antimonyl potassium tartrate) and the final solution is used for phosphate determination (10 mL for each 100 mL of the sample).

2.2. Colorimetric method

Colorimetric detection of phosphate artificial samples is done following Le Corre and Tréguer's method [18] and an Auto-Analyzer 3rd generation (AAIII Bran Luebbe) is used. Colorimetric detection of phosphate natural samples is developed following the method of Strickland and Parsons [19] and a spectrophotometer UV-VISIBLE LAMBDA 45 is used. The baselines are made with artificial seawater.

Reproducibility tests are performed for both spectrophotometers. The average precision obtained for artificial samples is 1.10%, whereas for natural samples this value is 2.37%.

2.3. Electrochemical method

Electrochemical measurements are carried out with a potentiostat µ-Autolab III (Metrohm). The reference electrode is an Ag/AgCl/KCl 3 M electrode (Metrohm). All the following potentials are given relative to this electrode. Measurements at a stationary or rotating disk electrode are recorded in a three electrode cell with a platinum counter electrode and gold or glassy carbon working electrode (Metrohm, diameter 3 mm). The working electrode is polished with lapping film sheet (3 M Aluminum Oxide, 1 µm) before the measurements.

The molybdenum electrode has a surface of 20 mm^2 (Goodfellow). Molybdate is produced by molybdenum anodic oxidation performed at a constant electrolysis current (50 mA) in a 5 mL cell.

The simultaneous production of molybdate and protons is based on the use of a cell divided in two parts by a Nafion membrane (N117 Du Pont^{TM} Nafion^R PFSA Membranes). The first half of the cell is filled with 3 mL of solution and the second half with 17 mL of solution. The first half contains the molybdenum, reference and sensing electrodes. The counter electrode is placed in the second half. Molybdate and protons are produced by molybdenum anodic oxidation performed at a constant electrolysis current (50 mA) during 500 s.

2.4. Seawater collection

The collection of seawater samples from four east–west transect lines was made during the Pelagico 1011-12-BIC OLAYA cruise aboard R/V Jose Olaya Balandra off Peru during austral spring 2010 (November–December), when intense upwelling occurs. Samples for phosphate analysis by both colorimetric and amperometric methods were collected during the leg from Puerto Pizzaro (3.67°S) to Salaverry (8.13°S) from November 10th to November 29th, 2010. Among the 22 CTD profiles performed during this leg, 7 vertical profiles were analyzed by both methods for phosphate determination.

Seawater was collected using 12 L Niskin bottles mounted on a cable equipped with a CTD-O$_2$ Sea Bird 25.

Samples were collected, frozen immediately and stored in 250 mL Nalgene plastic flasks then transported to the laboratory of the Chemical Research Unit of the Instituto del Mar del Peru (UIOQ-IMARPE) for analysis.

3. Results and discussion

3.1. Voltammetric and amperometric methods

The electrochemical determination of the non electroactive phosphate is based on the formation of a complex with molybdate. The complex is formed by the reaction of Na_2MoO_4 in an acidic solution (pH 1.0) to form a Keggin anion according to reaction (1). Molybdate is in large excess (20 mM) and the pH is adjusted with sulphuric acid.

$$PO_4{}^{3-} + 12MoO_4{}^{2-} + 27H^+ \rightarrow H_3PMo_{12}O_{40} + 12H_2O \tag{1}$$
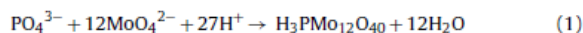
Cyclic voltammetry of the formed Keggin anion shows two reduction peaks at 0.32 V and 0.46 V and two oxidation peaks at 0.40 V and 0.53 V. The complexation takes about 60 s and cyclic voltammetry gives 4 correlation curves for concentrations greater than 5.0 µM. Unfortunately the concentrations of phosphate found in the open ocean are smaller (less than 3.0 µM) and in this concentration range the voltammograms show only one reduction and one oxidation peak which are not well marked because of the large ratio between the capacitive and the faradic currents.

To increase the sensitivity of the detection, an amperometric method was chosen. The working gold electrode was held at a constant potential of 0.29 V. Fig. 1 shows an amperometric linear
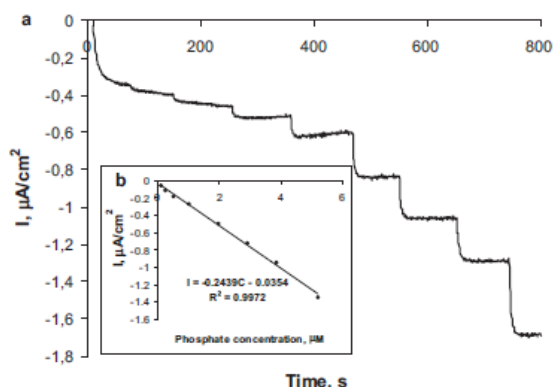
Fig. 1. Variation of current for the molybdophosphate complex measured by amperometry at a rotating gold electrode (0.29 V, 1000 rpm) as a function of time (a) and phosphate concentration (b). The calibration curve was achieved by addition of standard phosphate solution in the concentration range of 0.10–5.21 μM; molybdate concentration 20 mM, pH 1.0.

response in an experiment carried out in artificial seawater at pH 1.0 and with a concentration of molybdate of 20 mM. This calibration curve was obtained by addition of standard phosphate solution in the concentration range of 0.10–5.21 μM. The detection limit for this method is 0.05 μM. The detection limit was calculated as a signal measured between the highest and the lowest values of noise multiplied by three. The method is characterized by a good repeatability and the precision for each concentration is smaller than 3%. Amperometry is a very simple method, well adapted to the flow injection analysis, but the main drawback of this method for achieving an *in situ* long term sensor is that it requires the addition of molybdate and protons in the sample before measurements.

To optimize the method, influence of pH, electrode rotation rate and molybdate concentration were investigated. A pH range between 1.75 and 0.50 was examined by amperometry and we obtained the best results with a pH around 1.0. Fig. 2 shows the variation of current for a phosphate concentration of 1.0 μM in different pH conditions. The influence of the electrode rotation and molybdate concentration was studied by linear sweep voltammetry. Results show that the current increases with the angular frequency of the electrode rotation and with the concentration of molybdate. Fig. 3a shows the current versus potential curves for the molybdophosphate complex in different molybdate concentrations performed in artificial seawater containing phosphate at

constant concentration. No significant influence of the concentration of molybdate on current for the molybdophosphate complex was detected for concentrations larger than 20 mM.

The linear sweep voltammetry presented in Fig. 3b shows two reduction waves. In agreement with previous studies [8] the first reaction involves two electrons and the second three. Thus, the first reaction is the reduction of molybdate (VI) to molybdate (IV) and the second reaction is the reduction of molybdate (IV) to molybdate (I).

The voltammetry for the reduction of the phosphomolybdate species differs from that of the silicomolybdate complex [17] in several ways. The waves are not as well formed, they are less steep and they overlap to a greater extent. The limiting currents for the phosphomolybdate complex are lower than for the silicomolybdate one and they are not proportional to the radii of the microdisks, with the currents being less than expected. This characteristic is typical for electrode reactions where the electron transfer is preceded by a homogeneous chemical step which limits the rate of a protonation step or the rate of an isomerization which prevents rapid reduction of all the phosphomolybdate species in solution. This problem was already discussed by Carpenter et al. [8].

3.2. Oxidation of molybdenum

To avoid the addition of sodium molybdate in the sample we worked toward an electrochemical way to produce this ion in seawater medium. Molybdate is formed directly in the acidic medium by anodic oxidation of molybdenum at constant current of 50 mA in a 5 mL cell, according to reaction (2).

$$Mo + 4H_2O \rightarrow MoO_4^{2-} + 8H^+ + 6e^- \qquad (2)$$
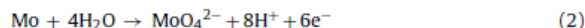
Electrochemical oxidation of molybdenum has been performed in several solutions [20,21] and in sea water [16,17]. However, our knowledge about the different forms of molybdates produced during this process is limited. Numerous works on molybdate solutions were done. The nature of the formed molybdate species depends strongly on the molybdate concentration and pH [22]. At very low concentrations ($<10^{-4}$ M) mononuclear species predominate. At higher concentrations numerous teams have shown the existence of the polynuclear species [23]. A longer oxidation time of molybdenum leads to higher molybdate concentration in the solution and the percentage of polynuclear species increases with oxidation time. Besides, the formation of polymolybdates consumes some protons and more and more complex polymolybdates are created with growing acidification. Having all this in mind, we assume that reaction (2) will change with time during the molybdenum oxidation.

3.3. Electrochemical production of molybdate and protons

In order to avoid the addition of both sodium molybdate and sulphuric acid, a method based on an electrochemical cell divided in two by a membrane was developed. Separation of the molybdenum anode from the cathode by a Nafion diaphragm eliminates the consumption of the protons on the platinum cathode. Thus, the protons formed according to reaction (2) accumulate in the anodic part of the cell. The optimal pH for the molybdophosphate complex formation was determined to be close to 1.0 (Section 3.1). To obtain this pH, it is necessary to oxidize the molybdenum electrode during 500 s at a stable current of 0.05 A in seawater starting with an average initial pH of 7.8. Reproducibility tests show a precision of 1.7% for this time of oxidation and the average value of pH is 1.02. During the oxidation we observed the evolution of molybdate and pH with time. Fig. 4 shows the evolution of the molybdate peaks in the reaction cell as a function of the molybdenum oxidation time
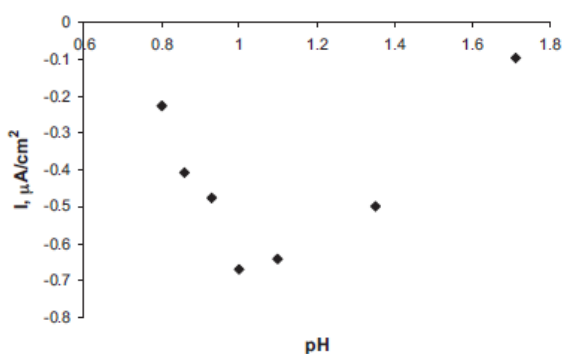

Fig. 2. Variation of current measured by amperometry at rotating gold electrode (0.29 V, 1000 rpm) as a function of pH for molybdophosphate complex performed in artificial seawater containing phosphate in concentration of 1.0 μM.
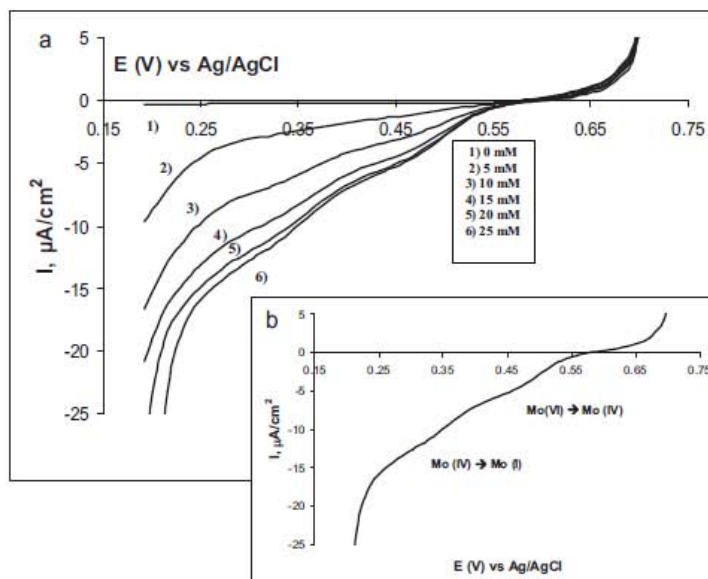
Fig. 3. Linear sweep voltammetry (5 mV/s) at a gold rotating disk electrode (1000 rpm) for molybdophosphate complex at pH 1.0 and different concentrations of molybdate (0, 5, 10, 15, 20, 25 mM), phosphate concentration 100 μM. (a) Optimization of molybdate concentration and (b) two steps of reduction of the molybdophosphate complex.

and pH. Molybdate reduction peak occurs at about −0.60 V. Moreover, the position of the peaks is shifted to more negative potentials for reduction peak and to more positive ones for oxidation peak as molybdenum oxidation goes along. Based on the influence of the rates of complex formation, difference in the electrochemical behavior is due to the formation of more and more complex polymolybdate species which are difficult to reduce and then to oxidize.

The molybdophosphate complex formed as described above can be detected in the electro-reduction process on the gold electrode at a potential of 0.29 V. This method gives a good linear response for phosphate in the concentration range of 0.33–3.20 μM and the detection limit is 0.12 μM ($I = -0.266C + 0.038$; $R^2 = 0.9973$; I in μA/cm^2). However, we also noticed a good linear correlation for smaller concentrations (0.10–1.0 μM) but with a lower sensitivity

$(I = -0.216C + 0.007$; $R^2 = 0.9992$; I in μA/cm^2). The detection limit was calculated as a signal measured between the highest and the lowest values of noise multiplied by three. The reproducibility tests reported in Table 1 exhibit a good precision in the concentration range usually found in the open ocean.

3.4. Silicate interferences

There is an obvious problem of cross interference in the ocean samples which contain both silicate and phosphate. Thus methods described above have to be adapted to overcome this challenge. A few approaches to avoid silicate interferences are proposed using differences in kinetics of complex formation [24], differences in electrochemistry of the two complexes and influence of pH on complex formation [8,25].

We observed by linear sweep voltammetry that the reduction of the molybdophosphate complex starts at a potential close to 0.55 V while the reduction for the molybdosilicate complex starts at 0.45 V. Fig. 5 shows the linear sweep voltammetry for both complexes in the potential range 0.20–0.70 V. Two reduction waves for each species clearly indicate that if we choose one of the potentials in the range at 0.45–0.55 V we would eliminate the interference from silicate. We found that for a potential of 0.50 V we do not obtain an amperometric signal for silicate while the signal for phosphate was exhibiting a linear correlation with concentration. However, this potential corresponds only to the first reduction wave and we lose some sensitivity. Besides, for the conditions where molybdate and protons were produced during anodic
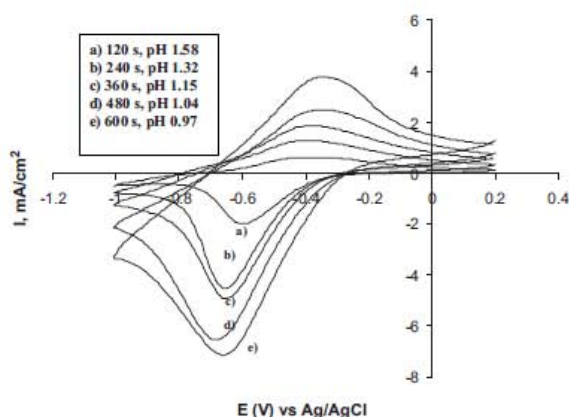
Fig. 4. Monitoring of pH and molybdate formation versus time: voltammograms obtained on stationary carbon glass electrode (200 mV/s) after several electrode time intervals of molybdenum oxidation in artificial seawater.

Table 1
Reproducibility tests for molybdophosphate amperometric detection obtained for different phosphate concentrations in artificial sea water samples. Each sample was measured 10 times.

Concentration (μM)	0.33	0.83	1.48	2.28	3.22
Standard deviation	0.11	0.33	0.42	0.92	1.19
Precision (%)	2.3	2.6	1.7	2.3	2.0
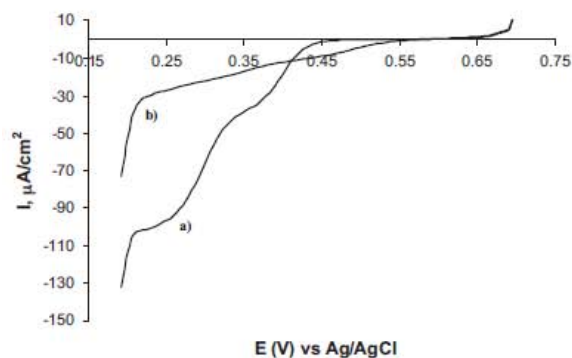
Fig. 5. Steady state voltammograms (5 mV/s) for molybdophosphate and molybdosilicate complexes on a gold rotating disk electrode (1000 rpm) in artificial seawater containing 100 μM of silicate (a) and 100 μM phosphate (b); molybdate concentration 20 mM, pH 1.0.

Fig. 7. Amperometric measurements made on a rotating gold electrode (0.29 V, 2000 rpm) for molybdosilicate and molybdophosphate complexes performed in artificial seawater. The signals were achieved by addition of standard solutions of: (a) silicate (5.0–140 μM) and (b) phosphate (0.49–3.30 μM); pH 1.0, ratio protons/molybdate = 70.

oxidation of molybdenum in seawater containing both silicate and phosphate species, we observe on the amperogram at a stable potential of 0.50 V not only the reduction of the molybdophosphate complex but also oxidation of other molybdate species formed during oxidation of molybdenum, which makes it impossible to detect phosphate.

Carpenter et al. [8] and Hodgson and Pletcher [25] indicated that at pH smaller than 0.50 there was no formation of the molybdosilicate complex. For this pH we did not obtain any signal for silicate in the concentration range found in the open ocean, while the signal for phosphate was well formed. Fig. 6 shows the amperometric response for silicate and phosphate under different pH conditions. We lose some sensitivity because a pH of 0.50 is not the optimized one. In addition, when molybdenum is oxidized in a sample containing both species, the molybdosilicate complex is formed at the beginning of this process and further acidification does not destroy it.

Zhang et al. [24] indicated that when working with a ratio of protons/molybdates close to 70 at pH 1.0 (meaning the molybdate concentration has to be close to 1.5 mM), the interference from silicate can be avoided. Although the method was used for colorimetric detection of phosphate in presence of silicate, we confirmed that it was also adequate using amperometry. According to reaction (2),

the ratio of protons/molybdate is 8 during the oxidation of molybdenum. We achieved an appropriate ratio of 70 by an extra addition of sulphuric acid. The last method seems to be the most promising one. Indeed, it does not require any modification of potential applied to the gold electrode during reduction of the molybdophosphate complex. Fortunately, the pH required for this method is 1.0 which happens to be the optimized value of pH we found. It will be thus easier to find a method for the protons production equivalent to this pH, than for example to go down to pH 0.50. Finally, with the molybdate concentration required for this method, the oxidation time is much shorter, 50 s in a 3 mL cell, than before (Section 3.3). Since the time of formation of the complex is about 60 s, the total reaction time is 110 s. Fig. 7 presents a calibration curve made in the mentioned conditions. It is clear that there is no signal for silicate, whereas the signal for phosphate exhibits a linear correlation in a concentration range 0.49–3.33 μM and with a detection limit of 0.22 μM. This latter method was used for the natural samples collected off Peru during the Pelagico 1011-12 cruise aboard the R/V OLAYA.

3.5. Comparison for sea water samples

Before applying this method to the natural samples, reproducibility of the method was tested for different phosphate concentrations representative of the seawater gradient reported in the Oxygen Minimum Zone off Peru and an intercomparison with the classical method was made. The reproducibility test performed on artificial sea water samples shows a precision on 2.1% for the highest phosphate concentration of 3.4 μM, 2.8% and 6.1% for intermediate concentrations of 2.2 μM and 1.2 μM, respectively and 6.3% for the lowest concentration of 0.5 μM. The reproducibility test was made with ten measurements for each sample. The intercomparison of the electrochemical method for artificial sea water samples with the laboratory classical method showed a good correlation with an average deviation of about 5.1%.

For the natural samples, the reproducibility tests were made at different CTD stations covering different *in situ* configurations (e.g. near the coast/off-shore, lower/higher latitude stations of the cruise, shallower/deeper depths) with a triplicate measurement on the same sample at each depth. Table 2 provides the obtained precision between 1.1 and 3.9% with an average value of 2.5%.

The typical vertical profiles of phosphate concentrations obtained offshore Peru in the coastal waters demonstrate that the electrochemical method is in excellent agreement with the colorimetric analysis conventionally used for seawater analysis (Fig. 8).

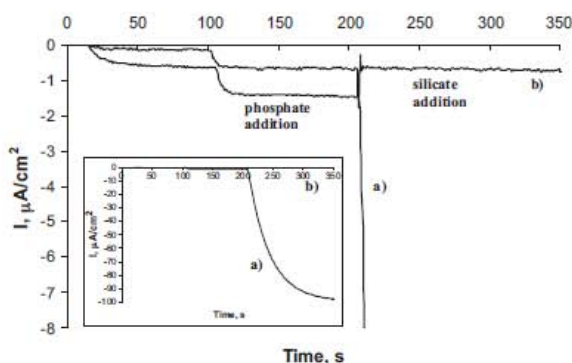**Fig. 6.** Amperometric response for molybdosilicate and molybdophosphate complexes on a gold rotating disk electrode (0.29 V, 1000 rpm) in artificial seawater. The signals were achieved by addition of standard phosphate solution in concentration of 3.0 μM and standard silicate solution in concentration of 150 μM; sodium molybdate 20 mM, pH 1.0 (a) and 0.50 (b). Inset presents the full signal for silicate when pH is 1.0.
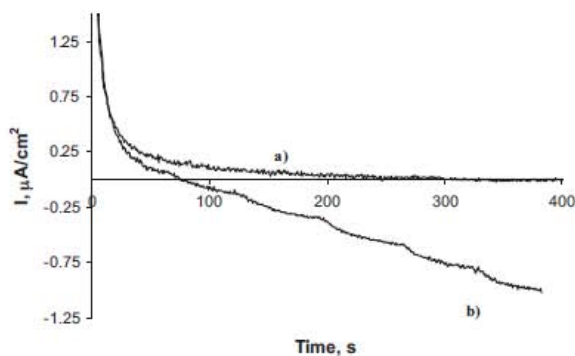
Fig. 8. Comparison of both methods, amperometry (black) and colorimetry (grey) at CTD stations 50 (a), 102 (b), 59 (c). Station 59 is situated very close to the coast and stations 50 and 102 more off-shore.

Table 2
Reproducibility tests made for natural phosphate samples (σ – standard deviation). Test made for the samples collected during the Pelagico 1011-12-BIC OLAYA cruise aboard R/V Jose Olaya Balandra.

Station	Depth (m)	Average (μM)	σ	Precision (%)
1	25	0.91	0.18	1.7
11	2	0.88	0.3	3.0
11	70	1.93	0.25	1.1
11	440	1.77	0.71	3.3
50	25	1.83	0.38	1.7
50	100	1.8	0.78	3.5
59	2	1.12	0.42	3.2
95	50	1.99	0.3	1.1
102	2	0.56	0.21	2.6
102	100	1.68	0.46	2.0
174	2	1.19	0.66	3.9

The average deviation obtained for all phosphate concentrations is 4.9%.

4. Conclusion

We have shown a thorough documentation necessary to set up an electrochemical method for phosphate detection in seawater. With molybdate and sulphuric acid addition to the seawater sample containing phosphate, we optimize the best conditions to produce the phosphomolybdate complex. We then created an electrochemical cell where molybdate ions and protons are produced by anodic oxidation of molybdenum in order to form phosphomolybdate complex without addition of liquid reagents. The created complex is detected electrochemically by means of amperometry with a detection limit of 0.12 μM.

We presented here a discussion about silicate interferences and we proposed three methods to solve this problem: detection of phosphate in presence of silicate by amperometry at a potential of 0.50 V, at pH 0.50 or at an appropriate ratio of protons/molybdate (70). The latter method was used during the "Pelagico 1011-12" cruise aboard the R/V OLAYA offshore Peru and showed that the amperometric approach is reliable for the analysis of phosphate in the water column. Thus, the method is very promising but presently appropriate ratio of protons/molybdate is achieved by an extra addition of sulphuric acid. We are currently working on introducing proton exchange membranes in order to avoid the acid addition in the cell. Identification of the molybdate species obtained during anodic oxidation of molybdenum in seawater

is also under investigation. This recognition is being performed by both electrochemical and spectroscopic methods. This study is crucial to entirely solve the problem with silicate interferences and to elucidate the complex chemistry of isopoly- and heteropoly-molybdates.

It is worth noticing that the investigated method can be used for analysis of phosphates in other aqueous environments such as lakes or rivers where silicate concentrations are negligible as compared to phosphate concentrations so that the analysis can be performed without interferences.

References

[1] T. Tyrrel, Nature 400 (1999) 525–531.
[2] A. Paytan, K. McLaughlin, Chem. Rev. 107 (2007) 563–576.
[3] W.V. Truesdale, J.S. Smith, Analyst 101 (1976) 19–31.
[4] L.I. Gordon, J.C. Jennings, A.A. Ross, J.M. Krest, WOCE, Method Manual. W.H.P. Office Report (1993) 68–69.
[5] A.G. Fogg, N.K. Bsebsu, Analyst 106 (1981) 1288–1295.
[6] S.M. Harden, W.K. Nonidez, Anal. Chem. 56 (1984) 2218–2223.
[7] L. Guanghan, W. Xiaogang, L. Yanhua, Y. Shenlai, Talanta 49 (1999) 511–515.
[8] N. Carpenter, A.W.E. Hodgson, D. Pletcher, Electroanalysis 9 (1997) 1311–1317.
[9] T. Matsunaga, T. Suzuki, R. Tomoda, Enzyme Microb. Technol. 6 (1984) 355–358.
[10] D. Liu, W.C. Chen, R.H. Yang, R.Q. Yu, Anal. Chim. Acta 338 (1997) 209–214.
[11] J. Liu, Y. Masuda, E. Sekido, J. Electroanal. Chem. 291 (1990) 67–79.
[12] M.N. Beg, M. Arshad, Indian J. Chem. 27A (1988) 460–462.
[13] N. Conrath, B. Gründig, S. Hüwel, K. Cammann, Anal. Chim. Acta 309 (1995) 47–52.
[14] J.J. Fernández, J.R. López, X. Correig, I. Katakis, Sens. Actuators B (1998) 13–20.
[15] V.G. Gavalas, N.A. Chaniotakis, Anal. Chim. Acta 427 (2001) 271–277.
[16] M. Lacombe, V. Garçon, M. Comtat, L. Oriol, J. Sudre, D. Thouron, N. Le Bris, C. Provost, Mar. Chem. 106 (2007) 489–497.

[17] M. Lacombe, V. Garçon, D. Thouron, N. Le Bris, M. Comtat, Talanta 77 (2008) 744–750.

[18] P. Le Corre, P. Tréguer, Contribution à l'étude de la matière organique dissoute et des sels nutritifs dans l'eau de mer. Caractéristiques chimiques du Golfe de Gascogne et des upwellings côtiers de L'Afrique du Nord-Ouest. Thesis. Université de Bretagne Occidentale. Brest. (1976) 490 pp.

[19] J. Strickland, T. Parson, Practical Handbook of Seawater Analysis, vol. 167, Fisheries Board of Canada Ottawa. Bulletin, 1972, 49–52.

[20] M. Bojinov, I. Betova, R. Raicheff, J. Electroanal. Chem. 381 (1995) 123–131.

[21] K. Wang, Y.-S. Li, P. He, Electrochim. Acta 43 (1998) 2459–2467.

[22] C.V. Krishnan, M. Garnett, B. Hsiao, B. Chu, Int. J. Electrochem. Sci. 2 (2007) 29–51.

[23] J.J. Cruywagen, A.G. Draaijer, J.B.B. Heyns, Inorg. Chim. Acta 331 (2002) 322–329.

[24] J.-Z. Zhang, C.J. Fischer, P.B. Ortner, Talanta 49 (1999) 293–304.

[25] A.W.E. Hodgson, D. Pletcher, Electroanalysis 10 (1998) 321–325.

Article 3: Jońca, J., Giraud, W., Barus, C., Comtat, M., Striebig, N., Thouron, D., Garçon, V., 2013, **Reagentless and silicate interference free electrochemical phosphate detection in seawater,** Electrochimica Acta, 88, 165-169

Reagentless and silicate interference free electrochemical phosphate determination in seawater

Justyna Jońca[a],*, William Giraud[a], Carole Barus[a], Maurice Comtat[b], Nicolas Striebig[c], Danièle Thouron[a], Véronique Garçon[a]

[a] *Laboratoire d'Etudes en Géophysique et Océanographie Spatiales, UMR 5566, 18 Avenue Edouard Belin, 31 401 Toulouse Cedex 9, France*
[b] *Laboratoire de Génie Chimique, UMR 5503, Université Paul Sabatier, 118 Route de Narbonne, 31 062 Toulouse Cedex, France*
[c] *Observatoire Midi-Pyrénées, UMS 831, Groupe d'Instrumentation Scientifique (GIS), 14 Avenue Edouard Belin, 31400 Toulouse, France*

ABSTRACT

An electrochemical method for phosphate determination in seawater was based on the oxidation of molybdenum in order to form molybdates and protons and subsequently, to create the phosphomolybdic complex electrochemically detectable by means of amperometry at a rotating gold disk electrode [J. Jońca et al., Talanta 87 (2011) 161]. To avoid silicate interferences, the method required an appropriate ratio of protons over molybdates equal to 70. Since the ratio of protons over molybdates created during molybdenum oxidation is only 8, the previous method still needed addition of sulfuric acid and thus was not free from addition of liquid reagents. In the present work, this aspect is solved by modification of the electrochemical cell construction. The method is now totally free from addition of any liquid reagents and gives a possibility to determine phosphate by amperometry in the concentrations range found in the open ocean with a detection limit of 0.11 μM. Having in mind the energy savings for future *in situ* sensor development, amperometry at rotating gold disk electrode was replaced by differential pulse voltammetry at static one. Phosphate can then be determined with a detection limit of 0.19 μM. Both methods are characterized by good reproducibility with an average measurements precision of 5.7% (amperometry) and 3.8% (differential pulse voltammetry). Results also show a good accuracy with an average deviation from theoretical values of phosphate concentration of 3.1% for amperometry and 3.7% for differential pulse voltammetry.

© 2012 Elsevier Ltd. All rights reserved.

1. Introduction

Phosphorus, in the form of phosphate, plays a key role in photosynthesis (*i.e.*, primary productivity) and the availability of this macronutrient in marine systems can strongly influence the marine carbon cycle and the sequestration of atmospheric carbon dioxide [1]. Thus, the biogeochemical cycle of phosphorus is one of the main research topics in chemical and biological oceanography, and measuring accurately the concentration of phosphate is very important.

Todays *in situ* monitoring of phosphate is based on a common method where the reaction of phosphate and molybdate in acidic medium is used in order to form the phosphomolybdate complex. This complex is then treated with ascorbic acid in the presence of antimony to yield the phosphomolybdenum blue as described

firstly by Murphy and Riley [2]. The reaction is followed by colorimetric detection at a wavelength of about 882 nm. ANAIS developed in our laboratory [3] is one of the *in situ* phosphate (and other nutrients) analyzers based on this method. These types of analyzers are characterized by good sensitivity and accuracy, but they are heavy and large. Additionally, they require addition of reagents and significant energy. To overcome these problems, progress toward miniaturization and decrease in energy consumption is crucial. Within a large number of analytical methods, electrochemistry provides promising reagentless approach to go further in miniaturization, decrease in response time and energy requirements. In aquatic systems, electrochemical methods are used routinely for monitoring pH by potentiometry, dissolved oxygen by amperometry [4], trace metals and speciation by voltammetry [5,6], conductivity and therefore salinity by impedimetry.

Electrochemistry also offers a wide range of possibilities for achieving an excellent phosphate determination in seawater with the following figures of merit: long lifetime, high precision, low detection limit, fast response time, good reproducibility but no autonomous electrochemical sensor for *in situ* phosphate detection exists nowadays. However, electrochemistry has been used

* Corresponding author at: Laboratoire d'Etudes en Geophysique et Oceanographie Spatiales, 14, av Edouard Belin, 31400 Toulouse, France. Tel.: +33 0561332913; fax: +33 0561253205.
E-mail address: justyna.jonca@legos.obs-mip.fr (J. Jońca).

for determination of phosphate in laboratory conditions. The determination of phosphate has been performed by pulse voltammetry with a great sensitivity [7], cyclic voltammetry [8,9] and amperometry [10,11]. Recently, a totally new electrochemical method was developed in our group for determination of silicate [12,13] and phosphate [14]. The method was based on the anodic oxidation of molybdenum in seawater in order to form silico- or phosphomolybdate complex electrochemically detectable either by means of cyclic voltammetry or amperometry. These reactions took place in an electrochemical cell divided in two by a non-proton exchange membrane in order to avoid protons reduction on the platinum cathode. Thus, molybdenum, working and reference electrodes were in the first compartment of the cell whereas the platinum electrode was in the second one. This method had an obvious drawback of cross interference in the ocean samples which contain both silicate and phosphate. Three solutions were proposed to address the silicate interferences issue [14], either by detection of phosphates in presence of silicates by amperometry at a suitable potential of 0.5 V or in a very acidic medium (pH 0.5) or with an adequate ratio of protons over molybdates equal to 70. The latter method was used for phosphate detection in the oxygen minimum zone (OMZ) offshore Peru during the Pelagico 1011-12-BIC OLAYA cruise in November–December 2010. The results showed an excellent agreement when compared to classical colorimetric measurements, but the method still required extra addition of acid to achieve the appropriate ratio of protons over molybdates [14].

In this work we will present the continuation of the development of the phosphate sensor along two routes. One is designing a new electrochemical cell including membrane technology to avoid any addition of liquid reagents. The second is to decrease energy requirements by switching to differential pulse voltammetry.

2. Experimental

2.1. Reagents and calibration standards

All solutions are prepared in Milli-Q water (Milli-pore Milli-Q water system) with reagent grade salts.

Artificial sea water for standards calibration, phosphate and silicate samples is prepared at a salinity of 34.4.

Working calibration standards are prepared as described in the WOCE operation and method manual [15] with potassium dihydrogen phosphate (KH_2PO_4, Merck) and sodium silicofluoride (Na_2SiF_6, Merck).

Phosphate artificial samples determinations by colorimetry are performed using reagents:

- An ammonium heptamolybdate solution (15 g of ammonium heptamolybdate in 500 mL of Milli-Q water).
- An acidic solution (140 mL of sulfuric acid, H_2SO_4 in 900 mL of Milli-Q water).
- An ascorbic acid solution (27 g of ascorbic acid in 500 mL of Milli-Q water).
- An antimonyl potassium tartrate solution (0.34 g of antimonyl potassium tartrate in 250 mL of Milli-Q water).

These solutions are mixed together (100 mL ammonium heptamolybdate, 250 mL sulfuric acid, 100 mL ascorbic acid and 50 mL antimonyl potassium tartrate) and the final solution is used for phosphate determination (10 mL for each 100 mL of the sample).

2.2. Colorimetric method

Colorimetric detection of phosphate artificial samples was done with a UV–vis spectrophotometer (Varian Inc. Cary 50, Australia) using 10 mm 100-QS quartz cuve (Hellma Analytics, Germany). The absorbance was registered at 882 nm following the method of Strickland and Parsons [16]. The baselines were done with artificial seawater. Reproducibility tests were performed and the precision of 2.25% was found.

2.3. Electrochemical method

Electrochemical measurements are carried out with a potentiostat μ-Autolab III (Metrohm). The reference electrode is an Ag/AgCl/KCl 3 M electrode (Metrohm). All the following potentials are given relative to this electrode. Measurements at a stationary or rotating disk electrode are recorded in a three electrode cell with a platinum counter electrode and gold working electrode (Metrohm, diameter 3 mm). The working electrode is polished with lapping film sheet (3 M aluminum oxide, 1 μm) and electrochemically cleaned in 0.5 mol L^{-1} sulfuric acid solution (5 scans, from 0.0 to 1.5 V, 200 mV s^{-1}) before each measurements.

The molybdenum electrode has a surface of around 100 mm^2 (Goodfellow). Molybdate is produced by molybdenum anodic oxidation performed at a constant electrolysis current of 50 mA or at constant potential of 2 V.

The simultaneous production of molybdate and protons with the appropriate ratio is based on the use of a cell divided in three parts. In the first one (1 mL), a primary molybdenum electrode is oxidized and thanks to a very thin (30 μm) proton exchange membrane (FuMaTech, fumapem^R F-930) only protons can pass through to the second compartment and thus acidify the medium to pH 1. In the second compartment (5 mL), a secondary molybdenum electrode is oxidized during a short time and thus achieving a ratio of protons over molybdates of 70. To avoid the reduction of protons formed during the two previous oxidations of molybdenum, the platinum electrode is placed in the third compartment which is in contact with the former two parts of the cell by a non-proton exchange membrane with thickness of 180 μm (N117 Du Pont^{TM} Nafion^R PFSA Membranes). During molybdenum oxidation, the platinum electrode acts as a cathode, whereas during phosphate determination it acts as a counter electrode. The schematic of the cell is presented in Fig. 1.

3. Results and discussion

3.1. In situ reagents formation in an electrochemical cell

Phosphate is not an electroactive species but the electrochemical detection is possible in acidic media (at pH 1) in presence of molybdate salts due to the following reaction (1) where the electroactive phosphomolybdate complex is formed [14].

$$PO_4^{3-} + 12MoO_4^{2-} + 27H^+ \rightarrow H_3PMo_{12}O_{40} + 12H_2O \qquad (1)$$
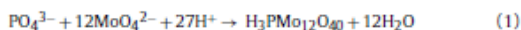
In order to eliminate the addition of molybdate and protons, a method based on anodic oxidation of molybdenum was developed [12,13]. Due to this process (2), all reagents required for phosphomolybdate complex creation are formed:

$$Mo + 4H_2O \rightarrow MoO_4^{2-} + 8H^+ + 6e^- \qquad (2)$$
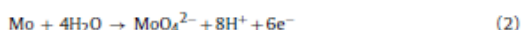
Since the silicomolybdate complex is formed at these conditions, the method described above has an obvious problem of cross interference in the ocean samples which contain both silicate and phosphate. A few methods to avoid these interferences are tested before using differences in electrochemistry of the two complexes, influence of pH on complex formation and differences in kinetics of complex formation by choosing an appropriate ratio of protons over molybdates of 70 [14]. The latter one was chosen and improved in this work.
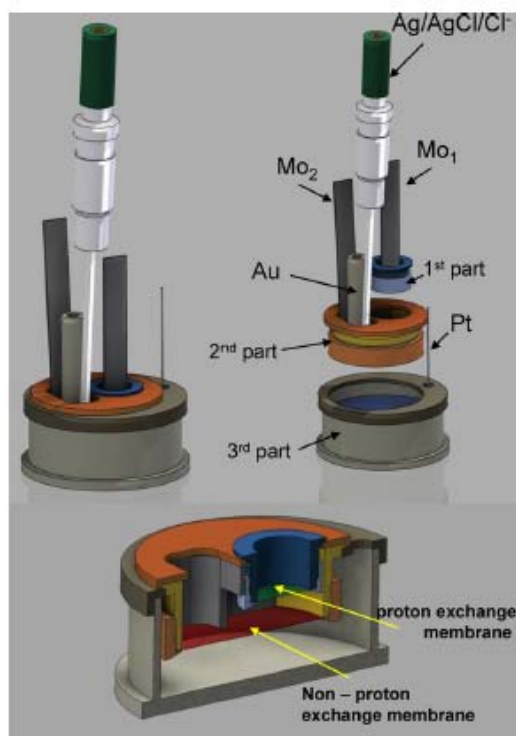
Fig. 1. Schematics of the electrochemical cell with application of membrane technology (Ag/AgCl/Cl⁻-reference electrode, Au-gold working electrode, Pt-platinum counter electrode, Mo₁-first molybdenum electrode, Mo₂-second molybdenum electrode, 1st part-first compartment of the cell with the proton exchange membrane, 2nd part-second compartment of the cell with the non proton exchange membrane, 3rd part-third compartment of the cell, simulating the open ocean).

Zhang et al. [17] indicated that when working with a ratio of protons over molybdates close to 70 at pH 1 (meaning the molybdate concentration has to be close to 1.5 mM), the interference from silicate can be avoided. Although the method was used for colorimetric detection of phosphate in presence of silicate, we confirmed that it was also adequate using electrochemistry. According to reaction (2), the ratio of protons over molybdate is 8 during the oxidation of molybdenum. At the beginning, we achieved an appropriate ratio of 70 by addition of acid [14]. In this work, we present a method where the desired ratio of protons over molybdate is achieved without addition of any liquid reagents. This method is based on the application of membrane technology and a special design of the electrochemical cell described in details in Section 2.3 (Fig. 1). Oxidation of the first molybdenum electrode was performed at a stable potential of 2 V since such high potential will ensure fast molybdenum oxidation and effective acidification of the solution in the second compartment. To achieve a desired pH of 1 in the second compartment, the first molybdenum electrode has to be oxidized during about 1000 s. This time is long but this is due to a large volume of the cell (5 mL) used in this work. The *in situ* sensor which will be developed in the future years will have a volume of a few hundreds μL and thus the reaction time will be much shorter. Excellent reproducibility of pH was achieved, when measuring pH in the second compartment after oxidation of the first
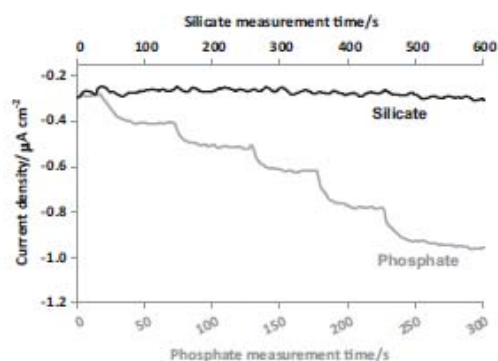
Fig. 2. Amperometric measurement made on a rotating gold disk electrode (0.29 V, 2000 rpm) for silicomolybdate (black) and phosphomolybdate (grey) complexes formed in artificial seawater during anodic oxidation of molybdenum. The signals were achieved by addition of standard solution of silicate (8.5–154.5 μM) and phosphate (0.59–3.49 μM), pH 1.0, ratio protons/molybdates 70.

molybdenum electrode-the precision calculated from 10 measurements is 2.0% with the average pH of 1.02. The second molybdenum electrode was oxidized in the second compartment at a stable current intensity of 50 mA during 80 s to ensure that concentration of formed molybdates is 1.5 mM as it is predicted by Faraday's law. The created phosphomolybdate complex was detected in the second compartment as described below.

3.2. Amperometric detection of phosphate in presence of silicate

The phosphomolybdate complex created as described above can be detected by electrochemical reduction at rotating gold electrode by amperometry at a potential of 0.29 V. Calibration curves for silicate and phosphate are presented in Fig. 2. It is clear that there is no amperometric signal for the silicomolybdate complex, whereas those for phosphomolybdate complex are well defined. The method gives a good linear response for phosphate in the concentration range found in the open ocean ($I = -0.1866C - 0.0066$, $R^2 = 0.9995$). The detection limit calculated as a signal measured between the highest and the lowest value of noise multiplied by three is 0.11 μM. The reproducibility tests reported in Table 1 exhibit quite good precision in the concentration range usually found in the open ocean. The average precision for the reproducibility test is 5.7%.

Amperometric method gives excellent possibility to detect phosphate in seawater but requires utilization of the rotating disk electrode which consumes energy and will complicate measurements in the future *in situ* sensor. Amperometry at static disk electrode shows no signals for phosphate in the concentration range found in the open ocean.

Classical cyclic voltammetry shows two reduction peaks at 0.32 V and 0.46 V and two oxidation peaks at 0.40 V and 0.53 V which give 4 correlation curves for concentrations greater than 5 μM [18]. Unfortunately the concentrations of phosphate found in

Table 1
Reproducibility test carried out for 10 measurements of amperometric or differential pulse voltammetric signal for adequate phosphate concentrations in artificial seawater.

	Phosphate concentration (μM)		
	0.65	1.60	3.01
Amperometry	5.5%	5.7%	5.8%
Differential pulse voltammetry	3.8%	4.0%	3.7%
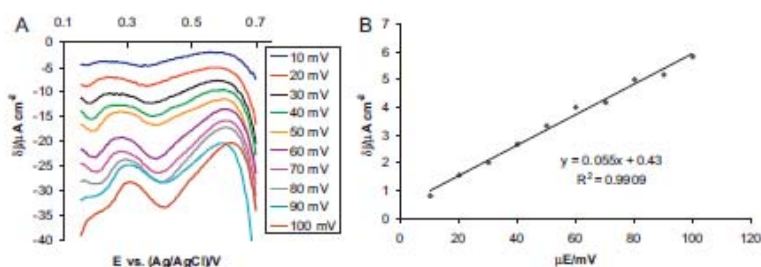
Fig. 3. (A) Differential pulse voltammetry for 3.49 μmol L^{-1} phosphomolybdate complex at different pulse amplitudes from 10 mV to 100 mV, (B) differential current density vs. pulse amplitude achieved from voltammograms presented in (A).

the open ocean are smaller (less than 3 μM) and in this concentrations range the voltammograms show only one reduction and one oxidation peaks which are very weak due to the high capacitive current as compared to the faradic one. The problem is associated with complicated electrode reactions where the reduction of complex on the gold electrode is coupled with an homogenous chemical step, protonation, which prevent rapid detection of the phosphomolybdate complex. This problem was discussed before [14,18]. Having all this in mind, we start to work toward the differential pulse method.

3.3. Phosphate detection using differential pulse voltammetry

The pulse amplitude was varied in the range 10–100 mV in order to find the best conditions for the phosphomolybdate complex detection. Fig. 3A represents the achieved voltammograms and Fig. 3B a plot of the differential current density vs. pulse amplitude. The results show an increase of differential current density value with an increase of pulse amplitude. In the same time, the peak width increases with pulse amplitude as well, which is characteristic for this type of detection method [19]. Besides, the potential peak (at about 0.25–0.30 V) is shifted slightly to more positive values as pulse amplitude increases. The second peak at more positive potentials is not well distinguished and thus impossible to measure. The peak is too close to potentials where formation of gold chlorides occurs at gold electrode in seawater at greater positive potentials. For further analysis, a pulse amplitude of 50 mV was chosen.

The phosphomolybdate complex was detected by differential pulse voltammetry at stationary gold electrode using pulse amplitude optimized above. The signals measured for phosphate in the concentration range found in the open ocean is presented in Fig. 4A. The calibration curve is described by equation $\delta j = 0.8082C + 0.9614$, $R^2 = 0.9897$ and the detection limit is 0.19 μM. Great care must be taken to measure properly the peak height. Here, we measure peak height as presented in Fig. 4B. The reproducibility tests reported in Table 1 exhibit a good precision. The average precision for the reproducibility test is 3.8%. For clarity and comparison, the reproducibility test for amperometry and differential pulse voltammetry were gathered in the same table. The results show that differential pulse voltammetry offers a better reproducibility.

3.4. Accuracy estimation for electrochemical and colorimetrical methods

An estimation of the deviation from theoretical values of phosphate concentration is provided for the classical colorimetric method, amperometry and differential pulse voltammetry methods. The same phosphate standards were used for all methods

to perform calibration curves and then 3 samples containing low (0.65 μM phosphate, 8.59 μM silicate), medium (1.60 μM phosphate, 57.1 μM silicate), and high (3.01 μM phosphate, 140.9 μM silicate) silicate and phosphate concentrations were
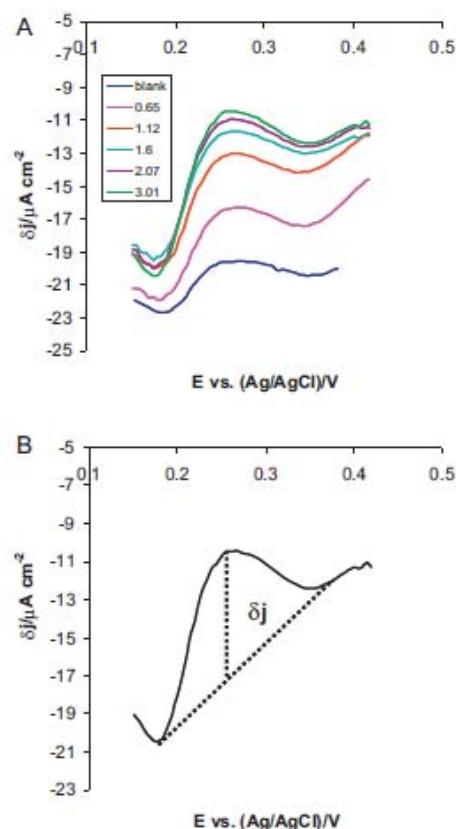
Fig. 4. (A) Differential pulse voltammetry measurement made on a gold disk electrode (at pulse amplitude of 50 mV) for phosphomolybdate complex formed in artificial seawater during anodic oxidation of molybdenum. The signals were achieved for different phosphate concentrations (0.65–3.01 μM); pH 1.0, ratio protons/molybdates 70, (B) method used in this work for determination of peak height.

Table 2

Comparison of colorimetric, amperometric and differential pulse voltammetric measurements for different phosphate concentration. Deviation between each method and theoretical value of phosphate concentration is given in brackets.

$[PO_4^{3-}]$ μM theoretical	$[Si(OH)_4]$ μM theoretical	$[PO_4^{3-}]$ μM by colorimetry	$[PO_4^{3-}]$ μM by amperometry	$[PO_4^{3-}]$ μM by differential pulse voltammetry
0.65	8.59	0.68 (4.6%)	0.63 (3.1%)	0.62 (4.6%)
1.60	57.1	1.61 (0.6%)	1.57 (1.9%)	1.56 (2.5%)
3.01	141	2.97 (1.3%)	2.88 (4.3%)	2.89 (4.0%)

tested. A good agreement between all methods confirms no interference from silicate. Accuracy comparison for all methods is presented in Table 2. The average deviation from theoretical values of phosphate concentration is 3.1% for amperometry, 3.7% for differential pulse voltammetry and 1.3% for colorimetry.

## 4. Conclusions

We described a thorough documentation necessary to set up an electrochemical detection of phosphate. Thanks to a special construction of an electrochemical cell and utilization of membrane technology coupled with molybdenum oxidation, the method is free from addition of any liquid reagents and free from silicate interferences. During molybdenum oxidation in a sample containing phosphate, the phosphomolybdic complex is formed. The complex is then detected by amperometry or differential pulse voltammetry on a gold electrode. The method allows detecting phosphate in the concentration range found in the open ocean with good detection limit, reproducibility and accuracy. The method will be tested for natural seawater samples as soon as it will be possible.

The further steps will be miniaturization and adaptation of the cell described above to the marine harsh environment (protection against corrosion, biofouling and high pressure) in order to achieve the first electrochemical *in situ* sensor for detection of phosphate in seawater. This sensor will be characterized by low energy consumption and quite fast response time due to the decrease of volume combined with application of large surface of membrane surfaces. We will be working simultaneously on calibrationless method as it was done for silicate in our team [20]. Additionally, long term behavior of gold electrode in seawater will be investigated and potential *in situ* cleaning procedure will be found.

References

[1] A. Paytan, K. McLaughlin, The oceanic phosphorus cycle, Chemical Reviews 107 (2007) 563.
[2] J. Murphy, J.P. Riley, A modified simple solution method for the determination of phosphate in natural waters, Analytica Chimica Acta 27 (1962) 31.
[3] D. Thouron, R. Vuillemin, X. Philippon, A. Lourenço, C. Provost, A. Cruzado, V. Garçon, An autonomous nutrient analyzer for oceanic long-term in situ biogeochemical monitoring, Analytical Chemistry 75 (2003) 2601.
[4] N.P. Revsbech, L.H. Larsen, J. Gundersen, T. Dalsgaard, O. Ulloa, B. Thamdrup, Determination of ultra-low oxygen concentrations in oxygen minimum zones by the STOX sensor, Limnology and Oceanography 7 (2009) 371.
[5] G.W. Luther III, B. Glazer, L. Hohmann, J. Popp, M. Taillefert, T. Rozan, P. Brendel, S. Theverge, D. Nuzzio, Sulfur speciation monitored in situ with solid state gold amalgam voltammetric microelectrodes: polysulfides as a special case in sediments, microbial mats and hydrothermal vent waters, Journal of Environmental Monitoring 3 (2001) 66.
[6] M.L. Tercier-Waeber, F. Confalonieri, G. Riccardi, A. Sina, S. Nöel, J. Buffle, F. Graziottin, Multi physical-chemical profiler for real-time in situ monitoring of trace metal speciation and master variables: development, validation and field applications, Marine Chemistry 97 (2005) 216.
[7] A.G. Fogg, N.K. Bsebsu, Differential pulse voltammetric determination of phosphate as molybdovanadophosphate at a glassy carbon electrode and assessment of eluents for the flow injection voltammetric determination of phosphate, silicate, arsenate and germanate, Analyst 106 (1981) 1288.
[8] N.G. Carpenter, A.W.E. Hodgson, D. Pletcher, Microelectrode procedures for the determination of silicate and phosphate in waters-fundamental studies, Electroanalysis 9 (1997) 1311.
[9] L. Guanghan, W. Xiaogang, L. Yanhua, Y. Shenkai, Studies on 1:12 phosphomolybdic heteropoly anion film modified carbon paste electrode, Talanta 49 (1995) 511.
[10] S.M. Harden, W.K. Nonidez, Determination of orthophosphate by flow injection analysis with amperometric detection, Analytical Chemistry 56 (1984) 2218.
[11] J.C. Quintana, L. Idrissi, G. Palleschi, P. Albertano, A. Amine, M. El Rhazi, D. Moscone, Investigation of amperometric detection of phosphate. Application in seawater and cyanobacterial biofilm samples, Talanta 63 (2004) 567.
[12] M. Lacombe, V. Garçon, D. Thouron, N. Le Bris, M. Comtat, Silicate electrochemical measurements in seawater: chemical and analytical aspects towards a reagentless sensor, Talanta 77 (2008) 744.
[13] M. Lacombe, V. Garçon, M. Comtat, L. Oriol, J. Sudre, D. Thouron, N. Le Bris, C. Provost, Silicate determination in sea water: toward a reagentless electrochemical method, Marine Chemistry 106 (2007) 489.
[14] J. Jońca, V. Leon-Fernandez, D. Thouron, A. Paulmier, M. Graco, V. Garçon, Phosphate determination in seawater: toward a reagentless electrochemical method, Talanta 87 (2011) 161.
[15] L.I. Gordon, J.C. Jennings, A.A. Ross, J.M. Krest, WOCE, Method Manual, W. H. P. Office Report, 1993, p. 68.
[16] J. Strickland, T. Parsons, Practical Handbook of Seawater Analysis, vol. 167, Fisheries Board of Canada, Bulletin, Ottawa, 1972, p. 49.
[17] J.-Z. Zhang, C.J. Fischer, P.B. Ortner, Optimization of performance and minimization of silicate interference in continuous flow phosphate analysis, Talanta 49 (1999) 293.
[18] J. Jońca, C. Barus, W. Giraud, D. Thouron, V. Garçon, M. Comtat, Electrochemical behaviour of isopoly- and heteropolyoxomolybdates formed during anodic oxidation of molybdenum in seawater, International Journal of Electrochemical Science 7 (2012) 7325.
[19] A. Bard, L.R. Faulkner, Electrochemical Methods: Fundamentals and Applications, 2nd ed., John Wiley and Sons, Inc., Hoboken, NJ, 2001.
[20] W. Giraud, L. Lesven, J. Jońca, C. Barus, M. Gourdal, D. Thouron, V. Garçon, M. Comtat, Reagentless and calibrationless silicates measurement in oceanic water, Talanta 97 (2012) 157.

179

SUMMARY OF ARTICLES 2 and 3

The two publications presented above showed the current state of the electrochemical phosphate sensor development. The Article 3 describes the continuation of the work described in Article 2 and thus, this summary corresponds to both publications.

The electrochemical determination of the non electroactive phosphate is based on the formation of a complex with molybdate. The complex is formed by the reaction with K_2MoO_4 in an acidic solution to form a Keggin anion (Carpenter et al., 1997).

$$PO_4^{3-} + 12\ MoO_4^{2-} + 27\ H^+ \rightarrow H_3P(Mo_{12}O_{40}) + 12\ H_2O \qquad\qquad (VI.\ 1.1)$$
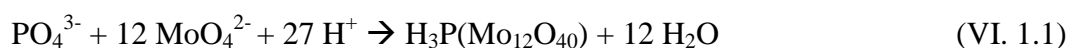
In order to eliminate the addition of molybdate and protons, a reagentless method is developed. Molybdate salts and protons are produced as the product of molybdenum oxidation in the reaction cell due to the following reaction (Lacombe et al., 2007, 2008):

$$Mo + 4\ H_2O \rightarrow MoO_4^{2-} + 8\ H^+ + 6e^- \qquad\qquad (VI.\ 1.2)$$

The created phosphomolybdate complex can be detected on a gold working electrode by means of amperometry with the detection limit of 0.12 μM. The method described above has an obvious problem of cross interference in the ocean samples which contain both silicate and phosphate. A few methods to avoid these interferences are tested using differences in electrochemistry of the two complexes, influence of pH on complex formation and differences in kinetics of complex formation by choosing an appropriate ratio of protons over molybdates of 70 (Jońca et al., 2011). The latter one was used during the Pelagico 1011-12 cruise aboard the R/V OLAYA offshore Peru.

The collection of seawater samples from four east-west transect lines was made during the Pelagico 1011-12-BIC OLAYA cruise aboard R/V Jose Olaya Balandra off Peru during austral spring 2010 (November-December), when intense upwelling occurs. The typical vertical profiles of phosphate concentrations obtained offshore Peru in the coastal waters demonstrate that the electrochemical method is in excellent agreement with the colorimetric analysis conventionally used for seawater analysis. The deviation obtained by comparing the amperometric and colorimetric analyses is 4.9% (Jońca et al., 2011) (Figure VI. 1). These results show great potential in the developed method for phosphate detection but it still required extra addition of acid to achieve an appropriate ratio of protons over molybdates (70). The solution to this problem is presented in Article 3.
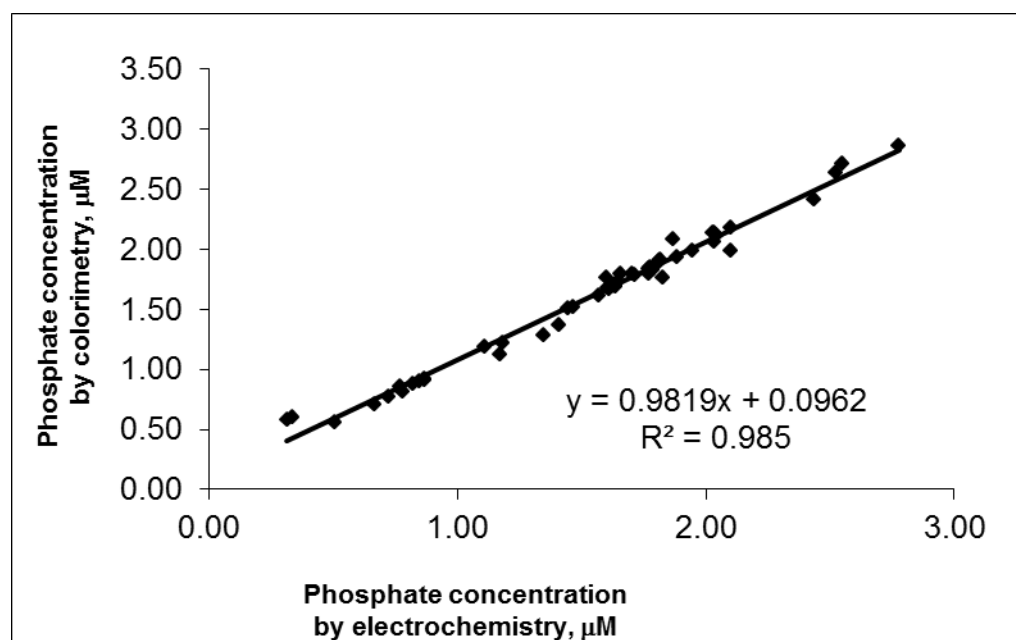
Fig. VI. 1. Deviation of amperometric analysis as compared to colorimetric measurements over our analyzed data set

According to reaction (VI. 1.2), the ratio of protons over molybdate is 8 during the oxidation of molybdenum. At the beginning, we achieved an appropriate ratio of 70 by addition of acid. Recently, we developed a method where the desired ratio of protons over molybdate is achieved without addition of any reagents. This method is based on the use of specific membrane technology and a special design of the electrochemical cell made by GIS laboratory (Groupe d'Intrumentation Scientifique) (Jońca et al., 2012, in press). The cell consists of 3 compartments. In the first one (1 mL), a primary molybdenum electrode is oxidized and thanks to a proton exchange membrane only protons can pass through to the second compartment and thus acidify the media to pH 1. In the second compartment (5 mL), a secondary molybdenum electrode is oxidized during a short time to produce 1.5 mM of molybdates achieving a ratio of protons over molybdates of 70. The third compartment is in contact with previous parts of the cell by a non-proton exchange membrane where a platinum cathode is immersed to avoid the reduction of protons formed during the two previous oxidations of molybdenum (Figure VI. 2).

The complex is detectable in the second compartment by means of amperometry or differential pulse voltammetry and the detection time is about 15 min. The detection time can be much shorter by decreasing the volume of the cell. The detection limit is 0.11 µM for

amperometry and 0.19 μM for differential pulse voltammetry. The reproducibility tests show average precisions of 5.7% (amperometry) and 3.8% (differential pulse voltammetry). Results show also quite good deviation with an average of 4.3% (amperometry) and 5.0% (differential pulse voltammetry) as compared with colorimetric measurements. Future work will be focused on miniutarisation and marinisation of the electrochemical cell.
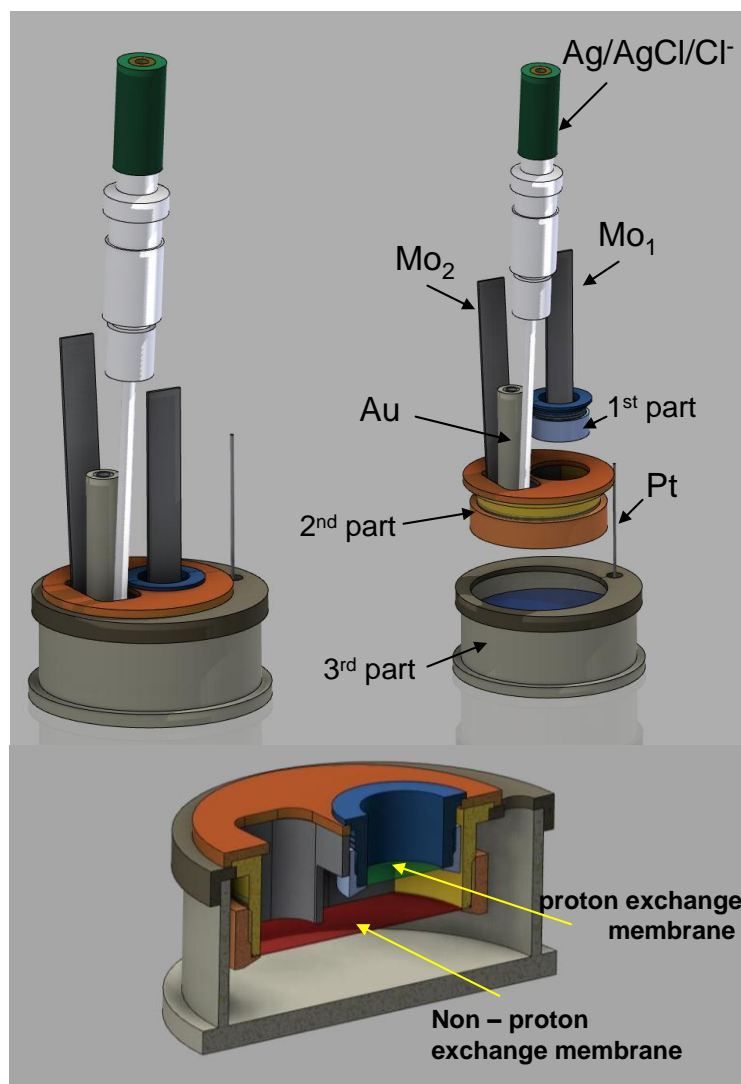
Fig. VI. 2. Schematics of the electrochemical cell.

CHAPTER VII:

ANALYSIS OF WATER MASSES OFFSHORE PERU

The previous chapters described the development of an electrochemical method for phosphate detection in seawater. The method was validated during an oceanographical cruise offshore Peru in November 2010 showing excellent agreement when compared with the classical colorimetric method (Jońca et al., 2011). Additionally, for the first time a relative phosphate minimum was noticed at depths of about 200 m. Some hypotheses about the source of this minimum are discussed but a definitive answer will require a retrospective detailed water mass analysis which can not be done within this PhD project.

The Eastern South Pacific is oceanographically a highly diverse region determined by coastal upwelling off Peru driven by alongshore winds. During this process, water masses rich in nutrients upwell to the surface forming one of the world most productive marine food webs. Additionally, the intermediate waters are characterized by low oxygen concentrations. The deoxygenation process has crucial implications on cycling of the macronutrients nitrate and phosphate by the occurence of microbial processes which drive the autotrophic system into a N limited system.

Contents

1. Pelagico 1011-12-BIC OLAYA cruise offshore Peru

Fig. VII. 1.1. (a) Map of the CTD stations where the samples for phosphate electrochemical detection were collected, (b) a satellite image of ocean colour from MODIS Aqua

The collection of seawater samples from four east-west transect lines was made during the Pelagico 1011-12-BIC OLAYA cruise aboard R/V Jose Olaya Balandra off Peru during austral spring 2010 (November-December), when an intense upwelling was occurring. Seawater was collected using 12 L Niskin bottles mounted on a cable equipped with a CTD-O_2 Sea Bird 25.

Samples for phosphate analysis by both colorimetric and chronoamperometric methods were collected during the leg from Puerto Pizzaro (3.67°S) to Salaverry (8.13°S) from November 10th to November 29th, 2010. Among the 22 CTD stations performed during this leg, 7 vertical profiles were analyzed by both methods for phosphate determination. Other nutrients were analysed using classical colorimetric method as described by Strickland and Parsons (1972). Fig. VII. 1.1a presents a map with some CTD stations where samples for phosphate determination were collected. Fig. VII. 1.1b presents a satellite image of ocean colour from MODIS-Aqua. This image corresponds to the same period of time that the leg where electrochemical analysis of phosphate was carried out. The image clearly indicates that between 3.67°S and 8.13°S both blue and brown waters, as mentioned by Bruland et al. (2005), were present.

The "brown" waters are associated with extremely high primary production; the satellite chlorophyll image shows very intense brown color in this region. The "blue" waters were described firstly by Strickland et al. (1969) and they are characterized by very low primary production and the concentration of nutrients is extremely high. These regions are also called HNLC (High Nutrient Low Chlorophyll) due to limitation in iron (Hutchins et al., 2002). The iron limitation is caused by the low rainfall which occurs only in the Andes (and not in the coastal range) and limited iron delivery from eolian flux of dust. On the other hand, the "brown" waters are associated with high iron input via upwelling. The suboxic water masses in contact with organic rich sediments release iron (in redox conditions) that could be supplied along the coast with macronutrients during upwelling occurring over these relatively broad shelf areas of northern and central Peru.

2. Mean circulation in the Oxygen Minimum Zone of the Eastern South Pacific

The Equatorial Current System is composed of quasi zonal currents: The Equatorial Undercurrent (EUC) and the primary and secondary Southern Subsurface Contercurrents (pSSCC and sSSCC) which flow eastward in the subsurface; and the South Equatorial Current (SEC) which flows westward near the surface (Montes et al., 2010). The other major system, the Peru Current system is composed of currents that are strongly influenced by the presence of the American landmass: the Peru Coastal Current (PCC) and the Peru Oceanic Current

(POC) near the surface; the Peru-Chile Countercurrent (PCCC) and the Peru-Chile Undercurrent (PCUC) in the subsurface. The various currents are presented in Figure VII. 2.1.
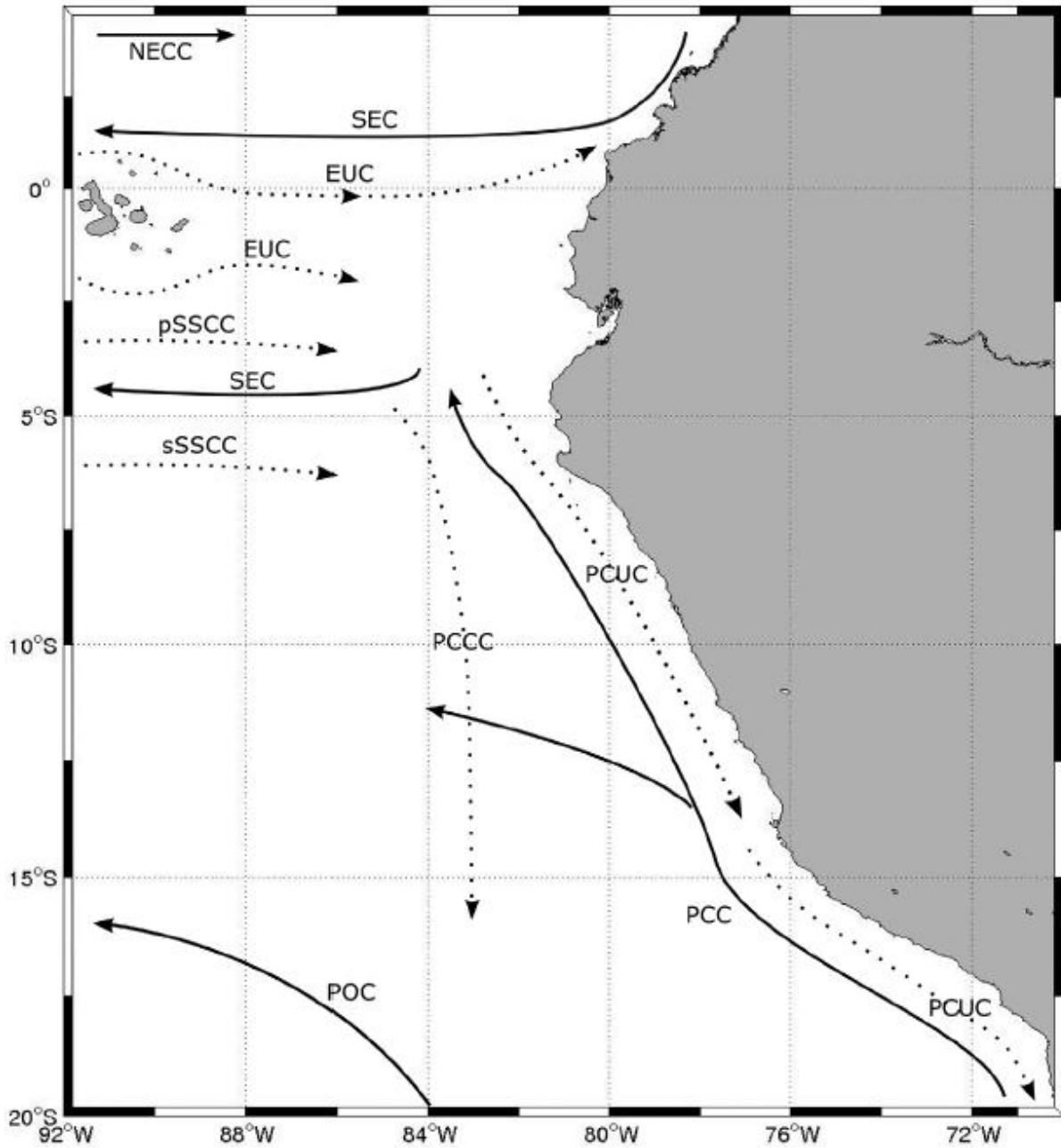
Fig. VII. 2.1. Oceanic circulation scheme for the eastern tropical Pacific. (Montes et al., 2010).

Coastal currents

The southern branch of the anticyclonic subtropical gyre of the south-eastern Pacific, named the South Pacific Current, flows towards the American coast between 35°S and 48°S. It then separates in two branches, the first flows southward (Cape Horn Current), the second flows northwards and is called the Peru Oceanic Current (POC).

The POC (known also as Chile-Peru Current) transports cold waters from the south to the equator where it may join the South Equatorial Current (SEC) (Chaigneau and Pizarro, 2005b) and is involved in the equatorial upwelling. This current is very wide (about 500 km) and can be present between the surface and greater depths (700m). The distance from the coast can vary between 500 and 1500 km.

The Chile Coastal Current (CCC) and the Peru Coastal Current (PCC) flow northward bringing cold, highly oxygenated Antarctic waters along the coast of Chile and Peru (Strub et al., 1998) in the near surface layers (0-100 m) with a 100 km width (Huyer et al., 1991), and their maximum velocity is located at the level of the thermal front generated by the upwelling of colder waters at the coast. Maximum upwelling for Peruvian coast takes place during austral winter when parallel winds are the strongest (Fiedler, 1994). The PCC current joins the South Equatorial Current (SEC) and upwells in winter.

The POC current together with PCC (and CCC) are often called the Humboldt Current. The Humboldt Current is one of the most productive marine ecosystems in the world, as well as the largest upwelling system. The cold, nutrient-rich water brought to the surface by upwelling drives the system high productivity (Graco et al., 2007). The Humboldts high rates of primary and secondary productivity support the world's largest fisheries; approximately 18-20% of the world's fish catch comes from the Humboldt Current (Willey, 2011). The species are mostly pelagic: sardines, anchovies and jack mackerel. The high productivity supports top marine predators such as marine mammals. The Humboldt Current is disturbed by the so-called El Niño effect, causing a rise in temperature of coastal waters, catastrophic rainfall in the Andes and the reduction of the perpetual snow cover, which cause water supply to the Andean rivers and thus floods and mud slides (Glantz, 2001).

The Peru-Chile Counter Current (PCCC), a southward surface current is observed 100-300 km from the coast (Strub et al., 1995, 1998) and it transports warm, salty Subtropical Waters. Processes explaining the dynamics of this counter-current, of direction opposed to the

density gradient are still poorly known. According to the modeling study (Penven et al., 2005), the PCCC is forced by a cyclonic wind curling north of 15° S in agreement with the Sverdrup relationship (Sverdrup, 1947), and then turns westward toward the open ocean.

The Peru-Chile Undercurrent (PCUC) known also as Gunther Current is a well-defined, poleward, subsurface flow, which extends over the continental shelf and slope off the west coast of South America. The PCUC can dominate the subsurface waters from 50 to 700 m depths but the core is situated at 100-300 m depth. The PCUC is the one that literally connects the tropics with the high latitudes (Figure VII. 2.1). The PCUC transports warm, salty Equatorial Subsurface Water from the eastern tropical Pacific to at least as far south as 48°S (Silva and Neshiba, 1979). This water mass in turn is the main source for the coastal upwelling off Peru and northern Chile (e.g. Huyer et al., 1987) and it carries low oxygen waters from equatorial regions into the ESP. Its dynamics is therefore a crucial issue for understanding the OMZ in the ESP.

Equatorial currents

The South Equatorial Current (SEC) flows westward near the equator and is predominantly controlled by the trade winds. The current is split into two branches by Equatorial Undercurrent (EUC) near the Galapagos Islands. The current is fed by cold waters from the Humboldt Current System (HCS). The SEC is weak on the east due to low winds, but speeds up at west due to slowdown of the EUC (Reverdin et al., 1994). The SEC also has two deeper branches directed towards the west, which could be due to a cyclonic spiral fueled by the SSCC (Southern Subsurface Countercurrent) (Kessler, 2006).

The Cromwell Current (also called Pacific Equatorial Undercurrent or just Equatorial Undercurrent - EUC) is an eastward-flowing subsurface current that extends the length of the equator in the Pacific Ocean. The current transports warm tropical waters to the east. The current is 400 km width and is 100 m under the surface of the ocean. The EUC is relatively narrow being only 30m deep. The EUC is separated into two branches near the Galapagos probably due to upwelling induced by the presence of the island (l'Eden and Timmermann, 2004). Additionally, some data suggest that part of the upper EUC upwells into the SEC (Wyrtki, 1963; Lukas, 1986; Strub, 1998). On the other hand, its lower layers are thought to be an important source of the water carried by the PCUC (Toggweiler et al., 1991; Fiedler and Talley, 2006).

The Southern Subsurface Countercurrent (SSCC) is the subsurface current oriented eastward present between 5°S and 10°S. The current is often separated into two branches pSSCC (primary SSCC) and sSSCC (secondary SSCC). It was suggested that both SSCCs could be complementary sources of PCUC waters (Lukas, 1986; Toggweiler et al., 1991). Such connections are certainly modified during active phases of El Niño during which substantial amounts of equatorial water are being advected along the Peruvian coast as far as 15-20°S (Kessler, 2006; Colas et al., 2008).

3. Description of waters masses offshore Peru

The main water masses characteristics offshore Peru (Strub et al., 1998, Graco et al., 2007, Ryabenko et al., 2012) are gathered in Table VII. 3.1. The T-S (temperature-salinity) and S-O_2 (salinity-oxygen), P-O_2 (phosphate-oxygen), P-S (phosphate-salinity), P-T (phosphate-temperature), P-Si (phosphate-silicate), N-P (nitrate-phosphate) and N-Si (nitrate-silicate) diagrams for 7 CTD stations analysed during the Pelagico cruise are shown in Figure VII. 3.1 A - H. The profiles of phosphate and oxygen as a function of depth are presented in Figure VII. 3.2.

The T-S and S-O_2 diagrams clearly indicate the water masses usually found in this region. The surface water from coastal CTD station 1 (3°39.94 S, 80°47.67 W) are characterized by high temperature of about 23 °C and very low salinity of 33.2. Salinity is low due to an excess of rainfall over evaporation and is characteristic of *Tropical Surface Water* (TSW). This water mass is associated with relatively low phosphate concentrations of about 0.6 μM. The silicate concentration was below 1.5 μM, and nitrate below 3 μM. Other coastal CTD stations 59 (4°49.99 S, 81°10.47 W) and 95 (5°59.96 S, 81°12.18) are different from this description. They present much colder and more salty characteristics typical of *Cold Coastal Water* (CCW). These waters are also associated with lower oxygen content than the *Tropical Surface Water*. The nutrient concentrations are also higher than of *Tropical Surface Waters.* Additionally, at station 59 the phosphate concentration is much lower than at station 95 (Figure VII. 3.2). This characteristic can be associated with the formation of "brown" and blue" waters. Other nutrient concentrations confirm this hypothesis: silicate and nitrate concentrations are much higher at station 95 than 59. Phosphate concentration for CCW "blue waters" varies between 1.3-2.7 μM, silicate between 18-26 μM and nitrate between 25.8-32

µM. For "brown" waters these values were in the range of 1.1-1.9 µM, 8.7-14.9 µM, 12.3-14.9 µM, respectively.

More offshore *Subtropical Surface Waters* (STSW) were found for CTD stations 102 (6°43.77 S, 80°20.02 W) and 174 (6°43.77 S, 82°26.54 W). This water mass is formed in the regions where evaporation greatly exceeds precipitation and thus, they are characterized by high salinity but the temperature can vary from 18-27°C (Wrytki, 1963). The phosphate concentration varies between 0.56-1.2 µM, silicate concentration between 1.3-2.5 µM, and nitrate concentration between 1.3-12.5 µM. Between the *Tropical Surface Water* and *Subtropical Surface Water* there is a water mass which is intermediate in properties and is called *Equatorial Surface Water*. This water mass is not a mixture of TSW and STSW but its properties are determined by seasonal advection of a colder water mass from the Peru Current and by equatorial upwelling (Wyrtki, 1963). The salinity is higher than for *Tropical Surface Water* but lower than *Subtropical Surface Water* and varies between 34.1-34.4. CTD stations 11 (3°39.83 S, 82°26.87 W) and 50 (4°59.95 S, 82°45.24 W) are located within this water mass. Phosphate concentrations here vary between 0.7-0.9 µM, silicate between 5-10 µM, and nitrate between 5.9-7.5 µM.

Since, the CTD stations were located very close to the coast, we did not find intermediate water masses like *Antarctic Intermediate Water* (AAIW) and/or *Eastern Pacific Intermediate Water* (ESPIW). Both AAIW and ESPIW are intermediate waters which penetrate into the Eastern South Pacific (ESP) bringing cold, salty waters, rich in oxygen and nutrients. AAIW is placed at greater depths (700-1200m) and is much colder than ESPIW (50-400) (Schneider et al., 2003).

T*able VII. 3.1. The main water masses characteristics offshore Peru.*

Water mass	Depth, m	Temperature, °C	Salinity	Oxygen, µM	Nitrate, µM	Phosphate, µM	Silicate, µM
TSW (Tropical Surface Water)	0 – 20[2]	20.4 – 26.1[1]	32.9 – 34.6[1]	97 – 223[1]	0.8 – 16[1]	0.3 – 1.4[1]	0.4 – 12.7[6]
ESW (Equatorial Surface Water)	0 – 30/40[2]	20.2 – 24.8[1]	34.2 – 34.9[1]	97– 272[1]	0.2 – 18[1]	0.6 – 1.4[1]	0.5 – 12.7[6]
STSW (SubTropical Surface Water)	0 – 100[2]	23.6 – 26.8[1]	35.5 – 35.6[1]	220 - 244[1]	1.4 – 5.1[1]	0.3 – 0.8[1]	0.1 – 7.7[6]
CCW (Cold Coastal Water)	0 – 50[4]	14.0 – 15.0[4]	34.9 – 35.1[4]	60 – 200[4]	5 – 10[4]	1.0 – 1.8[4]	10 - 20[4]
ESSW (Equatorial SubSurface Water)	50 - 550[1]	12.1 – 13.9[1]	34.8 – 35.0[1]	2 – 74[1]	0.0 – 34.5[1]	1.1 – 3.9[1]	10.7 – 42.8[6]
ESPIW (Eastern Pacific Intermediate Water)	50 – 400[3]	11 – 13[3]	34.1 – 34.3[3]	About 200[3]			
AAIW (Antarctic Intermediate Water)	600 – 1000[2]	4.2 – 6.0[1]	34.5 – 34.6[1]	18 – 63[1]	42 – 52[1]	3.1 – 3.6[1]	39 – 140
SASW (SubAntarctic Surface Water)	0 – 100[2]	13 – 15[2]	34.6 – 34.8[2]	206 – 247[4]	8.0 - 16[5]	1.0 – 1.4[5]	5.0 – 20[5]

[1]Ryabenko et al. 2012; [2]Graco et al., 2007; [3]Schneider et al., 2003, [4]Grados et al., 2009, [5]Silva et al., 2009, [6]Giraud, 2012
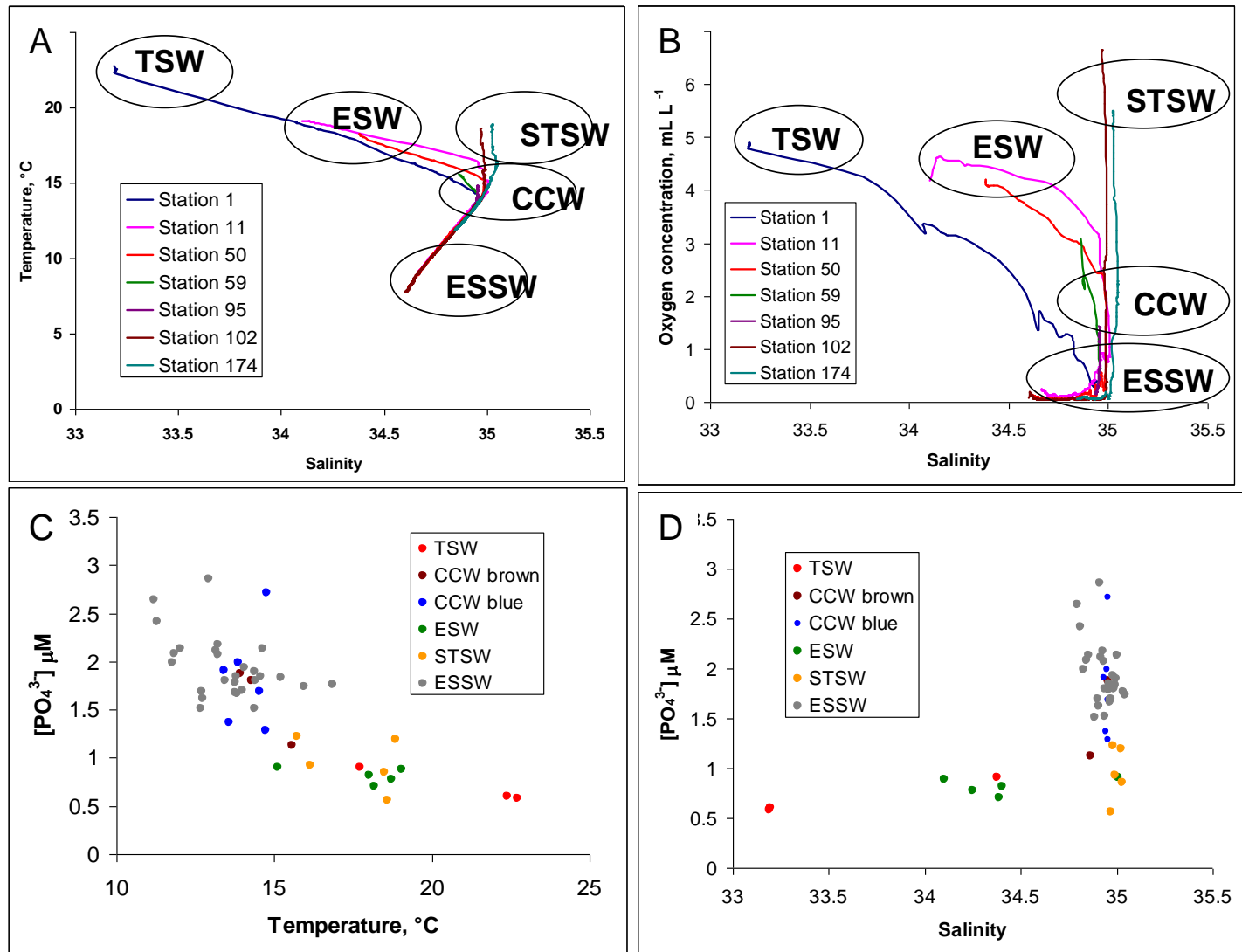
Fig. 3.1.(part 1) Diagrams T-S (A), O$_2$-S (B), P- T (C), P-S (D)
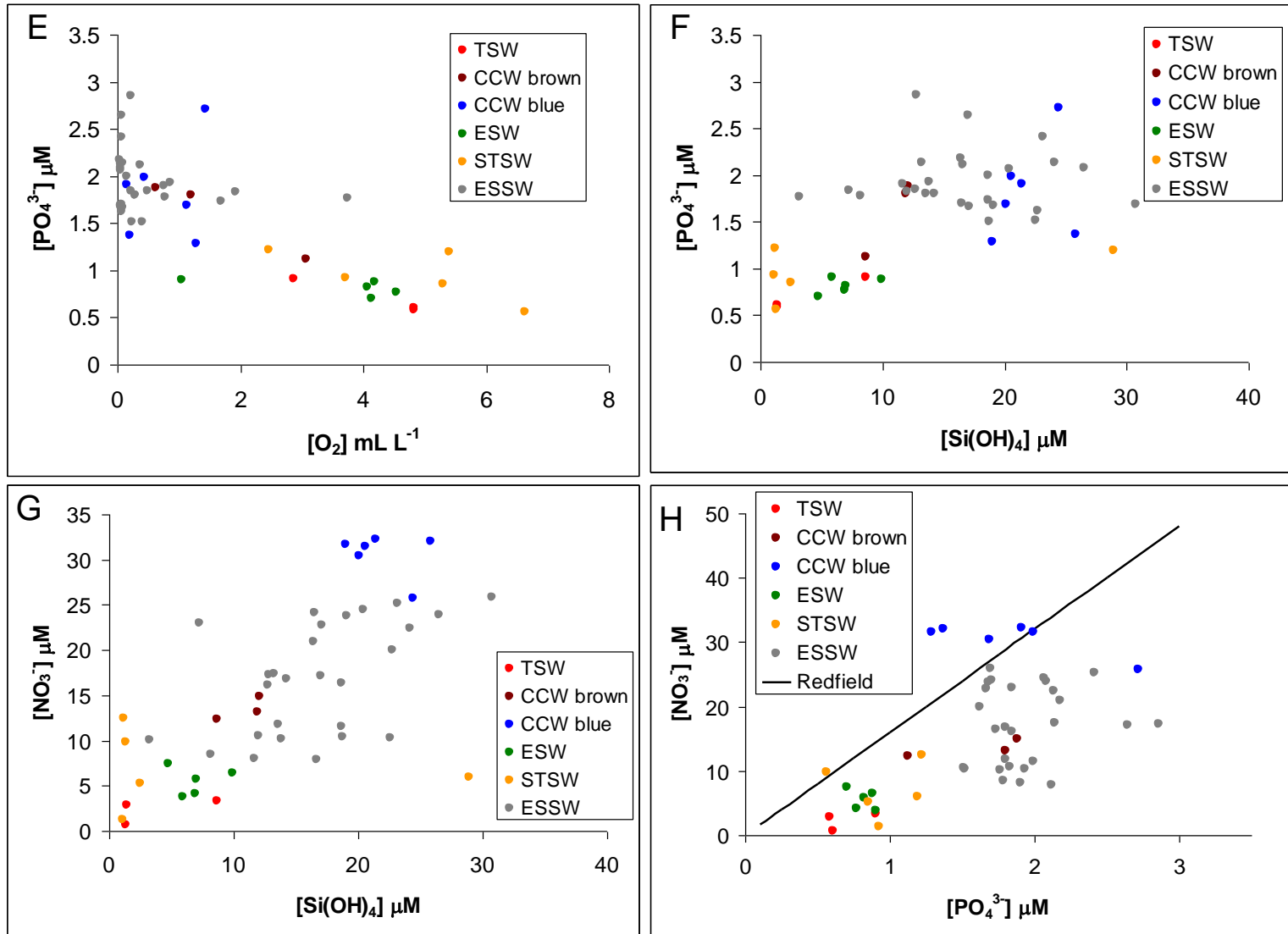
Fig. 3.1. (part 2) Diagrams P-O$_2$ (E), P-Si (F), N-Si (G), N-P (H)
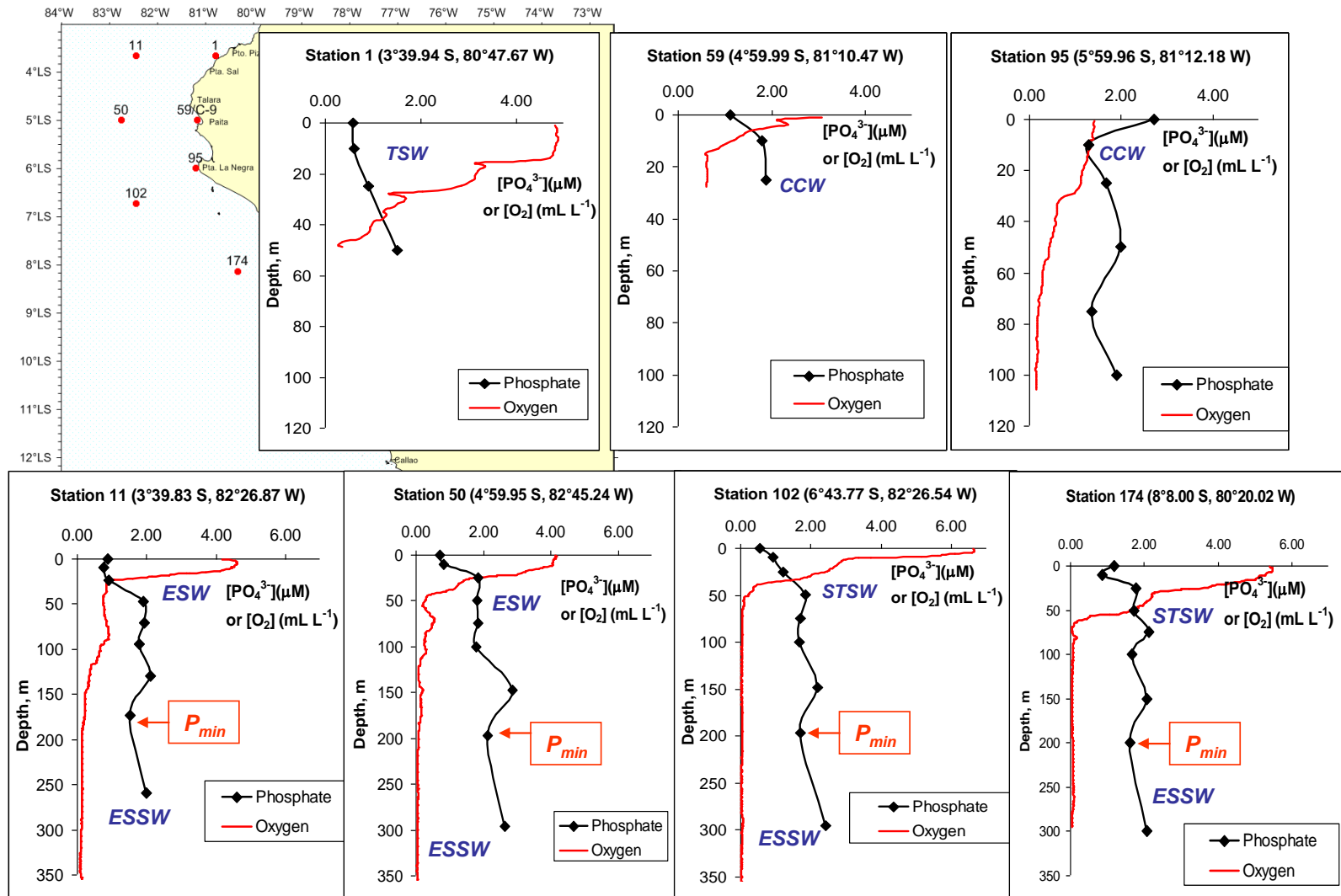
Fig. VII. 3.2. Phosphate and oxygen profiles from 3 coastal (top) and 4 offshore (bottom) Peru stations, P_{min}-phosphate minimum.

4. The source of relative phosphate minimum on the vertical profiles

The analysis of subsurface water masses clearly indicates the presence and dominance of the *Equatorial SubSurface Water* (ESSW) characterized by high salinity and very low oxygen concentrations (Figure VII. 3.2). Phosphate concentrations vary here between 1.5-2.9 µM, silicate between 3.0-30 µM and nitrate between 7.9-25.8 µM. However at depths ranging from 150-200 m a relative minimum in phosphate concentrations was observed. The concentration of phosphate at this depth varied between 1.5-2.1 µM. This relative minimum seems to appear at shallower depths as we move northward (Figure VII 3.2). It seems also that this relative phosphate minimum is more intense in the north than in the south. The difference between phosphate concentration at 200 m and 150 m (P_{200}-P_{150}) for CTD stations 11, 50, 102, 174 are -0.61, -0.72, -0.48, -0.45 µM, respectively. Both electrochemical and colorimetrical data showed similar values of this difference with excellent reproducibility of ± 0.04 µM and good accuracy of ± 0.07 µM when comparing the electrochemical method to colorimetric one. Thus, it is clear that the values of relative phosphate minimum are significant. This original observation needs to be fully documented examining data sets of all oceanographic cruises in the region. What are the origins of these relative phosphate minima? Is this phosphate minimum a permanent feature or is it seasonal? Are the underlying processes mostly of physical or biogeochemical origin or a complex mixture of both sources? The response to these questions requires a retrospective detailed water mass analysis over the past several years over central and northern Peru which can not be done within this work. However some hypotheses are discussed below.

4.1. Alongshore recirculation of subantarctic waters

It was shown by Montes et al. (2010) that subantarctic waters may have a stronger influence on Peruvian waters than it was previously thought. Montes et al. (2010) using virtual floats in a 3D physical model, showed an alongshore recirculation of subantarctic waters which can reach as far north as 3°S (Figure VII. 4.1). These waters are formed at great depths of about 1200 m. Indeed, a northward flow, with alongshore velocity of about 2 cm s^{-1}, could be identified in the model Eulerian fields just underneath the Peru-Chile Undercurrent (PCUC) extending down to 1500 m which feeds this injection (Montes at al., 2010). Water slowly upwells from abyssal depths into the PCUC while it is being carried northward. Once the virtual floats are within the PCUC at around 3°S, they start flowing poleward. During this

estimated 3 year time recirculation, waters get warmer (12.0-13.7°C), saltier (~ 34.9), and more depleted in oxygen (~0.2 mL L^{-1}).

The T-S diagram for water masses associated with relative this phosphate minimum was plotted together with characteristics of water masses found during the Pelagico cruise (Figure VII. 4.2). The linear extrapolation of obtained points shows that the water masses associated with a relative phosphate minimum present characterisics of the mixing of three water masses: ESSW (*Equatorial Subsurface Water*), STSW (*Subtropical Surface Water*) and AAIW (*Antarctic Intermediate Water*) and thus confirmed the influence of subantarctic waters on north Peruvian waters. Since the number of data is very limited it is not reasonable to calculate the contribution of each water mass using an inverse multiparametric method.
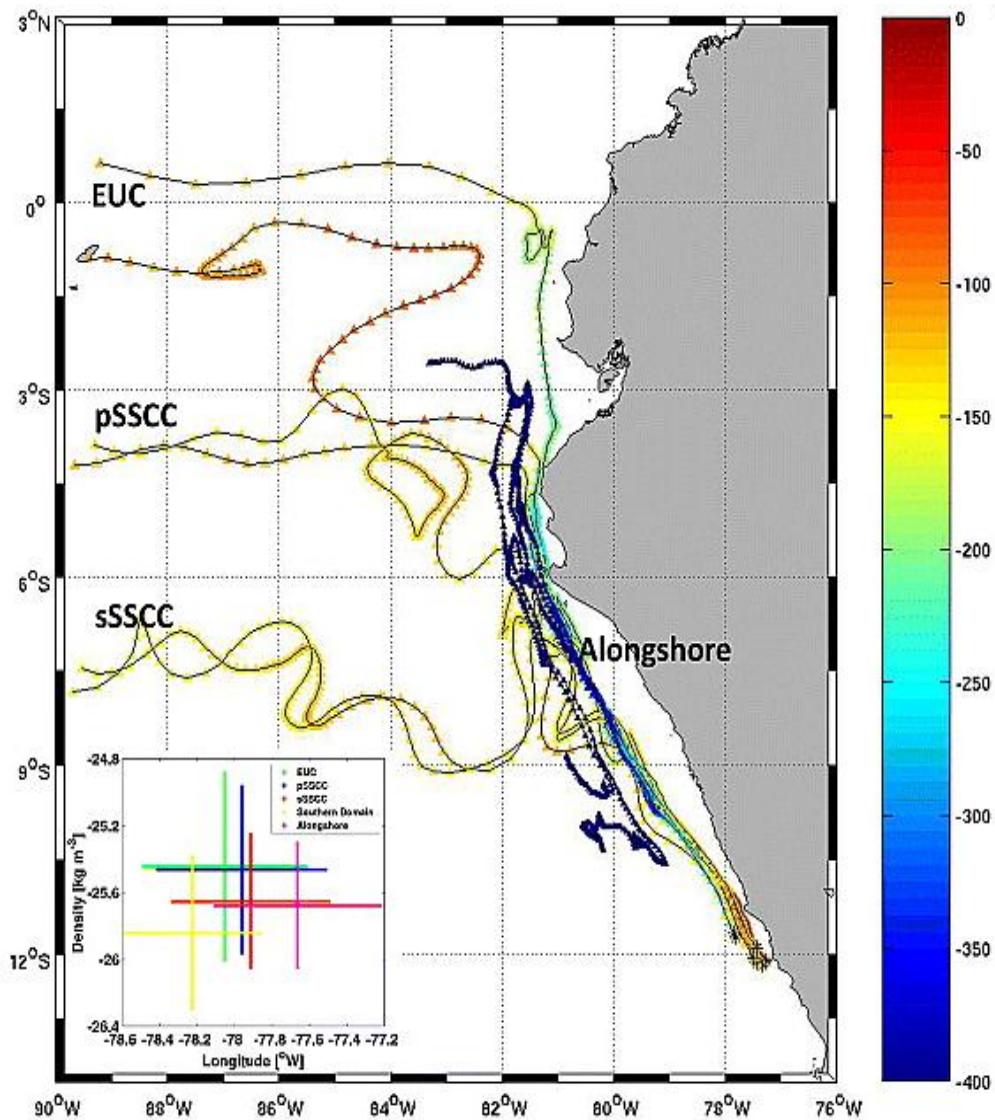
Fig. VII. 4.1. Alongshore recirculation of subantarctic waters offshore Peru (Montes et al., 2010) as evidenced in a 3D physical model.
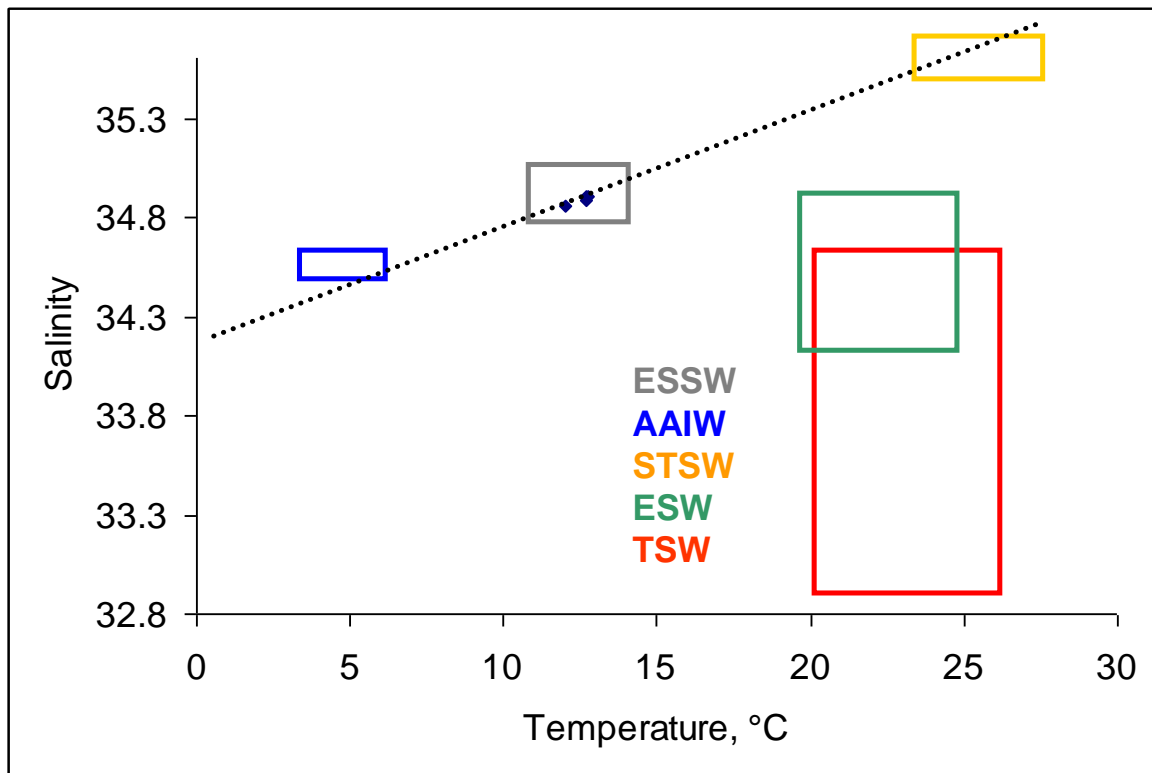
Fig. VII. 4.2. The T-S diagram for water masses associated with the relative phosphate minimum together with T-S characteristics range for different water masses found offshore Peru during the Pelagico cruise.

4.2. Complex biogeochemistry offshore Peru

The NO_3^- = f(PO_4^{3-}) diagram presented in Figure VII. 3.1 H for all 7 stations shows nutrient characteristics for all water masses observed during the Pelagico cruise. The deviation (average 8.9) from the canonical Redfield N:P ratio indicates that Peruvian waters are nitrogen limited. Such a low Redfield ratio was previously raported (Figure VII. 4.3-Franz et al., 2012). These characteristics are classical for waters where denitrification and anammox processes are taking place. Denitrification has crucial implications on cycling of the macronutrients nitrogen and phosphorus. The microbial processes anammox (anaerobic ammonium oxidation) (Kuypers et al., 2005, Hamersley, 2007, Galan et al., 2009), heterotrophic denitrification (Codispoti and Christensen, 1985) and DNRA (dissimilatory nitrate reduction to ammonium) (Lam et al., 2009) can occur within OMZs (Lam and Kuypers, 2011). Anammox and denitrification both represent large sinks of inorganic fixed N in anoxic and suboxic waters close to the shelf, thereby lowering the N:P stoichiometry and

driving the autotrophic system ultimately into N limitation. Furthermore, anoxic conditions in shelf sediments and shelf bottom waters enhance the release of reactive phosphate into the water column formely associated with iron hydroxides (Ingall and Jahnke, 1994) further enhancing negative deviation from the Redfield N:P ratio of 16:1.
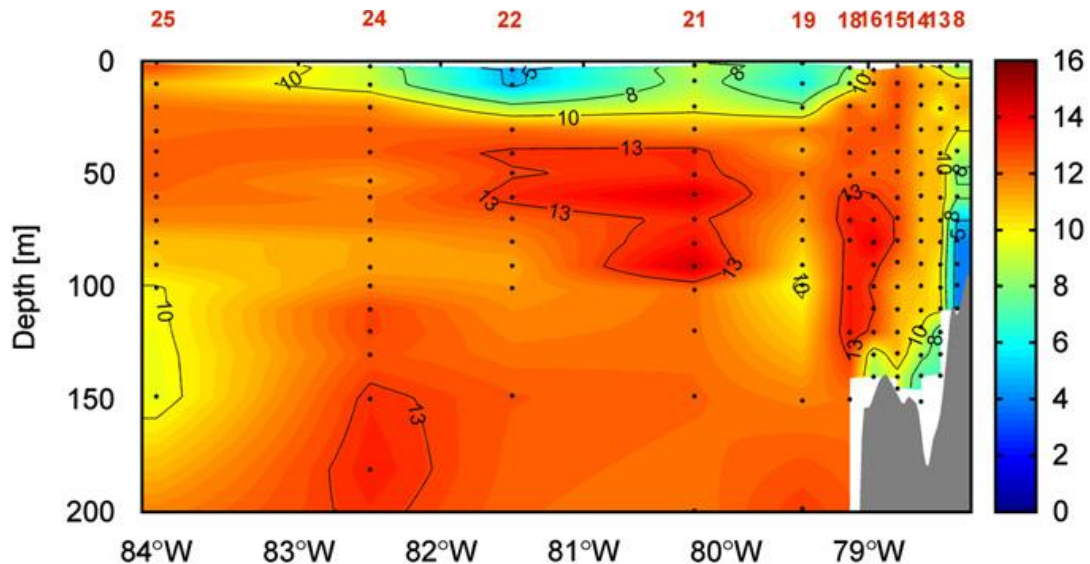
Figure VII. 4.3. Inorganic N:P stoichiometry in the water column along the complete 10°S transect during the M77/3 cruise on board of R/V Meteor (Franz et al., 2012).

Under such extreme conditions of nitrogen limitation, however, certain microorganisms like cyanobacteria utilize the nearly inexhaustible pool of dissolved N_2 as an alternative nitrogen source. Consequently, diazotrophic cyanobacteria could be the beneficiary of expanding OMZs. Nitrogen fixation is an essential process that biologically transforms atmospheric dinitrogen gas to ammonia, therefore compensating for nitrogen losses occuring via denitrification and anammox. This process requires a large amount of other nutrients like phosphate and iron. Consumption of phosphate can locally increase the ratio N:P and decrease the amount of phosphate excess (P*=inorg. P − inorg. N/16). In fact, the diagrams of N:P ratio as a function of depth show an increase of the ratio N:P at depths associated with an phosphate minimum (Figure VII. 4.4). Additionally, at depths of about 200 m the excess phosphate value seems to decrease indicating consumption of phosphate by cyanobacteria during the nitrogen fixation process (Figure VII. 4.5). Processes described above are still poorly known but according to Fernandez et al. (2011) the N_2-fixation can occur in the water column as deep as 400 m within the OMZ layer.
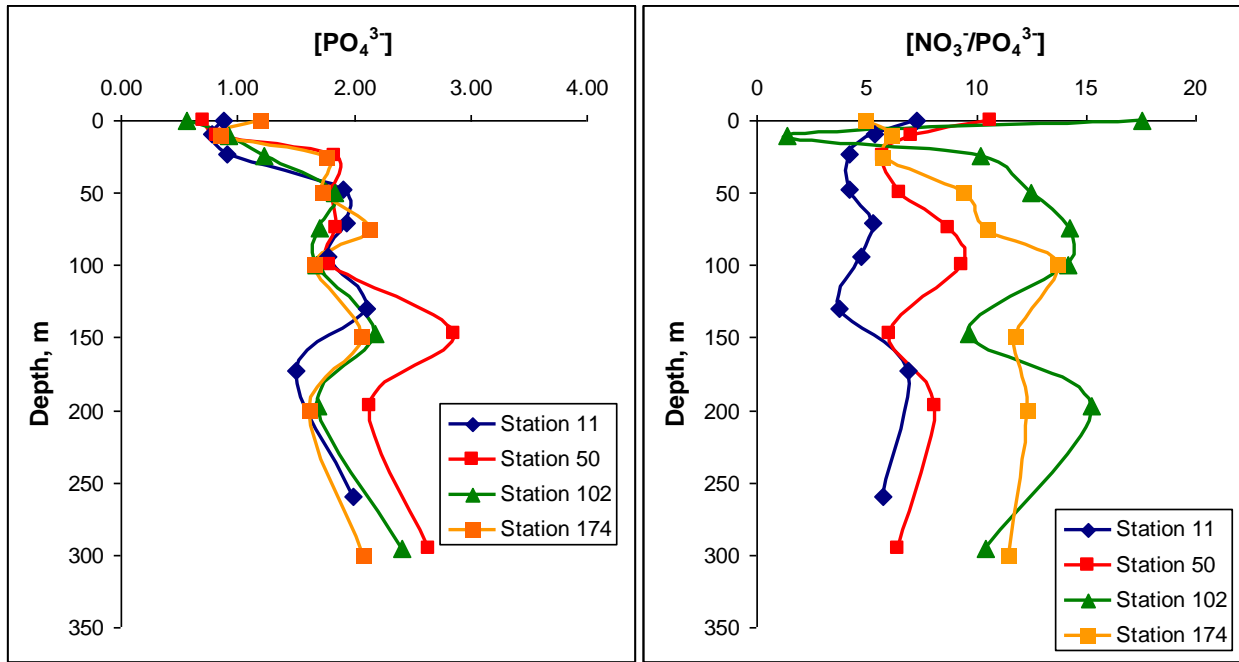
Figure VII. 4.4. Phosphate profiles (left) and NO_3^- / PO_4^{3-} (right) for the same CTD stations of the Pelagico November 2010 cruise.
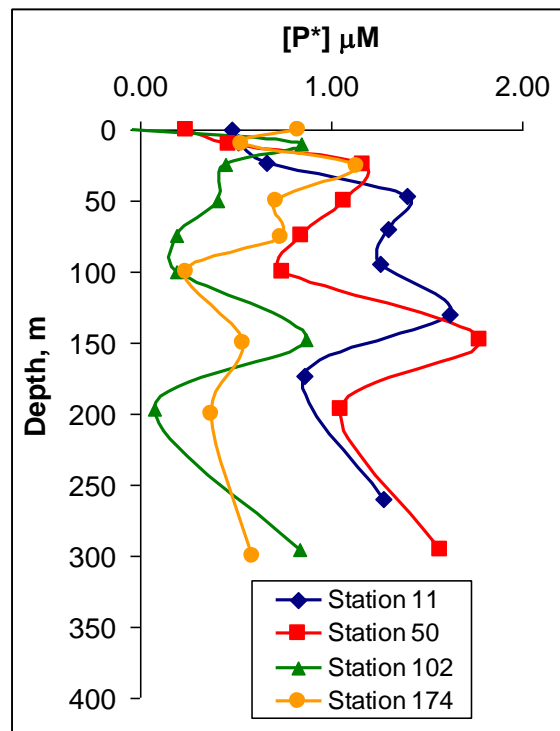
Figure VII. 4.5. Excess P (P*) according to the Redfield ratio of 16:1 for 4 offshore CTD stations analyzed during the Pelagico cruise.

Having a very limited data set from the Pelagico cruise it is very dificult to explain why this phosphate minimum associated with cyanobacteria activity occurs at about 150-200m. However, it seems that the presence of phosphate minima at this depth can be explained by the complex biogeochemistry in addition to the alongshore recirculation of subantarctic waters as mentioned in Section 4.1.

The injection of oxygenated AAIW into the Peru-Chile Undercurrent (PCUC) can cause modification of biogeochemical cycles. The presence of oxygen will lead to remineralisation and nitrification processes by aerobic activity. These processes consume oxygen and produce NO_3^-, NO_2^-, NH_4^+ leading system back to hypoxic conditions (Giraud, 2012). The locally increased nitrate concentration can magnify the denitrification and annamox processes by anaerobic organisms leading to production of gaseous nitrogen (N_2, N_2O). Finally, activation of N_2-fixation may occur in such extreme conditions leading to consumption of phosphate and thus influencing the vertical profiles of phosphate. The situation can be even more dificult if we consider that more than one process can take place at the same time. Figure VII. 4.6 presents the diagram $\delta[PO_4^{2-}]=f(\delta[NO_3^-])$, where $\delta[PO_4^{2-}]=$ $(P_{150}-P_{200})$ and $\delta[NO_3^-]=(N_{150}-N_{200})$ for water masses associated with this relative phosphate minimum.
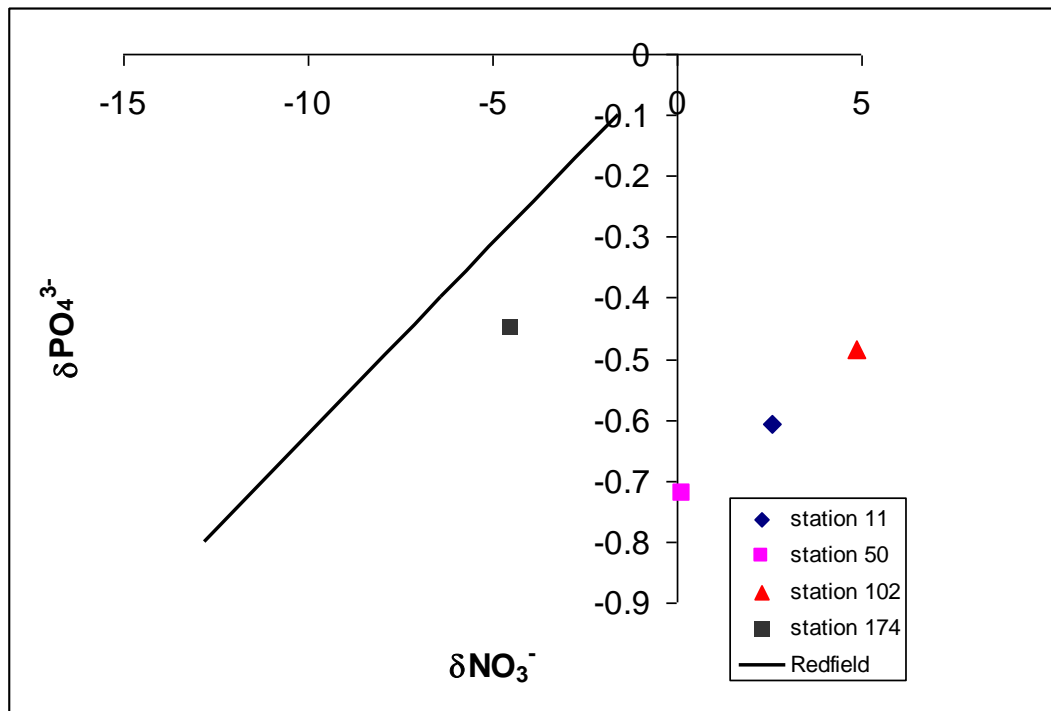
Fig. VII. 4.6. Diagram of phosphate and nitrate variations defined by difference in nutrients' concentrations at 150 and 200m for water masses associated with phosphate minimum.

Two cases can be noticed: phosphate minimum associated with nitrate minimum and phosphate minimum associated with nitrate maximum (Giraud, 2012; Paulmier, com. pers.). The first case is characteristic of the predominance of denitrification/anammox processes (which consume nitrate over nitrification/remineralization) associated with N_2-fixation (phosphate consumption). This description was found for the 174 CTD station from the Pelagico cruise where the weakest phosphate minimum was found. The second would be indicative of predominance of remineralization/nitrification processes (production of nitrate over denitrification/anammox) associated also with N_2-fixation (phosphate consumption, but no nitrate consumption). This characteristic is suitable for CTD stations 11, 50, 102.

5. Conclusions and perspectives

The oceanographic region offshore Peru is a very interesting area. This area is the site of permanent wind-driven coastal upwelling and inhabits a persistent, large and intense Oxygen Minimum Zone. It contributes to a significant fraction of fixed inorganic nitrogen loss via denitrification and anammox lowering the Redfield ratio of N:P. It seems that diazotrophic cyanobacteria could be the main beneficiary of this situation and might have a potential to replenish the inorganic N-deficit and reconstruct Redfield's nutrient stoichiometry via dinitrogen fixation process.

The analysis of water masses shows typical hydrological characteristics offshore Peru. At the surface *Tropical Surface, Cold Coastal, Equatorial Surface, Subtropical Surface Waters* were found. The subsurface waters were dominated by *Equatorial Subsurface Water* associated with extremely low oxygen concentrations. The N-P diagram clearly indicates that these water masses are all under nitrogen limitation. The Redfield ratio of N:P is extremely low (8.9). It is usually associated with microbial processes of denitrification and anammox. Additionally, a phosphate minimum was first observed at depth of ~200 m. It is quite dificult to provide the full scenario of explanations of this observation. However, some hypotheses were proposed. The water mass' characteristics observed at depths at the PO_4^{3-} minima could be associated with an alongshore recirculation of subantarctic waters. These waters flowing equatorward until about 3°S are injected into the PCUC, upwell and then flow back poleward, mixing with other Peruvian waters, and thus getting warmer, saltier and losing oxygen due to remineralization. Another hypothesis can be associated with the very complex biogeochemistry in this region. Low ratios of N:P can cause cyanobacteria blooms due to N_2 fixation even within Oxygen Minimum Zones. It is thus possible that dinitrogen fixation is

taking place in subsurface (200m) consuming large amounts of phosphate. The combination of physical and biogeochemical origins for the observed PO_4^{3-} minima is probably the most possible scenario but a definitive answer would require a retrospective detailed water mass analysis.

GENERAL CONCLUSIONS

To understand the factors controlling the biological carbon pump in the ocean, now and in the future due to global warming, we must better understand the functioning of coupled biogeochemical cycles of phosphorus, nitrogen, silica and iron. The long-term monitoring of the marine environment requires miniaturized autonomous sensors operating *in situ* with a long life time, low detection limit, low power consumption, a fast response, good reproducibility, resistance to biofouling and pressure. Electrochemistry offers a promising approach for further steps in miniaturization, and reduced response time and energy consumption.

This study is focused on phosphate and oxygen, two key compounds of the marine ecosystem. Improvement of the amperometric STOX sensor for ultra-low oxygen detection in seawater is presented. This part of the work was done during a three months stage at Aarhus University with some collaboration with the UNISENSE Company.

The project was, however, focused on phosphate sensor development and this part of the work was done at LEGOS laboratory with collaboration with LGC laboratory.

During my secondment at Aarhus University, improvement of STOX sensor for ultra-low oxygen concentrations was obtained. This improvement was achieved by a change in the sensor construction. Instead of electrodeposition of gold on platinum wire, gold plating on the silicon membrane was used to create the gold cathode. The method is based on the reduction of gold chloride by the solution of hydrazine hydrate. The comparison of the improved sensor and the traditional STOX sensor shows higher sensitivity (2-3 times) and faster response time (which is now 7 s instead of 16s). The temperature dependence remains the same in both cases. The average slope of this dependence is 2.36%/°C.

Recognition of isopoly- and heteropolyoxomolybdates obtained during oxidation of molybdenum in the sea water was performed. Studies have shown the formation of complexes at different oxidation states of molybdenum (V, VI) and proposed forms of complexes are: $H_4Si(Mo_2{}^{V}Mo_{10}{}^{VI}O_{40})$, $H_4Si(Mo_3{}^{V}Mo_9{}^{VI}O_{40})$, and $H_3P(Mo_6{}^{V}Mo_6{}^{VI}O_{40})$. Electrode reactions for these complexes represent reversible diffusion-controlled systems with coupled homogeneous reaction, probably protonation, which prevents the rapid electron transfer and influences the detection of phosphates and silicates. This work helps to discover which kinds of silico- and phosphomolybdate complex are formed, explains complicated electrode reactions and consequently helps to understand the difficulty of phosphate detection by electrochemistry. Thus, these results will help us to develop a first electrochemical sensor for *in situ* detection of phosphate (and silicate) in the ocean.

The electrochemical determination of electroinactive phosphate is based on the formation of a complex with molybdate due to a reaction with K_2MoO_4 in an acid solution (pH 1). The oxidation of the molybdenum is used to produce molybdate and protons without addtion of any liquid reagents. Three methods to solve the silicate intereference problem were developed and one based on an appropriate ratio between protons and molybdates equal to 70 was chosen and improved. Finally, thanks to the special design of the electrochemical cell with application of membrane technology, we are able to determine the phosphate concentration in the presence of silicates without addition of any liquid reagents by two electrochemical methods: differential pulse voltammetry and amperometry. The method was validated for natual seawater samples collected offshore Peru during the oceanographic cruise (Pelagico BIC Olaya-aboard R/V Olaya Balandra Jose) in November 2010. The average deviation obtained by comparing the amperometric and classical colorimetric methods is 5.1%.

Additionally, work on water mass analysis offshore Peru was done using data obtained from electrochemical measurements of phosphate during the cruise (Pelagico BIC Olaya – aboard R/V Olaya Balandra Jose). Hydrological characteristics show a signature of *Tropical Surface Water, Equatorial Surface Water, Subtropical Surface Water, Cold Coastal Water, and Equatorial SubSurface Water*-water masses usually found in this region. However, at depth of about 200 m, an interesting phosphate minimum was noticed. This minimum can be associated with the alongshore recirculation of subantarctic waters or/and complicated biogeochemistry with complex microbial processes coexising in this region: denitrification, nitrification, anammox, nitrogen fixation etc. Nitrogen fixation can be measured at great

depths and consumes phosphate leading to a higher than expected Redfield N/P ratio. Thus, the possible explanation of the relative phosphate minimum can be due to N_2 fixation carried out by cyanobacteria bloom at a 200 m. However, the definitive answer can be much more complicated and requires retrospective detailed analysis of water masses and biogeochemistry offshore Peru.

This thesis work opens different perspectives through development and deployment of autonomous sensors for the longer term.

Preliminary work performed at Aarhus University has shown a great potential for STOX sensor evolution. However, time spent on improving the STOX sensor was short (3 months). It would be necessary for a skilled builder to build a few more sensors of this new type and confirm the improved performances. Then monitoring of the stability of the signal during longer time (several months) in natural seawater will be necessary. The long-term stability can be obtained by combining the principle of the STOX electrode with optical oxygen sensors (Fisher et al., 2012). In addition, to increase the sensor robustness, possible avenues exist such as shielding a perforated tube or filling the sensor with a gel.

For phosphate sensor development, it will be necessary to continue monitoring of the signal stability over longer time (a few months) and to establish a protocol for *in situ* cleaning of the gold electrode. To do so, one may consider using multiple scans of potential in sea water until the residual current is low and stable. Next steps will be adressing the development of the mechanical and electronic parts of the sensor. Indeed, the measurement must be performed in a closed volume sample accurately the sea water. At the same time, a calibrationless method should be developed to make the sensor fully autonomous. Otherwise, we should consider an *in situ* calibration protocol by standard addition. The sensor will be characterized by a low power consumption and short response time due to the reduced volume combined with application of a large membrane surface. The adaptation of one sensor on autonomous vehicles profiling the water column (ARGO, AUV) would be the next step. Finally fixed moorings can allow the acquisition of long data time series at a fixed point. Indeed, within the AMOP project (Activities of research dedicated to the Minimum Oxygen Zone in the eastern Pacific), a shallow (200m) morring will be deployed next January 2013 offshore Callao, Peru, along 12°S at the IMARPE historical station N°5 for a 3 year period. It is planned that both the improved STOX and phosphate sensors will be adapted on the mooring line as soon as possible.

The results obtained during the oceanographic cruise offshore Peru were re-used for the analysis of water masses to explain the biogeochamical processes in this region. This work was done in collaboration with Mélanie Giraud and Aurélien Paulimer from our laboratory during her Master Thesis. Indeed, starting from our original observations of the phosphate minimum in subsurface such as measured during the November 2010 Pelagico cruise, Giraud (2012) examined a few other German cruises (Meteor 77 legs 3 and 4) in austral summer 2009 and 2010 in the region. She showed that a similar signature in phosphate concentration can be found. It will be of utmost interest to perform a complete characterization of these phosphate minima using all oceanographic data in the region to fully deconvolve the physical versus biogeochemical origins of these relative minima.

CONCLUSION GENERALE (français)

Pour comprendre les facteurs contrôlant la pompe biologique de carbone dans l'océan, maintenant et dans le futur, dans un contexte de réchauffement climatique, nous devons mieux connaître le fonctionnement couplé des cycles biogéochimiques du phosphore, de l'azote, de la silice et du fer. La surveillance à long terme de l'environnement marin requiert des capteurs autonomes, miniaturisés, opérant *in situ* avec une longue durée de vie, une limite de détection basse, une faible consommation d'énergie, un temps de réponse court, une bonne reproductibilité, ainsi qu'une résistance au biosalissures et à la pression. L'électrochimie offre des méthodes prometteuses pour atteindre ces objectifs.

Cette étude se concentre sur le phosphate et l'oxygène, deux composés principaux au sein des écosystèms marins. L'amélioration du capteur STOX pour la détermination de faibles concentrations en oxygène dans l'eau de mer est présentée. Cette partie du travail a été réalisée lors d'un stage de trois mois à l'Université d'Aarhus en collaboration avec la Société UNISENSE.

Mon projet de thèse a été, avant tout, axé sur le développement d'un capteur électrochimique pour la détermination du phosphate dont les travaux ont été effectués au laboratoire LEGOS en collaboration avec le Laboratoire de Génie Chimique, LGC de Toulouse.

Lors de mon stage dans la Société UNISENSE, une amélioration du capteur STOX pour la détermination des faibles concentrations en oxygène a été obtenue. Cette amélioration a été effectuée par un changement dans la construction du capteur. Au lieu d'électrodéposer de

l'or sur du platine, des particules d'or sont déposées sur du silicium pour créer la cathode d'or. La méthode est basée sur la réduction du chlorure d'or par une solution d'hydrate d'hydrazine.

La comparaison du capteur STOX traditionnel à la version améliorée montre une sensibilité plus élevée (2-3 fois) et un temps de réponse plus rapide (7 s au lieu de 16 s). Dans les deux cas, la dépendance de la température reste la même. La pente moyenne de cette dépendance est de 2,36% /° C.

Une reconnaissance des espèces isopolymolibdiques et hétéropolymolibdiques obtenues lors de l'oxydation du molybdène dans l'eau de mer a été effectuée. Des études ont montré la formation de complexes à différents états d'oxydation pour le molybdène (V, VI) et qui ont pour formule : $H_4Si(Mo_2^{V}Mo_{10}^{VI}O_{40})$, $H_4Si(Mo_3^{V}Mo_9^{VI}O_{40})$, et $H_3P(Mo_6^{V}Mo_6^{VI}O_{40})$. L'électrochimie de ces complexes montre un système réversible, contrôlé par la diffusion couplée avec une réaction homogène, sans doute une protonation, qui empêche le transfert rapide d'électrons et influe sur la détection des phosphates et silicates. Ce travail a permis de découvrir quels types de complexes silico- et phosphomolybdiques sont formés et rend compte de la complexité des réactions aux électrodes. Il contribue ainsi à comprendre les difficultés de détection des phosphates par l'électrochimie. Ces résultats peuvent aider à mettre au point un premier capteur électrochimique pour la détection *in situ* des phosphates (et des silicates) dans l'océan.

La détermination électrochimique du phosphate, espèce non électroactive, est basée sur la formation d'un complexe avec le molybdate en une solution acide. L'oxydation du molybdène est utilisée pour produire les ions molybdate et les protons sans ajouter de réactifs. Trois méthodes pour résoudre les interférences des silicates ont été étudiées et le choix s'est porté sur l'utilisation d'un rapport approprié entre les protons et les molybdates égal à 70. Finalement, grâce à la conception d'une cellule électrochimique et l'utilisation de membranes, nous sommes capables de déterminer les concentrations en phosphates en présence de silicates sans ajouter de réactifs, par deux méthodes électrochimiques : ampérométrie et voltammétrie impulsionnelle différentielle. La méthode a été validée avec les échantillons d'eau de mer naturelle collectés au large des côtes du Pérou au cours de la campagne océanographique Pelagico 1011-1012 BIC-Olaya à bord du R/V Jose Balandra Olaya en Novembre 2010. L'écart moyen obtenu en comparant les analyses ampérométriques et colorimétriques est de 5,1%.

En outre, un travail sur l'analyse des masses d'eaux au large du Pérou a été effectué en utilisant les données obtenues à partir de mesures électrochimiques des phosphates pendant la campagne en mer (Pelagico BIC Olaya à bord du R/V Jose Olaya Balandra). Les caractéristiques hydrologiques montrent la signature des Eaux de Surface Tropicale, des Eaux de Surface Equatoriale, des Eaux de Surface Subtropicale, des Eaux Froides Côtières, et des Eaux de SubSurface Equatoriale ; masses d'eau habituellement trouvées dans cette région. Cependant, à une profondeur d'environ 200 m, un minimum de phosphate atypique a été remarqué. Ce minimum peut être associé à la recirculation des eaux subantarctiques au large du Pérou et/ou à la biogéochimie complexe, riche de processus microbiens dans cette région : la dénitrification, la nitrification, l'anammox, la fixation de l'azote atmosphérique etc... La fixation de l'azote peut être mesurée à ces profondeurs importantes et consomme des phosphates induisant en rapport N/P supérieur à la valeur de Redfield. Cependant, la réponse définitive peut être beaucoup plus complexe et exige une analyse des masses d'eau plus détaillée et une surveillance de la biogéochimie au large des côtes du Pérou.

Ces travaux de thèse ouvernt différentes perspectives notamment dans le cadre du développement et du déploiement de capteurs atonomes à plus ou moins long terme sur des observatoires biogéochimiques.

Le travail préliminaire mené à l'Université d'Aarhus a montré un grand potentiel dans l'évolution du capteur STOX. Toutefois, le temps passé à l'amélioration des performances du capteur STOX (3 mois) fut très court. Il semble nécessaire de construire beaucoup plus de prototypes de ce type afin de confirmer ces acquis. Puis, il sera nécessaire de continuer le suivi de la stabilité du signal sur des temps plus longs (plusieurs mois) en eau de mer naturelle. La stabilité à long terme peur être obtenue en combinant le principe de l'électrode STOX avec les capteurs d'oxygène optiques (Fisher et al., 2012). De plus, pour accroître la robustesse du capteur, plusieurs voies existent comme le blindage d'un tube perforé ou remplissage du capteur par un gel.

En ce qui concerne la détection du phosphate il sera nécessaire de continuer le suivi de la stabilité du signal en function du temps et de mettre en place un protocole de nettoyage *in situ* de l'éléctrode d'or. Pour cela, il pourra être envisagé la réalisation de multiples balayages de potentiel en eau de mer jusqu'à l'obtention d'un courant résiduel faible et stable. Les prochaines étapes concernent le développement des parties mécanique et électronique du capteur. En effet la mesure doit être réalisée dans un volume fermé impliquant d'echantillonner de façon très précise l'eau de mer à analyser. Dans le même temps une méthode sans calibration devra être élaborée pour assurer une totale auonomie. Une

alternative serait d'envisager un protocole de calibration *in situ* par ajout de standards. Le capteur sera caractérisé par une faible consommation énergétique et un temps de réponse court en raison de la diminution du volume combiné à une application de membranes de grande surface. L'adaptation de notre capteur sur des véhicules autonomes profilant dans la colonne d'eau (ARGO, AUV) constitue l'étape suivante. Enfin l'implantation sur des mouillages fixes permettra l'acquisition de longues séries temporelles de données en un point fixe. En effet, dans le cadre du project AMOP (Activities of research dedicated to the Minimum Oxygen Zone in the eastern Pacific), un mouillage peu profond (200m) sera déployé en Janvier 2013 au large de Callao au Pérou, le long de 12°S à la station historique N° 5 de l'IMARPE pour une période de 3 ans. Il est prévu que le capteur STOX amélioré et le capteur phosphate soient adoptés sur cette ligne de mouillage aussitôt que possible.

Les résultats océanographiques obtenus pendant la campagne en mer au large du Pérou ont été re-utilisés pour l'analyse des masses d'eau et pour l'explication des processus biogéochimiques dans cette région. Ce travail a été fait en collaboration avec Giraud Mélanie et Paulimer Aurélien de notre laboratoire pendant un stage de Master 2 Recherche (Giraud, 2012). En effet, partant de nos observations originales sur le minimum de phosphate en subsurface tel que mesuré durant la camapgne océanographique Pelagico en Nevembre 2010, Giraud (2012) a étudié d'autres campagnes allemandes (Méteor 77 legs 3 et 4) pendant l'été austral 2009 et 2010 dans la région. Elle a identifié une signature similaire sur les profils de concentrations de phosphate. Il apparaît primordial de mener une caractérisation complète de ces minima de phosphate en utilisant l'ensemble des données océanographiques de la région afin de pouvoir déconvoluer les origines physiques versus biogéochimiques de ces minima relatifs.

ANNEXE

The purpose of this PhD thesis was to develop an electrochemical sensor for phosphate detection. However, thanks to a close collaboration within the team a work on silicate detection in seawater was done as well. As it was mentioned before, in acidic medium in presence of molybdate the silicomolybdic complex can be formed and detected in a similar way than for phosphate. Thus, a method for silicate detection was developed based as well on electrochemical oxidation of molybdenum in an electrochemical cell using membrane technology (Lacombe et al., 2007, 2008, Lacombe, 2007). The detection of silicate is less complicated since the electrode reactions are not limited visually by any homogenous chemical step (Jonca et al., 2012) and the electrochemical cell consists of two parts divided by one membrane which makes it easier to operate and then miniaturize. Recently, a calibrationless method was developed in our team based on the use of two electrodes of different size and applying two Fick's equations in order to calculate concentration and diffusion coefficient. The preliminary study shows good results for strong and medium silicate concentrations (50, 150 µM). Future step will be to work on this method for low silicate concentrations and to optimize a similar method for calibrationless phosphate detection. Currently, we are working also on miniaturization and adaptation of the silicate sensor to the marine environment. The purpose is to have soon both silicate and phosphate sensors adaptable on ARGO floats.

Contents

Article 4: Giraud, W., Lesven, L., Jońca, J., Barus, C., Gourdal, M., Thouron, D., Garçon, V., Comtat, M., 2012, *Reagentless and calibrationless silicates measurement in oceanic water,* Talanta, 97, 157-162

Reagentless and calibrationless silicate measurement in oceanic waters

William Giraud [a,1], Ludovic Lesven [b,1], Justyna Jońca [a], Carole Barus [a], Margaux Gourdal [a], Danièle Thouron [a], Véronique Garçon [a,*], Maurice Comtat [c]

[a] Laboratoire d'Etudes en Géophysique et Océanographie Spatiales, Centre National de la Recherche Scientifique, UMR CNRS 5566, 18 Avenue Edouard Belin, 31401 Toulouse Cedex 9, France
[b] Laboratoire Géosystèmes, UMR CNRS 8217, UFR des Sciences de la Terre, Université Lille 1, 59655 Villeneuve d'Ascq Cedex, France
[c] Laboratoire de Génie Chimique, UMR CNRS 5503, 118 route de Narbonne, 31062 Toulouse Cedex 9, France

A R T I C L E   I N F O

A B S T R A C T

Determination of silicate concentration in seawater without addition of liquid reagents was the key prerequisite for developing an autonomous in situ electrochemical silicate sensor (Lacombe et al., 2007) [11]. The present challenge is to address the issue of calibrationless determination. To achieve such an objective, we chose chronoamperometry performed successively on planar microelectrode (ME) and ultramicroelectrode (UME) among the various possibilities. This analytical method allows estimating simultaneously the diffusion coefficient and the concentration of the studied species. Results obtained with ferrocyanide are in excellent agreement with values of the imposed concentration and diffusion coefficient found in the literature. For the silicate reagentless method, successive chronoamperometric measurements have been performed using a pair of gold disk electrodes for both UME and ME. Our calibrationless method was tested with different concentrations of silicate in artificial seawater from 55 to 140×10^{-6} mol L^{-1}. The average value obtained for the diffusion coefficient of the silicomolybdic complex is $2.2 \pm 0.4 \times 10^{-6}$ cm^2 s^{-1}, consistent with diffusion coefficient values of molecules in liquid media. Good results were observed when comparing known concentration of silicate with experimentally derived ones. Further work is underway to explore silicate determination within the lower range of oceanic silicate concentration, down to 0.1×10^{-6} mol L^{-1}.

© 2012 Elsevier B.V. All rights reserved.

1. Introduction

Orthosilicic acid Si(OH)$_4$ or silicate is a key element in the control of the carbon cycle in natural waters (oceans and rivers). The source of silicate in aquatic media is mainly due to chemical weathering of silicate minerals. The delivery of silicate by rivers is influenced by lithology, weathering intensity and diatom production [1,2]. Another process in which silicate plays a key role is anthropogenic CO$_2$ sequestration through the biological carbon pump. Indeed diatoms, silica-shelled unicellular algae, require silicate to build their siliceous algal skeleton [3]. The C/Si/N/P molar composition of diatoms is proposed to be 106/15/16/1 [4]. These values also represent the ratios in which nutrients containing these elements are incorporated during phytoplankton growth and are released during phytoplankton decomposition and subsequent remineralization. As fast sinking particles, diatoms play a major role in exporting organic carbon to abyssal marine sediments and thus in sequestering CO$_2$ [5]. So, any change in silicon concentration in a globally warming ocean can alter the distribution and abundance of diatom species. Due to regional differences in spatial distribution, silicate constitutes also an excellent tracer of water masses in the ocean. Thus long term autonomous monitoring of the silicate concentration is of utmost importance to both understand changes in the biological carbon pump and to detect any modification in spreading and mixing of water masses.

In the literature, several methods including spectrophotometry, atomic absorption spectrometry, atomic emission spectrometry and high-performance liquid chromatography (HPLC) have been proposed for the determination of silicate [6]. The determination of silicate ion can also be performed by ion exclusion chromatography, with detection by post-column reaction [7].

In oceanography, determination of silicate is usually performed with an automatic colorimeter analyzer where measurement is based on the yellow color of a silicomolybdic acid. This complex is formed when ammonium molybdate is mixed with a solution of sulfuric acid and after reduction with ascorbic acid. The resulting color may be compared with that of standard solutions by spectrophotometry [8].

Long term monitoring in marine environments requires significant progress in miniaturization and decrease in energy consumption for the in situ autonomous instrumentation. Electrochemistry

* Corresponding author. Tel.: +33 5 61 33 29 57; fax: +33 5 61 25 32 05.
E-mail address: veronique.garcon@legos.obs-mip.fr (V. Garçon).
1 Co-first authors.

proves to be a promising methodological avenue for fulfilling these requirements and achieving excellent figures of merit (fast response time, robustness, good reproducibility, etc.) for a silicate sensor.

The method must be simple, based on basic fluidics with no liquid reagent, no solution for calibration and the possibility of self calibration. It should involve sensitive surfaces easily cleaned, insensitive to marine corrosion and biofouling. Dissolved nutrients such as silicate and phosphate are non-electroactive compounds. The electroinactivity of these compounds involves the setting up of a chemical reaction to transform them into a complex, characterized by heterogeneous electron transfer with metallic surfaces [9–13].

A method without addition of any liquid reagent using chronoamperometry has been developed based on the simultaneous formation of the molybdenum salt and protons on the anode of a divided electrochemical cell. Voltammetric detection of silicate was shown to be feasible within the range of concentrations found in the ocean (between 0.3 and 160×10^{-6} mol L^{-1}) in about 6 min. The detection limit was 1×10^{-6} mol L^{-1} [11,12]. The objective of the work presented here is to propose a calibrationless method for the *in situ* autonomous determination of silicate concentrations. The method is based on chronoamperometric oxidation of molybdenum followed by a time delay to allow the silicomolybdic complex formation and its detection by two successive chronoamperometric measurements on different sizes electrodes. The paper is structured as follows. Section 2 presents basics of diffusion phenomena and mathematical equations applied on some electrochemical problems. From these statements a calibrationless method is proposed in Section 3. To set up the method, ferricyanide is used to check accurately the radius of the disk electrodes, ferrocyanide to validate the calibrationless method and first results are presented with silicate in artificial seawater.

2. Diffusion as mass transport for direct determination of D_0 and C

Analytical electrochemical methods are in general based on the coupling between mass transport phenomena (convection, migration, diffusion) and heterogeneous electron transfer at the interface between an electronic conductor and species in solution. Convection and migration effects are neglected due to the absence of stirring and the presence of an electrolyte support respectively, which allows considering only diffusion, mostly in semi-infinite conditions [14]. The simplest method is chronoamperometry performed at constant potential. The mathematical approach consists of resolving the second Fick's law (the initial and infinite conditions are fixed and the method allows to determine the interfacial condition). The first step of the calculation leads to concentration profiles of the electroactive species at time t. The interfacial flux is then injected in the definition of the current intensity. Table 1 (2nd column) summarizes the operations leading to the relationship between the measured intensity value and the unknown concentration C_0^*. Only equations corresponding to planar electrodes are considered here since this geometry is the simplest to perform for our application. The different equations in Table 1 involve the intensity of the current I, the diffusion coefficient D_0, the concentration at infinite C_0^*, the concentration at the surface of the electrode C_0 ($x=0$), the number of transferred electrons n, the electroactive surface of the electrode A, the electroactive radius r_0, the normal distance to the surface of the planar electrode x, the time t, the electrical charge Q and the Faraday constant F. The Cottrell's equation shows the necessity to know n, D_0 and A, some variables generally determined with a calibration performed in the same conditions than

Table 1
Main steps for the resolution of second Fick's law in semi-infinite diffusion. Chronoamperometry (constant potential) at planar electrode is considered. D_0 in cm^2 s^{-1}; C_0^* and C_0 ($x=0$) in mol cm^{-3}; A in cm^2; and x in cm; t in s; Q in C and F in C mol^{-1}.

	Chronoamperometry at planar electrode
2nd Fick's law	$\frac{\partial C}{\partial t} = D_0 \frac{\partial^2 C}{\partial x^2}$
Boundary conditions	$C_0(x,0) = C_0^*$ $C_0(\infty, t) = C_0^*$ $C_0(0, t) = 0$ ($t > 0$)
Flux $-J = \frac{1}{nFA} = D_0 \left(\frac{\partial C_0}{\partial x} \right)_{x=0}$	$I = nFAD_0 \left(\frac{\partial C_0}{\partial x} \right)_{x=0}$
Concentration profile C_0	$C_0 = C_0^* erf \left[\frac{\partial C_0}{2(D_0 t)^{1/2}} \right]$
Intensity I	Cottrell's equation: $I = \frac{nFAD_0 C_0^*}{(\pi D_0 t)^{1/2}}$
Charge Q	$Q = \frac{2nFAD_0^{1/2} C_0^* t^{1/2}}{\pi^{1/2}}$

the measurement. However it appears essential to have theoretical or experimental tools to determine them.

For calibration, different strategies have been developed during decades. A direct determination of concentration has been proposed by electrical charge measurement but demanding a rigorous sample preparation [19,20]. Original methods for simultaneous determination are the use of two methods [21–23], measurements on electrodes with different forms [24,25]—planar or cylindrical [26], the use of one electrode on different timescales [27–32].

Before *in situ* measurements with the sensor, the determination of the diffusion coefficient value could be possible depending on different experimental conditions influencing its value such as conductivity or temperature. Indeed, if the *in situ* sensor in the ocean is equipped with conductivity and temperature probes, the data could be stored for an eventual correction. This estimation could be done on the lab bench using various electrochemical methods as described before. Another methodology for determining the diffusion coefficient D_0 value could be the "time of flight" [15–18]. However in order to have a more precise value and a simpler method for the determination of the diffusion coefficient, we propose here to use a direct simultaneous determination of both concentration and diffusion coefficient.

When solving second Fick's law for different geometries [14], the corresponding equation is composed of two terms, one of which is time dependent and the other is not. These two components correspond to the transient state governed by the Cottrell's equation ($I = nFAD_0 C_0^*/(\pi D_0 t)^{1/2}$, Table 1) and to a steady state achieved at longer times. As the current intensity is recorded *versus* time, one can easily plot I *versus* $t^{-1/2}$ for short times, the origin intercept and the slope of the linear regression curve will then give a linear system with two equations. From this system of two equations, one can select two out of the three unknowns: D_0, C_0^* and n. Original works done on these determinations were done by Lingane and Loveridge [25] and Brown [26] who proposed to determine values of n and D_0. Later, Kakihana et al. [27] used ultramicroelectrode (hereafter UME) for the accurate measurement of D_0. The development of theoretical solutions allowed Winlove et al. [28] to propose the simultaneous determination of D_0 and C_0^* of oxygen in solutions of albumin. In the early 90s, Amatore et al. [22] studied in details different possibilities among several calibrationless methods and they found good results with chronoamperometry at steady state with an UME. Denuault et al. [29] then confirmed these works. In a general manner, a calibrationless method can be set in using two electrochemical methods, the combination of which allows the

mathematical determination of both D_0 and C_0^*. Other different possibilities of sizes and geometries of electrodes can be combined for a calibrationless method: a ring UME associated with planar, cylindrical or spherical electrode or a planar electrode associated with a spherical or cylindrical electrode. More recently numerical improvements in modeling allow to foresee more complex miniaturized systems [31,32], which could be of particular interest for *in situ* measurements.

Different procedures for electrode constructions can be found in the literature in forms of rings, disks, spheres and cylinders made from materials such as gold, platinum, silver or carbon. As seen previously, the direct determination of electroactive species without calibration may require the successive measurement of current across two electrodes with different sizes or forms.

In the present study, we propose to associate a planar disk microelectrode (hereafter ME) of millimetric size and a planar disk UME of micrometric size. Both are used in semi-infinite conditions and the applied potential corresponds to the first reduction of the silicomolybdic complex [11,12]. Different mass transport regimes can be considered at planar electrodes during the measurement. For each electrode (ME and UME) and at very short times, the variation of current respects Cottrell's equation. Species present at a distance inferior to the diffusion layer from the surface of the electrode are reduced, leading to a relatively high current and creating a gradient of concentration. At relatively long experimental times, steady state is reached, governed by pure diffusional mass transport and a constant current is measured. Hemispherical diffusion brings species to the surface of the UME (Fig. 1a) while a linear diffusion, orthogonal to the surface (Fig. 1b), is observed for the ME (Fig. 1b). On the UME, with a radius r_{UME}, the resolution of the second Fick's law leads to the following term for the steady state:

$$I_{UME} = 4nFD_0C_0^*r_{UME} \qquad (1)$$

Depending on the size of the electrodes and time scale of the measurement, true diffusional steady state may be altered to the benefit of natural convection. This mass transport occurs when the thickness of the diffusion layer becomes comparable to the thickness of the convective-free domain [33,34]. In this study we took care to keep our experimental conditions under a pure diffusional mass transport.

The combination of Cottrell's equation (Table 1: $I_{ME} = nFA_{ME}D_0C_0^*/(\pi D_0 t_{ME})^{1/2}$ with $A_{ME} = \pi r_{ME}^2$; t_{ME} time of application of constant potential and I_{ME} the corresponding current intensity at each time t_{ME}) and Eq. (1) leads to the calculation of D_0:

$$D_0 = \frac{\pi}{16t_{ME}}\left(\frac{I_{UME}r_{ME}^2}{I_{ME}r_{UME}}\right)^2 \qquad (2)$$

Then determination of the concentration C_0^* is possible using Eq. (1) or Cottrell's equation. The theory of this calibrationless method was first checked with a well known electrochemical system, then tested in a second step in artificial seawater.
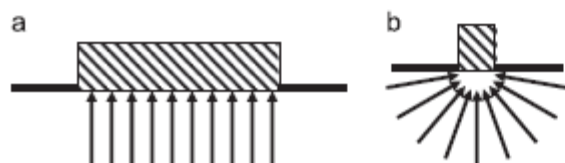

Fig. 1. Lines of diffusion field of the electroactive species arriving at the surface of a planar electrode (a) and an ultramicroelectrode (b).

3. Material and methods

3.1. Apparatus and electrodes

Amperometric measurements were carried out at room temperature (298 K) with a voltammetric analyzer comprising a PGSTAT 128N Metrohm equipped with an ECD module controlled by the GPES 4.9 software. A silver/silver chloride/KCl (3 mol L^{-1}) electrode and a platinum wire were used as the reference electrode and the auxiliary electrode, respectively. All potential values in this paper are given *versus* this Ag/AgCl/Cl$^-$ reference electrode purchased from Metrohm. For the calibrationless method a disk ME of 1.5 mm radius (Metrohm) or 0.5 mm radius (homemade) is associated to a disk UME of 12.5 μm or 25.0 μm radii (homemade). All homemade electrodes were prepared in the laboratory from a gold wire supplied by Goodfellow and sealed into an inert and electric insulating epoxy resin. Gold for homemade electrodes, platinum and molybdenum wires were supplied by Goodfellow.

Pre-treatment—before each experiment, the gold electrode surfaces were polished with alumina oxide paper 0.3 μm and rinsed with distilled water. Finally, cyclic voltammograms were carried out in 0.5 mol L^{-1} sulfuric acid (H$_2$SO$_4$) at 100 mV s^{-1} between 0 and 1.55 V until reproducible current–potential curves were obtained.

3.2. Reagents and solutions

All solutions were prepared in Milli-Q water (Millipore Milli-Q water system) and put into polypropylene containers. Glass cannot be used as it releases silicate in solution.

Artificial seawater was prepared with sodium chloride (NaCl) supplied by Merck to obtain a salinity of 34.5 g L^{-1}.

The electroactive surface of gold is activated in 0.5 mol L^{-1} H$_2$SO$_4$ solution prepared from a 98% H$_2$SO$_4$ solution from Merck.

Trihydrated potassium ferricyanide (K$_3$Fe(CN)$_6 \cdot 3$H$_2$O) and trihydrated potassium ferrocyanide (K$_4$Fe(CN)$_6 \cdot 3$H$_2$O) were purchased from VWR Prolabo and potassium chloride (KCl) from Merck. Argon gas was used to avoid ferrocyanide oxidation.

3.3. Analytical procedures

Electroactive surface determination—chronoamperometric measurements were performed in semi-infinite diffusion conditions on each gold working electrode. Time electrolysis depends on the electrode used: a potential of 0.2 V was applied for ferricyanide reduction during 60 s and 8 s for UME and ME, respectively.

Method without liquid reagent—the method used was adapted from the one described by Lacombe et al. [11,12], based on the oxidation of a molybdenum wire to form molybdates and protons. Experimentally, molybdenum, reference and working electrodes were placed in a 3 mL compartment. To avoid protons reduction, the counter electrode was isolated from the first compartment by a Nafion® membrane (N117 DuPont™ PFSA). Molybdates and protons were produced with molybdenum anodic oxidation at a constant potential of 0.8 V until a 14.0 C load was reached.

Calibrationless method—successive chronoamperometric measurements were performed *versus* time in semi-infinite diffusion conditions using a gold disk UME and a gold disk ME as working electrodes. For experiments performed with potassium ferrocyanide, a potential of 0.5 V was applied during 60 s on a gold disk UME and during 8 s on a gold disk ME. To analyze the silicomolybdic complex, a potential of 0.34 V was applied during 60 s on a gold disk UME and during 8 s on a gold disk ME.

Technicon Autoanalyser III—the reference colorimetric analysis of silicate was performed according to Tréguer et al.'s method

[35]. Laboratory colorimetric measurements were made with an Auto-Analyzer Technicon III (AAIII, Bran Luebbe). The concentration of the silicate solution, used for the preparation of silicate samples in artificial seawater, was precisely estimated with this technique.

4. Results and discussion

4.1. Electroactive surface determination

As the calibrationless method is very sensitive to the electroactive surface of each electrode (Cottrell's equation in Table 1 with $A_{ME} = \pi r_{ME}^2$ and Eq. (1)), first experiments were carried out to determine the electroactive radius of the working electrodes and check whether the proposed electrochemical equations are suitable. To achieve this, potassium ferricyanide in potassium chloride electrolyte was used as its diffusion coefficient which has been well established (ferricyanide: $D_0 = 6.95 \times 10^{-6}$ cm^2 s^{-1} at 25 °C in 0.2 mol L^{-1} KCl [36]). Three precise fresh solutions of ferricyanide potassium 7.5×10^{-3} mol L^{-1} were prepared in KCl 0.2 mol L^{-1}. Chronoamperometries were achieved on each electrode in semi-infinite conditions (three times for each solution) and the corresponding equations were applied for the disk ME and UME to determine r_{ME} and r_{UME}, respectively.

Knowing the diffusion coefficient D_0, the ferricyanide concentration C_0^* and the corresponding intensity I, the radii r_{ME} and r_{UME} have been calculated. Table 2 shows the comparison between the radius obtained experimentally and the geometrical radius as mentioned by the gold suppliers. The standard deviation obtained for the three determinations on experimental radii is excellent, equal or less than 0.6%. For the commercial electrode ($r_{ME} = 1.5$ mm), the mean value of electroactive radius, determined experimentally, is relatively much closer to the geometric value than for the homemade electrodes with different radii. For the homemade electrodes, observations with an optical microscope revealed an excellent

circular shape but deviations concerning the UME radii are slightly more important. Indeed, any deviation of a minute angle of the gold wire from the axis of the electrode body modifies the geometry of the electroactive surface towards an elliptic form instead of a perfect disk. Recent observations done with a Scanning Electronic Microscope have shown that the geometric surface is a well defined disk which makes Eq. 1 perfectly suitable. However, we observed on several UME the presence of a slight porosity. Given the quality of the gold material in our possession, we thus make the hypothesis for the time being that the geometric radius is close enough to the electroactive ones to perform the calibrationless method.

4.2. Calibrationless method with potassium ferrocyanide

It is proposed here to check the validity of the calibrationless method with the experimental materials used in the laboratory including the homemade UME. For the experiments, potassium ferrocyanide solution has been prepared in a 0.2 mol L^{-1} KCl electrolyte. The use of this compound presents a double interest as verification can be done on one hand on the diffusion coefficient, already estimated in a former study (ferrocyanide: $D_0 = 6.12 \times 10^{-6}$ cm^2 s^{-1} at 25 °C in 0.2 mol L^{-1} KCl [36]), and on the other hand on the concentration prepared accurately from potassium ferrocyanide salt.

The solution was prepared with argon bubbling to preserve ferrocyanide from oxidation. During the measurement, argon atmosphere was kept over the solution with a slow flux to avoid any stirring of the liquid, and to preserve the experimental semi-infinite diffusion conditions.

Chronoamperometry was successively applied on each electrode, and Cottrell's equation (Table 1) and Eq. (1) mentioned previously were used to estimate both diffusion coefficient D_0 and concentration of ferrocyanide C_0^*. Some tests were done for different concentrations of ferrocyanide on a couple of electrodes of radii 25.0 µm for UME and 1.5 mm for ME. As proposed in Section 4.1, geometrical radii were used for the calculations. The results are summarized in Table 3 and compared to the diffusion coefficient of ferrocyanide found by Bortels et al. [36] and the known concentration.

As it can be noticed in Table 3, the results are in good agreement with the diffusion coefficient value from literature. The repeatability of the measurement in the same solution is particularly good to determine a constant diffusion coefficient value. The concentration of ferrocyanide determined experimentally is also very close to the known value. These results give us some confidence in applying this calibrationless method for silicate determination.

4.3. Calibrationless method with silicate

Previous studies of the silicomolybdic complex by cyclic voltammetry have shown two successive and reversible reduction

Table 2
Determination of the electroactive radius r_0 of gold disk UME and gold disk ME with precise 7.5×10^{-3} mol L^{-1} potassium ferricyanide solutions in a 0.2 mol L^{-1} KCl electrolyte. Chronoamperometric measurements performed at 0.2 V during 60 s for UME and 8 s for ME.

Geometrical radius	Test 1		Test 2		Test 3	
	r_0	Std dev. r_0 (%)	r_0	Std dev. r_0 (%)	r_0	Std dev. r_0 (%)
$r_{UME} = 12.5$ µm	11.8 µm	0.3	12.5 µm	0.2	13.5 µm	0.3
$r_{UME} = 25.0$ µm	28.5 µm	0.5	29.6 µm	0.2	/	/
$r_{ME} = 0.5$ mm	0.44 mm	0.4	0.47 mm	0.5	0.48 mm	0.5
$r_{ME} = 1.5$ mm	1.49 mm	0.6	1.51 mm	0.4	1.53 mm	0.3

Table 3
Calibrationless method applied for the determination of ferrocyanide diffusion coefficient and its standard deviation (%) from the data obtained in the literature [36]. Chronoamperometric measurements performed at 0.5 V in 10 mL of potassium ferrocyanide solutions at different concentrations in a 0.2 mol L^{-1} KCl electrolyte.

r_{UME} (µm)	r_{ME} (mm)	D_0 ferrocyanide (10^{-6} cm^2 s^{-1})	% Error D_0	C_0^* known ferrocyanide (10^{-3} mol L^{-1})	C_0^* experimental ferrocyanide (10^{-3} mol L^{-1})	Error $= \frac{C_0^* \exp - C_0^* \text{known}}{C_0^* \text{known}}$ (in %)
12.5	1.5	6.16	0.7	3.45	3.43	−0.6
12.5	1.5	6.13	0.2	3.45	3.44	−0.3
12.5	1.5	6.14	0.3	5.16	5.16	−1.1
12.5	1.5	5.97	2.5	5.21	5.16	−1.1
12.5	1.5	6.36	3.9	7.32	7.17	−2.0
12.5	1.5	6.24	2.0	7.32	7.11	−2.9

waves involving two and three electrons transfer, respectively [9–12]. In the present study, results obtained come from the first reduction step of the silicomolybdic complex. Chronoamperometry was used with a potential applied at 0.34 V. Linearity was noticed between the current intensity and the concentration of the silicomolybdic complex for transient and steady states on ME and UME, respectively. For this reason the diffusion coefficient value is considered to be independent of the range of concentrations considered.

Silicate concentration was determined from the silicomolybdic complex with a reagentless method. A volume of 3 mL of a silicate solution was prepared in artificial seawater and introduced in the measurement cell. In the same compartment, a molybdenum electrode was placed with the reference and working gold ME and UME. The counter electrode was separated from the cell by a Nafion® membrane to avoid reduction of protons. This technical solution is also an advantage for the future development of an *in situ* sensor as the formation of gas in the measurement cell is prohibited. The molybdenum electrode was oxidized at 0.8 V until 14.0 C were reached, this charge was experimentally determined to obtain a pH lower than 1.5. During the oxidation of molybdenum, a black oxide layer covered the surface of the material, but this phenomenon did not affect the formation of molybdates and the achieved pH value. Indeed, some reproducibility tests, done on 10 oxidations of molybdenum, allowed reaching a pH value of 1.43 ± 0.02 and a reproducible current intensity measured for the reduction of the silicomolybdic complex (less than 3 standard deviations for 5 current intensity measurements of silicate concentration of 8.6×10^{-6} mol L^{-1}).

In the cell where molybdenum was oxidized, complexation of silicate with molybdates was carried out during 6 min under stirring, forming the electroactive Keggin anion $H_4Si(Mo_{12}O_{40})$ described in details by Lacombe et al. [11,12]:

$$Si(OH)_4 + 12MoO_4^{2-} + 24H^+ \rightarrow H_4Si(Mo_{12}O_{40}) + 12H_2O$$
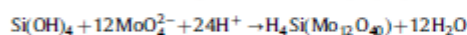
Successive chronoamperometric measurements of current *versus* time have been performed using a pair of gold disk electrodes of 12.5 or 25.0 μm radii for the UME and 1.0 or 1.5 mm radii for the ME. As good results were obtained with the calibrationless method applied to ferrocyanide, no prior determination of the electroactive surface was done before silicate determination and geometrical radii were used for the calculations. The potential was imposed during 8 s on the ME and during 60 s on the UME. Current as function of time (Fig. 2a) and steady-state current (Fig. 2b) have been used to calculate first the diffusion coefficient D_0 of the silicomolybdic complex with Eq. (2) and using the different radii values for the different pairs of electrodes.

Even if the method allows a theoretical detection of silicate, some characteristics of the voltammograms were verified systematically to apply the equations in correct conditions. Experimentally, the absence of stirring makes possible the hypothesis of semi-infinite conditions for the diffusion. Concerning data collected from the ME, the current intensity was systematically plotted *versus* $t^{-1/2}$ to verify the linearity of the correlation for times between 0.1 and 8 s, as shown in Fig. 2. This linearity shows that our experimental conditions respect Cottrell's equation (Table 1) and that the current is controlled by diffusion-controlled mass transport. To be sure to avoid both effects of double layer discharge at shorter times and limitation due to natural convection at longer times, we kept a range between 1 and 3 s for our calculations. For the UME, as time to achieve steady state current depends on several parameters [37], an experimental time of 30 s appeared sufficient to achieve steady state with a constant current intensity for a gold disk UME of 25 μm radius.

Different concentrations of silicate have been prepared from 55 to 140×10^{-6} mol L^{-1} in artificial seawater. The results obtained are reported in Table 4. The average value obtained for the diffusion coefficient of the silicomolybdic complex is $2.2 \pm 0.4 \times 10^{-6}$ cm^2 s^{-1} which is consistent with diffusion coefficient values of molecules in liquid media. Concerning the concentration, good results were observed when comparing known concentrations of silicate with experimentally derived concentrations. It must be noticed that the lowest deviation to known concentrations concerns the pair of electrodes of 12.5 μm and 1.5 mm radii for UME and ME, respectively. This can be explained by the fact that mass transfer behavior in these conditions is closer to the corresponding Cottrell's equation and Eq. (1) for ME and UME, respectively. Indeed, on one hand spherical diffusion is more predominant when the radius of the electrode is smaller and on the other hand perpendicular diffusion is much present for ME with a large surface. However, as compared to the excellent results with potassium ferrocyanide in Section 4.2, those obtained with silicate are less accurate. The main difference is the range of concentrations of silicate shifted towards lower concentrations as compared with potassium ferrocyanide. In these conditions, the required precision for the electroactive surfaces of both ME and UME becomes essential and the even slight presence of porosity might be an issue.

Starting from these results, further work is under progress with smaller radii for the UME and the use of gold from another supplier certifying the absence of porosity. As the size of the UME will be reduced, the main difficulty will be to acquire a current intensity under a few pico-amperes as noise will become predominant at this measurement scale. To get around this difficulty
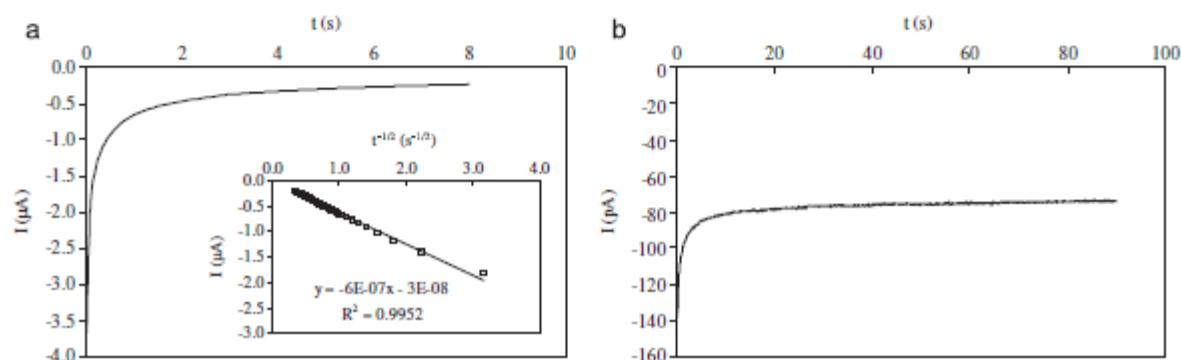

Fig. 2. Chronoamperograms performed at 0.34 V in 57.1×10^{-6} mol L^{-1} silicate in artificial seawater. (a) Reduction time of 8 s on the 1.5 mm radius gold ME. Regression of current intensity *vs* $t^{-1/2}$ plot for reduction of silicomolybdic complex in the range 0.1–8 s. (b) Reduction time of 60 s on the 25.0 μm gold disk UME.

Table 4
Calibrationless method applied for the determination of diffusion coefficient of silicomolybdic complex and concentration of silicate solutions prepared at different concentrations in artificial seawater. Amperometric measurements performed at 0.34 V in a volume of 3 mL of solution after oxidation of molybdate at 0.8 V to reach 14.0 C.

r_{UME} (µm)	r_{ME} (mm)	D_0 silicomolybdic complex (10^{-6} cm^2 s^{-1})	C_0^* known silicate (10^{-6} mol L^{-1})	C_0^* experimental silicate (10^{-6} mol L^{-1})	Error = $\frac{C_{exp}^* - C_{known}^*}{C_{known}^*}$ (in %)
25.0	0.5	1.4	55.2	52.4	−5.1
12.5	1.5	2.2	57.1	56.6	−0.9
12.5	1.5	2.4	107.3	107.3	0.0
12.5	0.5	1.9	139.7	152	8.8
25.0	0.5	2.3	139.7	136	−2.6
25.0	1.5	2.5	139.7	153.6	9.9
12.5	0.5	2.6	139.7	135.0	−3.4

some UME-arrays will be used that will allow the acquisition of a more acceptable signal and the increase of the signal to noise ratio. Building micro-devices with gold electrodes obtained by Chemical Vapor Deposition (CVD), where surface roughness of the electrode is highly reduced and its geometry accurately controlled, is the way forward to achieve perfect smooth surfaces. This process will allow us to obtain mass-produced electrodes (ME and UME) with miniaturized systems.

With a suitable protocol to electrochemically clean the electrode, reproducible results with a wider range of silicate concentrations ($0.1–140.0 \times 10^{-6}$ mol L^{-1}) are foreseen with our calibrationless method. This is the next step towards ANESIS, our Autonomous Nutrients Electrochemical Sensor *in situ* for silicate detection.

References

[1] D.J. Conley, Limnol. Oceanogr. 42 (1997) 774–777.
[2] D.J. Conley, P. Stålnacke, H. Pitkänen, A. Wilander, Limnol. Oceanogr. 45 (2000) 1850–1853.
[3] V. Smetacek, Nature 391 (1998) 224–225.
[4] A.C. Redfield, B.H. Ketchum, F.A. Richards, in: M. N. Hill (Ed.), The Composition of Sea-Water Comparative and Descriptive Oceanography, Interscience Pub, New York: 1963, pp. 26–77.
[5] P. Tréguer, P. Pondaven, Nature 406 (2000) 358–359.
[6] P. Tréguer, P. Le Corre, Manuel d'analyse des sels nutritifs dans l'eau de mer (Utilisation de l'autoanalyser II Technicon), 2nd edition, Université de Bretagne occidentale, France, 1975.
[7] L. Hua-Bin, F. Chen, J. Chromatogr. A 874 (2000) 143–147.
[8] D. Thouron, R. Vuillemin, X. Philippon, A. Lourenco, C. Provost, A. Cruzado, V. Garçon, Anal. Chem. 75 (2003) 2601–2609.
[9] N.G. Carpenter, A.W.E. Hodgson, D. Pletcher, Electroanalysis 9 (1997) 1311–1317.
[10] A.W.E. Hodgson, D. Pletcher, Electroanalysis 10 (1998) 321–325.
[11] M. Lacombe, V. Garçon, M. Comtat, L. Oriol, J. Sudre, D. Thouron, N. Le Bris, C. Provost, Mar. Chem. 106 (2007) 489–497.
[12] M. Lacombe, V. Garçon, D. Thouron, N. Le Bris, M. Comtat, Talanta 77 (2008) 744–750.
[13] J. Jońca, V. León Fernández, D. Thouron, A. Paulmier, M. Graco, V. Garçon, Talanta 87 (2011) 161–167.
[14] A.J. Bard, L.R. Faulkner, Electrochemical Methods: Fundamentals and Applications, second ed., Wiley, New York, 2000.
[15] B.J. Feldman, S.W. Feldberg, R.W. Murray, J. Phys. Chem. 91 (1987) 6558–6560.
[16] M. Mosbach, T. Laurell, J. Nilsson, E. Csöregi, W. Schuhmann, Anal. Chem. 73 (2001) 2468–2475.
[17] S. Licht, V. Cammarata, M.S. Wrighton, J. Phys. Chem. 94 (1990) 6133–6140.
[18] C. Amatore, C. Sella, L. Thouin, J. Electroanal. Chem. 593 (2006) 194–202.
[19] E. Beinrohr, M. Cakrt, J. Dzurov, L. Jurica, J.A.C. Broekaert, Electroanalysis 11 (1999) 1137–1144.
[20] E. Beinrohr, Accred. Qual. Assur. 6 (2001) 321–324.
[21] P.J. Lingane, Anal. Chem. 36 (1964) 1723–1726.
[22] C. Amatore, M. Azzabi, P. Calas, A. Jutand, C. Lefrou, Y. Rollin, J. Electroanal. Chem. 288 (1990) 45–63.
[23] M. Tsushima, K. Tokuda, T. Ohsaka, Anal. Chem. 66 (1994) 4551–4556.
[24] C. Biondi, L. Bellugi, J. Electroanal. Chem. 24 (1970) 263–270.
[25] J.J. Lingane, B.A. Loveridge, J. Am. Chem. Soc. 72 (1950) 438–441.
[26] O.R. Brown, J. Electroanal. Chem. 34 (1972) 419–423.
[27] M. Kakihana, H. Ikeuchi, G.P. Satô, K. Tokuda, J. Electroanal. Chem. 117 (1981) 201–211.
[28] P.C. Winlove, K.H. Parker, R.K.C. Oxenham, J. Electroanal. Chem. 170 (1984) 293–304.
[29] G. Denuault, M.V. Mirkin, A.J. Bard, J. Electroanal. Chem. 308 (1991) 27–38.
[30] D. Bustin, Š. Mesároš, M. Rievaj, P. Tomčík, Electroanalysis 7 (1995) 329–332.
[31] D. Menshykau, A.M. O'Mahony, M. Cortina-Puig, F.J. del Campo, F.X. Muñoz, R.G. Compton, J. Electroanal. Chem. 647 (2010) 20–28.
[32] P. Jenčušová, P. Tomčík, D. Bustin, M. Rievaj, Z. Dovalovská, Chem. Pap. 60 (2006) 173–178.
[33] C. Amatore, S. Szunerits, L. Thouin, J.S. Warkocz, J. Electroanal. Chem. 500 (2001) 62–70.
[34] C. Amatore, C. Pebay, L. Thouin, A. Wang, J.S. Warkocz, Anal. Chem. 82 (2010) 6933–6939.
[35] P. Tréguer, P. Le Corre, P. Courtot, J. Cons. Int. Explor. Mer 36 (1976) 289–294.
[36] L. Bortels, B. Van den Bossche, J. Deconinck, S. Vandeputte, A. Hubin, J. Electroanal. Chem. 429 (1997) 139–155.
[37] C. Amatore, C. Pebay, L. Thouin, A. Wang, J.S. Warkocz, Anal. Chem. 82 (2010) 6933–6939.

BIBLIOGRAPHY

Adornato, L., Cardenas-Valencia, A., Kaltenbacher, E., Byrne, R., Daly, K., Larkin, K., Hartman, S., Mowlem, M., Prien, R. and Garcon, V., 2010, *In Situ Nutrient Sensors for Ocean Observing Systems*, in Proceedings of OceanObs'09: Sustained Ocean Observations and Information for Society (Vol. 2), Venice, Italy, 21-25 September 2009, Hall, J., Harrison, D.E. & Stammer, D., Eds., ESA Publication WPP-306, doi:10.5270/OceanObs09.cwp.01

Archer, D., and Devol, A., 1992, *Benthic oxygen fluxes on the Washington shelf and slope: A comparison of in situ microelectrode and chamber flux measurements,* Limnol. Oceanogr. 37 (3) 614-629

Baar, H. J. W. de, P. W. Boyd, K. H. Coale, M. R. Landry, A. Tsuda, P. Assmy, D. C. E. Bakker, Y. Bozec, R. T. Barber, M. A. Brzezinski, K. O. Buesseler, M. Boyé, P. L. Croot, F. Gervais, M. Y. Gorbunov, P. J. Harrison, W. T. Hiscock, P. Laan, C. Lancelot, C. S. Law, M. Levasseur, A. Marchetti, F. J. Millero, J. Nishioka, Y. Nojiri, T. van Oijen, U. Riebesell, M. J. A. Rijkenberg, H. Saito, S. Takeda, K. R. Timmermans, M. J. W. Veldhuis, A. M. Waite, and C.-S. Wong., 2005, *Synthesis of iron fertilization experiments: From the Iron Age in the Age 595 of Enlightenment,* J. Geophys. Res. 110: 24 PP., doi:200510.1029/2004JC002601

Balino, B. M., Fasham M. J.R. and Bowles M. C., 2001, *Ocean biogeochemistry and global change,* IGBP No. 2

Bard, A., and Faulkner, L. R., *Electrochemical methods: Fundamentals and Applications, 2nd edition,* 2001, John Wiley and Sons, Inc. Hoboken, NJ

Barus, C., 2008, *Etude électrochimique de molecules antioxydantes et de leur association en milieux homogène et biphasique-Application aux produits dermocométiques,* Université Paul Sabatier, PhD Thesis, p. 67

Beaufort, L., Probert, I., de Garidel-Thoron, T, Bendif, E. M., Ruiz-Pino, D., Metzl, N., Goyet, C., Buchet, N., Coupel, P., Grelaud, M., Rost, B., Rickaby R. E. M., de Vergas, C., 2011, *Sensitivity of coccolithophores to carbonate chemistry and ocean acidification,* Nature 476, 80-83.

Bindoff, N. L., J. Willebrand, V. Artale, A, Cazenave, J. Gregory, S. Gulev, K. Hanawa, C. Le Quéré, S. Levitus, Y. Nojiri, C.K. Shum, L.D. Talley and A. Unnikrishnan, 2007, Observations: Oceanic Climate Change and Sea Level. In S. Solomon, D. Qin, M. Manning, Z. Chen, M. Marquis, K.B. Averyt, M. Tignor and H.L. Miller (Ed.), *Climate Change 2007: The Physical Science Basis. Contributions of Working Group I to the Fourth Assessment Report of the Intergovernmental Panel on Climate Change.* Cambridge: Cambridge University Press.

Bibliography
___

Bockris, J. O'M., Reddy, A. K. N., *Modern electrochemistry-An introduction to an interdisciplinary area, Vol. R.* Plenum Press, New York, 1970

Brandes, J. A., Devol, A. H., Deutsch, C., 2007, *New developments in the marine nitrogen cycle* Chem. Rev. 107, 577-589

Bruland, K. W., Rue, E. L., Smith, G. J., DiTullio, G. R., 2005, *Iron, macronutrients and diatom blooms in the Peru upwelling regime: brown and blue waters of Peru,* Mar. Chem. 93, 81-103

Bucher, R., 1983, *Electrolytes in polarographic oxygen sensors,* (ed. Gnaiger, E. and Forstner, H.) Springer, Berlin, p. 66

Buffle, J. and Horvai, J., 2000, *In situ monitoring of aquatic systems,* John Wiley and Sons Ltd

Canadell, J.G., Pataki, D., Gifford, R., Houghton, R.A., Lou, Y., Raupach, M. R., Smith, P., Steffen, W., 2007, in *Terrestrial Ecosystems in a Changing World,* eds Canadell JG, Pataki D, Pitelka L (IGBP Series. Springer-Verlag, Berlin Heidelberg), 59-78.

Carpenter N. G., Hodgson A. W. E. and Pletcher D., 1997, *Microelectrode procedures for the determination of silicate and phosphate in waters-Fundamental Studies,* Electroanalysis 9, No. 17, 1311-1317

Chaigneau, A., Pizzaro, O., 2005, *Mean surface circulation and mesoscale turbulent flow characteristics in the eastern South Pacific from satellite tracked drifters,* J. Geophysic. Res. 110, C05014

Chaigneau A., Pizarro O,. 2005, *Surface circulation and fronts of the South Pacific Ocean, east of 120°W..* Geophysic. Res. Lett., 32, L08605

Chan, F., Barth, J. A., Lubchenco, J., Kirincich, A., Weeks, H., Peterson, W. T., Menge, B. A., 2008, *Emegence of anoxia in the California Current large marine ecosystem,* Science 319, 920

Chesapeake Bay Foundation Reports, December 2008, cbf.org/badwaters

Chen, Z., Grierson, P., Adams, M. A., 1998, *Direct determination of phosphate in soil extracts by potentiometric flow injection using a cobalt wire electrode*, Anal. Comm. 34, 93-97

Cheng, W.-L., Jun-Wei, S., Wei, C., Chang, J. L. and Zen J.-M., 2010, *Activated nickel platform for electrochemical sensing of phosphates,* Anal. Chem., 82, 1157-1161

Chisholm S. W., 2000, *Stirring times in the Southern Ocean,* Nature 407, 685-687

Clement, A.C., and Peterson, L.C., 2008. *Mechanisms of abrupt climate change of the last glacial period*. Rev. Geophys., 46, RG4002, doi:10.1029/2006RG000204

Codispoti, L. A., Christensen, J. P., 1985, *Nitrification, denitrification and nitrous oxide cycling in the eastern tropical south Pacific Ocean,* Mar. Chem., 16, 277-300

Colas, F., Capet, X., McWilliams, J. C., Shcheptkin, A., 2008, *1997-1998 El Nino off Peru: A numerical study,* Prog. Oceanogr., 79, 138-155

Colling, A. B., 2004, *Ocean Circulation.* The Open University. Volume 3.

Compton, R. G., Sanders, G. H. V., 1996, *Electrode potentials,* Oxford Chemistry Prilers, Oxford, 92,

Compton, R. G., Banks, C. E., 2007, *Understanding voltammetry,* World Scientific Publishing Co., Singapore,

Cornejo, M., and Farijas, L., 2012, *Following the N_2O consumption at the Oxygen Minimum Zone in the eastern South Pacific,* Biogeosciences Discuss., 9, 2691-2707

Crank, J., 1989, *The mathematics of diffusion,* Clarendon Press, Oxford, 414

Dalsgaard, T., Canfield, D. E., Petersen, J., Thamdrup, B., Acun-Gonzales, J., 2003, *N_2 production by the anammox reaction in the anoxic water column of Golfo Dulce, Costa Rica.* Nature 422, 606–608

Delauney, L., Compère, C., Lehaitre, M., 2010, *Biofouling protection for marine environmental sensors,* Ocean Sci., 6, 503-511

Denman, K. et al., 2007, *Couplings between Changes in the Climate System and Biogeochemistry. In : Climate Change 2007 : The Physical Science Basis.* Contribution to Working Group I to the Fourth Assessment Report on the IPCC, Cambridge University Press, Cambridge, UK and New York, NY, USA

Denton, G. H. and Hendy, C. H., 1994, *Younger Dryas Age Advance of Franz Josef Glacier in the Southern Alps of New Zealand.* Science, 264(5164):1434-1437.

Denuault, G., 2009, *Electrochemical techniques and sensors for ocean research,* Ocean Sci., 5, 697-710,

Dhawan, S. K., Kumar, D., Ram, M. K., Chandra, S., Trivedi, D. C., 1997, *Application of conducting polyaniline as sensor material for ammonia,* Sens. Actuator B-Chem., 40, 99-103,

Diaz, R. J. and Rosenberg, R., 2008, *Spreading Dead Zones and Consequences for Marine Ecosystems,* Science 321, 926-929

Dickey, T. D., 2001, *The role of new technology in advancing ocean biogeochemical research,* Oceanography, 14, 417-425

Doney, S. C., Fabry, V. J., Feely, R. A., Kleypas J. A., 2009, *Ocean acidification: the other CO_2 problem,* Annu. Rev. Marine Sci. 1, 169-192

Drummond, L., and Maher, W., 1995, *Determination of phosphorus in aqueous solution via formation of the phosphoantimonylmolybdenum blue complex Re-examination of optimum conditions for the analysis of phosphate,* Anal. Chim. Acta 302, 69-74

Ejhieh A. N. and Neda, M., 2010, *Application of a new potentiometric method for determination of phosphate based on a surfactant-modified zeolite carbon-paste electrode (SMZ-CPE),* Anal. Chim. Acta 658, 68-74

Farias, L. Paulimer, A., Gallegos, L., 2007, *Nitrous oxide and N-nutrient cycling along the oxygen minimum zone off northern Chile,* Deep-Sea Res. 34, 164-180

Fernandez, C., Farias, L., Ulloa, O., 2011, *Nitrogen fixation in denitrified marine waters,* PloS ONE, 6 (6) e20536

Fiedler, P. C., Talley, L. D., 2006, *Hydrography of the eastern tropical Pacific: A review, Prog. Oceanogr.,* 69 (2-4), 143-180

Bibliography

Fiedler, P.C., 1994, *Seasonal and interannual variability of coastal zone color scanner phytoplankton pigments and winds in the eastern tropical Pacific*, J. Geophysic. Res.-Oceans 99, 18371-18384.

Fischer, J. P., and Wenzhofer, F., 2010, *A novel planar optode setup for concurrent oxygen and light field imaging: Application to the benthic phototrophic community,* Limnol. Oceanogr: Methods 8, 254-268

Fogg A. G. and Bsebsu N. K., 1981, *Differental-pulse voltammetric determination of phosphate as molybdovanadophosphate at a glassy carbon electrode and assessement of eluents for the flow injection voltammetric determination of phosphate, silicate, arsenate and germanate,* Analyst, Vol. 106, 1288-1295

Franz, J., Krahmann, G., Lavik, G., Grasse, P., Diimar, T., Riebesell, U., 2012, *Dynamics and stoichiometry of nutrients and phytoplankton in waters influenced by the oxygen minimum zone in the eastern tropical Pacific,* Deep-Sea Res. I, 62, 20-31,

Galan, A., Molina, V., Thamdrup, B., Woebken, D., Lavik, G., Kuypers, M. M. M., Ulloa, O., 2009, *Anammox bacteria and the anaerobic oxidation of ammonium in the oxygen minimum zone of nothern Chile,* Deep-Sea Res. Pt. II, 56, 1125-1135

Ganjali, M. Z., Norouzi, P., Ghomi, M., Salavati-Niasari M., 2006, *Highly selective and sensitive monohydrogen phosphate membrane sensor based on molybdenum acetylacetonate,* Anal. Chim. Acta 567, 196-201

Giraud, M., 2012*, Signature des phosphates dans l'OMZ du Pérou,* Master Thesis

Glantz, M. *Currents of change: Impacts of El Nino and La Nina on Climate and Society* 3rd ed. (Cambridge, U.K.: Cambridge University Press, 2001)

Glazer, B. T., Marsh, A. G., Stierhoff, K., Luther III, G. W., 2004, *The dynamic response of optical sensors and voltammetric electrodes to temporal changes in dissolved oxygen concentrations,* Anal. Chim. Acta, 518, 93-100

Glessmer, M. S., Park, W., Oschlies, A., 2011, *Simulated reduction in upwelling of tropical oxygen minimum waters in a warmer climate,* Environ. Res. Lett. 6, 045001, doi:10.1088/1748 9326/6/4/045001

Graco, M., Ledesma, J., Flores, G., Giron, M., 2007, *Nutrients, oxygen and biogeochemical processes in the Humboldt upwelling current system off Peru,* Rev. Peru. Biol. 14 (1) 117-128

Grados, C., Chaigneau, A., Graco, M., Ledesma, J., 2009, *Regional oceanographic scenery and water mass distribution in the coastal VOCALS REx region in October 2008,* The second VOCALS Meeting, University of Washington, Seattle

Greenblatt, J. and Sarmiento, J., 2004, *Variability and climate feedback mechanisms in ocean uptake of CO_2. In* The Global Carbon Cycle [Field, C. and Raupach, M., eds.], pp. 257-275. Washington: Island Press.

Gruber, N., M. Gloor, S. E. Mikaloff-Fletcher, S. Dutkiewicz, M. Follows, S. C. Doney, M. Gerber, A. R. Jacobson, K. Lindsay, D. Menemenlis, A. Mouchet, S. A. Mueller, J. L. Sarmiento, and T. Takahashi, 2009, *Oceanic sources, sinks, and transport of atmospheric CO_2, Global Biogeochem. Cycles*, 23, GB1005, doi:10.1029/2008GB003349.

Grundig, B., Wittstock, G., Rudel, U., Strehlitz, B., 1995, *Mediatore-modified electrodes for electrocatalytic Oxidation of NADH,* J. Electroanal. Chem., 395, 143-157

Guanghan, L., Xiaogang, W., Yanhua, L., Shenlai , Y., 1999, *Studies on 1:12 phosphomolybdic heteropoly anion film modified carbon paste electrode*, Talanta 49, 511-515

Gundersen, J. K., Ramsing, N. B., Glud, R. N., 1998, *Predicting the signal of O_2 microsensors from physical dimensions, salinity and O_2 concentration,* Limnol. Oceanogr., 43, 1932

Hale, J. M., 1983, *Factors influencing the stability of polarographic oxygen sensors*, In Polarographic Oxygen Sensors, ed. Gnaiger, E. and Forstner, H., Springer, Berlin, p. 3

Hamerseley, M. R., Lavik, G., Woebken, D., Rattray, J. E., Lam, P., Hopmans, E. C., Damste, E. C., Kruger, J. S. S., Graco, M., Gutierrez, D. Kuypers, M. M. M., 2007, *Anaerobic ammonium oxidation in the Peruvian oxygen minimum zone,* Limnol. Oceanogr. 52, 923-933.

Harden, S. M., and Nonidez, W. K., 1984, *Determination of orthophosphate by flow injection analysis with amperometric detection,* Anal. Chem., 56, 2218-2223

Helder, W., and Bakker, J. F., 1985, *Shipboard comparison of micro and minielectrodes for measuring oxygen distribution in marine sediments,* Limnol. Oceanogr., 30, 1106

Herstkotte, B., Alonso, J. C., Miro, M., Cerda, V., 2010, *A multisyringe flow injection Winkler-based spectrophotometric analyzer for in-line monitoring of dissolved oxygen in seawater,* Talanta, 80, 1341-1346

Hutchins, D. A., Hare, C. E., Weaver, R. S., Zhang, Y., Firme, C. F., DiTullio, G. R., Alm, M. A., Riseman, S. F., Maucher, J. M., Gessey, M. E., Trick, C. G., Smith, G. J., Rue, E. L., Conn, J., Bruland, K. W., 2002, *Phytoplankton iron limitation in the Humboldt Current and Peru,* Limnol. Oceanogr. 47, 997-1011

Huyer, A., Smith, R. L., Paluszkiewicz, T., 1987, *Coastal upwelling off Peru during normal and El Nino times,* J. Geophys. Res., 92 (14) 14297-14307

Huyer, A., Knoll, T., Paluszkiewic, T., Smith, 1991, *The Peru Undercurrent: A study of variability,* Deep Sea Res. Part A, 38, S247-S271

Ingall, E., Jahnke, R., 1994, *Evidence for enhanced phosphorus regeneration from marine sediments overlain by oxygen depleted waters.* Geochim. Cosmochim. Acta, 58, 2571-2575.

Jain A. K. Gupta V. K., Raisoni J. R., 2006, *A newly synthesized macrocyclic dithiooxamine receptor for phosphate sensing,* Talanta 69, 1007-1012

Johnson, K. S., 2009, *Observing biogeochemical cycles at global scales with profiling floats and gliders*, Oceanography Vol. 22, No. 3, 216-225

Johnson, K. S., Needoba, J., Riser, S., Showers, W., 2007, *Chemical sensor networks for the aquatic environment,* Chem. Rev., 107, 624-640

Johnson, K. S., 2003, *State of technology in the development and application of nutrient sensors,* Alliance for Coastal technology, 1-9

Jońca, J., Leon-Fernandez, V., Thouron, D., Paulmier, A., Graco, M., Garçon, V., 2011, *Phosphate determination in seawater: Towards an autonomous electrochemical method,* Talanta 87, 161-167

Kessler, W. S., 2006, *The circulation of the eastern tropical Pacific: A review,* Progr. Oceanogr. 69, 181-217

Keeling R. F., Kortzinger A., Gruber N., 2010 *Ocean deoxygenation in a warming world,* Annual Rev. Mar. 2, 199-229

Kérouel, R. and Aminot, A., 1987, *A procedure to reduce pre-analytical contamination during the analysis of dissolved nutrient elements (fingerprints, atmosphere, particulates) in seawater,* Mar. environ. Res., 22(1), 19-32

Kivlehan F., Mace W. J., Moynihan H. A., Arrigan D. W. M., 2007, *Potentiometric evaluation of calix (4)arene anion receptors in membrane electrodes: Phosphate detection,* Anal. Chim. Acta 585, 154-160

Kuhl, M., Revsbech, N. P., 2000, *Microsensors for the study of interfacial biogeochemical processes,* (ed. Boudreau, B. and Jorgensen, B. B., Oxford University Press, Oxford)

Kuypers, M., Lavik, G., Woebken, D., Schmidt, M., Fuchs, B. M., Amann, R., Jetten, S. M., 2005, Proc. Natl. Acad. Sci. USA 102, 6478 – 6483.

Kuypers M., Sliekers A., Lavik, Schmidt M., Jorgensen B., Kuenen J., Siminghe Damste J., Strous J., Jetten M., 2003, *Anareobic ammonium oxidation by anammox bacteria in the Black Sea,* Nature 422, 608-611

Lam, P., Lavik, G., Jensen, M. M., ven de Vossenberg, J., Schmid, M., Woebken, D., Gutierrez, D., Amann, R., Jetten, M. S. M., Kuypers, M. M. M., 2009, *Revising the nitrogen cycle in the Peruvian oxygen minimum zone,* PNAS, 106 (12) 4725-4757

Lam, P., Kuypers, M. M. M., 2011, *Microbial nitrogen cycling processes in Oxygen Minimum Zones,* Annu. Rev. Marine. Sci. 3, 317-245
Lawal A. T., Adeloju S. B., 2009, *Comparison of enzyme immobilisation methods for potentiometric phosphate biosensors,* Biosens. Bioelectron. 25, 406-410

Lee, K., Choi, S., Park, G., Wanninkhof, R., PENG, T., Key, R., Sabine, C., Feely, R., Bullister, J., Millero, F., and Kozyr, A., 2003, *An updated anthropogenic CO2 inventory in the Atlantic ocean,* Global Biogeochem. Cycles, 17(4):1116.

Levin L., 2003, *Oxygen Minimum Zones: Adaptation and community response to hypoxia*, Oceanography and Marine Biology 41, 1-45

Lin X., Wu X., Xie Z., Wong K.-Yin., 2006, *PVC matrix membrane sensor for fluorescent determination of phosphate*, Talanta 70, 32-36

Little B. J., Lee J. S., Ray R. I., 2008, *The influence of marine biofilms on corrosion: A concise review*, Electrochim. Acta, Vol. 54, 2-7

Lucas, R., 1986, *The termination of the Equatorial Undercurrent in the eastern Pacific,* Prog. Oceanogr. 16, 63-90

Luther III, G. W., Glazer, B. T., Ma, S., trouwborst, R. E., Moore, T. S., Metzger, E., Kraiya, C., Waite, T. J., Druschel, G., Sundby, B., Taillefert, M., Nuzzio, D. B. Shank, T. M., Lewis, B. L., Brendel, P. J., 2008, *Use of voltammetric solid-state (micro)electrodes for studying biogeochemical processes: Laboratory measurements to real time measurements with an in situ electrochemical analyser (ISEA)*, Mar. Chem. 208, 221-235

Luther III, G. W., Glazer, B., Hohmann, L. Popp, J., Taillefert, M., Rozan, T., Brendel, P., Theverge, S., Nuzzio, D., 2001, *Sulfur speciation monitored in situ with solide state gold amalgam voltammetric*

micorelectrodes: polysulfides as a special case in sediments, microbial mats and hydrothermal vent waters, J. Environ. Monitor., 3, 66

Maier-Reimer, E., Mikolajewicz, U., Winguth, A., 1996, *Interactions between ocean circulation and the biological pumps in the global warming,* Clim. Dyn., 12, 711-721.

Matsunaga, K., Kudo, I., Yanada, M., 1986, *Differential-pulse anodic voltammetric determination of dissolved and adsorbed phosphate in turbid natural waters,* Anal. Chim. Acta, 185, 355-358

Meehl, G. A., F.Stocker, T., D.Collins, W., P.Friedlingstein, Gaye, A., J.M.Gregory, A.Kithoh, R.Knutti, J.M.Murphy, A.Noda, S.C.B.Raper, I.G.Watterson, A.J.Weacer, and Zhao, Z., 2007, *Global climate projections - Chapter 10 In The Physical Science Basis.* Contribution of Working group 1 to the Fourth Assessment Report of the Intergovernmental Panel on Climate Change. Fourth Assessment Report of the Intergovernmental Panel on Climate Change. Cambridge University Press.

Millero F. J., Chemical oceanography, 3rd edition, 2006

Millero F. J. 2007, *The Marine Inorganic Carbon Cycle,* Chem. Rev., 107, 308-341

Montes, Y., Colas, F., Capet, X., Schneider, W., 2010, *On the pathways of the equatorial subsurface currents in the eastern equatorial Pacific and their contributions of the Peru-Chile Undercurrent*, J. Geophysic. Res., 115, C09003

Murphy J. and J.P. Riley, 1962. *A modified simple solution method for the determination of phosphate in natural waters. Anal. Chim. Acta,* 27, 31-36.

Nakamura H., Ikebukuro K., McNiven C., Karube I., Yamamoto H., Hayashi K., Suzuki M., Kubo I., 1997, *A chemiluminescent FIA biosensor for phosphate ion monitoring using pyruvate oxidase,* Biosens. Bioelectron., 12, No. 9-10, 959-966

Naqvi S. W. A., Gupta S., DileepKumar M., 1993, *Carbon dioxide and nitrous oxide in the Arabian Sea, In:McBean, G. A.Hantel M. (Eds.), Interactions between global climate subsystems: the legacy of Hann. (Geophysical Monograph; 15)* AGU, USA, 85-92

Naqui, S. W. A., Noronha, R. J., 1991, *Nitrous oxide in the Arabian sea,* Deep-Sea Res., 38, 871-891

Oschlies, A.. Schulz, K.G., Riebesell, U., Schmittner, A., 2008, *Simulated 21st century's increase in oceanic suboxia by CO_2-enhanced biotic carbon export.* Global Biogeochemical Cycles GB4008, doi:10.1029/2007GB003147

Paulmier A., Ruiz-Pino D., Garçon V., Farias L., 2006, *Monitoring of the Eastern South Pacific Oxygen Minimum Zone (OMZ) off Chile,* Geophysic.Res. Lett., 33, No. 20, 1-6

Paulmier A., Ruiz-Pino D., Garçon V., 2008, *The oxygen minimum zone (OMZ) off Chile as intense source of CO_2 and N_2O,* Continent. Shelf Res., 28,No. 20, 2746-2756

Paulmier A., Ruiz-Pino D., 2009, *Oxygen minimum zones (OMZs) in the modern ocean,* Prog. Oceanog. 80, 113-128

Paytan A., McLaughlin K., 2007, *The Oceanic phosphorus cycle,* Chem. Rev., 107, 563-576

Penven, P., Echevin, V., Pasapera, J., Colas, F., Tam. J., 2005, *Average circulation, seasonal cycle, and mesoscale dynamics of the Peru Current System: A modeling approach,* J. Geophys. Res., 110, C10021

Prien, R. D., 2007, *The future of chemical in situ sensors,* Mar. Chem., 107, 422-432

Quintana J. C., Idrissi L., Palleschi G., Albertano P., Amine A., El Rhazi M., Moscone D., 2004, *Investigation of amperometric detection of phosphate. Application in seawater and cyanobacterial biofilm samples*, Talanta 63, 567-574

Rahmstorf, S., 2003, *The current climate.* Nature, 421(6924):699-699.

Rahmstorf, S., 2006, *Thermohaline ocean circulation.* Encyclopedia of Quaternary Sciences.

Redfield A. C., 1958, *The biological control of chemical factors in the environment,* Am. Sci. 64, 205-221.

Reid, J. L., 1997, *On the geostrophic circulation of the Pacific ocean patterns, tracers, and transports,* Prog. Oceanog. 39, 263-352,

Reimers, C. E. and Glud, R. N., 2000, *In situ chemical measurements at the sediment-water interface,* In chemical sensors in oceanography ed. Varney, M., Gordon and Breach

Reverdin, G., Frankignoul, C., Kestenare, E., McPhaden, M.J., 1994, *Seasonal variability in the surface currents of the equatorial Pacific*, J.Geophysic. Res. 99, 20323-20344

Revsbech N. P., Larsen L. H., Gundersen J., Dalsgaard T., Ulloa O., Thamdrup B., 2009, *Determination of ultra-low oxygen concentrations in oxygen minimum zones by the STOX sensor*, Limnol. Oceanogr.: Methods 7, 371-381

Revsbech, N. P., 1989, *An oxygen microelectrode with a guard cathode,* Limnol. Oceanogr. 34, 474

Revsbech, N. P. and Jorgensen, B. B. 1986, *Microelectrodes: their use in microbial ecology,* Adv. Microb. Ecol., 9, 293

Roemmich, D., W.J. Gould and J. Gilson, 2012: *135 years of global ocean warming from the Challenger Expedition to the Argo Program Nature Climate Change*, DOI: 10.1038/NCLIMATE1461.

Roemmich D., Gilson J., 2009, *The 2004–2008 mean and annual cycle of temperature, salinity, and steric height in the global ocean from the Argo Program*, Progr. Oceanog., 82, (2), 81-100

Roemmich, D., S. Riser, R. Davis, and Y. Desaubies, 2004, *Autonomous profiling floats: Workhorse for broadscale ocean observations.* Mar. Technol. Soc. J., 38 (2), 21-29.

Ryabenko, E., Kock, A., Bange, H. W., Altabet, M. A., Wallace, D. W. R. 2012, *Contrasting biogeochemistry of nitrogen in the Atlantic and Pacific oxygen minimum zones,* Biogeosciences Discuss., 8, 8001-8039

Sabine, C., Feely, R., Gruber, N., Key, R., Lee, K., Bullister, J., Wanninkhof, R., Wong, C., Wallace, D., Tilbrook, B., Millero, F., PENG, T., Kozyr, A., Ono, T., and Rios, A., 2004, *The oceanic sink for anthropogenic CO2.* Science, 305(5682):367-371.

Saeed M. A., Powell D. R., Hossain Md. A., 2010, *Fluorescent detection of phosphate by a highly selective chemosensor in water*, Tetrahedron Letters 51, 4904-4907

Sarmiento, J. and Gruber, N., 2002, *Sinks for anthropogenic carbon*. Physics Today, 55(8):30–36.

Schnaider, W., Fuenzalida, R., Rodriguez -Rubio, E., Garces-Vargas, J., 2003, *Characteristics and formation of Eastern South Pacific Intermediate Water*, Geophysic. Res. Lett., 30 (11) 1581

Siegenthaler, U., Stocker, T. F., Monnin, E., Luthi, D., Schwander, J., Stauffer, B., Raynaud, D., Barnola, J. M. et al., 2005, *Stable Carbon Cycle–Climate Relationship During the Late Pleistocene,* Science 25, 1313-1317

Silva, N., Rojas, N., Fedele, A., 2009, *Water masses of the Humboldt Current System: Properties, distribution, and nitrate deficit as a chemical water mass tracer for Equatorial Subsurface Water off Chile,* Deep-Sea Res. II, 56, 1004-1020

Silva, N., Neshiba, S., 1979, *On the southermost extension of the Peru-Chile Undercurrent,* Deep -Sea Res., 26, 1387 - 1393

Stramma, L., Johnson, G. C., Sprintall, J., Mahrholz, V., 2008, *Expanding Oxygen Minimum Zone in the tropical oceans,* Science 320, 655-658

Stramma, L., Schmidko, S., Levin, L., Johnson, G. C., 2010, *Ocean oxygen minima expansions and their biological impacts*, Oceanogr. Res. Papers, 57, 587-595

Stramma, L., Oschlies, A., Schmidtko, S., 2012, *Anticorrelated observed and modelled trends in dissolved oceanic oxygen over the last 50 years,* Biogeosciences Discuss. 9, 4595-4626

Strickland, J. D. H., Eppley, R. W., de Mendiola, B. R., 1969, *Phytoplankton populations, nutrients and photosynthesis in Peruvian coastal waters,* Bol.-Inst. Mar. Peru 2, 4-45

Strickland, J. D. H. and Parsons, T. R., 1972, *A practical handbook of seawater analysis.* Second Edition, Bulletin 167. Fisheries Research Board of Canada, Ottawa

Sunda W. G. (2010), *Iron and the carbon pump,* Science 327, 654-655

Strub, P. T., Mesias, J. M., Montecino, V., Rutlant, J., Salinas, S., 1998, *Coastal ocean circulation off western South America. Coastal Segment (6, E).* En A. R. Robinson & K. H. Brink [eds.], The Sea. Wiley. New York. 273-313

Strub, P.T., Mesias, J., James, C., 1995, *Satellite observations of the Peru-Chile countercurrent.* Geophys. Res. Lettr., 22, 211-214.

Sverdrup, H. U., 1947, *Wind-driven currents in a baroclinic ocean, with application to the equatorial currents of the eastern Pacific.* Proc. Natl. Acad. Sci. USA, 33, 318-326.

Takahashi, T., S. C. Sutherland, R. Wanninkhof, C. Sweeney, R. A. Feely, D. W. Chipman, B. Hales, G. Friederich, F. Chavez, A. Watson, D. C. E. Bakker, U. Schuster, N. Metzl, H. Yoshikawa-Inoue, M. Ishii, T. Midorikawa, Y. Nojiri, C. Sabine, J. Olafsson, Th. S. Arnarson, B. Tilbrook, T. Johannessen, A. Olsen, Richard Bellerby, A. Körtzinger, T. Steinhoff, M. Hoppema, H. J. W. de Baar, C. S. Wong, Bruno Delille and N. R. Bates, 2009, *Climatological mean and decadal change in surface ocean pCO$_2$, and net sea–air CO$_2$ flux over the global oceans,* Deep Sea Res. Part II, 56, 554-577

Tanaka, T., Miuran M., Ishiyama, T., 2001, *Adsorptive voltammetric determination of orthophosphate at a glassy carbon electrode,* J. Trace, Microb. Tech. 19 (4) 591-599

Tarazona, J., Gutierrez, D., Paredes, C., Indacochea, A., 2003, *Overview and challenges of marine biodiversity research in Peru,* Gayana 67 (2) 206-231

Tercier-Waeber M. L., Confalonieri F., Riccardi G., Sina A., Nöel S., Buffle J., Graziottin F., 2005, *Multi Physical–Chemical profiler for real-time in situ monitoring of trace metal speciation and master variables: Development, validation and field applications*, Mar. Chem, 97, (3-4), 216-235

Tercier-Waeber, M. L., Buffle, J., Confalonieri F., Riccardi G., Sina, A., Graziottin, F., Fiaccabrino, G. C., Koudelka-Herp, M., 1999, *Submersible voltammetric probes for in situ real time trace element measurements in surface waters, groundwater and sediment-water interface,* Meas. Sci. Technol., 10, 1202-1213

Thamdrup, B., Dalsgaard, T., Jensen, M. M., Ulloa, O., Farias, L., Escribano, R., 2006, *Anaerobic ammonium oxidation in the oxygen-deficient waters off northern Chile,* Limnol. Oceanogr. 51, 2145-2156.

Thouron, D., Garçon, V., 2006, *ANAIS: Analyzeur de sels nutritifs autonome in situ: 1995-2005: développement, validation, fiabilisation, Avenir?.* Rapport d'audit LEGOS, Toulouse. INSU/CNRS, pp 45

Thouron, D., Naudin, J. J., Labaron, P., Oriol, L., Lacombe, M., Comtat, M., Le Bris, N., Garçon, V., 2006, *Monitoing des nitrates en millieu côtier. Le capteur autonome ANAIS en baie de Banuyls/Mer. AEI.*

Thouron, D., Vuillemin, R., Philippon X., Lourenço A., Provost C., Cruzado, A., and Garçon, V., 2003, *An Autonomous Nutrient Analyzer for Oceanic Long-term in situ biogeochemical monitoring,* Anal. Chem., 75, 11, 2601-2609.

Toggweiler, J. R., Dixon, K., Broecker, 1991, *The Peru upwelling and the ventilation of the South Pacific thermocline,* J. Geophys. Res., 96, 20467-20497

Toggweiler, J. R. and Russell, J. 2008, *Ocean circulation in a warming climate.* Nature, 451(7176):286-288.

Trojanowicz, M., Lewenstam, A., Krawczyk, T. K. V., Lahdesmaki, I., Szczepek, W., 1996, *Flow injection amperometric detection of ammonia using a polypyrrole-modified electrode and its application in urea and creatinine biosensors,* Electroanal., 8, 233-243,

Udnan Y., McKelvie I. D., Grace M. R., Jakmunee J., Grudpan K., 2005, *Evaluation of on-line preconcentration and flow-injection amperometry for phosphate determination in fresh and marine waters.,* Talanta 66, 461-466

Whitfield, M., Jagner, D., 1981*, Marine electrochemistry: A practical introduction,* Wiley, 542

Willey, N., 2011, *Humboldt Current*, Culp Press

Winkler, L. W., 1888, *Die Bestimmung des im Wasser gelosten Sauerstoffes,* Ber. Dtsch.Chem. Ges. Berlin, 21, *2843*

Wunsch, C. (2002). *What is the thermohaline circulation?* Science, 298(5596):1179-1180.

Wyrtki, K., 1963, *Circulation and water masses in the Eastern Equatorial Pacific Ocean*, Int. J. Oceanol. Limnol. 1 (2) 117-147

Vaquer-Sunyer A and Duarte C. M., 2008, *Thresholds of hypoxia for marine diversity*, PNAS 105, 15452-15457

Varney, M. 2000, *Chemical sensors in oceanography,* Gordon and Breach: Amsterdam, The Netherlands, 2000 (Eds.), 333

Vuillemin, R., Thouron, D., Gallou, G., Pares, L., Brient, B., Dubreule, A., Garçon, V., 1999, *ANAIS : Autonomous nutrient analyzer in situ.* Sea Technol., 40, 75-78

Yao T., Takashima K., Nanjyo Y., 2003, *Simultanous determination of orthophosphate and total phosphates (inorganic phosphates plus purine nucleotides) using a bioamperometric flow-injection system made up by a 16-way switching valve,* Talanta 60, 845-851

Zoski, C. G., 2007, *Handbook of electrochemistry,* Elsevier B. V.

Zou Z., Han. J., Jang A., Bishop P. L., Ahn C. H., 2007, *A disposable on-chip phosphate sensor with planar cobalt microelectrodes on polymer substrate*, Biosens. Bioelectron. 22, 1902-1907

Justyna Jońca

Electrochemical methods for autonomous monitoring of chemicals (oxygen and phosphate) in seawater: Application to the Oxygen Minimum Zone

PhD advisor: Véronique Garçon, Maurice Comtat

Co – advisor: Niels Peter Revsbech (secondment at Aarhus University)

Abstract

Developing new sensors for improving our understanding of the coupled biogeochemical cycles constitutes an immense challenge. Electrochemistry provides promising reagentless methods by going further in miniaturization, decreasing the response time and energy requirements and thus increasing our observing capacities in the ocean. This study is focused on phosphate and oxygen, two key compounds of the marine ecosystems. Improvement of the amperometric STOX sensor for ultra-low oxygen detection in seawater is presented. The improvement was achieved by changing sensor construction and preliminary studies showed higher sensitivity and faster response time. A novel electrochemical method for phosphate detection was developed. The method is based on anodic oxidation of molybdenum in seawater in order to form the phosphomolybdic complex, electrochemically detectable by means of amperometry or voltammetry. Thanks to special construction of an electrochemical cell including specific membrane technology, the method does not require addition of reagents and is free from silicate interferences. The method was tested during Pelagico 1011-12-BIC OLAYA cruise offshore Peru in 2010. The Peruvian water masses analysis was also performed using data collected during this cruise.

Key words: *in situ* autonomous observatories, open ocean, Oxygen Minimum Zone, phosphate, oxygen, STOX sensor, electrochemistry, water masses.

Research field: Analytical chemistry, oceanography

Laboratoire d'Etudes en Géophysique et Océanographie Spatiales

UMR 5566 – CNRS/IRD/UPS/CNES – Observatoire Midi Pyrénées

14 av Edouard Belin 31400 Toulouse, France

Justyna Jońca

Méthodes électrochimiques pour la surveillance autonome des espèces chimiques (oxygène et phosphate) dans l'eau de mer : Application aux Zones de Minimum d'Oxygène

Directeurs de la thèse : Véronique Garçon, Maurice Comtat

Co – encadrant : Niels Peter Revsbech (stage à l'Université d'Aarhus)

Résumé

Le développement de nouveaux capteurs pour améliorer notre compréhension des cycles biogéochimiques dans l'océan représente un immense défi. L'électrochimie offre des méthodes de détection sans ajout de réactifs, avec un temps de réponse court, une faible consommation d'energie, la possibilité de miniaturisation et donc d'augmenter significativement nos capacités d'observation de l'océan. Cette étude se concentre sur le phosphate et l'oxygène dissous, deux composés principaux au sein des écosystèms marins. Une amélioration du capteur STOX pour la mesure des faibles concentrations d'oxygène a été obtenue. Celle-ci repose sur un changement dans la construction du capteur et les résultats préliminaires ont montré une sensibilité plus élevée et un temps de réponse plus rapide. Une nouvelle méthode électrochimique pour la détection des phosphates a été développée. Le procédé est basé sur l'oxydation du molybdène dans l'eau de mer pour former le complexe phosphomolybdique, électrochimiquement détectable sur l'or par ampérométrie ou voltammétrie. Grâce au développement d'une cellule électrochimique adaptée, utilisant la technologie membranaire, la méthode ne nécessite pas d'ajout de réactif liquide et s'affranchit de l'interférence des silicates. La méthode a été testée pendant la campagne en mer Pelagico 1011 à 1012-BIC OLAYA au large du Pérou en 2010. Une analyse des masses d'eaux au large du Pérou a été réalisée grâce aux données recueillies au cours de cette campagne.

Mots clés : observatoires *in situ* autonomes, océan ouvert, Zone de Minimum d'Oxygène, phosphate, oxygène, capteur STOX, électrochimie, masses d'eaux.

Domaine de recherche : chimie analytique, océanographie